High Resolution Wide Field Surface Plasmon Microscopy

by Graham Stabler, MEng

Thesis submitted to The University of Nottingham
for the degree of Doctor of Philosophy, Sept 2004

Abstract

This thesis presents the development of a high resolution wide field speckle illuminated interferometric surface plasmon microscope. This system is based on a Linnik interferometer and uses a high NA oil immersion objective for the excitation of surface plasmons. The confocal response of the microscope and high surface field enhancement due to surface plasmon excitation lead to high resolution and high contrast of weak surface structures and films. The microscope was also demonstrated in two other modes of operation, a sensing mode where the distributions seen in the back focal plane of the sample objective could be used to determine the optical parameters of the sample and a conventional surface plasmon microscope mode where image enhancement was created through the use of polarizers and optical masks. Results are presented that show the microscope as capable of imaging results comparable or better than that in the literature and without the need to scan. Hence the system is shown to be wholly suitable to biological and research fields interested in thin films and surface reactions.

Acknowledgements

Firstly I would like to thank EPSRC for funding my research. I'd then like to thank Mike Somekh, my supervisor, for many enlightening, vibrant and occasionally heated discussions on the topic of my thesis. Without his vast experience and guiding hand I would not have been able to produce this work.

Amongst my collegues I would like to thank Ian Stockford, a fellow student and lab mate for making the hard times bearable, for discussing ideas and of course for answering my stupid questions. I would also like to thank Nick Sawyer, Mark Pitter, Steve Sharples and Dr See for disscussion on subjects as diverse as speckle illumination and thesis writing. Amongst the departmental staff I would particularly like to thank Kevin Last, Malcolm Gibbons and Ron Whitehead for providing the necessary help in building the mechanical assemblies for the experiment and for teaching me many workshop skills. I would also like to thank Rod Dykeman for preparing some of the samples used in the experiments.

Thanks also go to some of my friends who have made the latter portions of the PhD experience most enjoyable, they include Paul Robson, Andrew Goodman, Steve Bull, Phil Bream and Andreas Pain.

Last but not least I would like to thank my Mum who has supported me all the way through my academic career, good times and bad, without whose support I would have given up long ago.

Contents

Chapter 1

Introduction

The work presented in this thesis concerns the realization of a wide field surface plasmon (SP) microscope with high spatial resolution and high sensitivity to the refractive index and thickness of the sample. The instrument makes use of a high NA oil immersion objective to excite surface plasmons in a wide field, speckle illuminated, analogue of a scanning confocal interferometer. The system extends the work described in the thesis of S. Liu [1] where such a scanning system was presented.

The work that is to be described in the following chapters will be preceded by a brief overview of the use of surface plasmon resonance in the characterization of thin films and surface features. Then the evolution of optical systems that make use of the phenomena, from sensors to high resolution microscopes will be described. A change in methodology will also be shown that allows the exploitation of the more sensitive phase effects associated with surface wave propagation. This chapter is not a comprehensive review of all microscopy techniques utilizing surface plasmon

propagation but rather seeks to put this work in context, notable techniques such as near field surface plasmon microscopy for example will not be discussed as they are not readily compatible with biological microscopes.

1.1 Introduction to surface plasmon resonance

There are many areas of scientific, engineering and medical interest that involve the study, classification and imagery of thin films and chemicals in contact with a surface.

The key problems with sensing and characterizing thin films optically, is the fact that they are thin[2]. This means that the optical path of light passing through the material is very short and the materials effect on the amplitude and phase of the light, small. This is especially so for the case of film thicknesses of less than the optical wavelength. The refractive index is often the only factor that provides sufficient sensitivity to distinguish between materials in sensing applications and provide contrast in microscopy unless the material is highly absorbing where reflection and transmission methods may be used as they are in bulk sensing/microscopy. A simple example of a glass tumbler held underwater demonstrates the inherent difficulty in imaging structures with very similar refractive indices, the problem is not trivial. Thickness measurements are also key to the production of some thin films such as those produced by the Langmuir-Blodgett method[3]. So systems that can detect or image changes in thickness parameters are also of interest.

It is therefore beneficial to find a way of increasing the optical effect of the layers being studied. One way to increase the optical effect of such a thin film is to allow the light to propagate laterally through the film before re-emitting, to allow this to happen the film must form part of a leaky waveguide structure. Conventionally this would mean that the film would be surrounded by cladding of lower refractive index, this again is rather impractical. Looking at the profile of a guided mode of this sort shows that the field decays evanescently into the cladding and is hence affected by the cladding properties. This is the case for whichever layer is used as the waveguide. This fact allows a single sided solution of guiding layer and sample layer followed by air (for example).

To get the best sensitivity in this situation the field extending into the sample layer must consist of as much of the propagating energy as possible. As stated by Yeatman [2] this can be achieved by making the guiding layer thin and of high refractive index. One way to achieve this is to use a thin metal layer as the waveguide.

Using a suitable optical set-up it is possible to excite a surface wave in the electron lattice of a thin metal layer. The perturbation in the electron cloud and associated electromagnetic wave is known as a surface plasmon polariton, surface plasmon or SP as it will be abbreviated to for the duration of this thesis. The wave is tightly confined to the metal surface, decaying evanescently in directions perpendicular to the plane of propagation both into the metal and sample layer. Because the field is confined to the very surface and because boundary conditions across the interface must be met, the evanescent field intensity in the sample layer

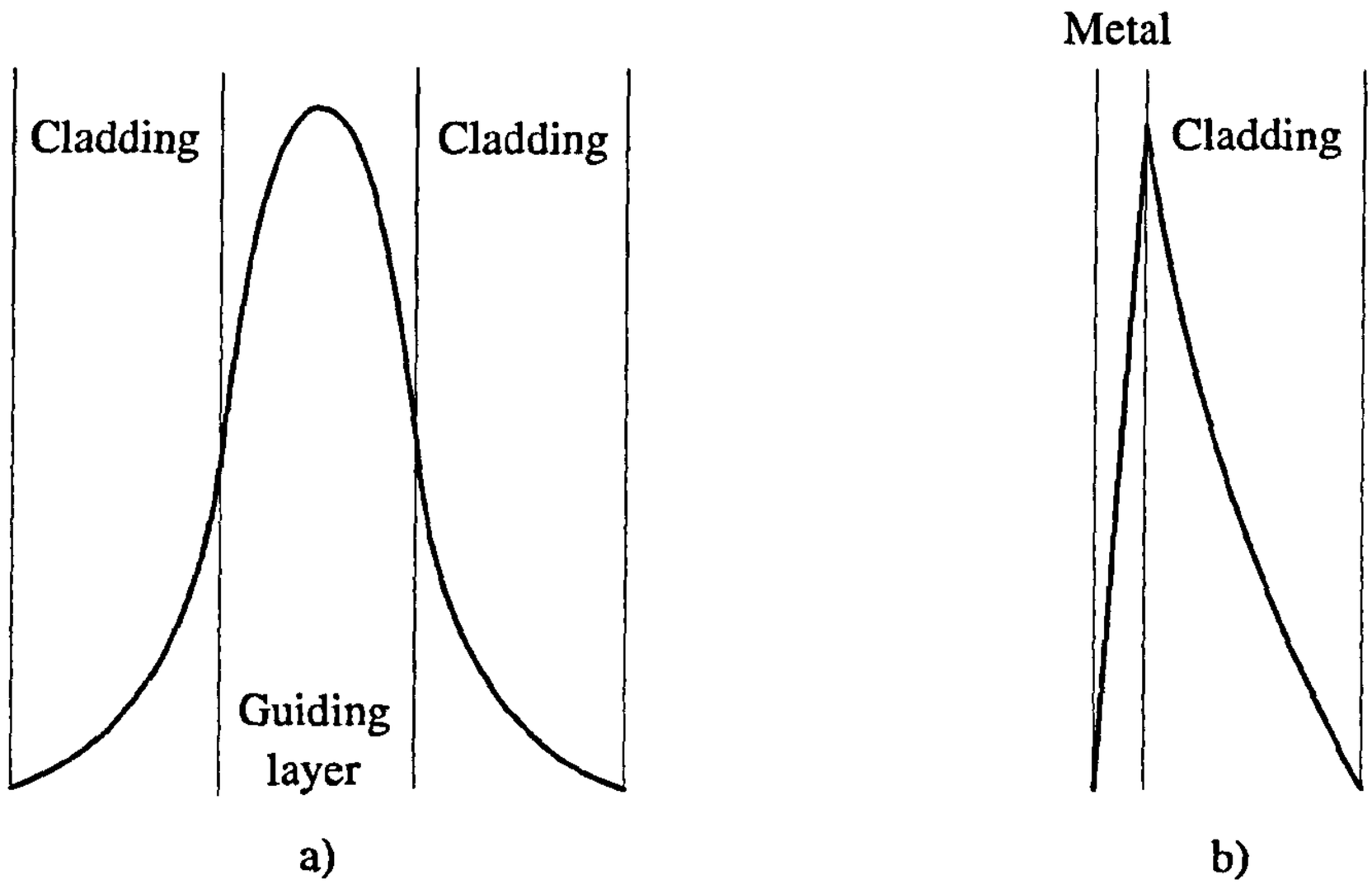

Figure 1.1: *Field intensity for a) waveguide and b)SP structures*

is also high compared to a normal guided mode where the amplitude will begin to drop off before the interface. This can be seen graphically in figure 1.1.

One important fact about SPs is that to excite them requires more momentum than that of light in free space. Coupling mechanisms such as prisms and gratings must be used to increase the k vector of the incident light. Many of the first experiments used a right angled prism in the so called Kretschmann configuration [4]. The basic set up can be seen in figure 1.2. A metal layer is deposited on the hypotenuse of the prism and the incident light beam proceeds through one of the shorter faces, gaining momentum in the prism due to the higher refractive index. On striking the metal surface the light may excite surface plasmons if the incident k-vector matches that of the surface plasmon mode. The generated SP may re-radiate as the process

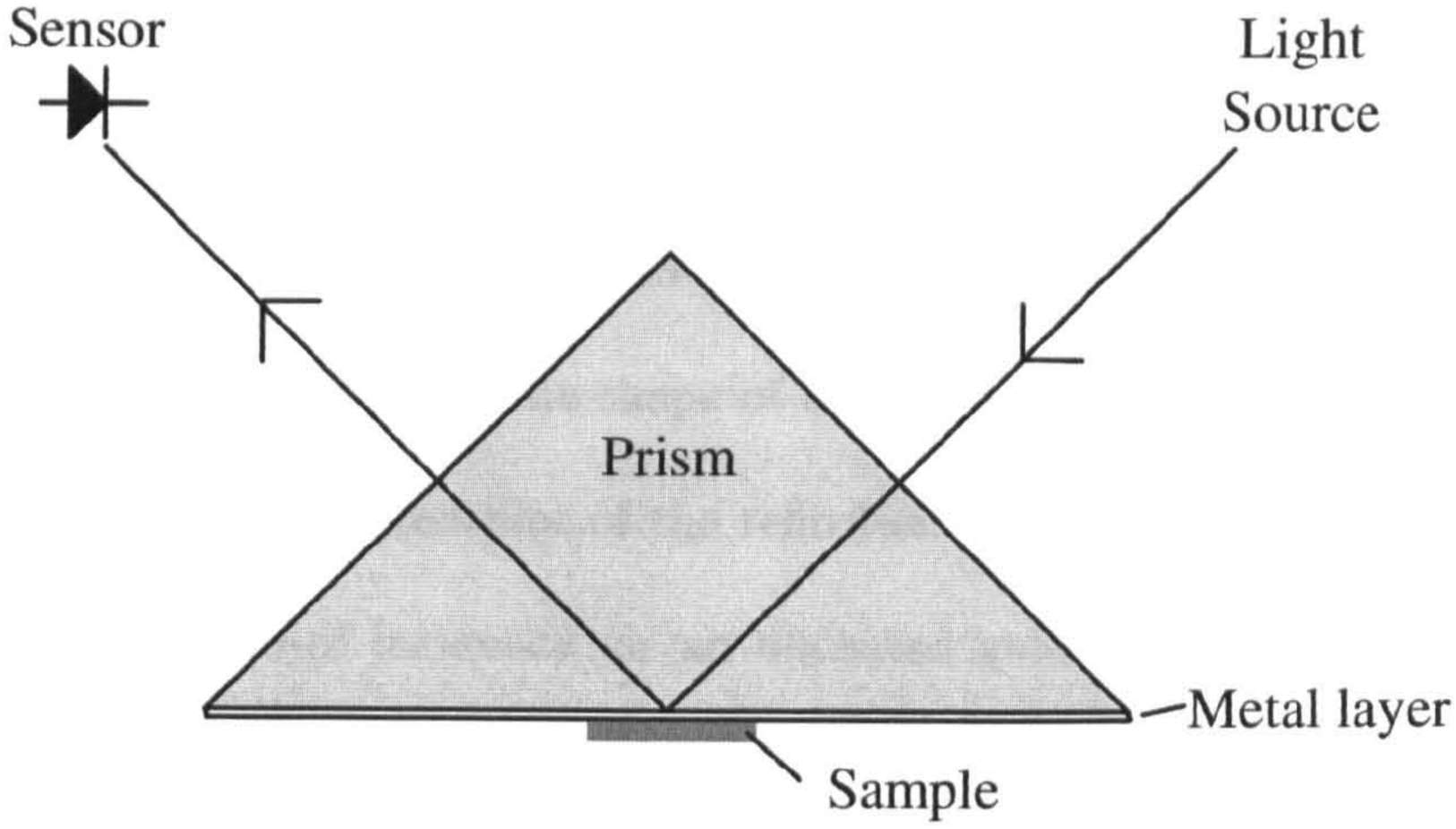

Figure 1.2: *Kretschmann configuration for surface plasmon excitation*

of excitation and emission is reciprocal, however, some of the energy coupled into the SP is lost as heat in the metal lattice ohmically. This is seen as a minima in the reflection coefficient of the gold [5] and has also been measured directly using acoustic methods [6][7]. The light that is not absorbed or that re-radiates, leaves the prism by the other short face and is focused on a sensor such as a photodiode.

It was mentioned that the k vector of the incident light and SP must match in order to excite SPs. This is because the metal layer is a waveguide structure with a finite number of solutions to Maxwell's equations that produce guided waves. Unlike most wave guide structures the form of the solution is quite simple for a uniform metal film. All that is required is a plane wave at the correct angle with its electric field vector perpendicular to the metal surface. This is so the incident field and the electron cloud may "synchronize" creating the surface wave.

The basic principle of using the reflectivity minima in sensing is to operate the system at a fixed angle that lies on the slope of the resonance where the gradient is highest. When a layer is added to the metal surface the angle at which the resonance occurs increases but the shape of the resonance stays roughly the same. Figure 1.3 shows a simulated plot of the reflection coefficient for p-polarized light plotted against angle of incidence for an uncoated gold film of 43.5nm thickness and the same film with a 6nm thick layer of SiN_4 added. The resonance moves considerably and due to that movement the reflected intensity at a fixed angle will also vary sensitively with the surface thickness. In a similar way, the resonance moves with a change in refractive index for a layer of fixed thickness. This basic method of surface plasmon resonance (SPR) sensing has found widespread use in many different fields [8][9][3][10][11]. The actual reflectivity profile observed varies with all parameters of the optical structure. This includes the metal refractive index and thickness as well as the sample properties. The resonance is also highly affected by the illumination wavelength. Longer wavelengths create sharper resonances and so produce higher sensitivity, this is because the SPs propagate further along the metal/sample interface. As was described earlier the increase in optical path length naturally leads to a greater effect on the incident light. Work was carried out by H. de Bruijn et al [12] on choosing wavelength and metal for best sensitivity.

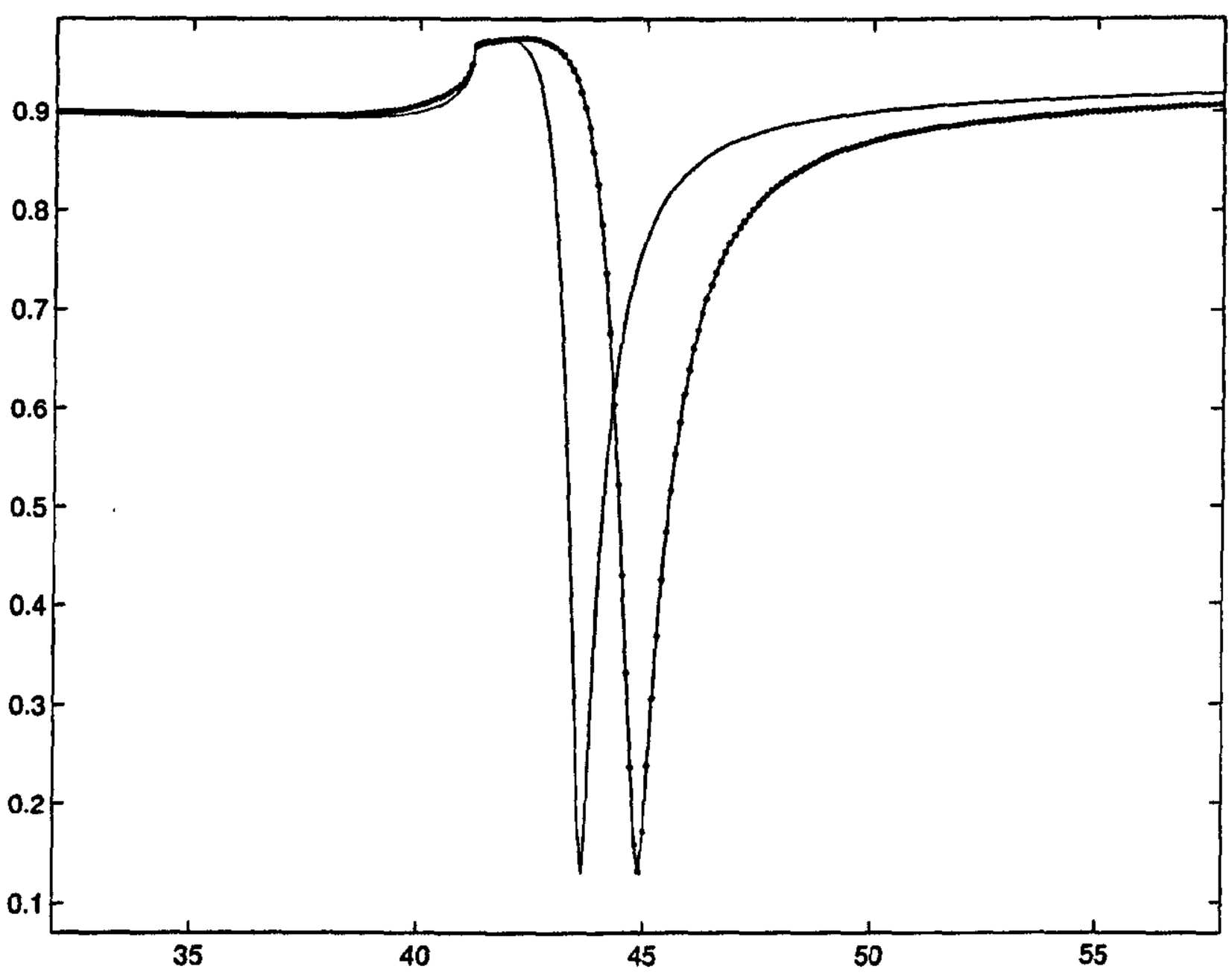

Figure 1.3: *Rp plotted against incident angle for 43.5nm Gold, uncoated (solid) and coated with 6nm of SiN4 (solid-dot)*

1.2 Surface plasmon microscopy

The term surface plasmon microscopy is often used to describe the exploitation of the minima in reflection co-efficient in an imaging configuration. More generally it can be described as any imaging formation process that utilizes the excitation of SPs in order to gain contrast. This may use the amplitude dip, the phase shift or a mixture of the two. The ability to produce images showing the lateral variation in refractive index or thickness on a surface is important in any application where the structure of low contrast samples in contact with a surface are of interest. This can include simple imagery of mechanically produced structures or biological samples such as cells but can also be used to monitor the binding of chemical or biological entities to the metals surface. In some instances the surface may be prepared such as to be functionalized allowing only the analyte of interest to bond, creating a contrast. In these situations real time imaging is also of interest and hence speed of data aquisition and image formation is of key importance. Furthermore imaging can be used to perform high throughput screening processes if the sample is prepared as a matrix of samples to be tested.

An extension of the SPR sensor concept was suggested by Yeatman et al [13] shortly followed by Rothenhäusler et al [14]. Both described and demonstrated systems capable of imaging the lateral variation of film thickness or refractive index.

Yeatman initially imaged 3Å thick dielectric structures on the surface of silver using a scanning technique. A focused laser beam was used to excite SPs in a local

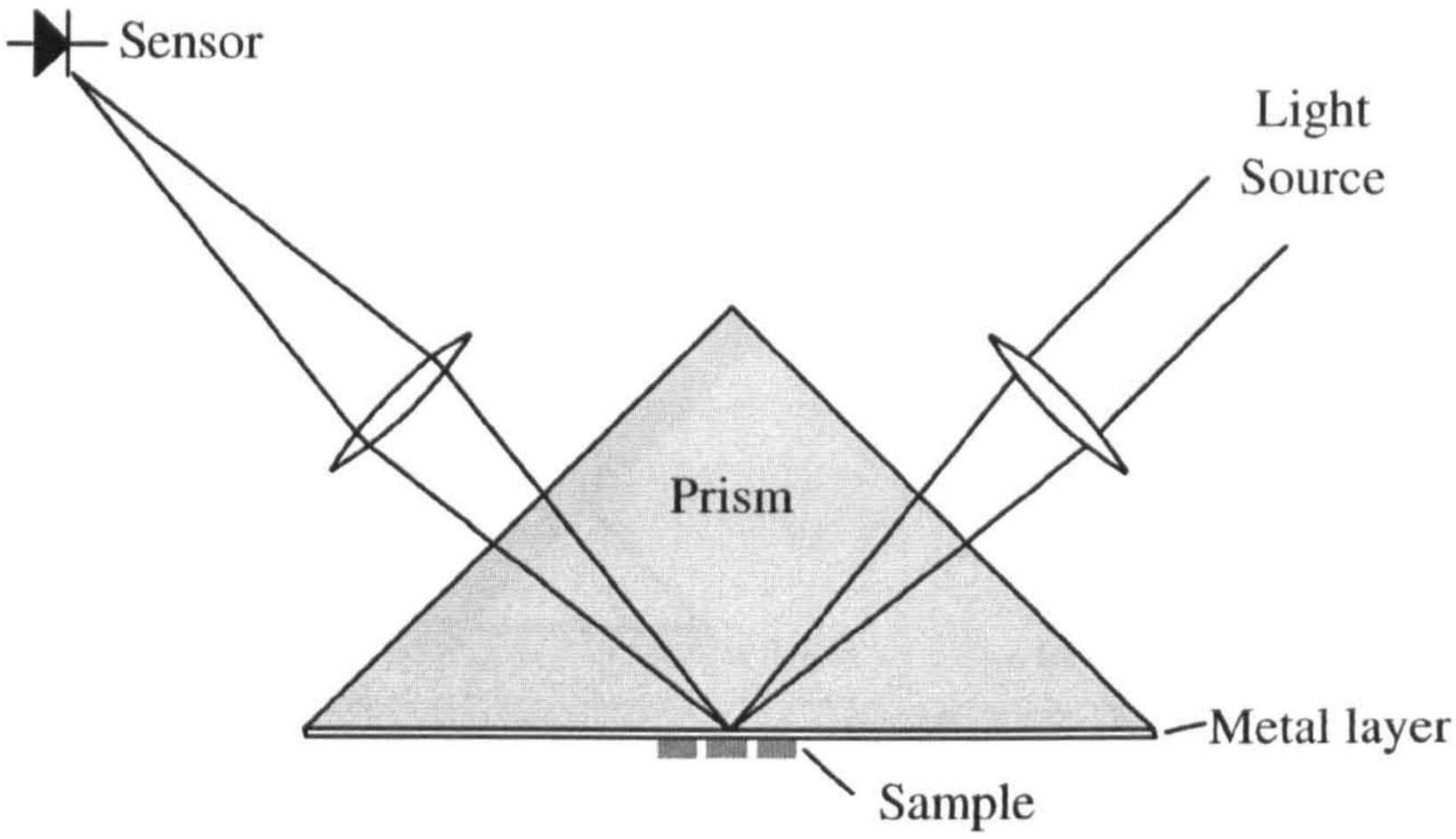

Figure 1.4: *Scanning SP microscope by Yeatman et al [13]*

area through the prism and the reflected energy Fourier back converted to a photo diode. The structure could then be scanned to build up an image. The system may be seen in figure 1.4. They also demonstrated wide field imaging as per the system shown in figure 1.5. The sample was illuminated with a collimated beam before being imaged to a camera, parts of the sample at resonance would appear dark and those off resonance, light. Rothenhäusler presented an identical wide field system as well as a dark field version where the imaging optics face the rear of the metal layer as seen in figure 1.6. Areas that are resonant appear bright as coupled SPs radiate from the inherent roughness of the material [15]. This dark field method allows the imaging of scatterers such as sharp transitions in structure and particles however it does not usually provide much contrast due to thickness or refractive index variations.

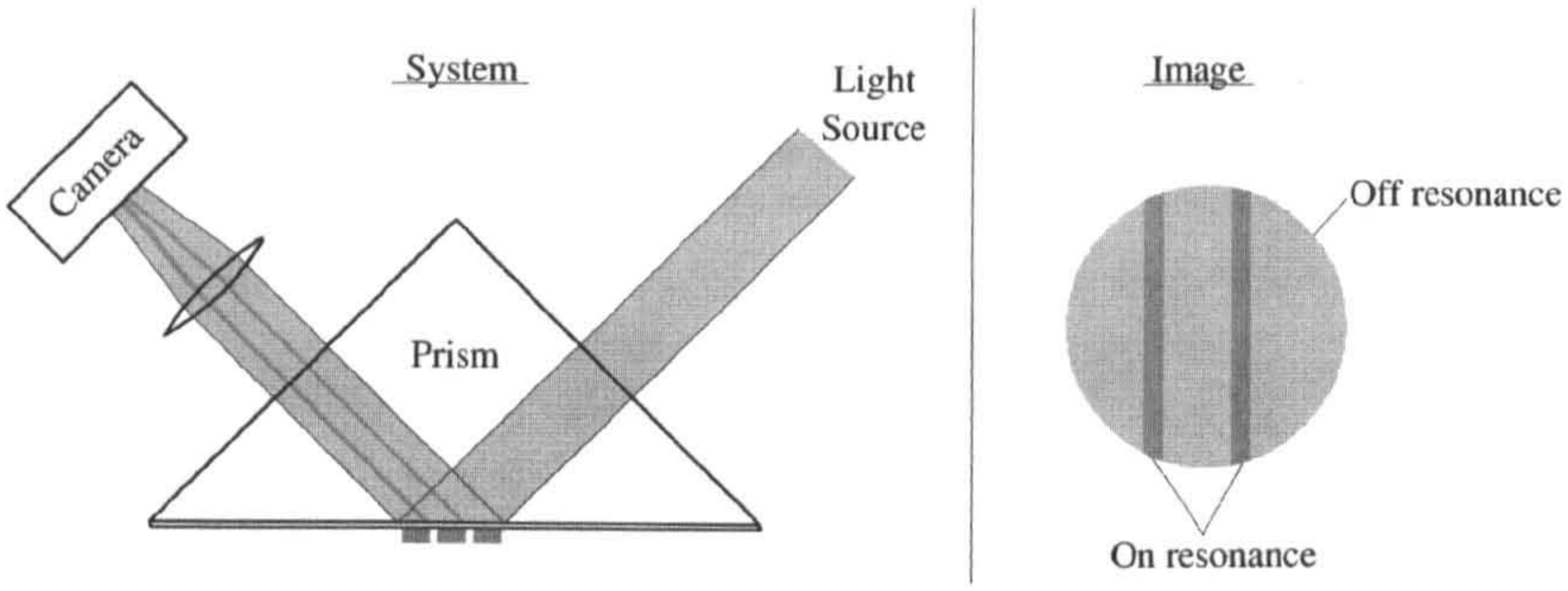

Figure 1.5: *Wide field SP microscope by Yeatman et al [13]*

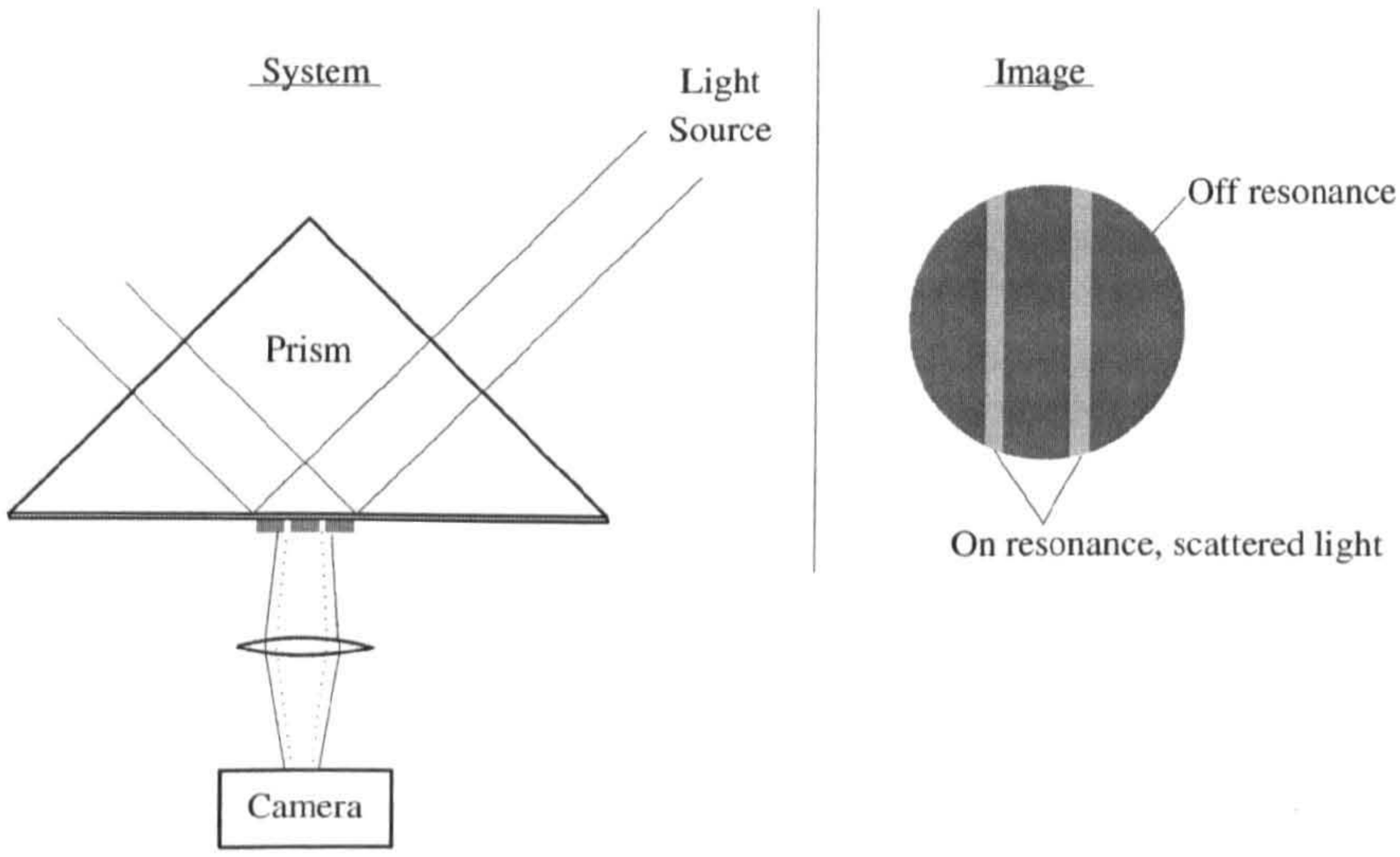

Figure 1.6: *Surface plasmon microscope operated in dark field by Rothenhäusler et al [14]*

Both Yeatman and Rothenhäusler mention the effect of SP propagation length and direction on imaging resolution in their papers. The ability to resolve objects is of key importance in microscopy so this will now be expanded upon.

1.2.1 Resolution and sensitivity in SPM

Some of the initial work that relates to resolution in SP microscopy was done by Z. Schlesinger et al [16] who showed experimentally in the IR wavelength that on meeting the edge of a dielectric structure (thickness variation in this case) that SPs would tend to couple into bulk radiation as well as into non-resonant SP modes. They performed an experiment with a dielectric layer of finite length and showed that some of the bulk modes generated at the first edge would propagate to the second edge almost parallel with the surface and on reaching the second edge, could be coupled back into the metal as SPs with their phase shifted with respect to the bound SPs (due to differing phase velocity). This created an interference signal dependent on the structure length and material. .Although not directly relevant to microscopy the work shows that SPs propagating across boundaries can couple both into the new structure but also into radiation modes. Theory was also developed for single edges using mode analysis [17] and for gap/barrier structures that represent a general case [18]. The theory of a Fabry-perot type interferometer for IR wavelengths much like the experimental set up of [16] was also developed [19].

Rothenhäusler et al then performed Kretschmann configuration based experiments on dielectric gratings and showed that total internal diffraction could occur

[20]. Single angle illumination was used on a grating structure which could provide extra momentum to the SPs producing a number of diffracted orders seen in the reflected beam. A wavelength was chosen such that the the propagation length of the SPs was much less than the width of the grating structures. This meant that most generated plasmons would decay before reaching a boundary and so a usual Fresnel treatment of the structure was adequate. The two parts of the grating could be treated separately and indeed showed separate resonances.

Rothenhäusler et al expanded upon this the following year by looking at the variation of the reflection coefficient of a grating with with incident angle [21]. They used a collimated beam capable of illuminating several lines of a dielectric grating and found that when the structure was larger than the SP propagation length that the resonances of each material were clearly and separately defined i.e. the corresponding responses of $R_p(\theta)$ added linearly. When illuminating finer structures, or when using a longer wavelength the two distinct resonances merged into one at the average angle of the two, weighted by the area covered by each. This suggested that when plasmons are likely to cross the boundaries between materials there is an averaging effect. Other resonances were also seen due to the grating vector adding to the incident wave vector to satisfy the conditions for plasmon excitation. This is another example of the fact that plasmons can propagate from one region into another and in addition shows the importance of propagation length.

Rothenhäusler et al then moved their attention to the specific effects of the propagation over boundaries by performing interference experiments in the visible

spectrum [22][23] similar to those Schlesinger et al had done in the IR band. A metal film had a partial coating of a dielectric applied so as to produce a step transition. The sample was then illuminated in a Kretschmann arrangement at the resonance of the uncoated region such that generated SPs would cross the step. On reaching said step the SPs excited in the uncoated metal with a propagating constant of k_0 couple into radiation modes and an SP mode with modified propagation constant k_1. These SP's are coherent with the incident field but not resonant with it so decay laterally away from the edge. Although the coated region of the sample is not resonant with the incident field, if the coating is sufficiently thin a non-resonant evanescent field will still be produced with propagation constant k_0. This can interfere with the decaying SP as they are coherent. The interference produces a ripple in the imaged field with a period proportional to the wavelength. The various components may be seen in figure 1.7. The experimental setup is essentially identical to the SP microscope systems devised by Yeatman and Rothenhäusler so the effect will be seen when imaging and has a direct influence on the resolution that can be achieved with these microscope configurations. The results of Rothenhäusler showed that as the wavelength and hence the SP propagation length increased, the interference extended further out into the coated region. Further to this is the fact that SPs with shorter propagation lengths have more chance of decaying before reaching the edge.

This theory was more recently improved upon by Berger et al [24] where account was made for the incident field as well as for the non-resonant plasmon field it

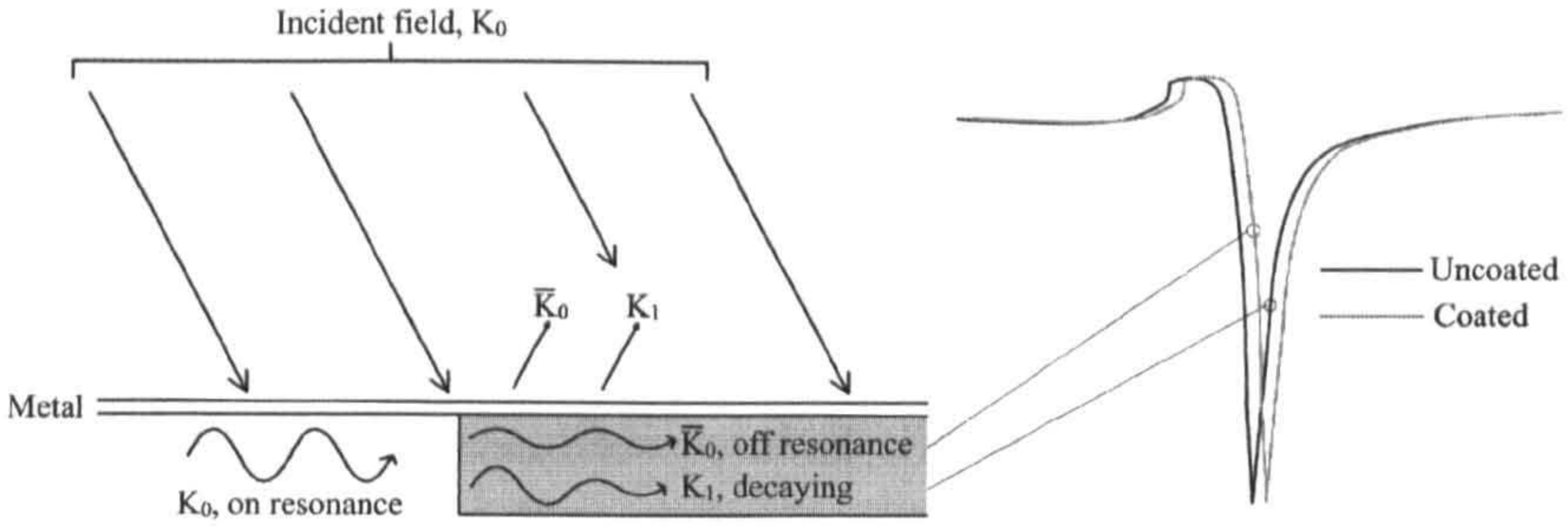

Figure 1.7: *Components of interference when SPs propagate over an index step*

produces.

Although it had been suggested that the propagation direction affects the resolution it was not until experiments on a SP based liquid crystal light valve were performed by Yeatman et al [25] that the point was explicitly made experimentally. In the experiments performed the resolution acquired was highly dependent on the propagation direction of the generated SPs with respect to the LC grating structures.

1.2.2 Methods of resolution improvement

It was at this point that a number of strategies to ensure high resolution while maintaining the sensitivity that makes SP microscopy attractive in the first place were devised. It was known that for high sensitivity a long wavelength was required, but also that on crossing a boundary the SP corresponding to a long wavelength would decay over a large distance and interfere with off resonance SPs from the driving beam, smearing the structure and reducing the resolution. One method was

to keep a suitably long wavelength but orientate the sample such that the SPs did not cross any boundaries. This of course is not possible for structures other than a grating or step. H. Bruijn et al [26] devised a system whereby a number of images could be recorded with the sample rotated with respect to the SP vector. The system may be seen diagrammatically in figure 1.8. A simple L shaped structure is shown, this could be a refractive index or thickness variation. The sample is positioned against a metal layer deposited upon a hemispherical prism. This prism allows rotation of the object with respect to the illumination and imaging optics without change in the incident angles or path lengths. Three example images of the structure are also shown for various orientations. It can be seen that although not all features are sharp in any one image that they are all sharp in at least one of them. The paper also reveals some other problems concerning resolution and prism based microscopes, firstly the physical size of the prism limits the numerical aperture (NA) of the imaging lens due to the working distance required. Secondly the surface is being imaged at an angle so the resolution is reduced further. The result of these two factors is that even with the benefit of rotating the sample the resolution was still not diffraction limited.

A distinct tack was taken by Berger et al [27]. They re-framed the question of how to get high resolution with high sensitivity by assuming that the wavelength used, would be chosen to give best resolution. The question then became, how can the image quality be increased such that contrast is not lost? They introduced a number of techniques, a) They increased the dynamic range of the images by taking

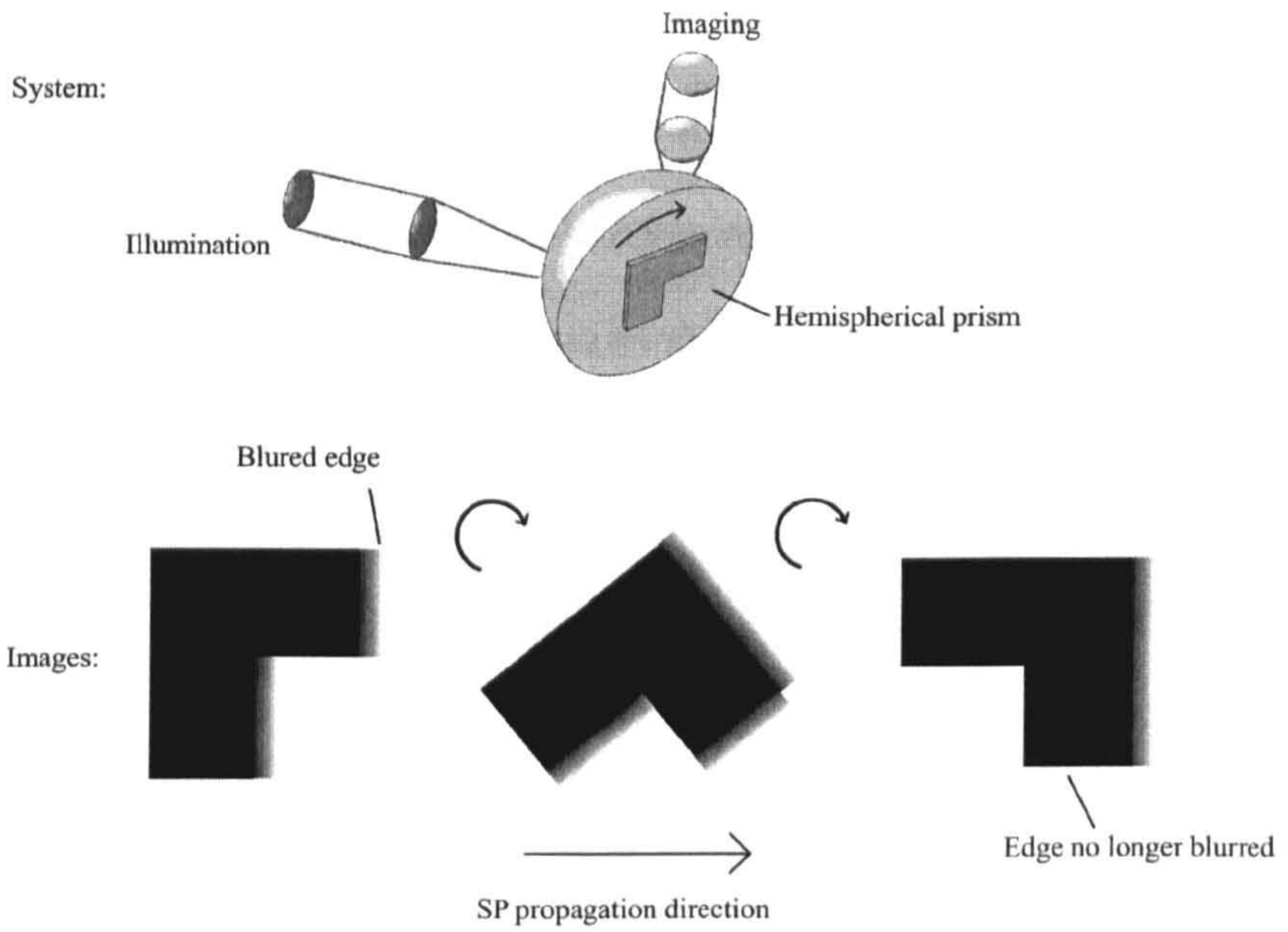

Figure 1.8: *Surface plasmon microscope using rotation of the sample to increase resolution [26]*

several images at a time before adding them. The main reason for this is to allow the application of digital contrast improvement techniques. The increased number of quantization levels means that the quantization is less visible with amplification.

b)An extension of a, by integrating over several images they also reduced noise due to low light levels. c) They removed spurious interference terms and lateral inhomogeneities in the incoming laser beam by taking images with both s and p polarization. The p-polarized image contains the lateral variation due to SPR and spurious interference terms due to imaging optics and source. The s-polarized image contains only the spurious terms and so after a suitable linear transform the s and p-polarized images could be processed leaving an improved image. The final resolution obtained was found to be around $2\mu m$, this it was suggested was limited by the lateral inhomogeneities of laser source and the objective.

To summarize the two methods of improvement it could be said that Bruijn side-stepped the problem of resolution with long wavelengths and that Berger made the best of short wavelengths. In both cases the fundamental problem of prism based imaging with coherent light was present. Low NA objectives are required unless micro prisms were used and even in that case the angled nature of the substrate can lead to problems with depth of field [26].

Yeatman has summarized much of the resolution and sensitivity issues involved with SPM and developed models to predict each and the relationships between them [2].

1.2.3 Objective based excitation

It has already been stated that the k-vector of the incident light used to excite SPs must be greater than that of free space. The prism based systems described up to now are not the only way to achieve this condition. Other than grating based coupling methods that do not lend themselves to imaging the key things required for the SP excitation are a medium of high refractive index against the metal and the correct incident angle. Oil immersion objective lenses use a drop of oil between the front optic of the lens and the sample. These oils are typically matched to the cover slips used in the microscope systems they are designed for and so are of adequate refractive index. The incident angle is limited by the numerical aperture which is directly proportional to the maximum angle produced on the sample. Objectives up to around 1.65 NA are available commercially and even allow excitation for aqueous samples.

Kano et al [28] showed that SPs could be excited on silver films with an objective lens of 1.3NA in the Kretschmann-Raither configuration as seen in figure 1.9. They produced a mathematical model that showed that when the exit pupil or back focal plane (BFP) of the lens is illuminated with a plane wave that a laterally localized SP was generated. The localization is caused by the interference of the SPs on the sample surface. The term localization is a confusing one as it suggests that the SPs are some how corralled into a small area and it has been used in this sense when describing SPs on metallic particles. This is not the case for the focused beam, the

SPs propagate through the optical axis adding up in phase to create a region of high intensity and then propagate onwards. The localization is just a focus, there is concentration but no confinement. Kano then conducted experiments to prove the theory by placing a micro bead on the surface of the silver to act as a scatterer. This particle was smaller than the SP propagation length and only scattered when on the optical axis, in other words coincident with the SP focal spot. The scattering could be imaged with a lower NA air objective on the rear of the sample. It was not suggested if increasing the beam intensity might make the scatterer visible when away from the focal spot. Assuming there is enough incident intensity, plasmons that had already passed through the focal spot might still scatter off the particle.

They also showed in simulation and in practice that the exact shape of the localized SP illumination could be changed according to the input polarization. As will be described in later sections the BFP of an objective is a direct map of incident angle at the sample, from the optical axis where the incident light is normal to the sample the angle increases with radial position to a maximum value defined by the NA. SP resonance occurs over a narrow angular range, reducing the amount of light reflected by the sample, and so a dark ring is formed at the radial position corresponding to these angles when the BFP is imaged. Polarization is another factor that effects SP excitation, p-polarized light is required. In order to produce totally p-polarized light at the sample the input polarization must be radial. This is possible with special set ups [29]. When the input polarization is linear there are regions of pure p-polarization on the axis of the input polarization and regions of

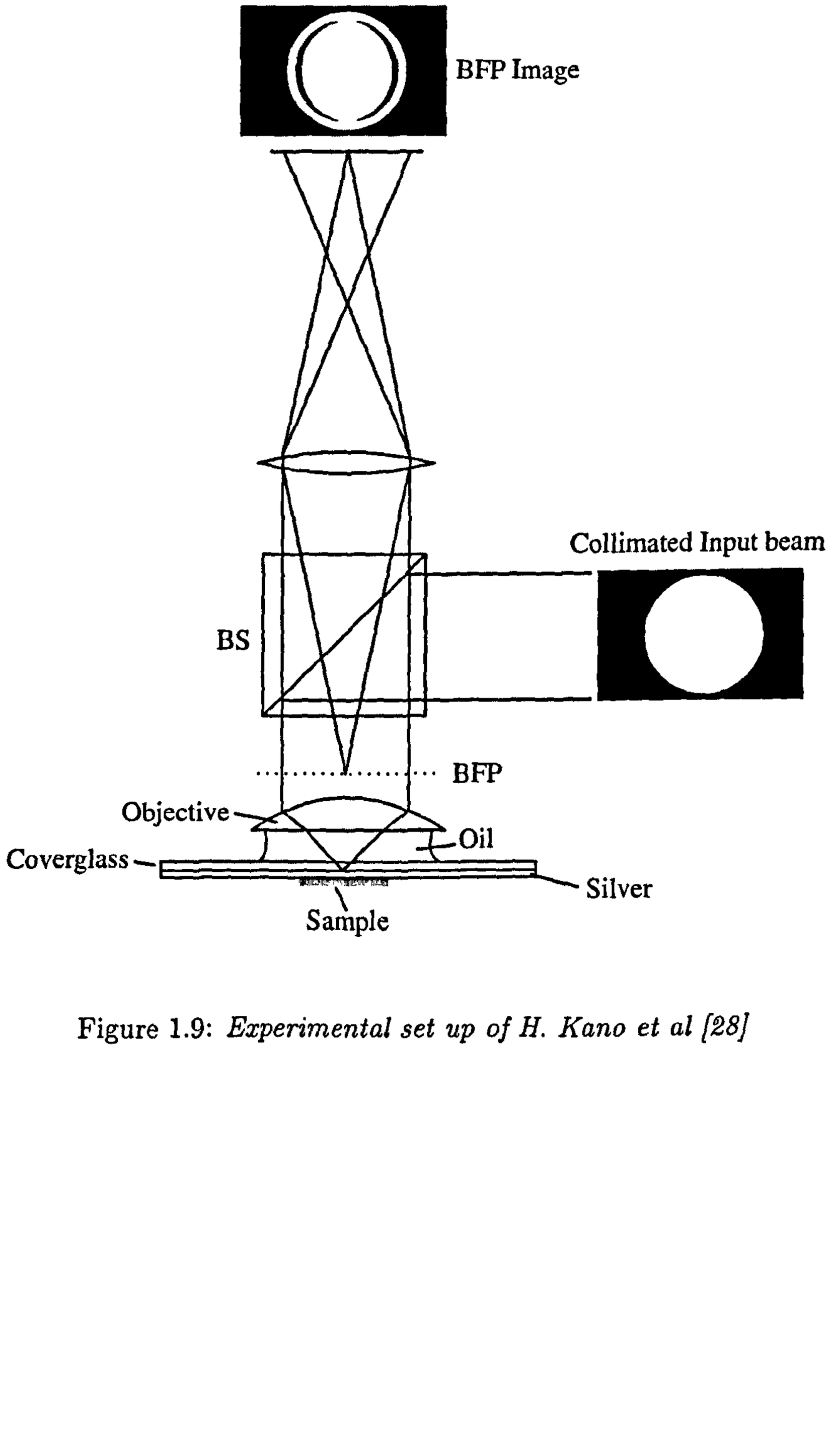

Figure 1.9: *Experimental set up of H. Kano et al [28]*

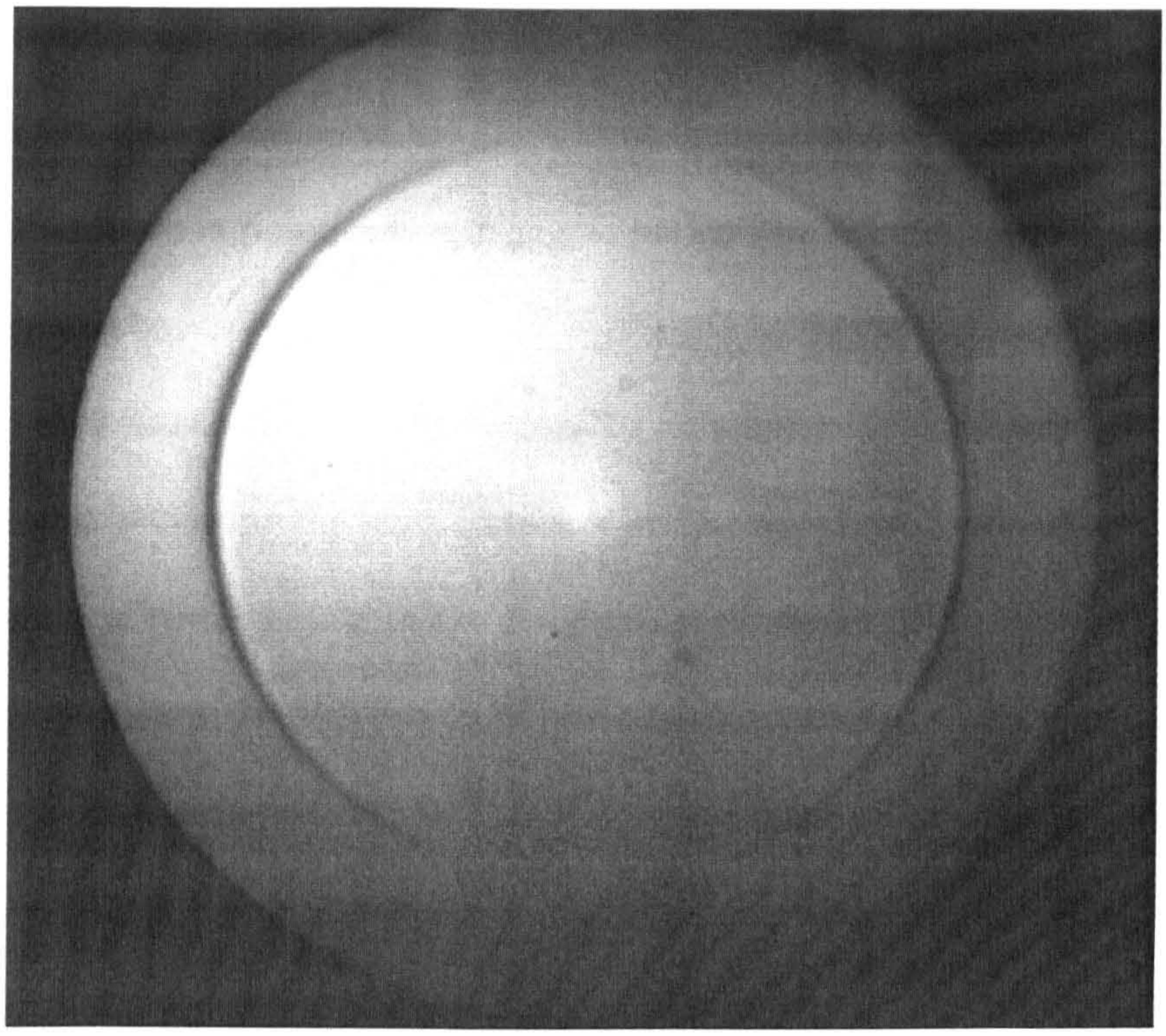

Figure 1.10: *Example BFP distribution showing crescent shaped resonances due to linear input polarization*

pure s-polarization on the axis perpendicular to this. In between there is a mixture of the two. Because of this, the resonance does not appear as a ring but rather as a pair of crescents. An example BFP image may be seen in figure 1.10, this will be described in detail later. The asymmetry of excitation was shown to affect the field intensity at the sample creating side lobes on the distribution. A final note was that the sample itself could effect the localization, presumably by affecting some focusing plasmons differently as might occur on the edge of a diffractive step.

The images taken of micro scatterers showed one potential microscopy applica-

tion however relying on scattering and surface roughness is not suitable for many samples. The concentration of the SP field at focus is an interesting effect but how this might be used in practice as a means to higher resolution in the bright field was not touched upon.

Kano et al extended their observations by measuring the thickness of Langmuir-Blodgett films [30] using the same system of excitation. This was done by measuring the diameter of the crescents in the BFP compared to an uncoated sample. From these measurements the film thickness could be deduced and layers down to 3.4nm were successfully detected. They also tried circularly polarized light which gives a symmetrical BFP distribution and made measurement easier. They failed to comment on the possible effect on the SP localization. It is an important point to note that the dynamic range of this system is greater than that of prism based SPR systems where with thicker layers the resonance may move off the illumination angle altogether.

Once the sensitivity of the measurement had been proven it was a simple task to extend the technique to scanning microscopy as was indeed done by Kano et al [31]. The coverslip with metal coating and sample were placed on a piezoelectric scanning stage and images of the back focal plane taken at each point. These were then processed on a PC to produce grey levels dependent upon the layer thickness before being assembled into an image.

It was stated earlier that the localization of the surface plasmons is in fact a concentration. In the case of detecting scattered light in the dark field this is of

obvious benefit as light will be more strongly scattered at this 2-dimensional focus. In the case of an imaging system based on the measurement of the angular position of resonances seen in the back focal plane the usefulness is less clear. The radius of the resonance seen is dependent on the properties of the material on which the SPs were excited. What happens to the SPs after that does not affect the position of the resonance so the fact that the SPs focus does not matter. The resolution should be equal to the spot size of the focused beam rather than the focal spot of the SPs. They were able to image micro particles down to 1.5μm but it was found that artifacts in the BFP images due to coherent noise made it impossible to improve on this. A mention was made that when using linear polarization the resolution was affected in one direction due to the asymmetrical probe. It is a little unclear but they seem to refer to the asymmetrical intensity distribution. The excitation distribution is also asymmetrical as there will be little or no excitation in the direction of s-polarization and in the area of the focal spot corresponding to this. The shape of the spot that can excite SPs is hence an oval and will give differing resolution in each direction.

In an effort to improve on the resolution obtained by Kano et al, Tanaka et al produced a scanning system using multiple photo detectors instead of a camera [32]. The basic system may be seen in figure 1.11, a collimated light source illuminates the BFP of the objective which focuses the beam to a spot creating localized SPs as before. The exit pupil is imaged to a plane containing 4 pinholes each is placed at the radial position corresponding to the resonant dip for an uncoated sample. Two lie on the line of the x-axis and two on the y-axis. Behind each pinhole is a

photo diode which is in turn connected to a PC. The sample is scanned by means of a piezo positioning stage controlled by the same PC. As the sample is moved with respect to the focused beam the radius of the resonant dip changes as it did in the case of Kano's microscope. In this case however the system is analogous to the simple prism based SPR sensors as the photo diodes interrogate the BFP over only a small range of angles. The contrast comes from the movement of the resonance with respect to the fixed detection angle.

It is obvious that to perform this kind of imaging four sensors are not required, but in order to answer questions of resolution with respect to propagation direction that were left unanswered by Kano these were included. Images of grating structures were recorded using circular input polarization with each sensor in turn. The images produced using the sensors that are perpendicular to the grating vector give identical results and show a resolution of around 1.5μm. The images created by the sensors that are parallel to the grating vector were also identical to each other but of much lower contrast and resolution.

The main benefit of this microscope is the reduction in coherent noise. This it was claimed is due to averaging of speckle over the area of the pin holes and also due to the scanning nature of the system. Despite this the resolution obtained was no higher than that of Kano et al even in the case of SP propagation along the grating. This could in part be due the the way the resolution was defined as Kano et al did not produce a line scan of the step response.

The reasons for the loss of resolution due to SP propagation perpendicular to

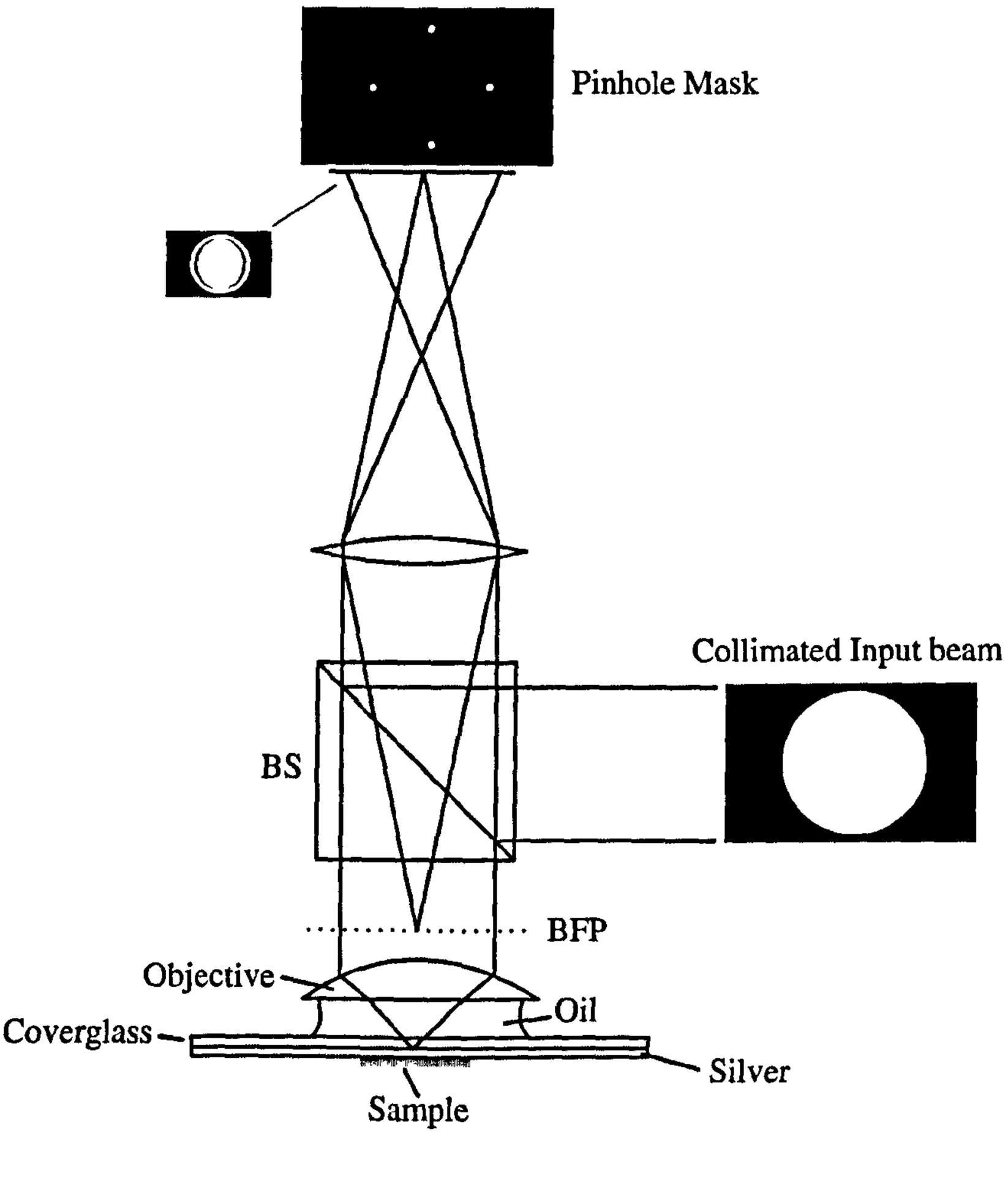

Figure 1.11: *Experimental set up of T. Tanaka et al [32]*

the grating should be explained further. Tanaka et al used circularly polarized light to illuminate the sample and the back focal plane distribution was shown to be symmetrical and so it is reasonable to assume that the field distribution seen at the sample will be too. Even if this was not proven explicitly by Kano et al, it was shown for the similar case of radial polarization. The main difference being the efficiency of producing a symmetrical polarization field.

It was supposed that the loss of resolution was due to the reasons outlined by Berger et al [24] already described. In that instance, SPs propagating across a boundary were coupled into a decaying mode in the covered region and together with non-resonant modes, would interfere with the incident beam. The experiments of Berger et al differ in two important ways to that of Tanaka's. Firstly the grating structure used was capable of supporting SPs in both coated and uncoated regions, and secondly there was incident light on both regions while imaging took place. In the work of Tanaka et al, the step response was created using a step made from a cover slip too thick to allow SP generation and the grating used for imaging was made from a 400nm layer of photo resist which again suppresses SP excitation totally. This negates the possibility of a decaying SP in the coated regions. The nature of the focused illumination means that even if SPs did propagate past the refractive step there would be no incident field for them to interfere with. Finally the nature of the observed loss of contrast is different. In the case of Berger's results destructive interference was seen in regions that were off resonance (appear bright) at the edge of the resonant areas so the dark resonant areas appear to be smudged into the light

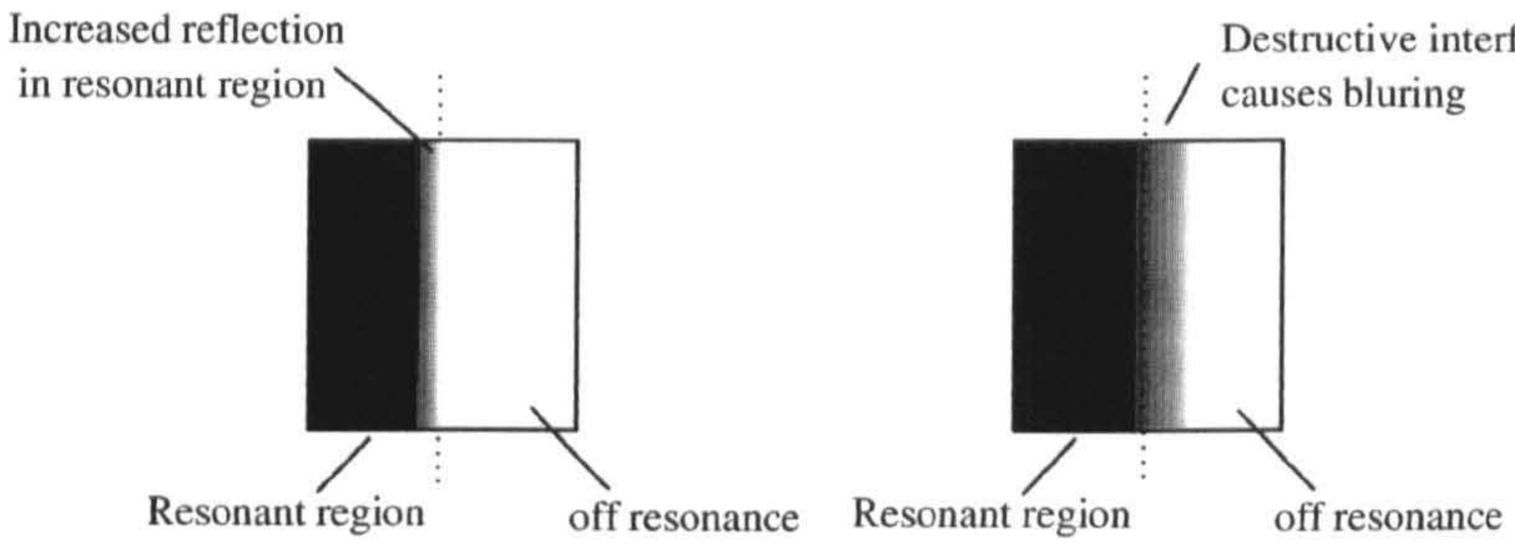

Figure 1.12: *The difference in resolution loss between the work of Berger et al and Tanaka et al. In the case of Berger, plasmons re-radiate in the none resonant region causing destructive interference whereas in Tanaka's work there is an increase in the reflection co-efficient in the resonant region close to the boundary*

none resonant areas. In Tanaka's results the intensity of the reflected light in the resonant regions close to non-resonant regions was increased. The difference may be seen in figure 1.12. There is a small mention of possible reflections at the edge that cause a similar effect however this was not predicted in Berger's model and was considered outside of the scope of the paper. It is assumed that Tanaka et al did not refer to this phenomenon.

Nevertheless, a loss in contrast was observed that was dependent upon SP propagation direction. There seems to be a simple explanation; the fact that the structure consisted of materials that either supported SPs or did not means that the contrast should be extreme, the photo detectors will either measure a low value (for the bare gold) or a high value for the coated gold. The loss of contrast could simply be said

to come from more light being collected (at that angle) when probing the gold close to the edge than away from it. One simple explanation is that SPs propagating away from the focus toward the edge may scattered by it. It may be thought that this light will not contribute to the signal because it is a scanning system, however, it is only the illumination that should be thought of as focused. Because the detection system interrogates the Fourier plane of the objective it can contain components that are from regions out of the optical focus. For this reason scattered light may increase the light levels seen at the photo detectors. As the proximity of the probe to the edge increases the scattering would also increase because the SP that is scattered will have decayed less. This corresponds to the observations of Tanaka et al.

It can be concluded that although the localization effect is one of interest and obvious direct use in imaging particles in the dark field it has not been harnessed by either of these systems as they both rely on the resonant crescent on the back focal plane. The position of which is not affected by the localization but whose depth may be affected by scattering from SPs away from the focus. This leads to the conclusion that the main advantages of these systems is that they use high NA objectives perpendicular to the sample. Of the two methods that of Kano would seem to be preferred as it will be unaffected by light scattered off axis and has higher dynamic range. However improvement would be needed in order to reduce the coherent noise in the BFP and circular polarization might be preferred for symmetrical resolution.

1.2.4 Phase based surface plasmon sensing and imaging

The use of the resonance in the amplitude reflection coefficient is the most widely used method of getting sensitivity/contrast from SP propagation, however, the amplitude tells only half of the story. Figure 1.13 shows the phase of the reflection coefficient R_p for the same sample structures as figure 1.3. A rapid step in the phase can be seen with the point of maximum gradient centered on the resonant amplitude dip. This phase profile, just as the amplitude coefficient did, moves when the system parameters are changed. The difference is that the gradient of the phase jump is much steeper than that of the resonance dip. This means that higher sensitivity can be expected.

A number of experimental set ups from the literature will now be described however the exact technical details of the experimental setups will not be elaborated upon as they are not directly relevant to this thesis. Nor is this a comprehensive review of phase techniques in SP sensing/microscopy. Some systems may be described in greater detail in forthcoming chapters where they are of particular relevance.

Nelson et al first demonstrated the use of the phase step in a SP based sensor [33]. A Kretschmann prism setup formed one mirror of a heterodyne interferometer. Modulation was performed with an acousto-optical device and the beating reference and sample signals were detected by separate photo diodes. The phase was then deduced electrically using phase detection circuitry. The authors describe theory predicting the variation in phase shift with the refractive index and present results

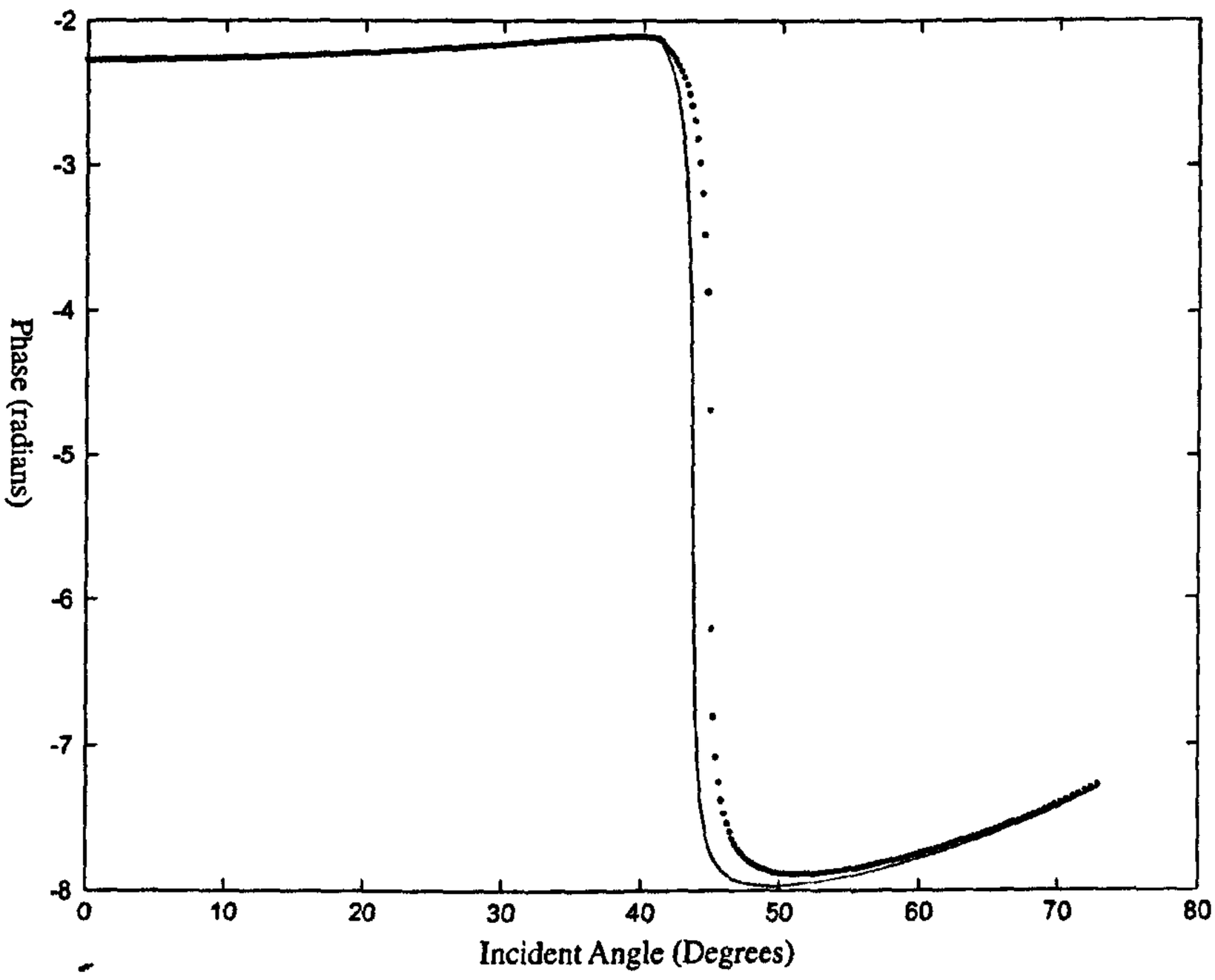

Figure 1.13: *Phase of Rp plotted against incident angle for 43.5nm Gold, uncoated (solid) and coated with 6nm of SiN4 (dotted)*

that support this. They predict the resolution of refractive index measurement to be $5x10^{-7}$ refractive index units with a well designed system. Another important point raised in their paper is the importance of the choice of metal film thickness and also that the device be operated at the resonant angle. This of course is the point of highest sensitivity but also of lowest light levels, raising potential problems with the SNR.

Kabashin et al later developed a much less complicated sensor based on a Mach-Zehnder interferometer [34]. The experimental setup may be seen in figure 1.14 The illuminating beam is split into two by a beam splitter whereupon the beams reflect on the sample mounted in a Kretschmann prism setup and reference mirror alike. The reflected beams are then combined and shone onto a CCD camera and wide-aperture photo-diode. The phase shift induced by the sample was measured by monitoring the movement of the fringes on the CCD camera. The amplitude response was also recorded using the photo-diode. The samples used were gaseous, passed over the metal film within a flow cell. They were able to detect changes in refractive index down to 10^{-6} which was the limit of the gas preparation methods. Even though they were not able to test the absolute limit of their system they were able to establish that it gave approximately thirty times more sensitivity to refractive index change than provided by conventional SPR measurements.

Grigorenko et al elaborated on the nature of the phase step in their paper describing the first implementation of a surface plasmon phase microscope [35]. They showed that the form of the phase jump seen at resonance was highly dependent

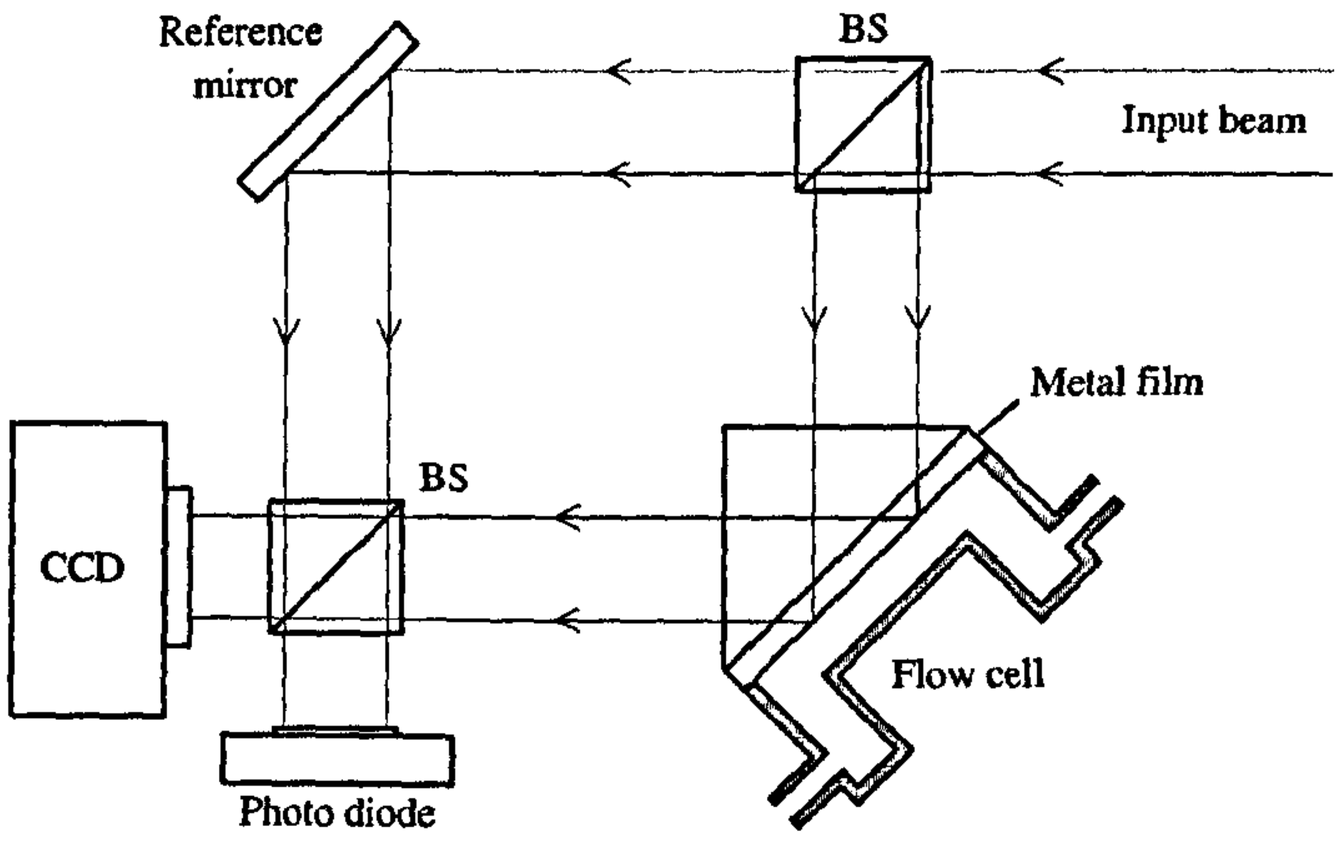

Figure 1.14: *Experimental set up of A. Kabashin et al [34]*

upon the metal layer thickness because the jump is due to a zero in the system parameters. Effectively as the phase of the system is undefined with zero amplitude the phase can undergo an abrupt shift as the system parameters pass through or close to the zero. The depth of the plasmon resonance is highly dependent upon the metal thickness and indeed any dielectric layer applied to it and so affects the shape of the phase jump. When the metal layer is too thin, the phase shift reduces monotonically and when too thick, it increases monotonically. When it is chosen for the deepest minima, however, it displays the Heaviside step type response. The system they describe is another example of a Mach-Zehnder interferometer. A p-polarized collimated laser beam was split by a beam splitter forming a sample and reference beam. The sample beam was used to excite plasmons in a Kretschmann prism con-

figuration that again formed one mirror of the interferometer. The reference beam was reflected by a reference mirror before being recombined with the sample beam by a second beam splitter. The combined beam then passed through a set of imaging optics before striking a CCD camera. The imaging optics were setup to make the CCD camera and sample conjugate. The system could be operated in two regimes; fringe mode and Zernike phase contrast mode. In the former mode, phase shifts on the sample could be seen as distortions of the interference pattern and in the latter mode additional polarizers and a phase retarder were added to allow visualization of the phase shifts. The system could also be used for conventional measurement of amplitude by blocking the reference arm. Using this system, ultra thin droplets of fatty acids were imaged when in the conventional amplitude mode nothing could be seen. The layers were estimated to be 1Å thick. They were also able to image a 5Å layer of Si corresponding to three monoatomic layers. Further to this they were able to monitor in real time the reaction of gold with self-assembling thiol molecules dissolved in a solvent. The excellent sensitivity of the method had already been proven but with the addition of imaging in 2D, monitoring surface reactions with ultrathin/transparent layers could now be performed. An important point to note however is that this system operates at a single angle at the resonance, the price paid for such high sensitivity is a loss of dynamic range.

In the same year Kabashin et al published a result from a sensor based system that combined phase contrast with polarization contrast [36]. A collimated beam with rotatable linear polarization was focused onto the sample in a Kretschmann

configuration allowing variable components of s and p-polarization and also containing a range of incident angles. As only the p-polarized component of light reflected at the plasmon resonance excites plasmons two effects on the polarization of the light are seen after the prism. Firstly the p-component of light is attenuated and secondly a shift in phase is seen between the s and p components. The former effect causes a rotation of the polarization of the light that has excited plasmons whereas the latter causes the polarization to become elliptical. The relative contributions to the polarization change from these two effects are dependent upon the sample. The important point is that by illuminating with a mixture of both s and p-polarizations the rotation and ellipticity may be used to gain further contrast. A Babinet-Soleil phase compensator was added to the output arm of the system, this consists of two plates that may be slid across each other changing the relative phases of s and p components. This allowed the ellipticity of the reflected beam to be removed by putting s and p polarizations in phase. The resultant should be a linearly polarized component rotated with respect to the original input polarization. By adding a polarizer this portion of the beam may be blocked and as it corresponds only to light that has excited plasmons resonantly it increased the depth and hence slope of the amplitude reflection dip. This was observed with a CCD camera which recorded the amplitude over the range of incident angles in the illumination. The resonant dip was seen to be enhanced by the addition of the polarization and phase optics by an order of magnitude. Unlike the previous methods this one is not interferometric and does not show the extreme increase in sensitivity however it does show another

way to enhance the sensitivity of SPR based systems by taking advantage of phase shifts between s and p-polarizations.

The phase based methods that have been described up to now all make use of the Kretschmann configuration but as it has already been established this is not the best optical set up for imaging. Now an advanced technique will be described that maintains the benefits of phase shift based contrast and improves the optical characteristics.

1.2.5 Advanced phase imaging

The phase shift seen at resonance is a powerful marker for the plasmon resonance and can give incredibly high sensitivities. It does however have a disadvantage, the severe lack of dynamic range, this is also a problem for SPR based sensors and microscopes but even more so for phase systems especially when the metal film thickness is optimized. A second disadvantage that is seen in the phase based microscopes described in the literature and indeed in most SPM systems generally is the poor optical characteristics furnished by the Kretschmann configuration for imaging.

The subject of spatial resolution which has not been touched upon in the literature with respect to phase imaging must also be a consideration when producing high resolution images.

Somekh et al [37] published work describing a scanning SP microscope that combines the advantages of a high NA oil immersion imaging system and phase contrast.

The system also improves upon the resolution by making use of the localization seen in objective based SPMs. The system will be described in detail in chapter 2 so only a brief description will be presented here. Basically, the high NA objective, coverslip and sample, formed one arm of a Michelson interferometer. The other was formed by a mirror. Each arm was modulated electro-acoustically to produce a beat frequency in the light detected on a photo diode. The electro-acoustic devices used to shift the frequency were locked together and the driving signals mixed to provide a coherent reference for a lock-in amplifier used to detect the amplitude of the detected signal. The output of the system was termed V and the response when the objective was defocused was known as the V(z). The observed response was analogous to that described by A. Atalar et al [38] in an acoustic microscope system based on Rayleigh waves. An oscillation was observed in the output as the lens was brought closer to the sample and into negative defocus. This was found to be due to the interference of the axial components of the incident waves with the waves resulting from surface wave generation that had incured a different phase shift due to defocus. The same was seen by Somekh et al. The exact period of the oscillations depends on the sample properties. Hence at a fixed defocus, parts of the sample that differ in thickness or in refractive index give different values of V. This is the mechanism of contrast of the microscope. The image was then built up by scanning the object with a piezo xy stage.

Several points must now be made about the imaging mechanism of the microscope. Firstly the fact that the objective lens is operated in defocus may seem

alarming, however, much like the other phase based SP microscopes this system extracts information from light that results from SPs that have propagated across the sample. In the case of a defocused objective the plasmons will be excited in a ring and focus to a spot as described earlier. The focal spot represents a common path for all the excited plasmons and so the response is weighted toward this region. This means that although the lens itself is not at focus the optical system as a whole is still at a form of focus. The "rays" may simply be thought of as being bent to be parallel to the sample when they meet it before being unbent when they leak. In a way the system represents another way of gaining more contrast from a thin sample, not only does the light propagate laterally through the thin sample but is does so many times simultaneously, multiplying the effective optical path length.

The previously reported causes of lost resolution are largely irrelevant as they were due to SPs being generated in one region resonantly before emitting in another to interfere with the incident beam. This caused a decrease in the light reflected in that region and so blurred the edges. For this system the phase dictates the system response. Besides, as the illumination covers a large angular range the entire sample will be at resonance. Finally as the means of contrast is not resonant in itself it has a higher dynamic range than previously seen phase based microscopes although with a sensitivity more akin to amplitude based systems. This microscope represents a very powerful tool for the imaging of thin films and biological specimens. Super high NA objectives also make it possible to image sample in aqueous solutions. The only disadvantage of the system is the relative complexity and the scanning mode

of operation which is too slow for live monitoring of reactions etc.

The subject of this thesis is the expansion of this microscope into wide field. This was done by building a wide field confocal microscope with speckle illumination. A system of this sort was described by Somekh et al and was used for conventional amplitude and phase microscopy [37]. The system made use of a spinning diffuser disk to produce rotating speckle illumination which was in turn imaged to the BFPs of two matched objectives in a Linnik interferometer setup. One objective was focused on the sample, while the other was focused on a mirror which could be moved by a piezo actuator. A set of four images were taken and a phase stepping algorithm applied to extract phase and amplitude information. The speckle pattern was not seen in the images due to temporal averaging of the CCD camera. However, the speckle formed an important part of the system. Firstly it created a set of random angles in the back focal plane to produce wide field illumination and secondly it gave a confocal response to the microscope. Interference would only occur when the speckle correlated in 2D space and more importantly in defocus. This leads to the use for wide field SPM as this response is much the same as for the heterodyne system described previously. It may be considered that each point on the image of the sample in this wide field system is a miniature version of the scanning system, localized from adjacent points by the requirement for speckle correlation. As only four images are captured for each phase/amplitude image it leads to fast image acquisition and potentially identical contrast and resolution making the microscope system a much more appealing prospect to researchers in thin films and biology.

1.3 Layout of thesis

The basic background and context of the work to be described in this thesis have been covered in this chapter. Chapter 2 provides the reader with the necessary background to understand the operation and design of the system described and also covers the work this thesis is founded on in more detail. Chapter 3 covers the design of the optical system in detail and the choices taken in instrumentation. Chapter 4 shows images of the BFP for various samples showing another mode of operation of the microscope as a sensor. Chapter 5 presents intermediate results taken with the instrument in a new SP microscopy mode. Chapter 6 presents the results of full interferometric wide field SP imaging. Chapter 7 draws conclusions about the work presented and suggests potential future avenues of investigation.

Chapter 2

Background

2.1 Introduction

In this chapter background information required for the design of the proposed microscope will be described. Moreover, some of the literature mentioned in chapter 1 will be described in further detail as this work builds on what has been done before.

2.2 The back focal plane

The relationship between the back focal plane and the front focal plane or sample plane of an objective is very important in the development of any microscope. In the case of an SP based microscope it is even more important as the back focal plane provides a means to control incident angles as well as a way of understanding the resonances and imaging mechanisms. This section will explain the relationship

in more depth and also show the importance of considering the polarization of the incident light.

The Fourier transform may be performed on data to produce a plot of its frequency spectra. The frequency may be temporal, spatial or simply a mathematical abstraction. Each frequency component is calculated as an integral of all the data with constants determined by the specific frequency in question. This is of course a rather obvious point but there are physical processes that rely on the same principle. For example, a distribution of light can be thought of as a collection of point sources of varying amplitude and phase, emanating spherical waves as per Huygens principle. The light falling on one point of a distant plane is a summation of a portion of light emitted from all of these point sources. The exact integral changes for each point on the distant plane as the relative distances change. This is Fraunhofer diffraction, the mathematical form of which is identical to a Fourier transform. The far field of a light distribution is hence a Fourier transform in the spatial domain of that distribution.

A lens, because of its ability to curve a wavefront due to varying optical path length (thickness or refractive index) is able to bring the far field to its focal plane. It is well know from ray optics that a point source at one focal plane will produce a plane wave at the other. The point source is the Dirac delta function and the plane wave shows wide band and equal frequency components as expected. The same is true for other optical distributions such as a sinusoid, this will produce two delta functions in the back focal plane, representing the fundamental frequency of the

distribution in positive and negative spatial frequency space. Of course they are not ideal delta functions as they are convolved with the aperture of the lens but this is the same for any transform performed on a non-infinite data set.

The relevance of the effect to this thesis is the fact that just as a point on the axis of one focal plane maps to a plane wave normal to the lens in the other, a point off the axis also maps to a plane wave but angled in accordance to the shift theorem. This means that the light distribution seen at one plane may be used to describe the distribution seen on the other in terms of a summation of plane waves with varying amplitude and phase. This representation of the field is known as the angular spectrum. Figure 2.1 shows a few points in one plane mapping to plane waves in the back focal plane. Point A maps to a wave perpendicular to the axis, point B to some angle to it. There would, in reality be a continuum of points and plane waves. As was discussed in chapter 1, SP excitation only occurs at specific resonant angles when the incident light satisfies the conditions for coupling energy into the surface wave. If an oil immersion objective is used to excite SPs then considering the front focal plane in terms of its angular distribution one should expect only a small subset of the plane waves to excite surface plasmons. All of the plane waves map to a point in the back focal plane but it is only those that excite SPs that will be reduced in amplitude. Hence when the exit pupil is viewed, i.e. the BFP imaged after reflection, points in the distribution corresponding to SP excitation will also have reduced amplitude.

Just as with the prism based systems discussed in chapter 1 the polarization

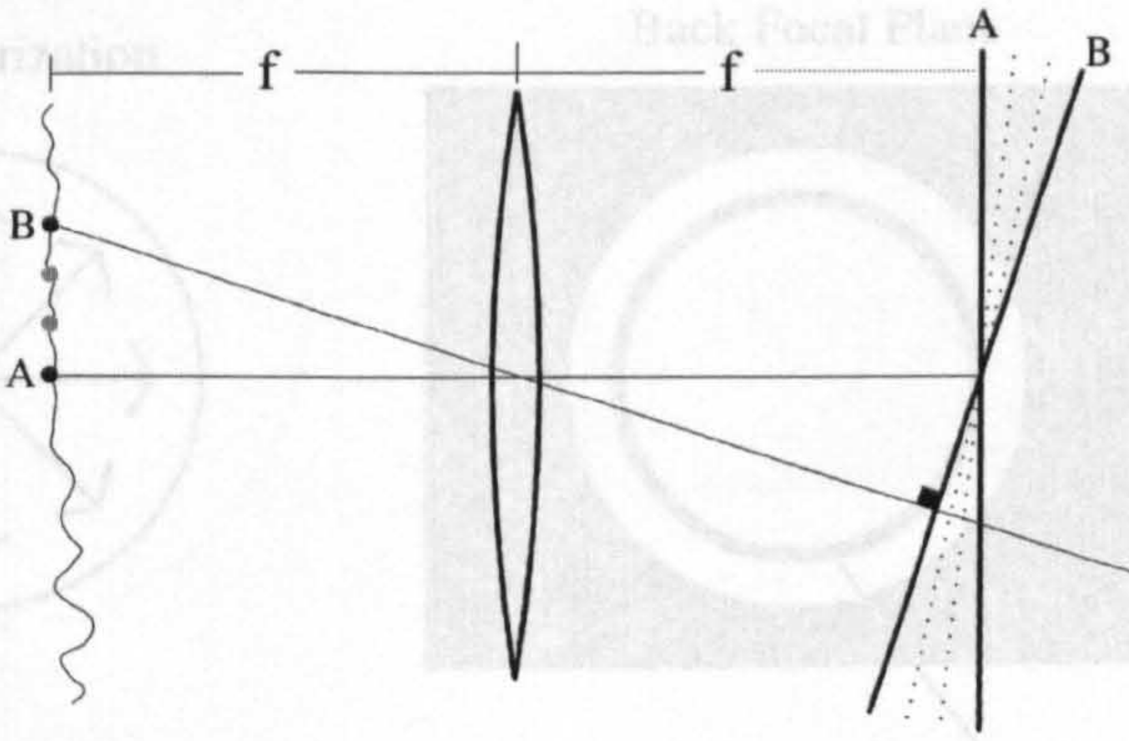

Figure 2.1: *A field distribution, Fourier transformed by a lens and represented by an angular spectrum.*

of the incident plane waves is also important. If the case of radial polarization in the back focal plane is considered then all of the incident plane waves will be p-polarized and able to excite SPs if they are at the resonant angle. Figure 2.2 shows this arrangement and the expected distribution seen at the BFP. As can be seen a dark ring appears at a position away from the axis corresponding to incident waves at resonance with the sample. In the case of linear polarization the situation is more complex. If a point in the back focal plane is considered then this point has a radial position that dictates the incident angle of the corresponding plane wave. It also has an azimuthal position that not only dictates the direction in which the plane wave hits the sample but also varies the relative components of s and p-polarization. Figure 2.3 shows how such a point may be resolved in to a p-polarized hence radial component and s-polarized, tangential component. The

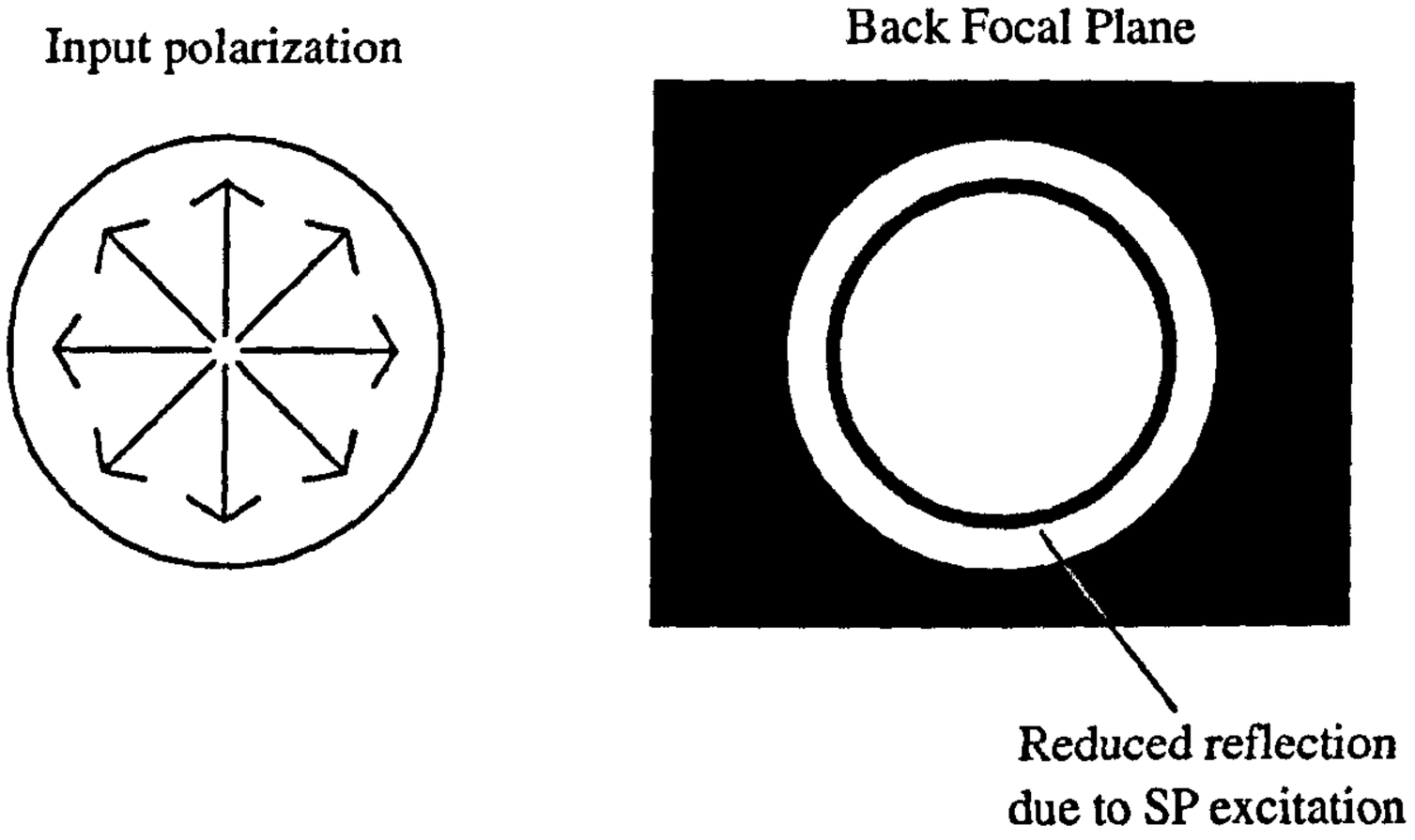

Figure 2.2: *The expected back focal plane distribution for radial polarization*

diagram shows the input polarization orientated horizontally so it is obvious that on the x-axis the polarization is purely p and on the y-axis the polarization is purely s. In between there is a mixture of the two varying from fully p to s. Therefore in this case all of the light at the resonant angle on the x-axis will excite SPs and none of the light on the y-axis will. Moving from p to s polarization the resonance will gradually disappear producing a crescent distribution. In some cases there may be more than one resonance and it is also possible to see such effects due to multiple layer structures where TIR can produce a resonance at a given angle.

2.3 Fresnel treatment of reflection coefficients

The system described in this thesis makes use of the phase shift in the reflection coefficient of p-polarized light at the SP resonance, the amplitude reflection coefficient

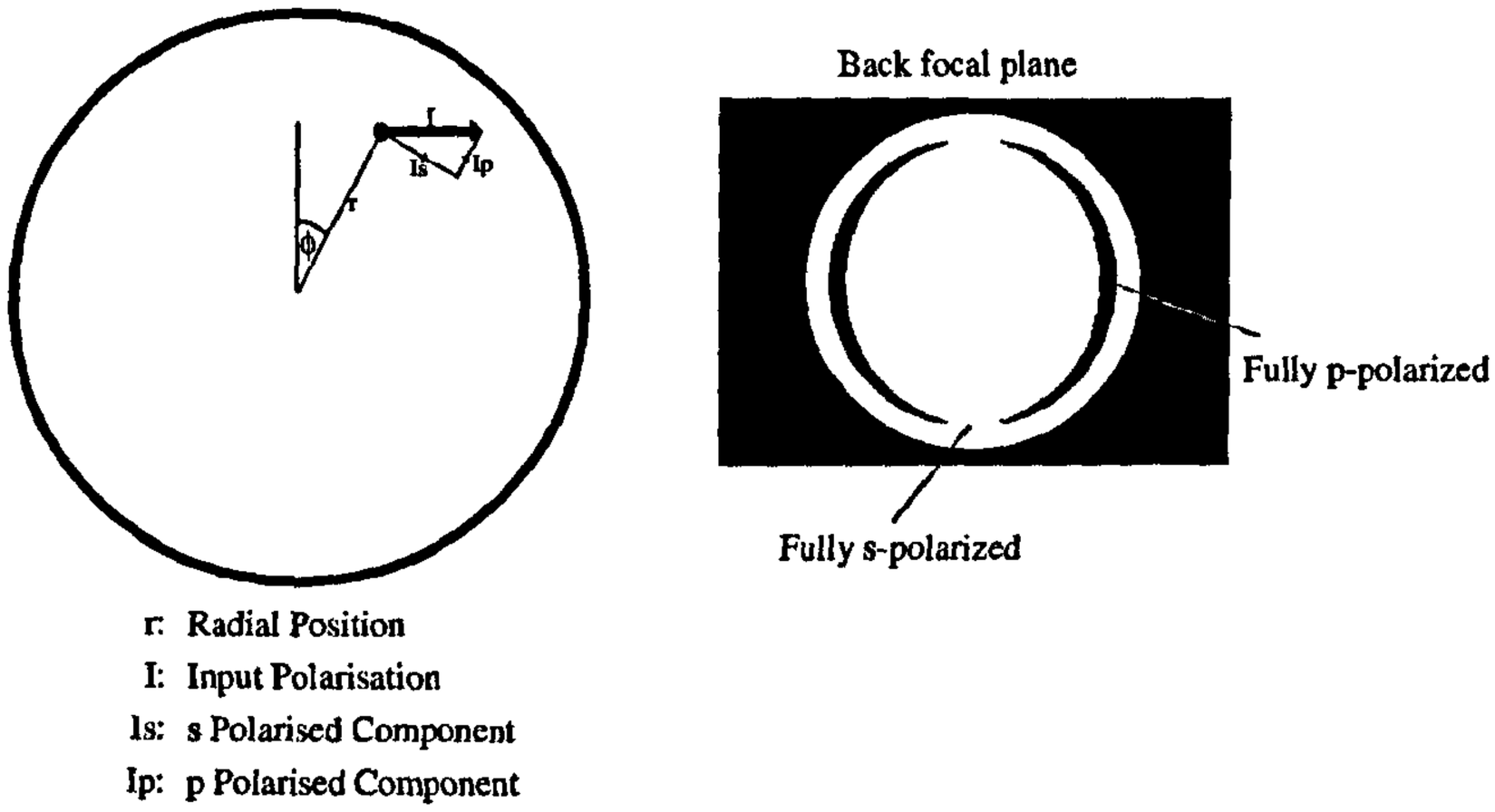

Figure 2.3: *Components of input polarization*

also shows a dip corresponding to excitation of SPs. In order to model the response of the microscope the reflection coefficients were calculated using computer programs formulated within the group based on the method described in ref [39]. Although a detailed description is not warranted the general theory behind the determination of the coefficients helps in understanding the meaning of the phase shift. The following will consider a 3-layer dielectric system of ambient material, film and substrate for simplicity. The procedure is identical for materials with complex refractive indices such as the metal layers used for SP excitation but the physical picture becomes complicated. The basic method may also be expanded to multiple layer structures by application of a matrix formulation.

The structure may be seen in figure 2.4. A ray corresponding to a plane wave originating in the ambient region strikes the sample. A portion of this plane wave is specularly reflected and the rest transmitted into the film layer. On meeting the

second boundary between film and substrate the wave is again split into reflected and transmitted components. The reflected component arrives back at the ambient-film boundary and is again divided into reflected and transmitted components where it may continue doing the same as it traverses the film. The amount of light reflected and transmitted at a single reflection event can be determined by the Fresnel complex reflection coefficients. These are determined themselves by the application of Snell's law and the matching of tangential E and H fields across the boundary. The figure

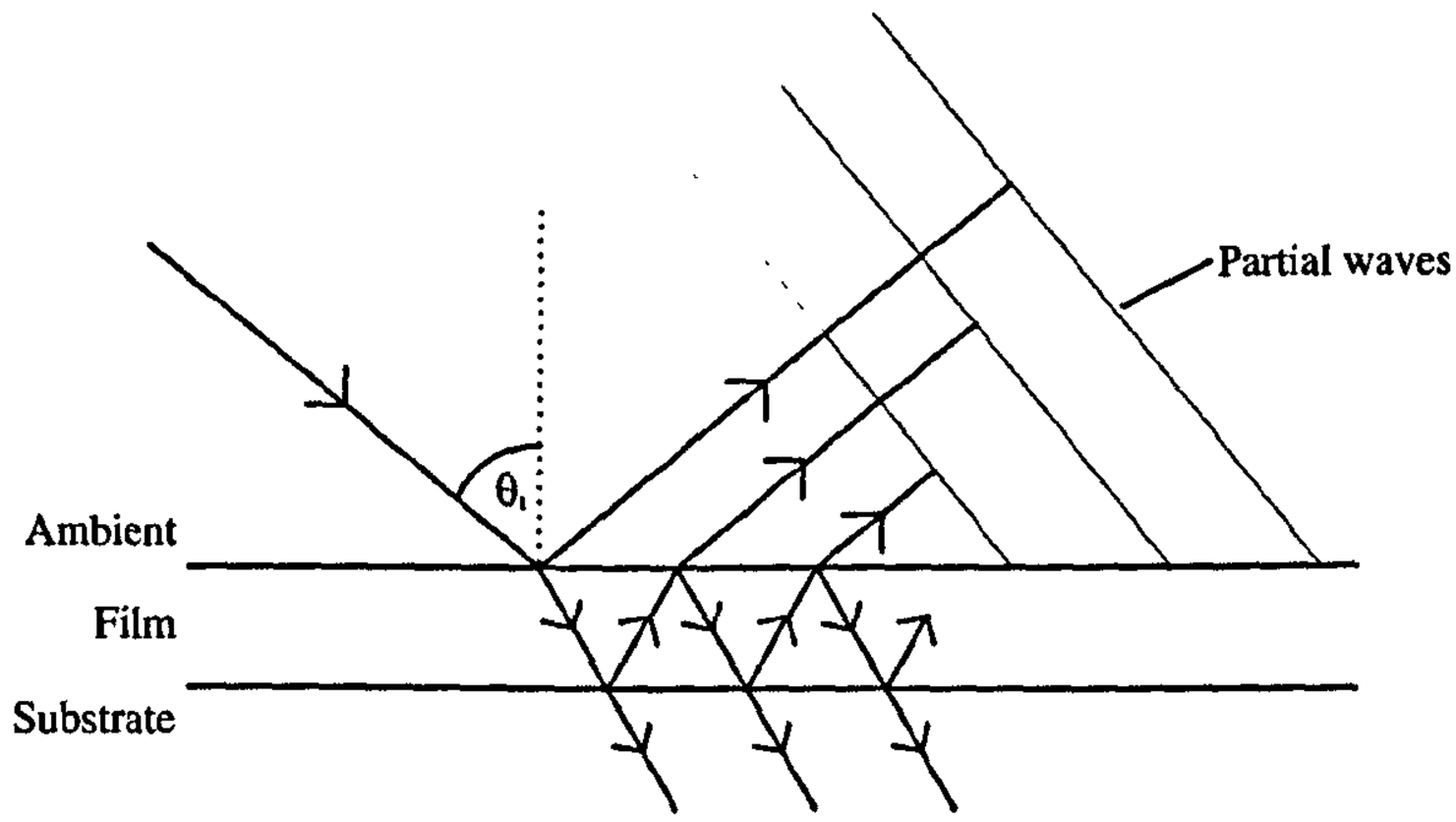

Figure 2.4: *Reflection of a plane wave from a three-layer dielectric structure*

only shows a single ray but the plane wave extends to infinity, so each of the directly reflected components can therefore be thought of as secondary sources that are each in phase and as such produce a partial plane wave. Likewise the light reemitting from the film after reflecting at the film-substrate boundary forms another partial wave and so on. The overall reflection co-efficient is determined by the summation

of these partial waves.

The reflection co-efficients differ for s and p polarizations because the Fresnel complex-amplitude and phase co-efficients depend on the tangential components of the field and hence the reflection coefficients of a layers structure also display the dependence.

The plasmon excitation which creates a dip in the amplitude reflection coefficient and shift in the phase coefficient is indicative of the generation of a surface wave as the energy is largely trapped by the structure and absorbed ohmically, any reemitted light will tend to have been translated laterally and is hence phase shifted with respect to the incident field.

Now that the general background has been discussed, more in depth coverage of the systems of relevance in the literature will be presented.

2.4 Review of Scanning Plasmon Interferometer

In order to develop the wide field version of the heterodyne interferometric scanning microscope developed by Somekh et al [40] it is necessary to first consider how that system worked so that the important elements of the design are retained.

The experimental configuration of the scanning SP microscope previously devised can be seen in figure 2.5. The light source is a 15mW HeNe laser with a wave length of 633nm. This is divided into a reference and sample beam by a non-polarizing cube beam splitter. The reference beam passes through a Bragg cell that is driven from a

signal generator at a frequency of 80MHz. This produces a set of diffracted orders, the first of which has an 80MHz shift in optical frequency. The angle and power of the Bragg cell is adjusted such that the power in the zeroth (unshifted) and first order are equal. The first diffracted order, shown by a dotted line, is discarded and the zeroth order after reflection on the reference mirror returns back through the Bragg cell whereupon it is again diffracted. The zeroth order is this time discarded and the first order collected by a lens and focused onto a photo detector.

The same process occurs in the sample arm, the beam is diffracted and the diffracted light discarded. The zeroth order is expanded 10 times by the sample arm optics before illuminating the back focal plane of the objective. The light focused onto the sample is then collected by the objective before propagating back through the beam expander. The now de-magnified beam passes through the second Bragg cell (driven at 80.01MHz) and the first order is focused onto the same photo diode.

The interference of the sample and reference beams creates a beat frequency at the sum and difference of the two components. In the case of this system the driving frequencies were 10kHz apart and the difference frequency, also 10kHz, was chosen for detection as it matched best the electronics available. To detect the interference signal and extract amplitude and phase information a lock-in amplifier was used. This takes the signal from the photo diode and a reference signal to selectively filter all but the wanted frequency. The reference can be produced by mixing the outputs of the oscillators that drive the Bragg cells electrically or by using a third signal generator. In the latter case the signal generators must be locked together to ensure

they are coherent with the reference generator.

The data produced by the Lock-in includes phase and amplitude information and may be read directly on the LCD display or by a PC with the relevant interface.

To produce an image the sample is scanned in X and Y using a piezo translator stage and values recorded at a matrix of points, these can then be built into an image using appropriate software. The process is a slow one taking 10s of minutes but results are good with sub micro resolution and high contrast as described in ref [40].

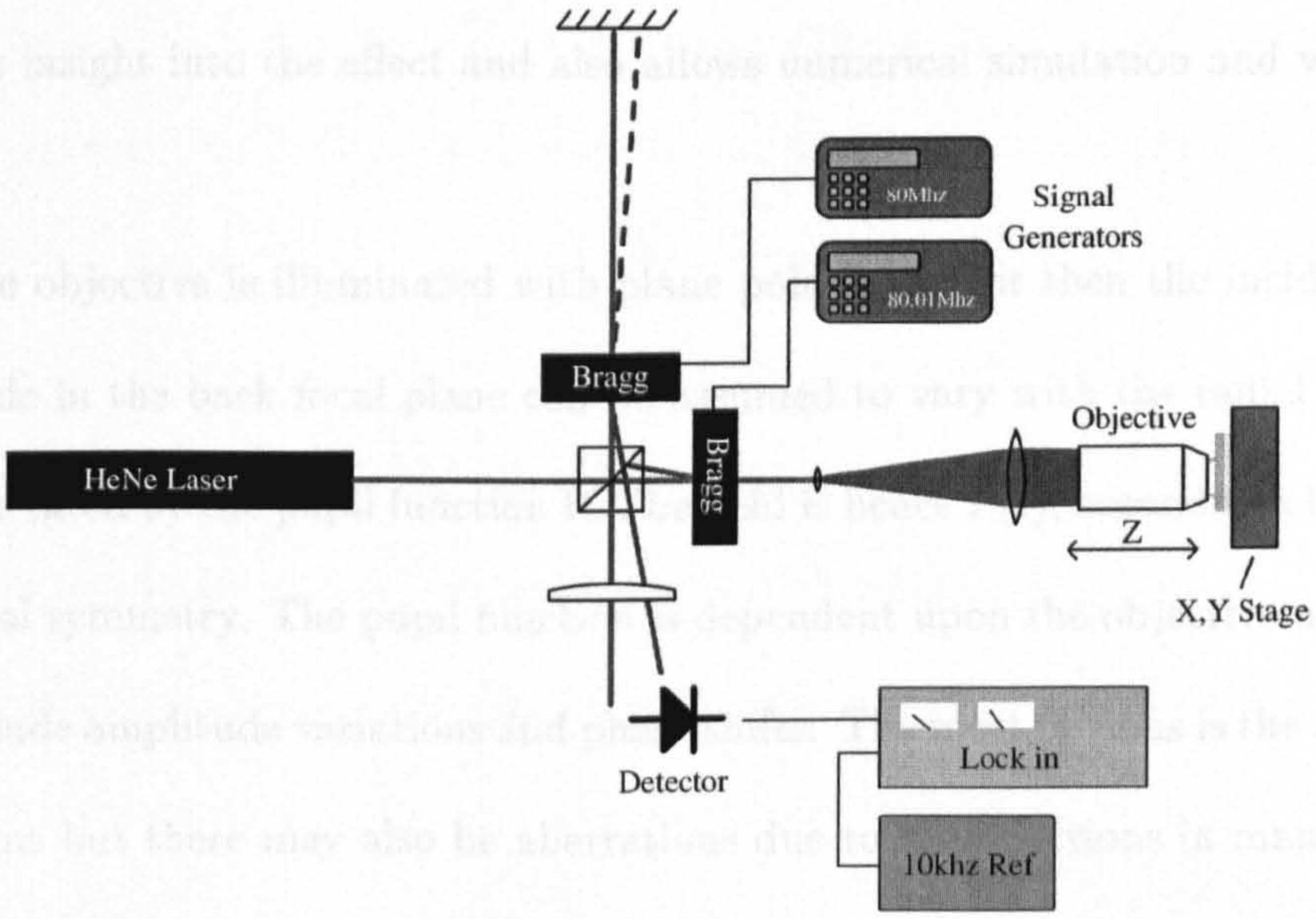

Figure 2.5: *High resolution scanning microscope layout.*

2.4.1 Use of defocus in achieving high contrast

In order to increase contrast in the scanning system it was found advantageous to operate the microscope with negative defocus i.e. the objective is moved toward the sample such that the distance between the objective and sample is less than the focal length. V(z) refers to the response of the interferometric scanning plasmon microscope, V changing with the defocus of the objective z.

Before discussing further the ramifications of the V(z) response produced when a sample is imaged, a mathematical expression for the response will be derived. This provides insight into the effect and also allows numerical simulation and visualization.

If the objective is illuminated with plane polarized light then the incident field amplitude in the back focal plane can be assumed to vary with the radial position and is dictated by the pupil function P. The field is hence P(r), assuming a lens with rotational symmetry. The pupil function is dependent upon the objective used, and may include amplitude variations and phase shifts. The most obvious is the aperture of the lens but there may also be aberrations due to imperfections in manufacture and materials.

Figure 2.3 shows the the aperture of the BFP and a point a distance r from the optical axis, at an azimuthal angle ϕ. It is known from the angular spectrum approach of Fourier optics [41] that the field at this point creates a plane wave at the front focal plane (sample plane) with an incident angle of $\theta = \arcsin(r \sin \theta_{max})$,

where θ_{max} is the maximum angle of incidence that can be produced by the lens and r is the normalized radius. It can therefore be seen that there is a direct mapping between the radial position on the BFP and the sine of the incident angle at the sample plane. As P is a function of r and can hence be considered a function of $\sin\theta$, P shall be redefined as $P(\theta)$ to simplify the notation and allow integration in terms of angle only.

Figure 2.3 also shows how the linearly polarized input light can be resolved into two polarization states. One component is p-polarized, that is, orientated radially such that its electric field vector lies parallel to the plane of incidence. The other component has its electric field vector perpendicular to the plane of incidence and is known to be s-polarized. The relative components of s and p polarization vary with the azimuthal angle from being fully p-polarized when $\phi = 0$ to fully s-polarized when $\phi = \pi/2$. As the reflection coefficient is dramatically different in both amplitude and phase between s and p polarizations this factor is very important.

The amplitude and phase of the incident plane wave produced by a point in the BFP with an azimuthal angle of ϕ and a radial position such that the incident angle is θ is given by:

$$E_i = P(\theta)(R_p(\theta)\cos(\phi) + R_s((\theta))\sin(\phi)) \tag{2.1}$$

Where R_p and R_s are the reflection coefficients for p and s polarization components.

There is also a phase shift added to the plane wave that is dependent upon the defocus. Figure 2.6 shows the difference in physical path length between plane waves incident at θ passing through the optical axis for focused and negatively

defocused samples. The total change in physical path length is given by $2z\cos\theta$ due to reflection and so the change in optical path length is $2zn\cos\theta$. Where n is the refractive index of the coupling oil and k is the wavenumber in free space ($2\pi/\lambda_{free}$). Negative z corresponds to the reduction of the sample to objective distance. The relation also holds true for positive defocus but with a positive sign. The wave

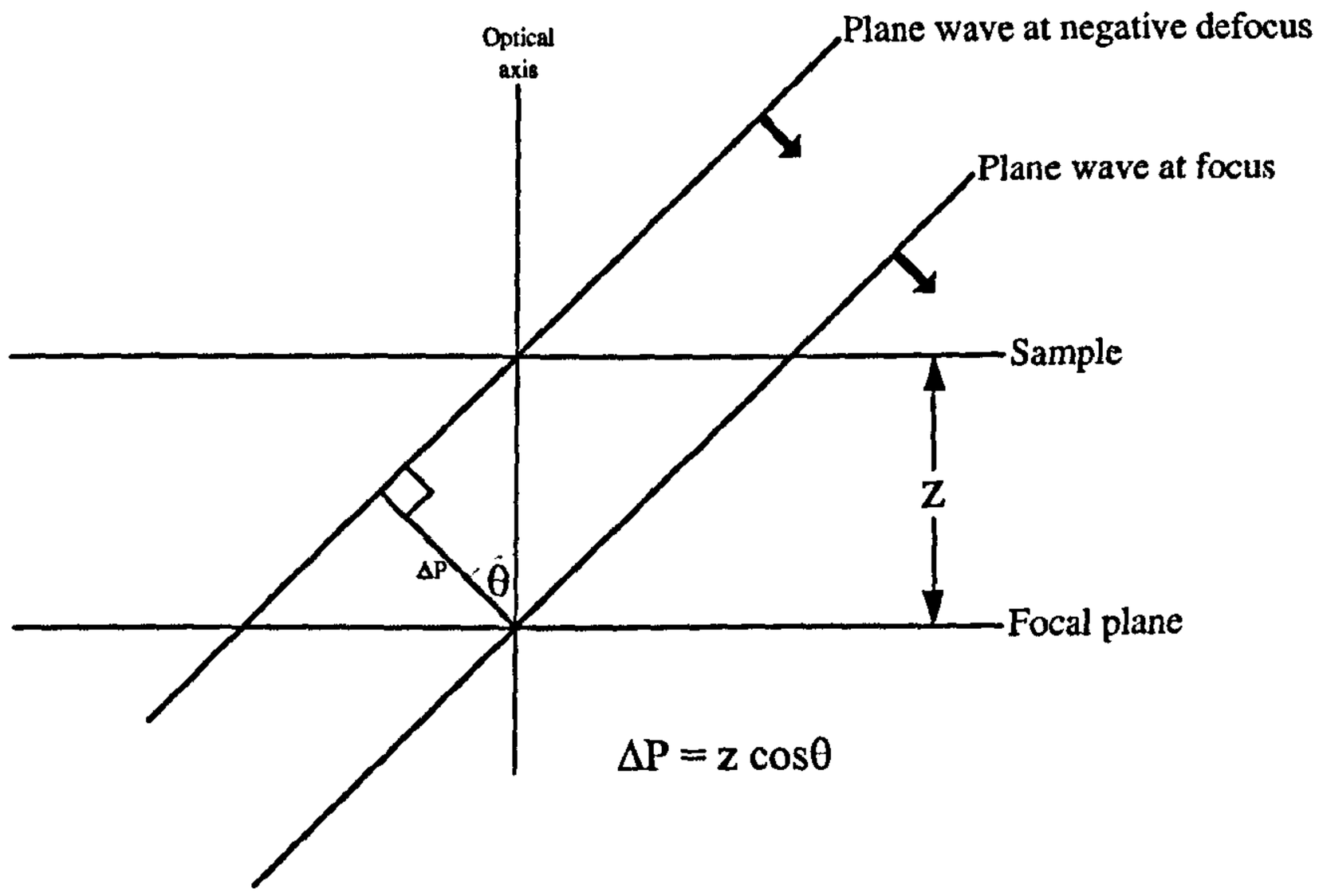

Figure 2.6: *Phase shift due to defocus*

immediately after reflection is therefore given by:

$$E_r = P(\theta)(R_p(\theta)\cos(\phi) + R_s(\theta)\sin(\phi))exp(j2nkz\cos\theta) \tag{2.2}$$

The light returns through the objective to the original point of excitation and must be resolved into the direction of the original input polarization as only this component interferes with the reference beam and contributes to the system output V.

The reflected light at the point (r, ϕ) corresponding to incident angles (θ, ϕ) is hence given by:

$$E_r = P^2(\theta)(R_p(\theta)\cos^2(\phi) + R_s(\theta)\sin^2(\phi))exp(j2nkz\cos\theta) \quad (2.3)$$

The P^2 term comes from the fact the light passes through the pupil function twice.

This field is interfered with a plane reference beam E_o such that the frequency shifted output from the heterodyne interferometer is given by:

$$\Re(E_r E_o^*) \quad (2.4)$$

Where * represents the complex conjugate.

The output of the system is a summation of all the points in the BFP and can be written, omitting constant terms, as:

$$V(z) = \iint P^2(\theta)(R_p(\theta)\cos^2(\phi) + R_s(\theta)\sin^2(\phi))exp(j2nkz\cos\theta)d\theta d\phi \quad (2.5)$$

2.4.2 V(z) for samples not supporting surface plasmons:

As was shown earlier the shift in phase of a point in the BFP due to a defocus z is given by $2knz\cos\theta$. Therefore the rate of change of phase with defocus is $2kn\cos\theta$. Points on the BFP close to the axis have the greatest rate of change of phase and points off axis have a lower rate of change. Therefore, as the objective is defocused, the outer components increasingly lag the axial ones and the well known phase curvature associated with a defocused lens is seen at the BFP. The signal V is the interference signal between the returned wave front and the reference. As shown in

equation 2.5, with a plane reference beam this reduces to a summation of all the points in the BFP, each of which has a phase and amplitude. If the phases of the components are equal then the vectors add up to produce a large value of V. This is the case for the objective at focus, when the phase shift is zero for all components. At defocus however the rapidly varying phase *across* the bfp means that most of the components cancel and only the axial angles (when $\cos\theta$ varies slowly with θ) add up in phase. The overall effect is that the response V reduces smoothly with negative defocus assuming a well designed objective with a suitable pupil function.

2.4.3 V(z) for samples supporting plasmons:

Figure 2.7 shows a typical simulated $V(z)$ response for a sample consisting of a plain 43.5nm gold layer. As can be seen there are ripples in the negatively defocused region. There is also some oscillation in the positively defocused region but that is due to the choice of pupil function. Too sharp an edge creates a slight sinc response and this could be also be seen in simulations of non plasmon supporting structures. In practice and with good optics, no oscillation is seen when plasmons are not present. For example when imaging a thick metalized mirror. If any two points on the BFP with different radial positions are considered then it is already know that the phase shift due to defocus will will differ due to the different incident angles. Therefore if these two components are interfered with the reference beam the result is an oscillation in V with varied z as the two components come in and out of phase with each other.

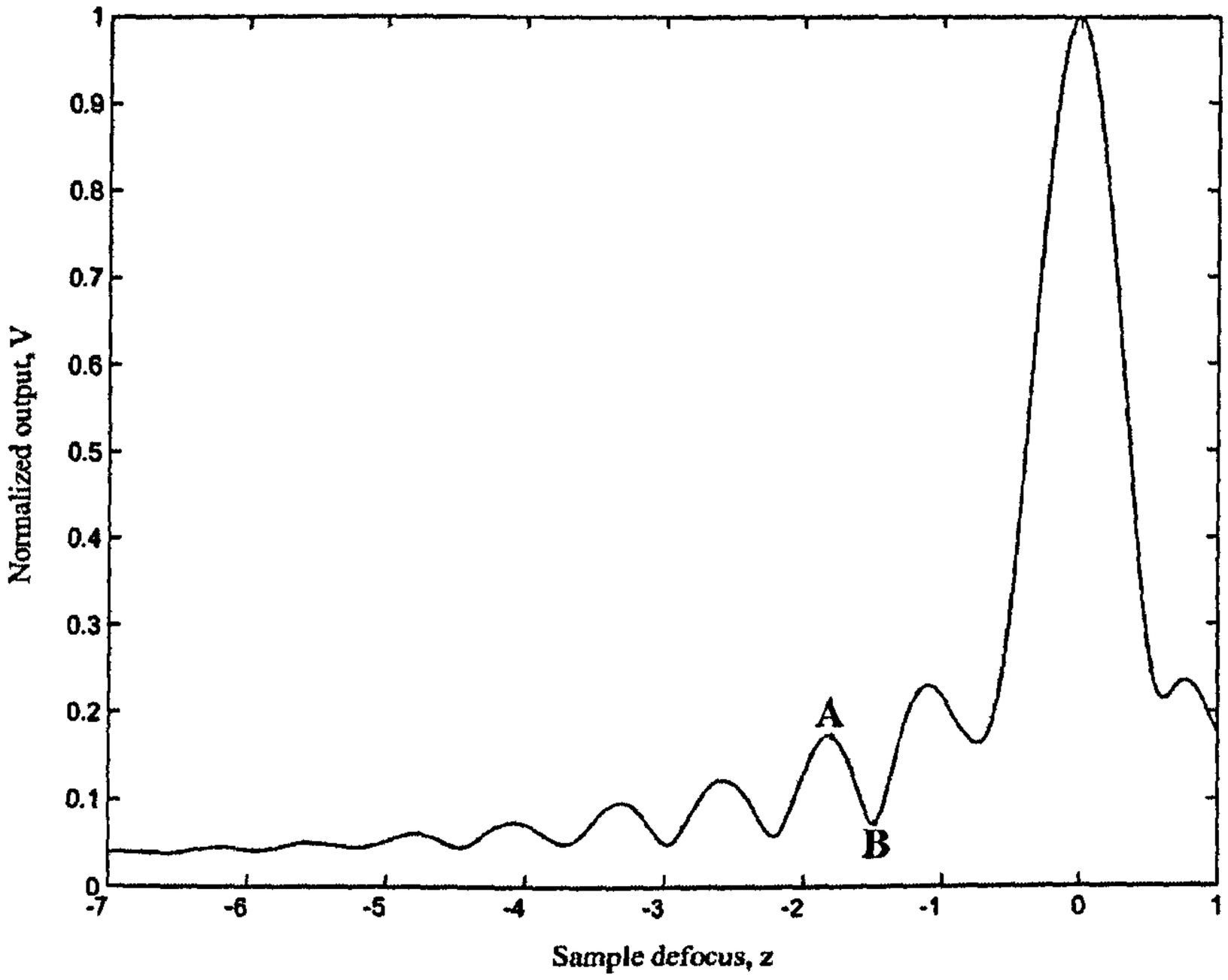

Figure 2.7: *Simulated $V(z)$ response for a planar 43.5nm thick gold sample (defocus in microns)*

As was shown for a sample that does not support SPs the rapid phase curvature of the wavefront due to defocus means that only the axial components of the BFP contribute greatly to the interference signal. However, as discussed in section 1 there is a phase shift in the reflection coefficient at angles associated with the excitation of SPs. The phase of the reflection coefficient for p-polarized light, R_p, shifts rapidly at the SP resonance θ_p. This means that plane waves at these incident angles suffer an additional fixed phase shift. This shift is superimposed on the general curvature but does not follow the $\cos\theta$ variation. Because it does not follow this variation it does not tend to be canceled as in the case of a sample that does not support SPs.

There are therefore two main contributions to the interference, one consists of the axial angles, these do not cancel because of the slower phase variation. The second is the light that corresponds to plasmon excitation. The oscillation in V is due to the relative phase shifts of these components changing with defocus.

To demonstrate this effect, vector diagrams showing the components that are summed to produce V at two values of z were produced for a single plane of incidence. Each component of the summation is a complex number and hence a vector, the plots show the cumulative summation of the vectors. For example the 3rd point of the plot is the summation of the first 3 vectors and the 5th the first 5. The line that can be described between the origin and the last value is V for that value of z. The order in which the points are added up does not make a difference to the final resultant but it is logical to sum them from the lowest incident angles to the greatest. In the case of a mirror sample the plot is a straight line at focus when all the contributions are in phase and as the defocus is increased the line curls due to the phase curvature across the wavefront. This spiral gradually tightens with increasing defocus. The spiraling suggests that the curved portion of the wavefront is not contributing to the interference term as the components are canceling each other.

In figure 2.8 a plot for the defocus marked A in figure 2.7 is shown. And in figure 2.9 a plot for the same sample but backed with water to prevent plasmon generation. The point corresponding to the main minima in the reflection coefficient due to plasmon excitation is marked with a dot. In the case of the sample with no

SP excitation the vector spiral can be seen to be quite symmetrical as would be expected. When SPs are excited, however, there is a clear kink in the spiral pushing the resultant away from the axis of symmetry. In fact the symmetry is being lost before the main resonance dip but the main effect is around the resonance when the phase of the reflection co-efficient is varying rapidly.

In figures 2.10 and 2.11 similar plots for point B of figure 2.7 are shown. In the case of the plasmon supporting sample the resultant is smaller. This is because as the spiral has unraveled and the tip (resultant) has been pushed to the other side of the spiral axis due to the plasmon perturbation. Whereas in the case where plasmons are suppressed the tip of the vector remains reasonably central to the spiral and so merely increases the resultant slightly. Essentially a certain amount of the spiraling that corresponds to the components canceling is straightened by the plasmon phase shift producing a portion of the components that can beat with the lower angles. These angles are the greatest component of the resultant because they are the least spiraled or in other words the most in phase. Figures 2.12 and 2.13 show simplified phasor diagrams for the plasmon supporting sample at point A and B respectively. V is split into three vectors, the first corresponds to the angles below the plasmon resonance, the second (dotted) corresponds to angles around the resonance and the third, angles beyond the resonance. In the case of point A, the second (plasmon) vector is adding up in phase with the first (DC) vector to produce a local maxima in the V(z). At point B the plasmon vector is out of phase with the DC vector reducing the resultant. The third vector has little effect in both cases.

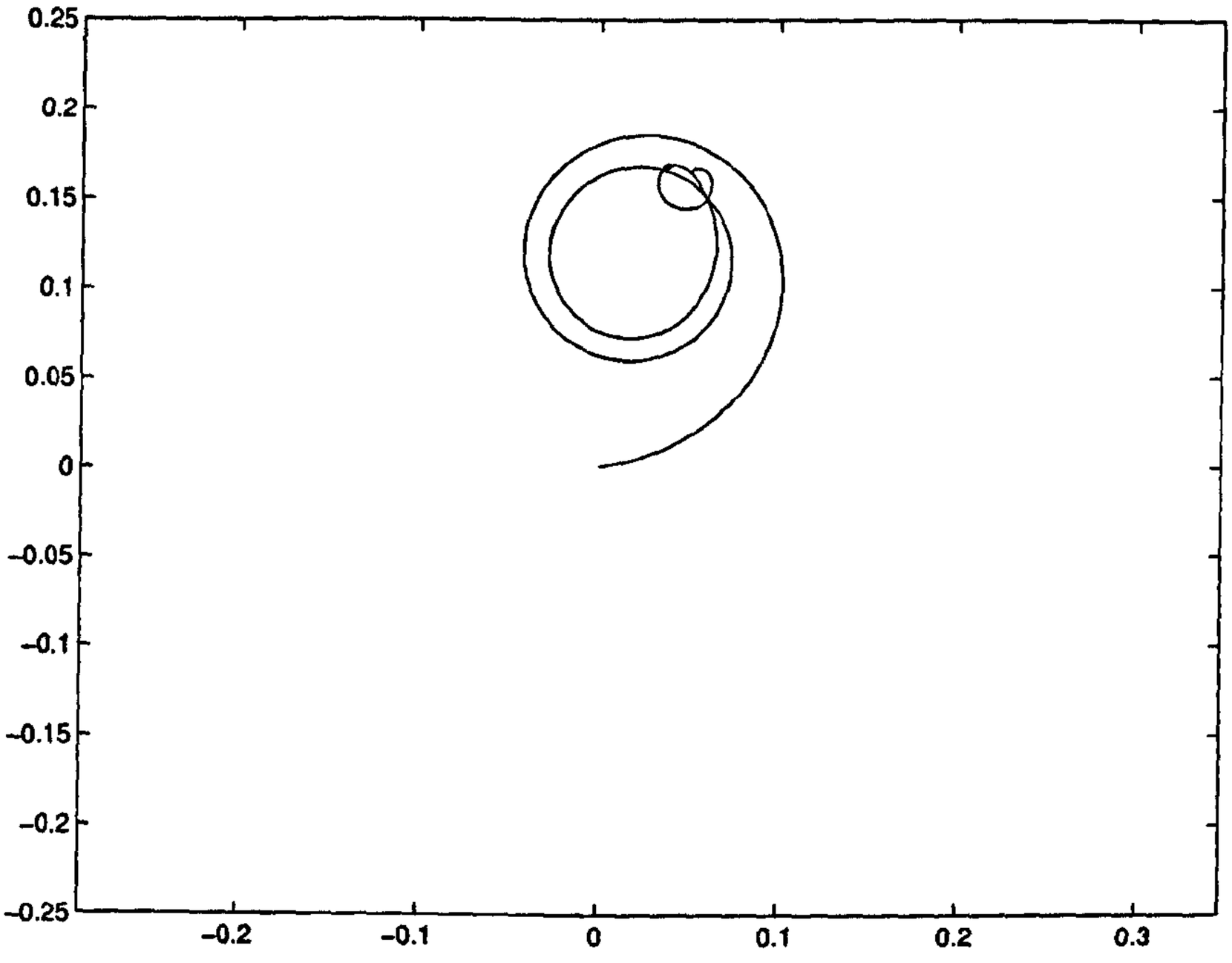

Figure 2.8: *Vector diagram for V at point A of figure 2.7 (plotted in complex space)*

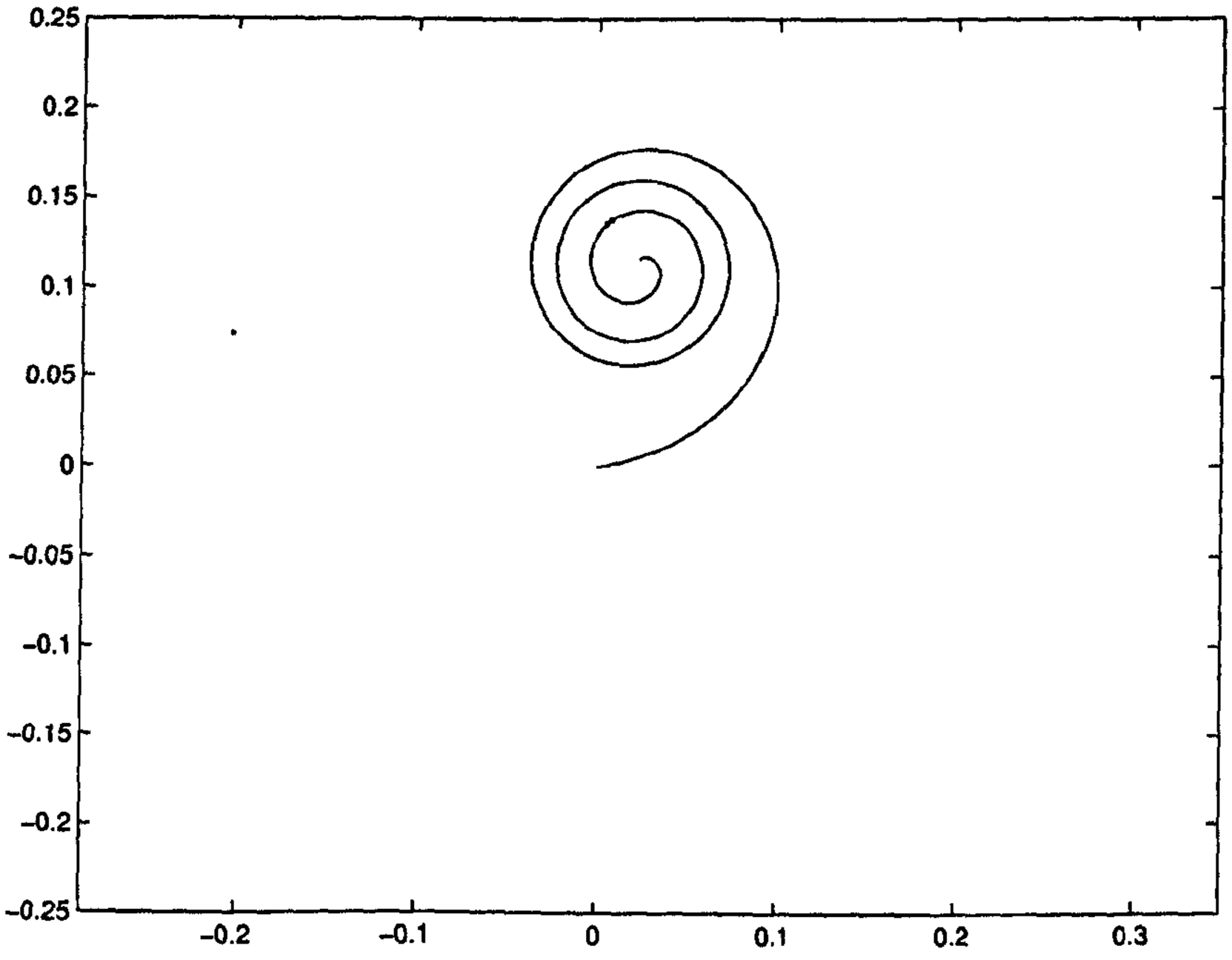

Figure 2.9: *Vector diagram for V at point A of figure 2.7 when plasmons are suppressed (plotted in complex space)*

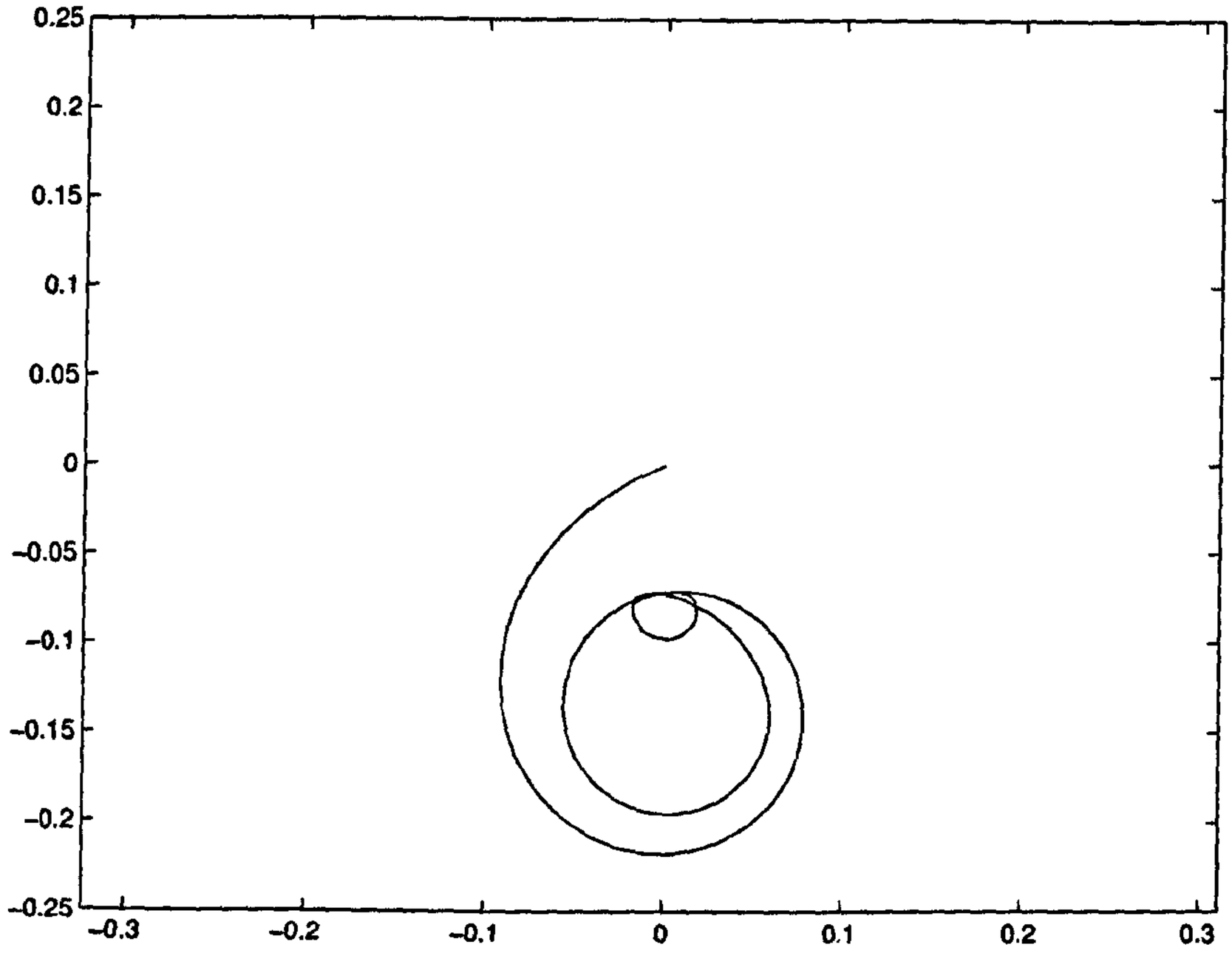

Figure 2.10: *Vector diagram for V at point B of figure 2.7 (plotted in complex space)*

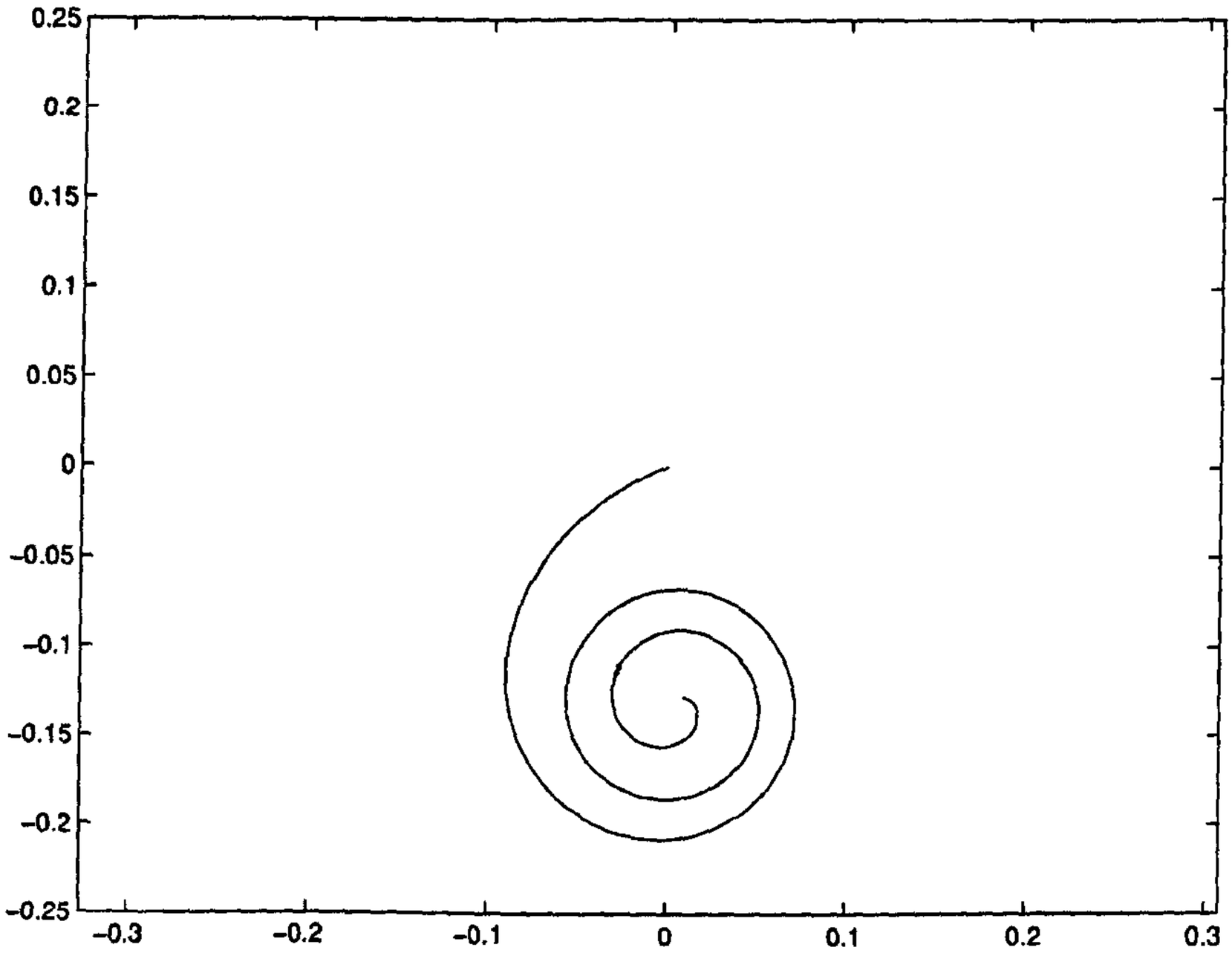

Figure 2.11: *Vector diagram for V at point B of figure 2.7 when plasmons are suppressed (plotted in complex space)*

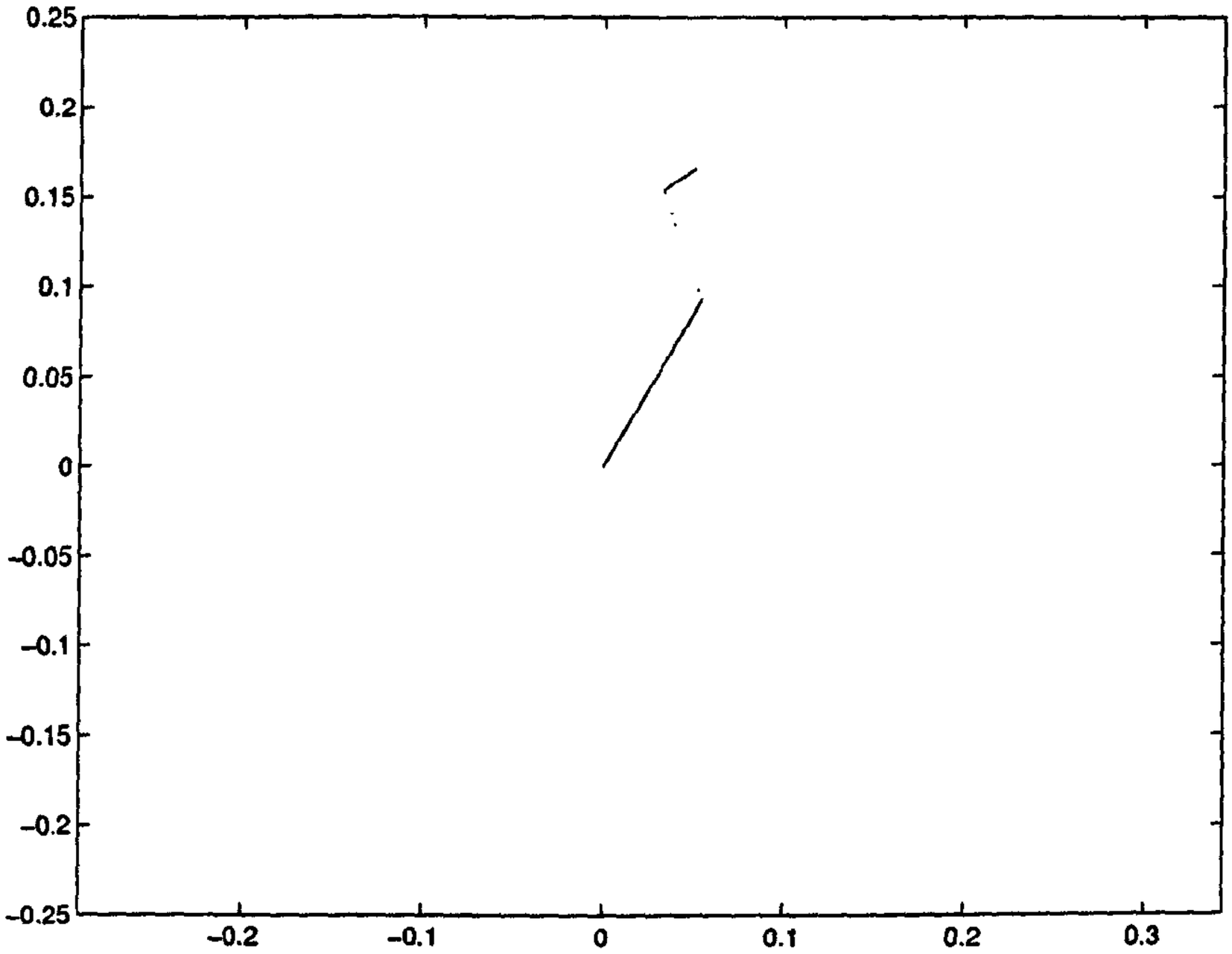

Figure 2.12: *Simplified Vector diagram for point A of figure 2.7 (plotted in complex space)*

To calculate the period of the oscillation the components of the incident light that contribute to the oscillation, those on axis and at the plasmon resonance only need be considered.

The phase of the light on the axis varies as $2knz$ and the light at the plasmon angle as $2knz\cos\theta_p$ the difference in phase between the two contributions expanding k to $2\pi/\lambda_f$ is given by:

$$\frac{4\pi nz}{\lambda_f}(1-\cos\theta_p) \tag{2.6}$$

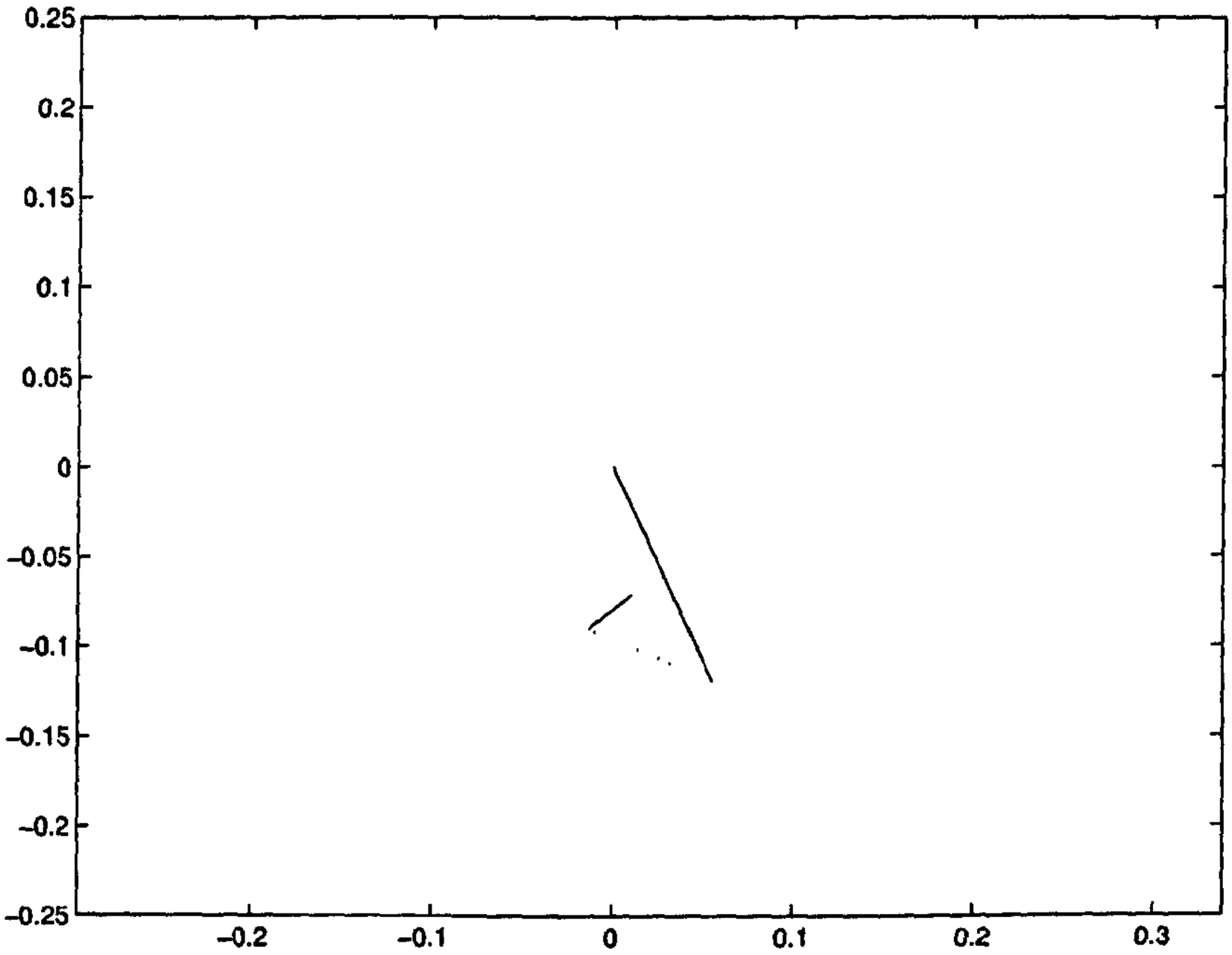

Figure 2.13: *Simplified vector diagram for point B of figure 2.7 (plotted in complex space)*

Equating to 2π and rearranging:

$$\Delta z = \frac{\lambda_f}{2n(1-\cos\theta_p)} \tag{2.7}$$

Equation 2.7 shows the usefulness of the $V(z)$ response. The angles that produce plasmons are known to be relatively high due to the requisite k-vector and so the value of $\cos\theta_p$ varies quickly with θ due to the high gradient of the cosine. This means that two points on the same sample with differing values of θ_p, due perhaps to a deposit on the metal, will have greatly differing periods of $V(z)$. Figure 2.14 shows V(z) curves for a 43.5nm thick gold layer; the first plain gold, the second with a 20nm

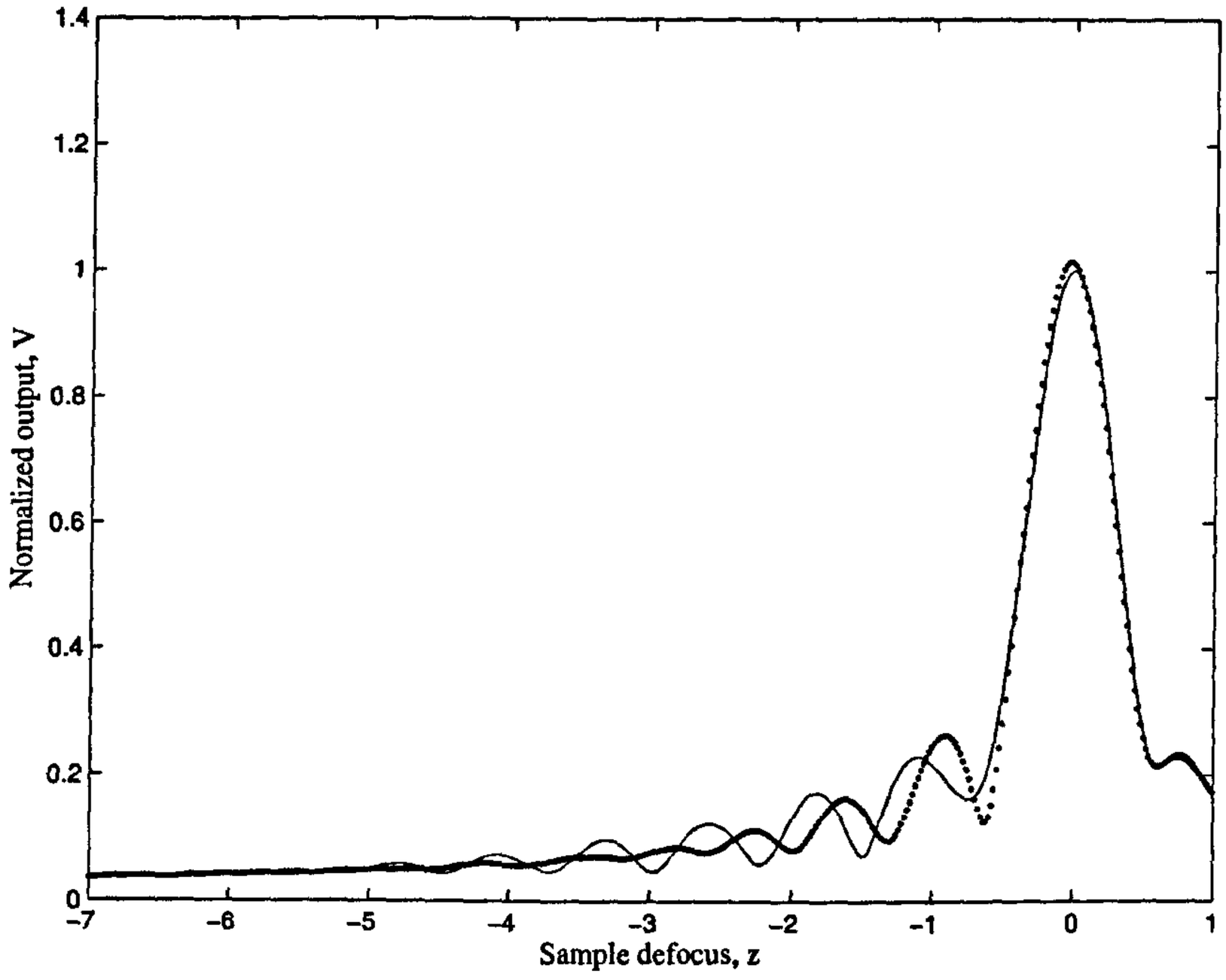

Figure 2.14: *Simulated V(z) responses for an uncoated 43.5nm thick gold layer (solid line) and the same layer coated with 20nm of SiO_2*

thick layer of SiO_2. As can be seen the periods differ greatly despite the thinness of the added layer. At the focus the values of V are almost identical but away from focus the contrast between the two samples varies periodically. At a suitably chosen defocus the response of the microscope V will therefore be highly sensitive to the additional layer. In practical microscopy the objective can be scanned over a surface to form an image. Because the slope of the contrast between the two V(z) curves is less than that of the phase shift in the reflection co-efficient the dynamic range is higher. The sensitivity therefore, is likely to be somewhat lower although the limits of sensitivity have never been defined. One other factor is the choice of defocus. It

is an easy enough task to find the focus and to add a defocus but the exact defocus required for good contrast will depend on the sample imaged. Samples that are not binary may require images to be taken at more than one defocus position. This is another reason why a wide field version of the system is so attractive as images may be taken in real time while adjustment is made to the defocus position.

This explanation does however bring up the obvious question of what happens to the resolution when the objective is operated in defocus. It turns out that the resolution is not especially degraded by the defocus.

2.5 Resolution in defocused scanning system

As was shown in chapter 1 there is a focusing effect on the sample surface when an objective is used to excite surface plasmons. The SP field adds in phase on the optical axis creating large field enhancement. This is also the case for the defocused objective. Figure 2.15 shows the situation. A plane wave illuminates the BFP of an oil immersion objective in defocus producing a field distribution with a phase curvature. Because of the curvature, SPs may only be excited at a certain radius corresponding to the point where the local curvature equates to the wave vector for SP excitation. The excitation therefore occurs over a ring or more precisely in the case of illumination with linear polarization over two crescents. The excited SPs then propagate through the optical axis forming a focus with high field enhancement. To achieve resolution greater than the defocused spot size the microscope must be more

sensitive to the axial region of the spot than to other parts of the focal spot. The situation is rather complex, however the fact that all of the excited SPs propagate through the axial focus bodes well for the resolution. High resolution of less than 1μm has been observed but a thorough analysis has not been performed to determine the exact resolution mechanism. The full analysis is beyond the scope of this thesis however some suggestions for common sample types will be presented here.

2.5.1 Homogeneous response

When the focal spot is over a single medium the response is as discussed in section 2.4, i.e. the output depends on the specific defocus and the angle of SP excitation. This represents the main mechanism of contrast.

2.5.2 A small scatterer

SPs on meeting dielectric boundaries can emit bulk radiation. For a scatterer of a size much smaller than the propagation length the amount of scattering will be at a maximum when the object is at the SP focus. Although the SPs decay away from the point at which they are excited the focus has the highest energy density of any point within the spot. It is also the case that the light scattered from the focus will be in phase and will therefore form a large component in the integral that determines V. A scatterer that is away from the optical axis will scatter much less light and the scattered light will tend not to be in phase. If several objects are within the focal spot then there will be some blurring much as might be seen in

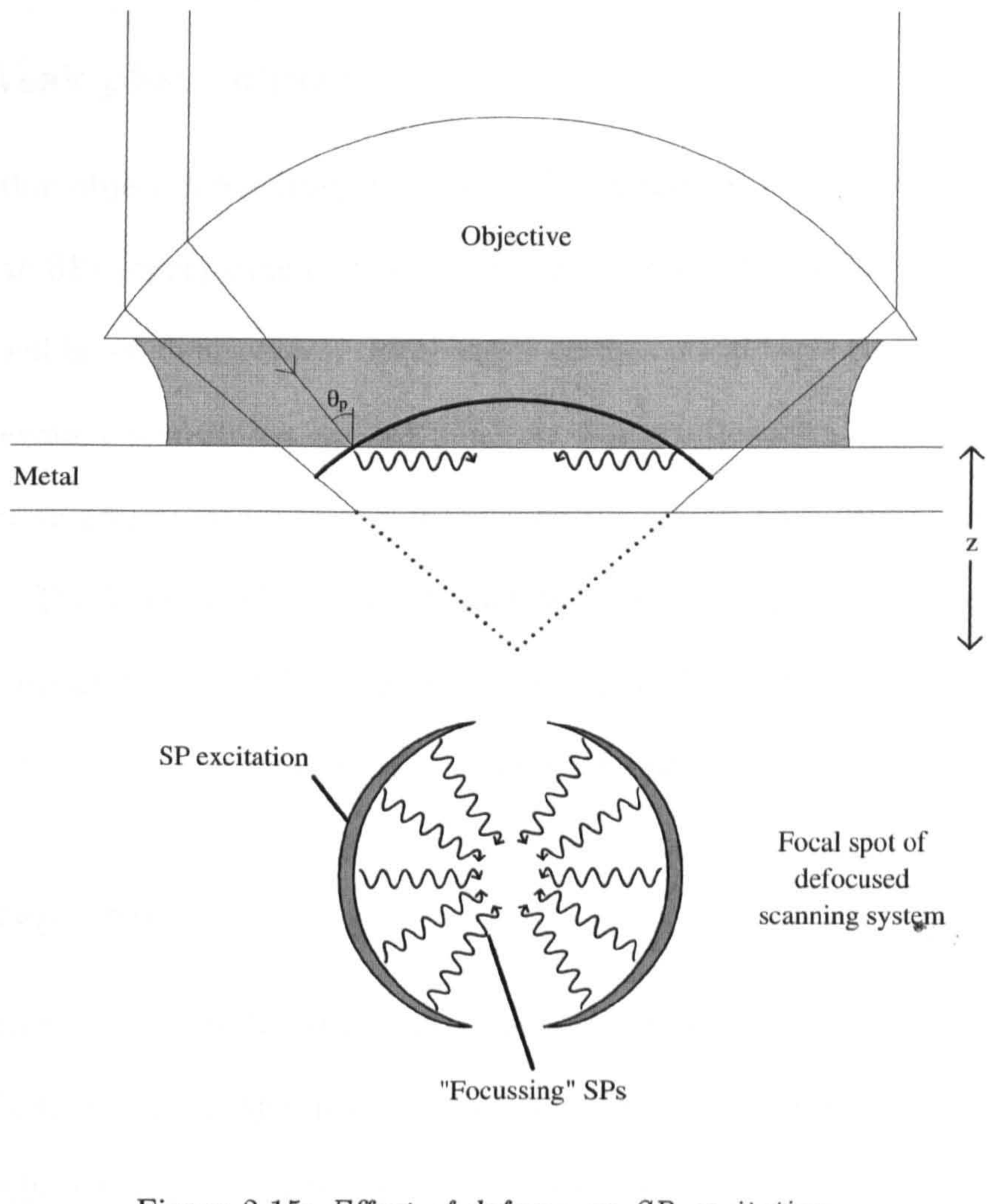

Figure 2.15: *Effect of defocus on SP excitation*

any confocal system however assuming that only a portion of the SP propagating over small scatterers is scattered the central spot should still be by far the greatest component of the output.

2.5.3 Weak phase object

A weak or thin object is less likely to scatter SPs however it may impart a small phase shift to SPs propagating over it. If the object is small then the effect on a specific SP will be small however if the object is on the optical focus then the small effect is integrated over all the excited SPs. As was mentioned in chapter 1 the sensitivity of an optical measurement depends on the optical path length through the material. The focusing effect therefore increases the optical path length as each short path through the object forms part of an integral. When the object is off the optical axis it will only effect a cone of SPs and so the effect is reduced.

2.5.4 Step object

A step in refractive index or thickness can produce scattering and this will represent one mode of contrast on an edge. It is complicated by the fact that the light scattered will have a different emission angle and hence phase shift depending on the direction it propagates over the boundary. The scattered light from SPs in a region where the excitation angle is such that reemitted light is out of phase with the axial reference will produce components at the edge that will tend to reduce V. Likewise those from a region that produces reemitted SPs that are in phase with the axial reference

will increase V. The scattering will therefore be identical when the step is on the axis. Therefore half of the incident light will produce a value of V corresponding to one material and half to the other. The overall effect will be a value of V that is intermediate to the two. When the optical axis it just over the edge however, the relative amount of scattering resulting from SPs in each region will change with more coming from the side on which the focus lies.

When the step is a weak scatterer then this effect will be less pronounced. In this situation the main reason for a sharp transition will come from the fact that on propagating over the boundary the SPs will not only be coupled into a new mode but will also be refracted slightly forming a new focus. The importance of the coupling into a new mode is that the V(z) response depends upon the difference between the phases of the axial light and that apertured by the SP phase shift. The phase of the light corresponding to SP excitation due to defocus is a function of the incident angle but also the angle of emission that is normally identical. If an SP propagates over a boundary however, the emission angle changes and so does the phase shift associated with the defocus. The effect is to produce a component of V that equates to a sample of intermediate properties between the two regions. This is at least closer to the properties of the region in which the optical axis resides than the other region. The new focus formed by refraction means that the majority of reemission occurs off the optical axis, this adds an additional phase gradient to the contribution which will tend to be rejected by the confocal response of the microscope.

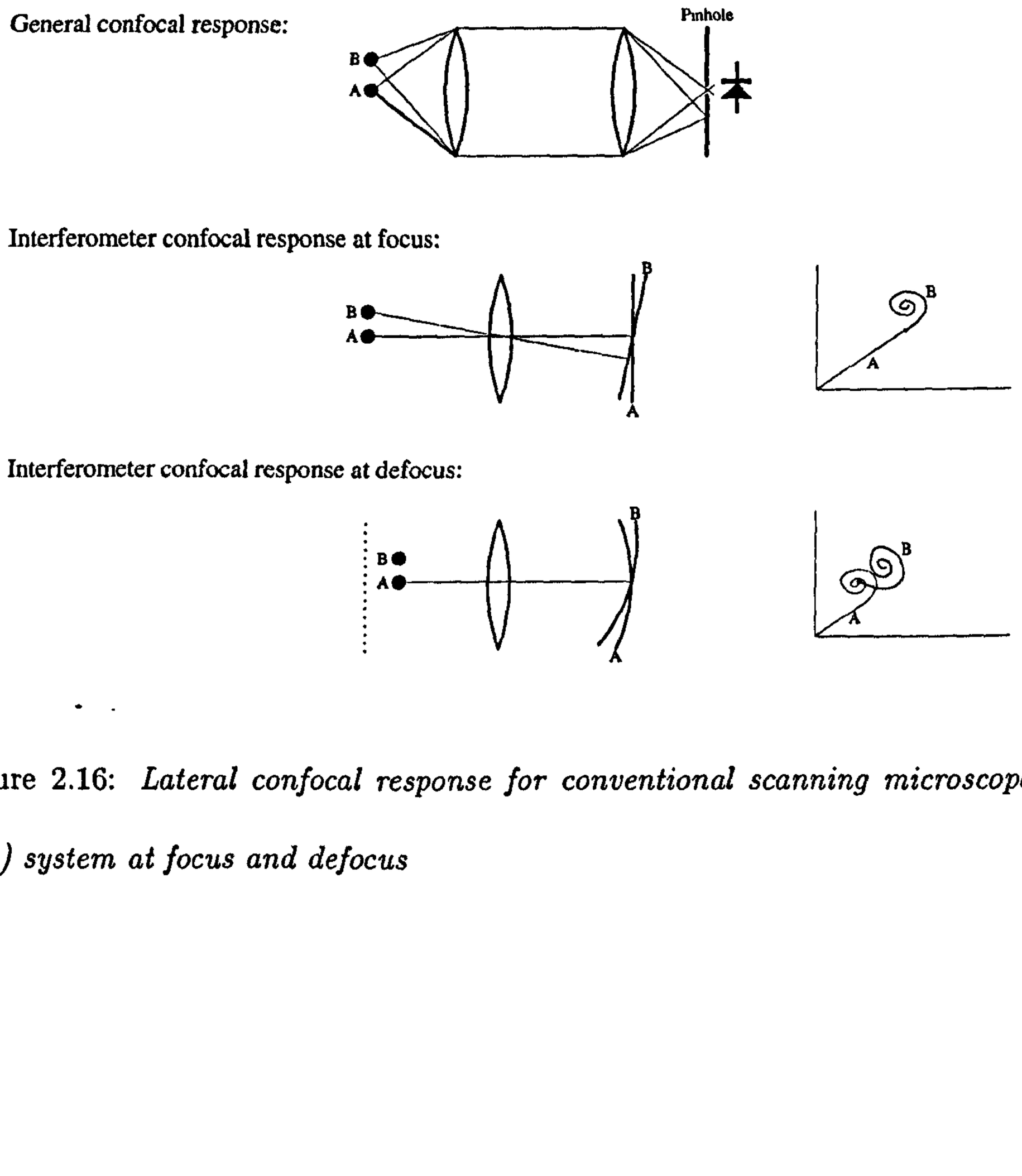

Figure 2.16: *Lateral confocal response for conventional scanning microscope and V(z) system at focus and defocus*

The confocal response

Up to now this aspect of the microscope has not been mentioned directly. The basic concept of a confocal response can be seen at the top of figure 2.16 a conventional confocal scanning microscope has a pinhole added in front of the detector, now objects that lie off the focal spot have less effect on the response and also the side lobes of the focal spot which are a jinc type function can be truncated. As such, the microscope has improved resolution. This same principle also works for depth discrimination as defocused objects will produce an enlarged spot which is predominately blocked by the pinhole. The scanning system described here does not have a physical pinhole but rather a virtual one. Considering the in focus case first, the second part of figure 2.16, light emitted from the central spot will produce a plane wave at the back focal plane, light emitted off axis will also produce a plane wave but with a phase gradient. When these two waves are interfered with the reference the on axis contribution will be much larger as it has zero phase gradient. The off axis contribution will tend to cancel itself out. A vector diagram much like those shown previously can be seen showing the addition of these two components, although it might be more usual to sum the distributions before plotting the diagram the result is the same. Just as for the conventional confocal microscope this system also has a confocal response in depth, as the objective is defocused the field in the BFP is curved more and more and interferes less with the reference. However, depth discrimination is meaningless in a surface based microscope and we have seen that

the defocus is necessary for contrast. The question is, does the microscope lose its lateral confocal response because of defocus. The answer would seem to be no although it may be somewhat degraded. The final part of figure 2.16 shows the case of the system at defocus, this time the two contributions produce waves with phase curvatures. The on-axis component A, produces a spherical wave symmetric with the optical axis whereas contribution B produces a similarly curved wave front but with the addition of a linear phase gradient. The effect, as may be seen in the phasor diagram is that the response tends toward the axial portion of the on axis contribution A. When SPs are excited there are also phase perturbations on the spherical waves, these too will tend to contribute more when the background phase-gradient is less.

2.6 Discussion

The exact weightings and validities of each of these effects requires formal mathematical analysis or numerical simulation but the main point would seem to be that the SP focus represents a point where more light will be emitted than anywhere else and where emitted light will add in phase when interfered. It is also a point that is common to all SP propagation paths, this would seem to be the essence of the operation. The above mechanisms suggest ways that the response of the microscope is biased to the central SP focus, however the exact output given by the microscope may not be that expected for the material from the V(z) theory. As was touched

on earlier this system is a microscope rather than a scanning sensor, after all, if a sample has three regions of differing refractive index some parts may not be visible at certain defocus positions. The important thing is to be able to see variation in the structure and have some contrast, this again reinforces the benefits of a wide field system where images can be taken quickly at different defocuses.

A wide field system which is analogous to this scanning heterodyne interferometer will now be described.

2.7 Wide field speckle illuminated microscopy

The wide field, amplitude and phase confocal microscope with speckle illumination described by Somekh et al [37] was originally devised to combine the advantages of scanning confocal microscopy with the inherent speed and lower cost of a wide field system. The advantages of a scanning confocal system over a conventional microscope are improved depth discrimination, elimination of flare and improved lateral resolution. With the possible exception of improved resolution these advantages are not relevant to an SP microscope which looks only at surface structures but the fact that this wide field system has an almost identical response to its scanning counterpart means that the general technique may also be applied to the conversion of the scanning heterodyne interferometer already described to wide field. To this end the general operation of such a microscope system will be described.

The basic concept of a scanning confocal microscope is to image the point being

measured into the centre of a pin-hole. Contributions to the beam reflected from the sample that are not at the focal spot laterally and in depth tend to be filtered by the pinhole. A number of methods have been shown in the literature to provide a confocal response with wide field operation. One is the tandem optical microscope that scans with a rotating Nipkow disk, the problem with this method is the low light level in illumination as the pinholes must be separated sufficiently to avoid cross talk [42]. A second method is to use orthogonal coding so that the temporal coherence of adjacent pinholes is minimized, removing the cross-talk [43] while increasing light levels due to a more dense distribution. Finally structured light has also been used to provide optical sectioning and confocal response in a wide field system [44]. The technique described here may be thought of as a subset of this method, the illumination effectively has the pinholes built in.

Figure 2.17 shows the system configuration. A laser source is first expanded by a pair of lenses before striking a ground glass diffuser. The diffuser is mounted on a suitable spindle such that it may be rotated at high speed. A pair of lenses then image the speckle distribution seen at the diffuser onto the back focal planes of two matched objectives via a beam splitter. One objective focuses onto the sample to be imaged, while the other focuses onto a reference mirror. The light exiting the objectives is then recombined by the beam splitter and the surface of the mirror and objective simultaneously imaged onto a CCD camera. The importance of the speckle is two-fold; it produces wide field illumination because of the random angular spectrum in the BFP and also it provides the means of gaining a confocal

response. The speckle pattern that is imaged onto the BFPs of the objectives is Fourier transformed by them into another speckle pattern as the Fourier transform of a random distribution is another random distribution. The speckle pattern on the sample and reference are hence identical. When the image is produced the two speckle patterns will interfere but only if the speckle correlates. The individual speckles act much like pinholes as they will only interfere with their matching speckle in the other arm of the interferometer. If for example the microscope is defocused then a single speckle in the sample plane spreads out in the image plane. Only the part of it that overlaps with the matching "pin-hole" on the reference will contribute to the interference signal. Hence the response is reduced with defocus. Likewise the same localization occurs laterally so crosstalk is greatly reduced. For this system the final image is produced by phase stepping the reference mirror to extract the amplitude and phase of the interference signal. To do this an image is recorded in at least 3 different but known reference mirror positions, the envelope of the interference can then be used to produce the amplitude and phase information.

The system was shown to demonstrate the expected confocal response and allow rapid capture of amplitude and phase images over a wide area of the sample. This and the relative simplicity of the system makes it an ideal candidate for the proposed wide field SP interferometer.

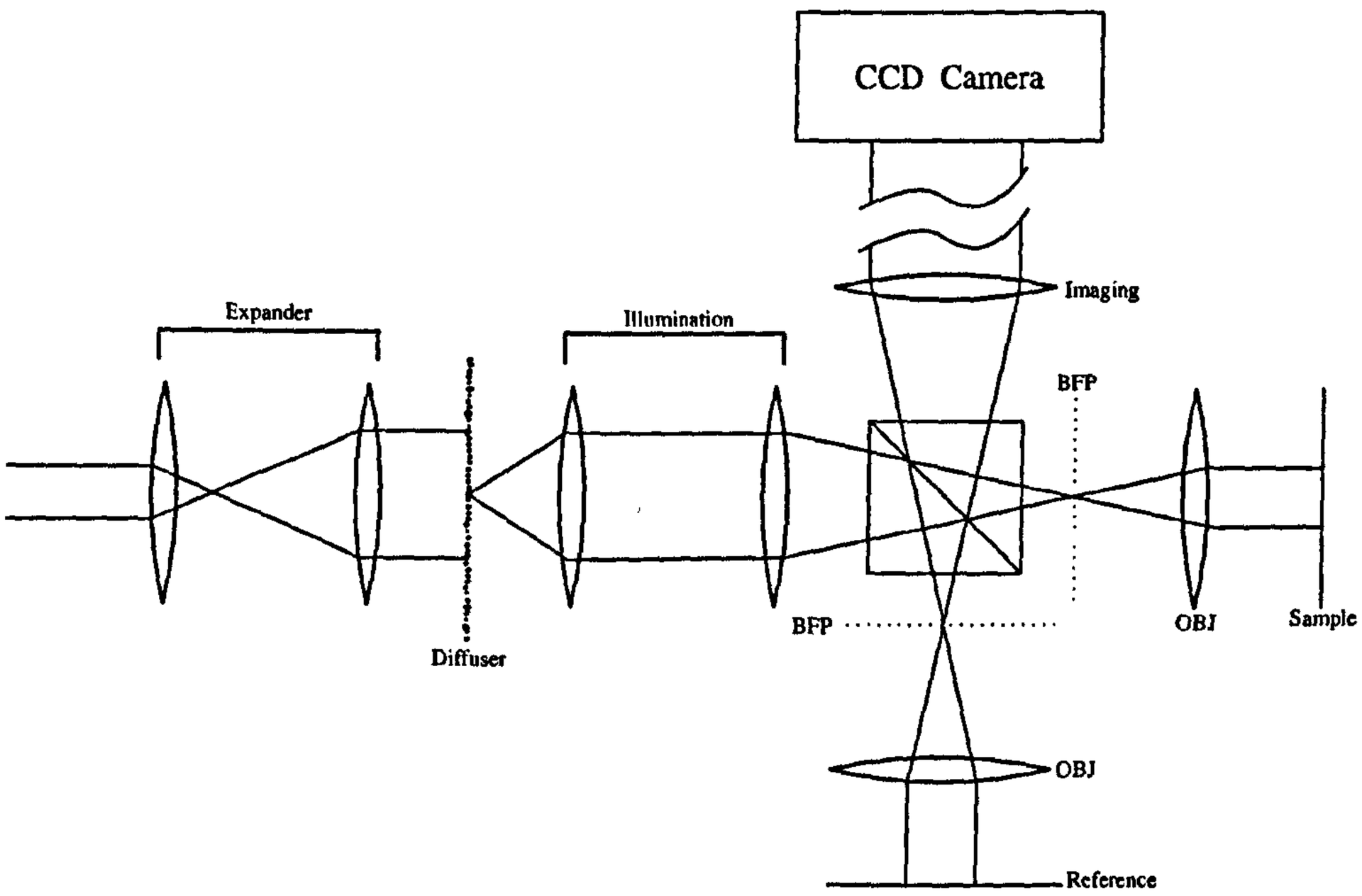

Figure 2.17: *System configuration for a wide field amplitude and phase confocal microscope with speckle illumination*

2.8 Summary

In this chapter the concept of the BFP and its relationship with the front focal plane was described. The concept of angular spectrum was also covered. The idea behind the calculation of reflection coefficients for layered media was explained and as such the concept of phase shift in a reflection coefficient could be understood. This lead to the description and explanation of the scanning system that the instrument presented in this thesis is based upon. It was shown that the phase shift associated with SP resonance was used to provide contrast in the microscope and that this only occurred at defocus. The literature shows that resolution is not lost with defocus and some suggestions are made as to why as this relates directly to the wide field version of the system. Finally a wide field microscope was described that makes use of speckle illumination to produce virtual pinholes for confocal response and wide field illumination, this microscope is the analogue of its scanning counterpart and forms the basis of the extension of the scanning SP microscope to wide field.

Chapter 3

Instrumentation

3.1 Introduction

The design and construction of a high NA microscope is not trivial, proper choice of optics and alignment is critical to good performance. In this chapter the instrument constructed for this work will be described and the decisions taken and factors considered during the design phase will be presented.

The instrument may be roughly divided into two sections, the illumination section and the imaging section. Both play an important role in the final image quality. Sections devoted to the design of both will follow a brief overview of the layout and operation of the microscope.

3.2 Overview

Before describing the design of the microscope it is worth reviewing the requirements.

The instrument is essentially the wide field speckle microscope described in ref [37] and chapter 2, it must therefore provide wide field speckle illumination of a sample and reference objective lens in a Linnik interferometer arrangement. There must also be the capability to step the reference mirror by controlled amounts to allow the use of a phase stepping algorithm to extract the amplitude and phase. On top of these general requirements are those specific to surface plasmon microscopy (SPM). Most importantly the sample objective must be capable of exciting SPs. There must also be access to the BFP to allow filtering or masking of the illumination. Finally it must be possible to translate the sample for alignment and to capture images quickly, preferably in an automated way especially with respect to the defocus for V(z) scans. With this brief in mind the instrument was designed. It may be seen in figure 3.1 and detail of the sample objective in figure 3.2.

Beginning with the illumination section, a 10mW HeNe laser with a beam diameter of 1mm strikes a rotating diffuser disk to produce a speckle pattern. This speckle pattern is imaged by lens F1 and F2 to a plane where masks may be placed. This plane is then imaged onto the BFP of the high NA oil immersion sample objective and reference objective via a non-polarizing beam splitter. The objectives then illuminate the sample and reference mirror. In each case the reflected light is imaged by the respective objective and lens F5 onto a CCD camera. The exit pupil

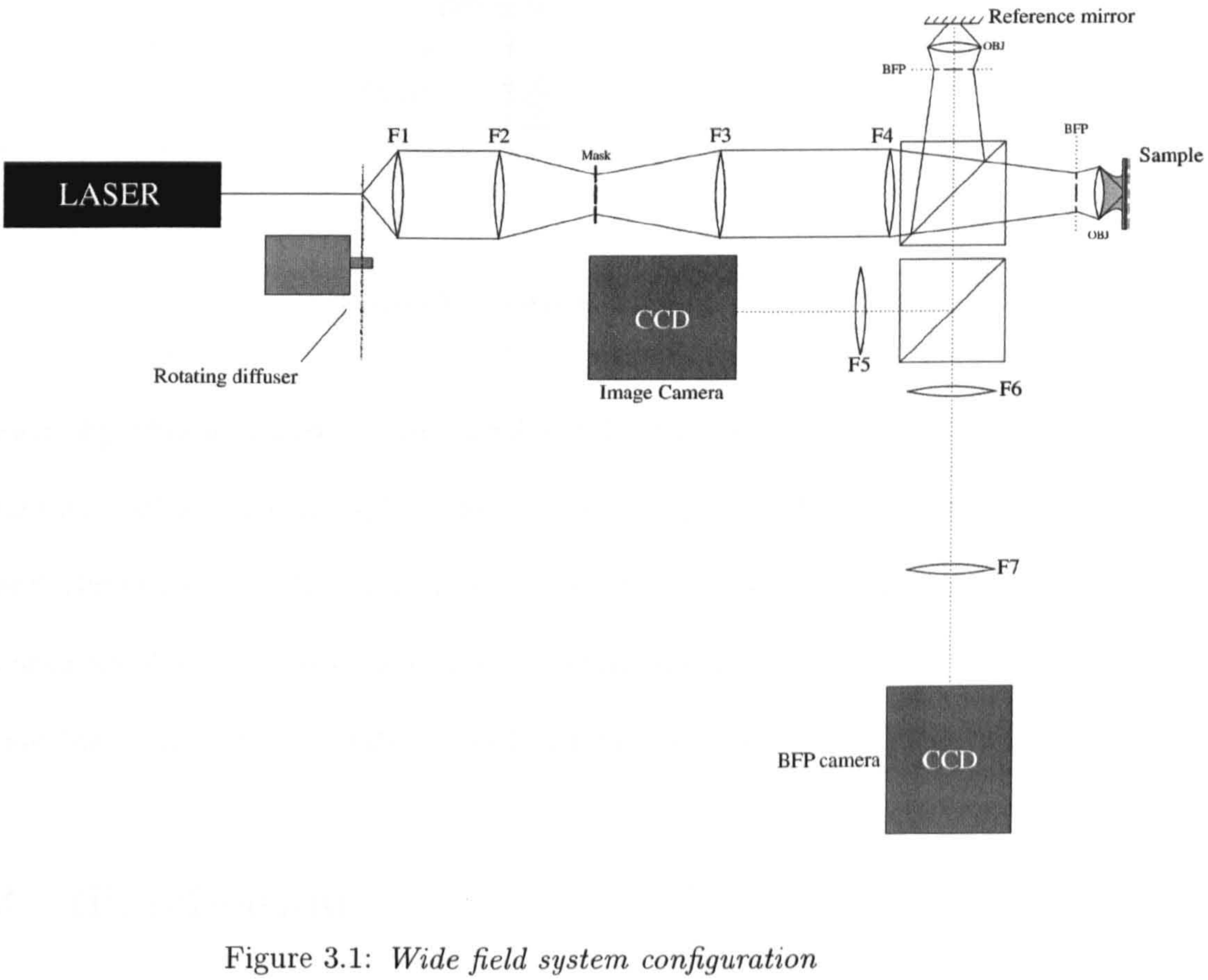

Figure 3.1: *Wide field system configuration*

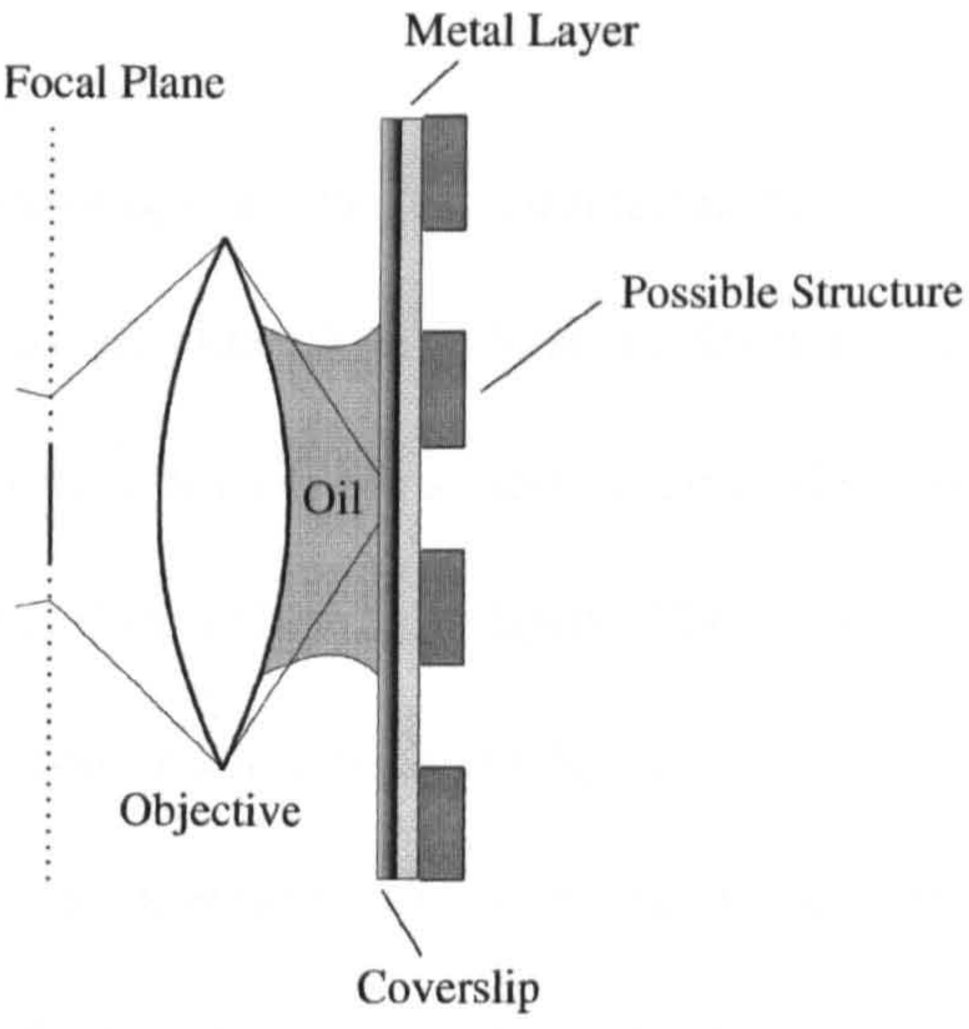

Figure 3.2: *Objective detail*

of each objective is imaged by lenses F6 and F7 onto a second CCD camera. A further non-polarizing beam splitter allows both sample and BFP imaging systems to work simultaneously. However, when imaging the BFP of the sample objective it was usual to block the reference arm of the interferometer.

The instrument will now be described in greater detail

3.3 Illumination

In order to image a structure it must first be illuminated. The illumination is one of the most important parts of this microscope as it affects the field of view, the image quality and the excitation of SPs.

3.3.1 Speckle

The operation of the microscope in the full interferometric mode relies on the confocal response provided by speckle illumination as described in chapter 2. It was therefore necessary to produce a suitable source of such illumination. Laser speckle is caused by the interference of diffuse laser light. When two plane waves interfere, fringes are normally seen but when a coherent light source is given a random phase variation the interference is likewise random as the diffuse light comes in and out of phase in a random fashion. It is the destructive interference that provides the boundaries of the "specks", that give speckle its name.

The size of the speckle observed is clearly related to its angular spectrum, large speckles will consist of lower spatial frequencies than smaller ones. The size of the speckle is dictated by how often the diffused light interferes destructively in the spatial domain. If two interfering plane waves are again considered the spatial frequency of the fringes is dependent on the rate of change of phase difference between them. Speckle might be thought of as a large set of plane wave pairs, all producing fringes in different directions. The more random the phase profile, the higher the phase gradient between these pairs and the higher the frequency of the fringes that produce the speckle pattern. The importance of speckle size and the angular spectrum of the speckle comes from the need to produce wide field illumination. The imaging arm will be set up for a specific field of view and this must be illuminated if images are to be produced. If the speckle has no angular frequencies within it i.e.

is a plane wave, then this will be focused to a spot on the sample. By adding sufficient randomness to the distribution, the field is not focused on the optical axis but spreads over an area of the sample. It is important therefore to consider this when firstly making or purchasing the diffuser and secondly when designing the imaging optics. It is quite possible for a speckle distribution of adequate angular range to be imaged with a low NA optical system such that it is filtered and can no longer produce the required illumination area.

When designing the illumination section of the system these three things must therefore be considered:

- The speckle size and hence angular spectrum.
- The full illumination of the BFP.
- The NA of the illumination optics.

The speckle size is dictated by the grain size of the diffuser and the magnification of the imaging optics. If a ground glass diffuser is used then the grain size will be controlled by the grinding medium, often a diamond paste. The speckle distribution may then be magnified by the imaging optics in order to completely fill the BFP. This is the second point, only when the BFP is completely illuminated and preferably over illuminated will the full NA of the objective be used. The amount of magnification required will vary depending on the objective but more importantly on the source. If the diffuser is illuminated with an expanded beam, less magnification is required to fill the BFP and more speckle will appear there. The speckle will therefore

have a higher angular spectrum at the BFP and produce a wider illumination area. If the beam diameter is reduced the magnification needs to be increased and less speckles will be seen in the BFP, this corresponds to a lower angular spectrum and smaller field of illumination. Finally the NA must be sufficient to ensure the angular spectrum of the speckle is not overly degraded.

3.3.2 The diffuser system

As was mentioned above, diffusers can be produced from glass and indeed plastics such as Perspex. These can be ground using a suitable diamond paste to give the desired amount of diffusion i.e. to provide just sufficient diffusion to remove the zero order and ensure sufficient numerical aperture at the back focal plane. Any further diffusion beyond this point only reduces the amount of light that may be collected by the optics. Originally a 5mm thick Perspex disk was used but severe vibrations at higher rotational speeds made interferometry impossible despite the assembly being mounted on vibrational insulators. The disk was then replaced with a polycarbonate copy of only 1.5mm in thickness. The reduced thickness and mildly flexible nature of the polycarbonate allows the disk to flex, neutralizing imbalances and instabilities. This leads to a diffuser set up that produces much less vibration. One drawback of this is that the undulation of the disk does produce more turbulence in the surrounding air, another factor that can effect interferometric systems. To reduce this effect a housing was mounted around the disk with apertures to allow light passage. An interesting side effect of using the polycarbonate disk is the effect

it has on the polarization of the light. The HeNe laser used was linearly polarized but on passing through the diffuser became unpolarized. This is thought to be due to the long polymer chains in the plastic creating birefringence, the effect was obviously averaged by the rotation to give pseudo-random polarized light. For most of the experiments performed a linear polarizer was used to provide pure linearly polarized light with the advantage that the plane of polarization could be altered using only the polarizer. The laser did not need to be rotated, nor did a 1/2 wave plate need to be employed. Despite the relatively high performance of the disk in terms of the diffusion properties and vibration produced, improvements were sought. A polymer film used for the production of PCB masks was tried, this film is approximately 0.1mm thick, is flexible and is diffuse. The material allows a small amount of zero order through causing a small bright spot to be detected in the centre of the BFP images however the effect on sample imaging is negligible especially when a mask or interferometry is employed. This disk provides almost vibration free rotation at higher speeds than before (due to a lower load on the motor) and also does not require careful machining or alignment, the disk being cut to shape using scissors.

Once the source had been produced the optics could be chosen to image the speckle onto the BFPs of the objectives. As has already been mentioned it is important to fill the aperture to provide full NA illumination. It was thought prudent to overfill the BFP by a factor of around 1.5 as the naturally Gaussian nature of the illumination might otherwise effect the imaging. The lenses used for this purpose were all 25mm diameter doublets. These provide aberration free performance over

the range of NA required for the illumination and are relatively economic. The magnification was split between the two parts of the illumination section with a greater amount being performed by lenses F1 and F2 so that F1 could be of lower focal length for good light collection.

3.3.3 Objective selection

Before moving on to the imaging section of the system the objectives used in the system will be described. The objective used in the sample arm of the microscope was a Zeiss α PlanFLUAR 100X 1.45NA for oil immersion. The α stands for the optimal NA giving the highest resolution possible with a 100X objective and oil of refractive index 1.518. The oil used was Zeiss fluorescence free Immersol F. Fluar refers to the fact that the objective is suitable for fluorescence imaging, a useful feature for some of the other work carried out in the group. Plan refers to the flat field of view. The objective was chosen because it is suitable for most non-aqueous imaging and also for some aqueous imaging when special layers are used. The layers produce guided waves rather than SPs but can be dependent upon SP propagation and so are of interest in the field of SPM as well as in their own right.

The reference objective is another point of interest. It is traditional to produce Linnik interferometers with matched objectives. This is obviously the ideal but when dealing with high NA objectives the economic considerations come into play. Essentially all the reference objective must do is Fourier transform the speckle distribution on the BFP and then inverse Fourier transform it after reflecting on the

mirror, in other words it must reverse the direction of the beam without the phase shift associated with reflection. Assuming the objective is of high enough NA to retain the modest angular spectrum requirements of the speckle illumination and does not produce any serious aberration then a low NA objective should perform the task adequately as indeed it did. An Olympus 0.13 NA infinity corrected objective was chosen due to availability.

3.4 Imaging

The mechanical and automation aspects of the sample and reference mirror will be covered later and so the imaging section of the instrument will be described. Considering first the sample imaging optics. The image that is to be captured by the CCD camera can be thought to comprise of a set of overlapping point spread functions. The pixels of the CCD camera sample this image at discrete points. The sampling theorem should therefore be applied. That is to say that at least 4 pixels should be allowed for each point spread function. Any less than this and the image will be undersampled and will not represent the full NA of the objective. From this criterion the maximum magnification can be determined from the field of view that it corresponds to. Once the field of view is known the calculations to find the required angular spectrum of the illumination and NA of the illumination optics are trivial.

Imaging the BFPs of the objectives was considered essential, most importantly

the BFP images may be used for the design of masks and for the registration of the masks with the BFP resonances. Secondary to this is that the BFP is an excellent aid to alignment, showing a response even when no image is visible as long as SPs are being excited. The images produced are also of interest in their own right as they give insight into the effects of the imaged structures on SP excitation that images cannot. The choice of lenses F6 and F7 was not critical and chosen to simply use as much of the CCD area as possible.

Now that the optical elements of the design have been described, attention will be switched to the collection of data from the system.

3.5 Automation and control

The instrument described consists of several items that must interface with the control PC. This can be for reasons of data capture, alignment or spatial scanning. In this section the components that allow this will be briefly described.

3.5.1 Motion control

These components allow precise positioning for alignment and scanning capabilities.

Reference mirror

The reference mirror was mounted in a kinematic stage to allow angular adjustment and alignment but it also needed to be adjusted for focus with the reference objective.

A boxed or partially boxed system makes this difficult so the mirror was mounted on a small servo and leadscrew type stage with a resolution of 0.1μm. The mirror also needed to be stepped distances of around 0.08μm for the phase-stepping algorithm, the motorized stage was not capable of this and so a single axis piezo stage with crossed roller bearings was added. This device used strain gauge feedback and servo control to ensure the correct position of the mirror. The high quality bearing system also ensures that the motion is in a single axis. The stage has a range of around 15μm and so the motorized stage was still required for general alignment.

Sample

For the purpose of alignment and also to allow scanning in defocus, a means of moving the sample with respect to the objective under computer control was required. A second motorized stage was decided upon as it gives reasonable resolution and also allows the sample to be withdrawn a large distance from the objective, allowing the sample to be removed without a danger of changing the objective alignment.

3.5.2 Camera control

CCD cameras were used to capture images of sample and back focal plane. These were connected to an image capture card in the control PC via a switch box for camera selection. A serial link was also used to modify the shutter speed so that the camera was not saturated.

3.5.3 Automation and data capture

All the components of the system that have just been described were controlled via a single visual C++ application written specifically for the task. This communicates via serial link to the camera and piezo stage and by motion control cards to the two servo stages. Images could be captured from the frame grabber card as well as displayed live. With all the components automated it was a simple task to write experiment specific algorithms that synchronize motion and data capture.

3.6 Mask Construction

To enable certain areas of the back focal plane to be blocked masks were manufactured. As different samples require differing masks in-house processes were developed, otherwise it would have been possible to have the masks printed onto glass as per lithographic artwork. A number of methods were tried, the most versatile of which was photo etching. The process involves the coating of thin metal sheet with a photo resist, this is then exposed to ultraviolet radiation through a mask printed with a laser printer on to a suitable film. The photo resist is then developed, softening the unexposed areas. The softened photo resist falls away from the metal surface leaving a pattern of photo resist on the surface of the metal. The metal sheet could then be placed in an acid bath where the exposed metal was etched away. In theory the best results can be had from etching the mask on both sides of the metal sheet. This is because the etching is isotropic and causes undercutting, by etching from

both sides the etching time is approximately halved and the undercutting reduced. It was found in practice to be difficult to accurately align the masks and so single sided etching was used on 0.1mm brass shim with an adhesive tape backing. This proved to be effective and undercutting could be corrected by adjusting the artwork.

A second method of mask production was also employed, this is less versatile but for some of the masks gave better results, especially those with small apertures. These masks were machined from brass in a watchmakers lathe. Using micro drills centralized apertures down to 0.1mm could be produced. The masks consisted mainly of small disks of around 3mm in diameter with or without an aperture. The machined disks were glued to a 25mm diameter cover-slip with epoxy to allow them to be mounted in conventional lens mounts. In some cases when a transparent annulus was required the mask was made in two parts, a central disk and an outer ring. After the inner ring was bonded to the cover-slip the outer ring could be aligned using a stereo microscope before being glued in place.

Both of these methods produced adequate results but for totally flexible masking a transmissive LCD might be used in the BFP to perform filtering. A slightly slower method would be to utilize a desktop slide printer. These can produce high resolution images onto film very quickly. Software could be created to semi-automate the design process. The user could select points on the back focal plane image produced by the system to define regions where the light should be blocked. For well established sample types it would also be possible to fully automate the mask production by using edge detection techniques on the BFP images.

The masks were mounted on a manual (x,y,z) positioning stage for adjustment of focus and position.

3.6.1 Optical alignment

In high NA optical systems, errors in alignment tend to be amplified and any interferometer system can be sensitive to surrounding vibrations and air flow. The mechanics of the optical system and its alignment are therefore very important.

This system was built on a standard optical bread board. All optical components were then mounted onto this. Extensive use of magnetic mounts was made in the illumination section of the microscope. These mounts allow optical components to be removed from the system quickly and replaced with precision. A beam expander was also set up on such a mount. Once the laser was made parallel to the breadboard then this beam expander could be inserted and aligned. It could then be added or removed as required. Lenses F1 and F2 were aligned as a beam expander using a shear-plate to check for collimation. Then lens F3 could be aligned in the same way with F1 removed. Finally F4 was added with F2 now also removed. Both objectives were aligned with only F4 and the beam expander in the illumination arm. The expanded beam focused into the BFP of the objectives should produce a collimated beam coming out of the sample/mirror side of the objective on the optical axis when aligned correctly. In reality the beam is not collimated especially for the high NA objective. In this case the spot size was minimized on a distant target. The angular alignment of the objectives was also important. They were held in mounts that kept

their axis parallel to the optical bench thus setting one angular axis. The second axis was set by fixing a coverslip to the back of the objective mount with a drop of oil. This produces a back reflection that could be aligned with the incident beam using an iris but also allowed light to propagate through for the positional alignment. The imaging optics were set up in a similar way to the illumination optics. A mirror was placed in front of the sample objective and aligned such that a collimated beam into the objective (all imaging optics removed) would produce a collimated beam coming out. Then if F4 was added the outgoing beam would be focusing and F5 could be aligned. F6 was initially aligned as for F5, F6 was aligned as for the first optics. Camera positions were defined by ensuring that F6 and F5 were illuminated with a plane wave, then the CCD cameras were monitored to ensure they were at the focus. The final stage of the alignment process was to ensure that the two speckle patterns from each objective were correlated. This is most easily done by looking at the sample image; with the system aligned as described only moderate adjustment of the reference mirror should be required to obtain fringes. The most important adjustment is in fact the focus of the sample objective, this needed to be within about 1μm of the focus to get good contrast. Once fringes are observed then the reference mirror can be adjusted to produce a single large fringe. This can be seen most easily by tapping the optical bench. A final point is that the system was found to be highly sensitive to airflow. The air conditioning system was turned off and tubes were added to the sample and reference arms to prevent the optical path lengths from being altered by airflow.

The system described in this chapter is the final embodiment for wide field interferometric imaging, however, the microscope may also be operated in two other modes when the reference arm is blocked. Chapter 4 shows how the system may be used for sensing homogeneous samples by using the back focal plane to deduce layer thickness or refractive index. Chapter 5 shows how the imaging arm of the system may be used in a standard microscopy mode allowing, with the use of filtering, good contrast and resolution.

These additional modes of operation consist of the component parts of the full instrument and each benefit from the advantages of speckle illumination. They offer in themselves useful ways of interrogating the sample as stand-alone systems or may be used in conjunction with the final implementation to form a multipurpose microscope/sensing system.

Chapter 4

Back focal plane imaging

In chapter 1 various microscopy and sensing methods that utilize the BFP distribution of high NA oil immersion objectives were described. These methods in one way or another measure the position of the resonant dips. One of the major problems encountered by others while trying to take measurements and produce images was the existence of coherent noise. As laser light is highly coherent, interference is usually seen due to spufious reflections within optical components. This may be minimized by the use of anti reflectance coatings but it will always be present to some degree. An example of the kind of image that is produced with coherent light is shown in figure 4.1. It was produced with this system by removing the diffuser before replacement with a beam expander. The many overlapping fringes visible make taking measurements difficult.

The imaging techniques described in the literature all use collimated illumination to interrogate a small area on the sample. The microscope presented in this thesis

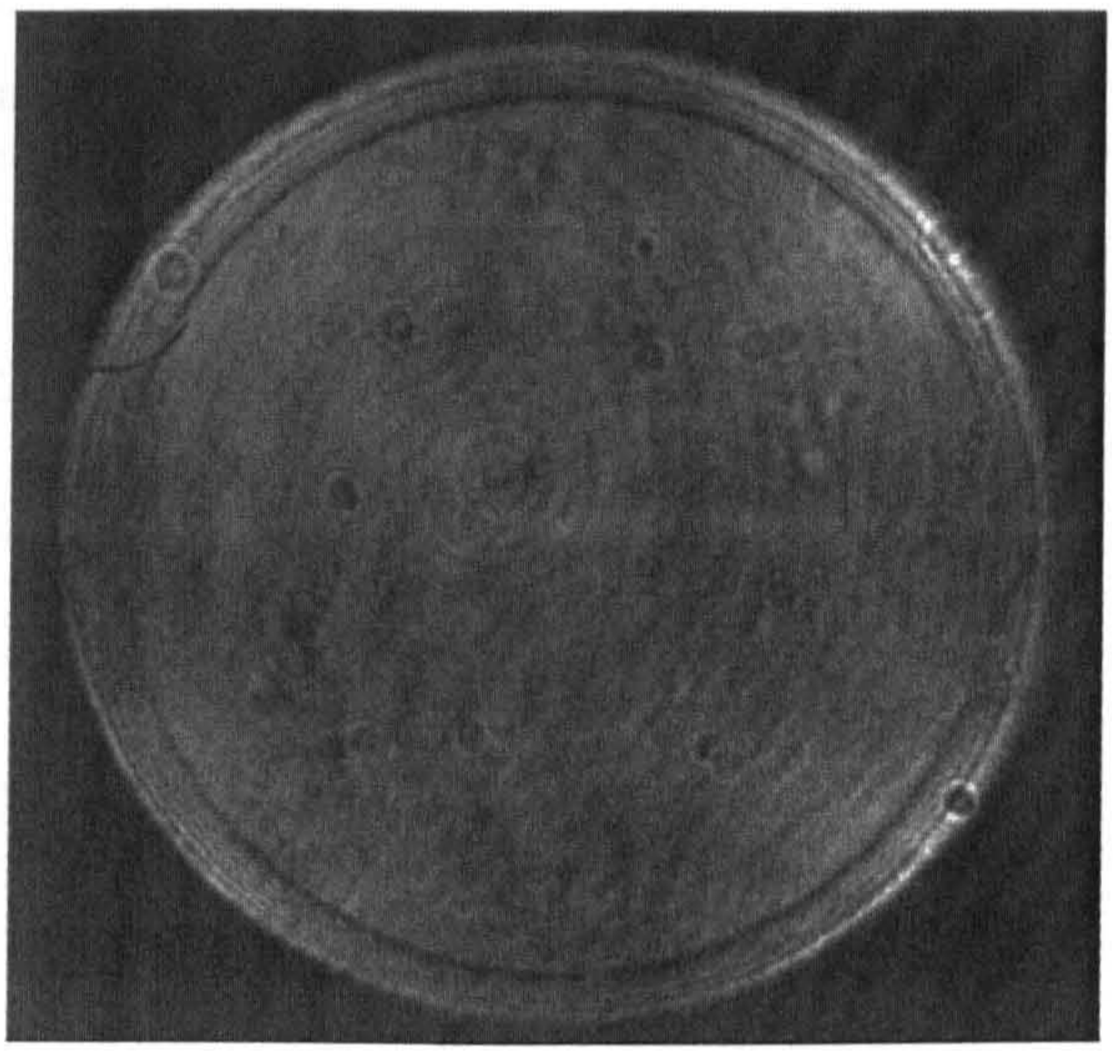

Figure 4.1: *A typical BFP image produced with coherent illumination*

produces a wide field of illumination and so the BFP represents the entire structure illuminated, for this reason measurement of the BFP could not be used in an imaging system apart from for low resolution scanning.

In sensing applications the size of the area interrogated is less important. For the microscope system described here the field of illumination is approximately 100μm which is still quite small for sensing applications. For plane samples the BFP of this microscope shows reflectance versus angle for s and p polarizations simultaneously and also provides high dynamic range when taking measurements. The advantage in this configuration is that the averaged speckle illumination removes coherent noise producing BFP images that are much sharper than those seen in the literature.

In this chapter a number of BFP images for a variety of planar samples will be shown. The reference arm of the system was blocked for all measurements.

Case	Overlayer thickness	Water backing
1	air	no
2	400nm SiO_2	no
3	400nm SiO_2	yes
4	520nm SiO_2	yes
5	520nm SiO_2	no

Table 4.1: *Summary of samples interrogated*

Table 4 summarizes the measurements taken and the samples used. Each sample consisted of a cover slip with a 43.5nm thick layer of gold deposited upon it before a further layer consisting of air or SiO_2. In some instances the rear cavity of the sample holder was also filled with water.

To begin with, let us consider case 1, a plain gold sample of 43.5nm thickness. The back focal plane distribution may be seen in figure 4.2. A single resonance is seen on each side of the BFP, this corresponds to p-polarized light. That is the input polarization lies horizontally to the page as it will for all further images. The resonant dips are found to be clear and sharp and easily measured if needed. Figure 4.3 shows a cross-section taken from the image that effectively shows $(R_p)^2$. The x-axis of the graph has been scaled to show the angle corresponding to the radial positions in the BFP. This plot may be compared to that seen in figure 1.3 seen in chapter 1. The angle at which the dip occurs is around 0.5 degrees higher than that expected. This is probably due to the difficulty in defining the exact aperture of the

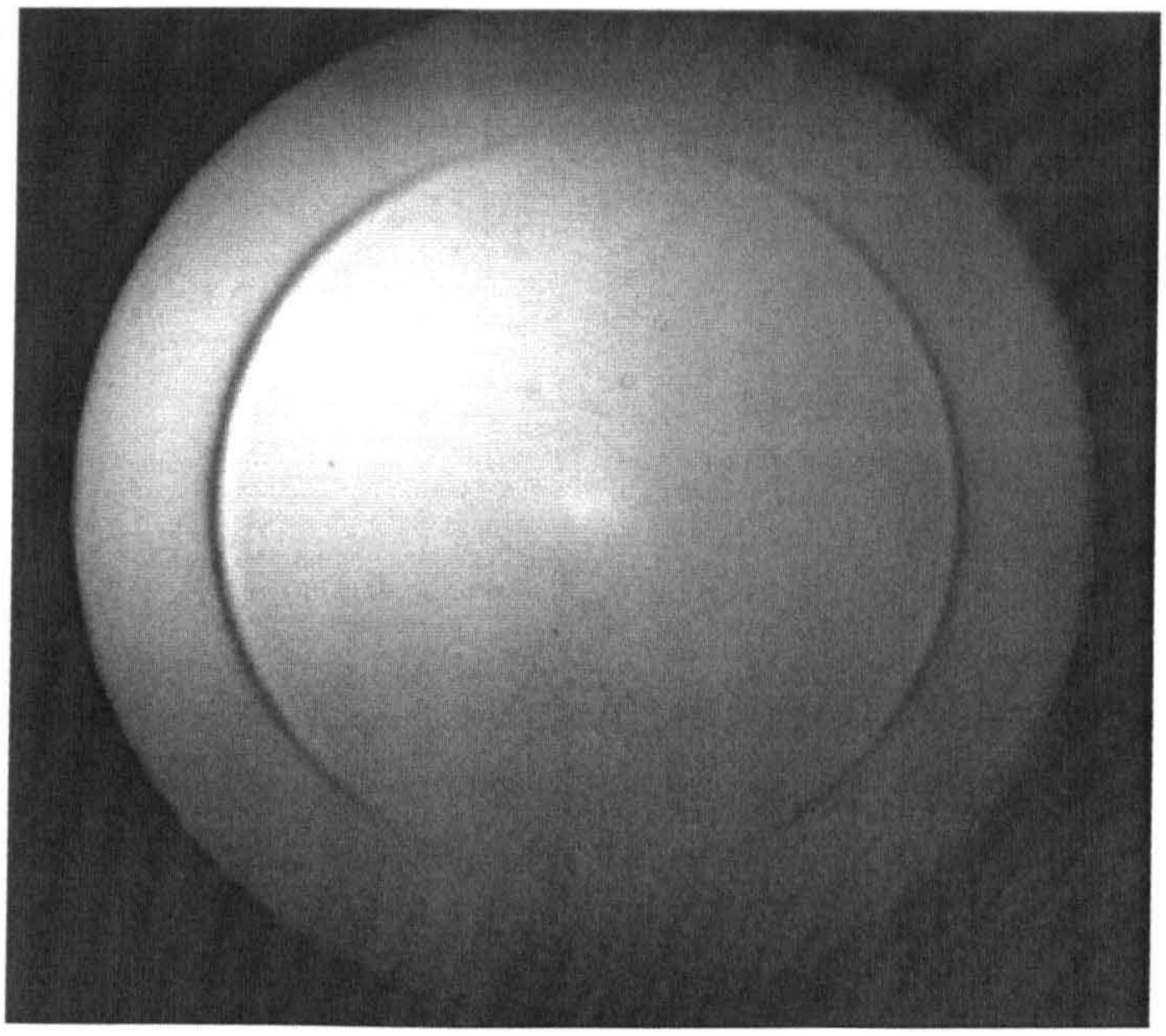

Figure 4.2: *BFP of planar 43.5nm gold sample*

BFP and shows the importance of reference samples if absolute measurements are to be taken. Results could be improved still further by using a 12-bit CCD camera.

For cases two to five the sample has a layer of $Si0_2$ applied to the gold. In order to understand the origins of the resonances it is useful to consider the resonances observed at intermediate layer thicknesses. Samples for these thicknesses were not available but are easily simulated and results for p and s-polarizations may be seen in figures 4.4 and 4.5 respectively. The resonance in the p-polarized case can be seen to increase in angle and width with increasing layer thickness until it eventually disappears. Later at a layer thickness of around 250nm a new resonance comes into existence. It will be noticed that it appears at the critical angle which suggests that

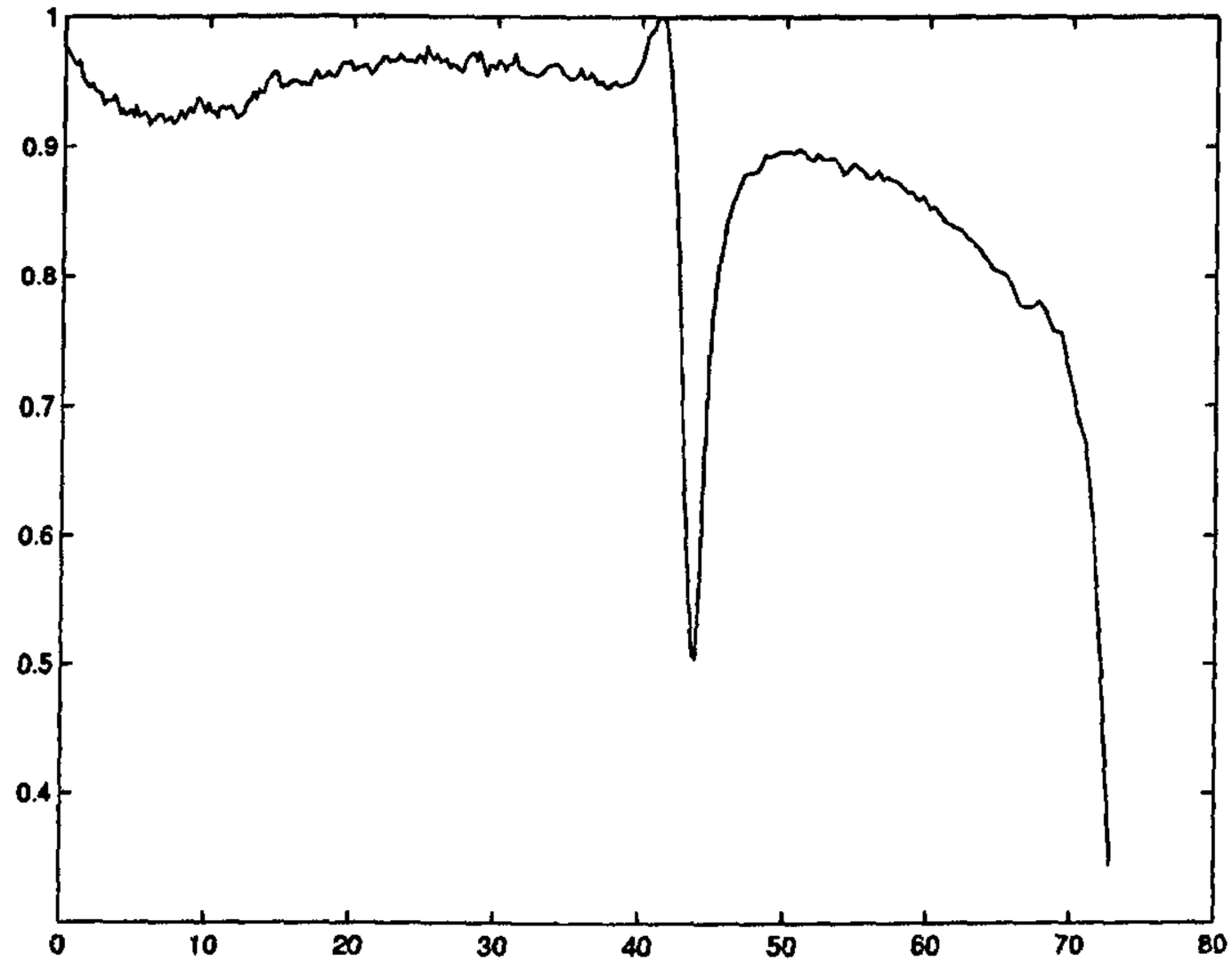

Figure 4.3: *Experimental plot of $(R_p)^2$ for a planar 43.5nm thick gold sample*

is is a guided wave existing in the additional layer. For s-polarization, figure 4.5, a resonance is not seen until there is a reasonable layer thickness. This is again a guided wave mode as SPs cannot be excited with s-polarized light. As with the p-polarized SP resonance this resonance increases in angle but becomes more sharp. At around 420nm layer thickness a second resonance comes in to existence and again begins to move to higher angles.

The results of simulation can now be compared with the measured BFP distributions. Figure 4.6 shows the back focal plane distribution of case 2, a 400nm thick overlayer and no water backing. Figure 4.7 shows simulated plots of the reflected intensities and these can be seen to correspond well with the images although the second resonance in the s-polarized direction is not visible, this is possibly the re-

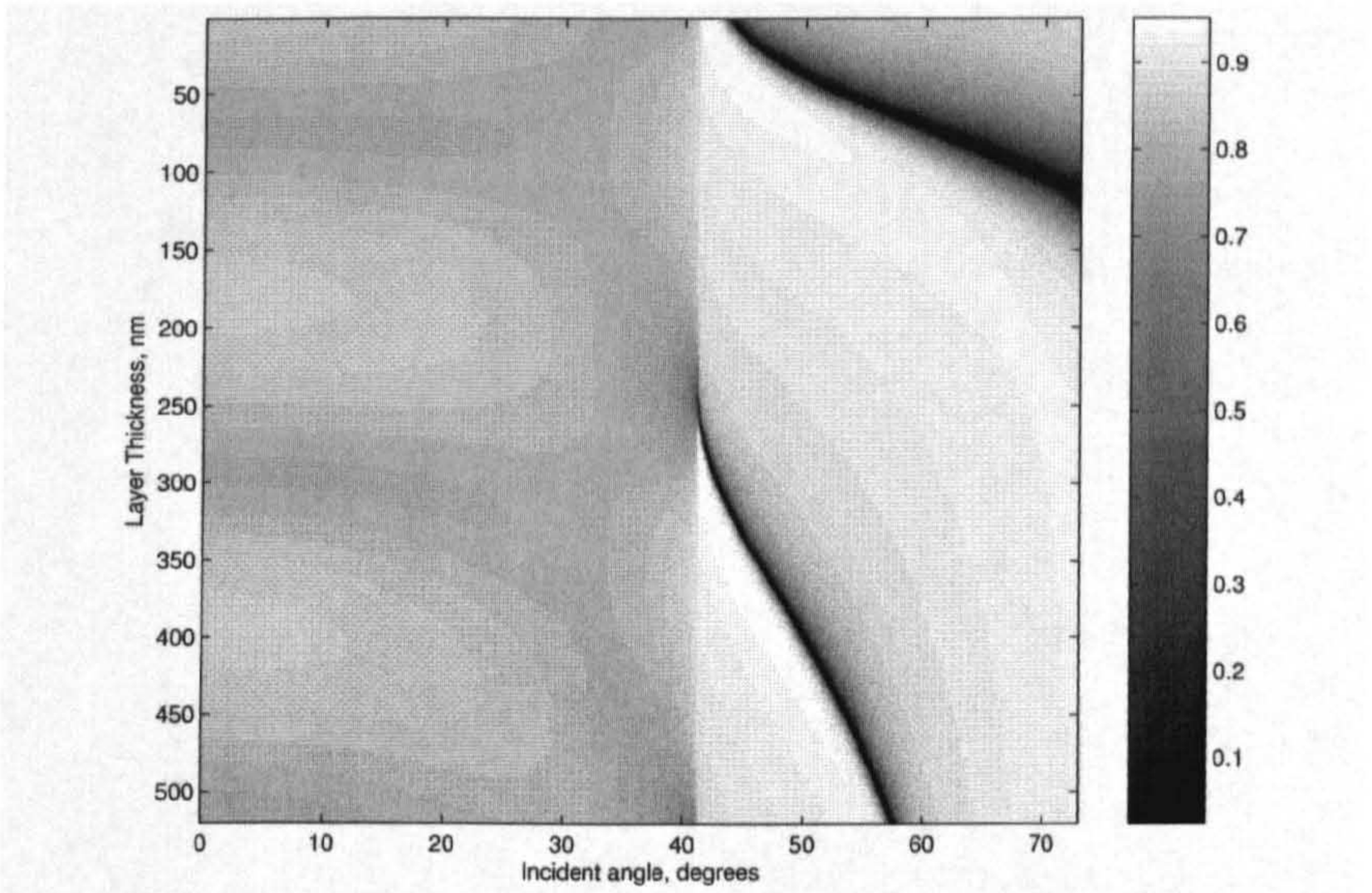

Figure 4.4: *The reflection coefficient Rp plotted as a function of incident angle and layer thickness*

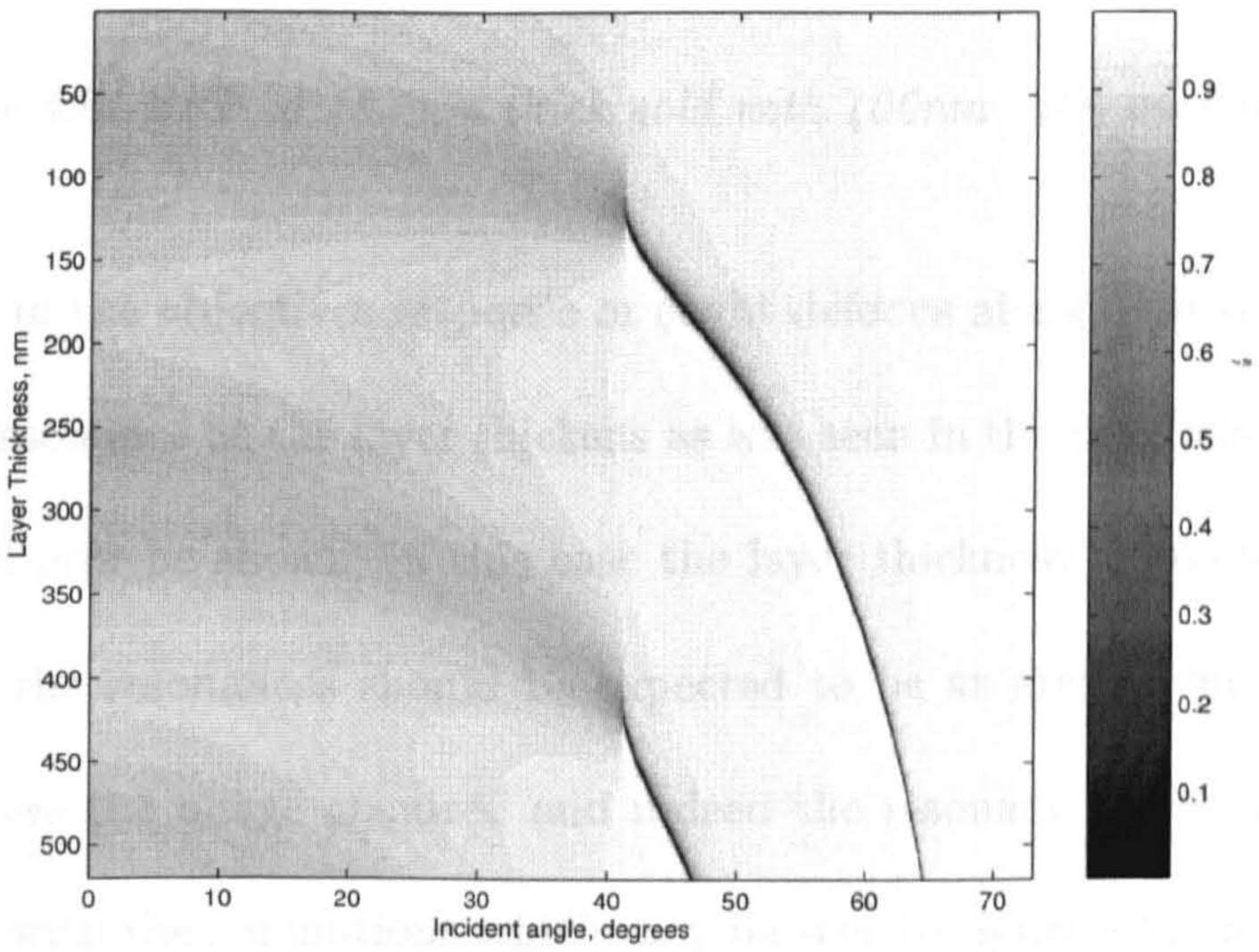

Figure 4.5: *The reflection coefficient Rs plotted as a function of incident angle and layer thickness*

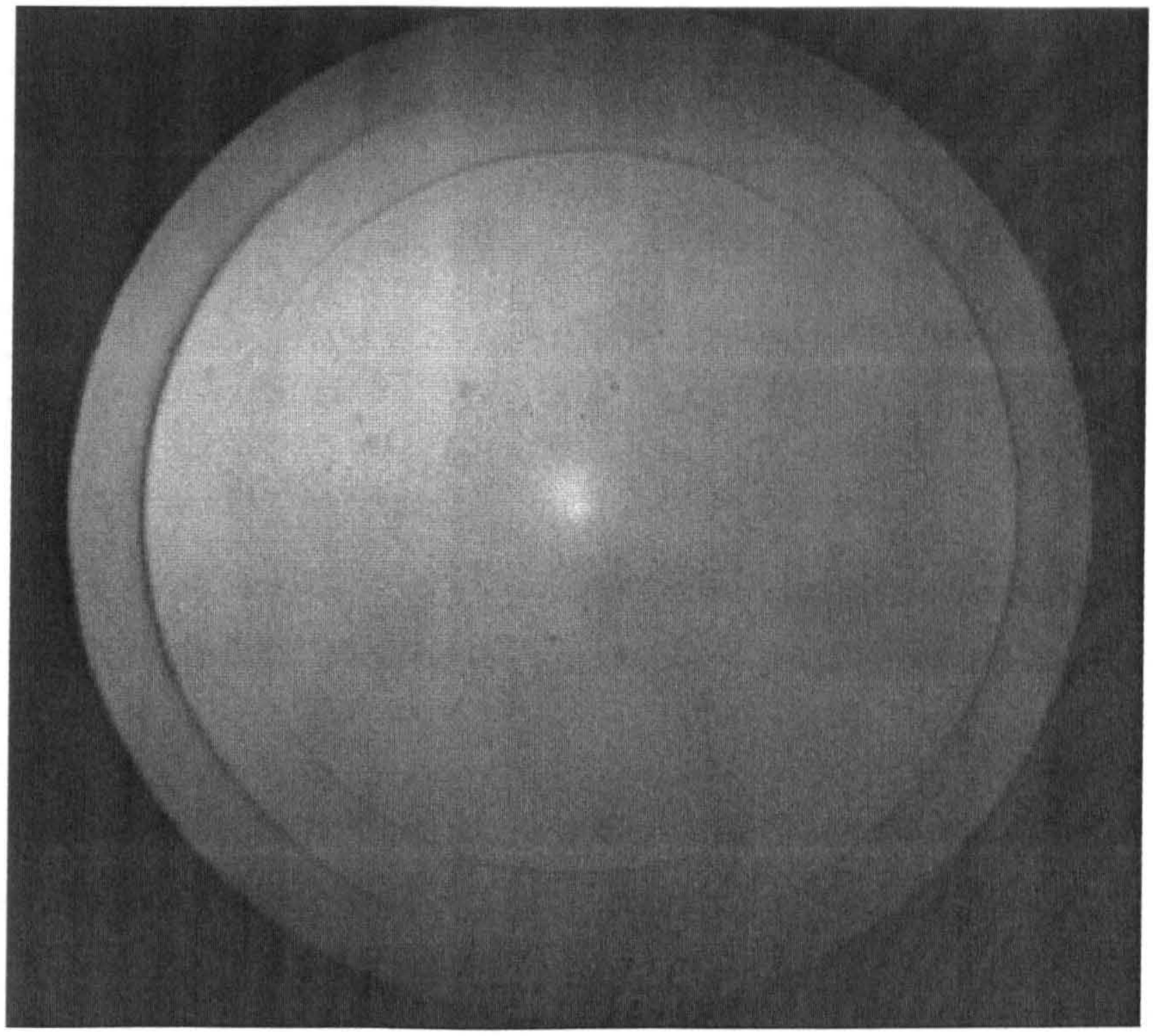

Figure 4.6: *BFP of 43.5nm thick gold with 400nm SiO_2 over layer*

sult of roll-off in the objectives response or slight defocus along with the decreasing width of the resonance as the layer thickens as was seen in the previous simulations.

Case 4 will now be shown, in this case the layer thickness is greater than that of case 2 and the resonances should be expected to be at greater incident angles. Figure 4.8 shows the image acquired and indeed the resonant angles are increased in accordance with the simulations which may be seen in figure 4.9. In fact, a trace of the outer s-polarized resonance may be seen in this image. As this is at a greater incident angle than for the 400nm layer case it does suggest that problem may not

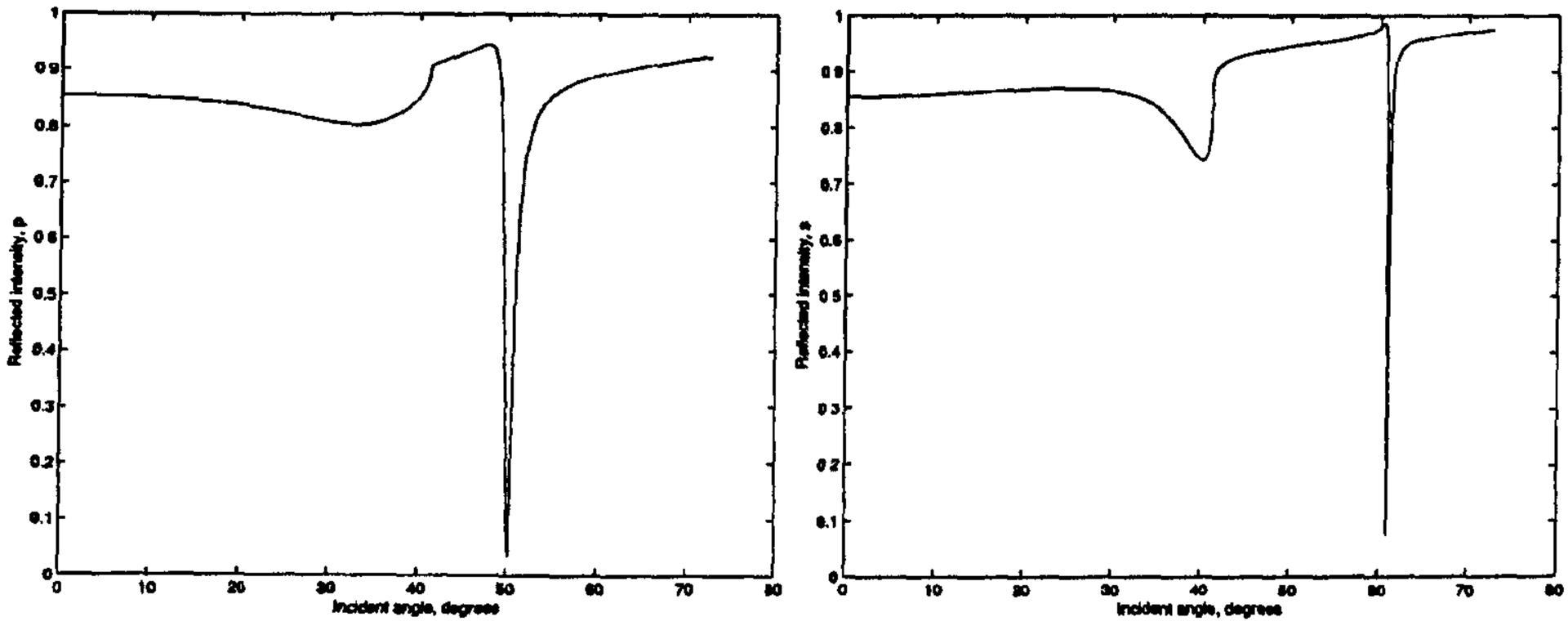

Figure 4.7: *Simulated plots of* $(R_p)^2$ *and* $(R_s)^2$ *for 43.5nm thick gold with 400nm* SiO_2 *over layer*

be one of roll-off but rather defocus or poor illumination.

The sample holder was designed such that the rear cavity could be flooded with fluid. This was done with distilled water and results for both samples recorded. As before it is useful to understand the origins of the resonances observed. Figure 4.11 shows the p-polarized case. The plasmon resonance is almost completely suppressed and in practice is not observed at zero layer thickness. The critical angle for the system is increased by the water backing and this is indicated by the general increase in reflected intensity at around 60 degrees. When the layer thickness gets to around 400nm a resonance occurs at the critical angle and increases in angle with layer thickness. This is again a guided wave resonance. Figure ?? shows the the results for s-polarized light. In this case the resonance occurs at a lower layer thickness and appears to be much sharper.

The experimental results for a layer thickness of 400nm and 520nm with a water

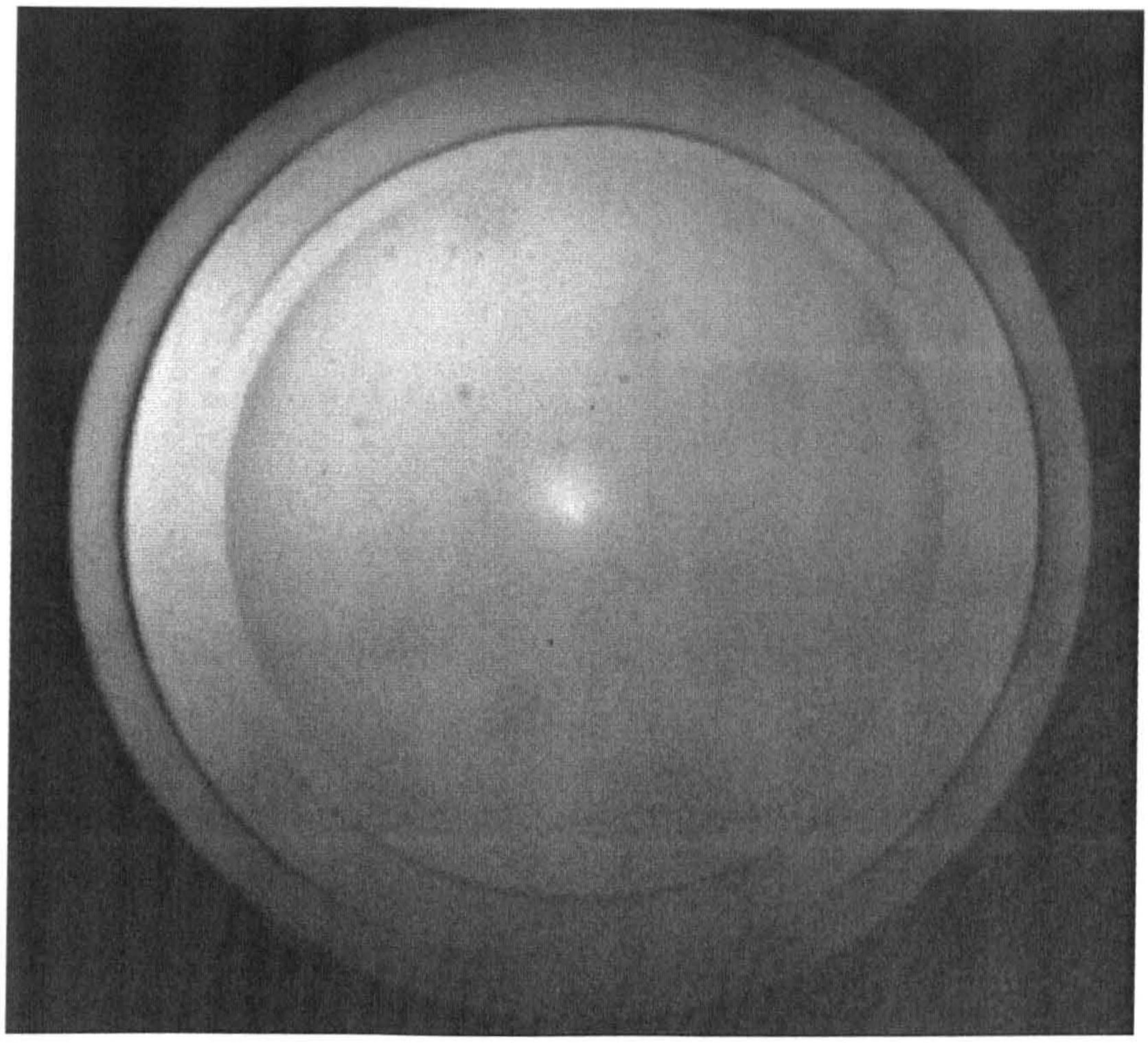

Figure 4.8: *BFP of 43.5nm thick gold with 520nm SiO_2 over layer*

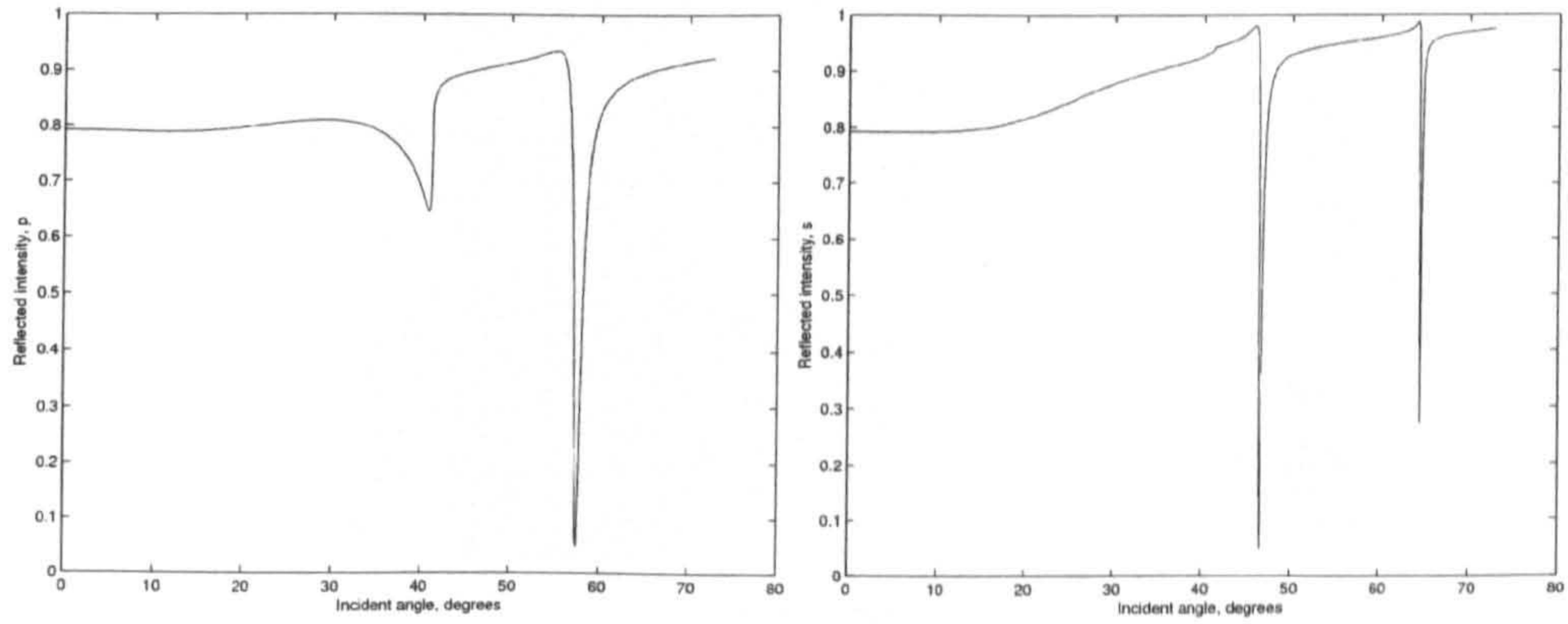

Figure 4.9: *Simulated plots of $(R_p)^2$ and $(R_s)^2$ for 43.5nm thick gold with 520nm SiO_2 over layer*

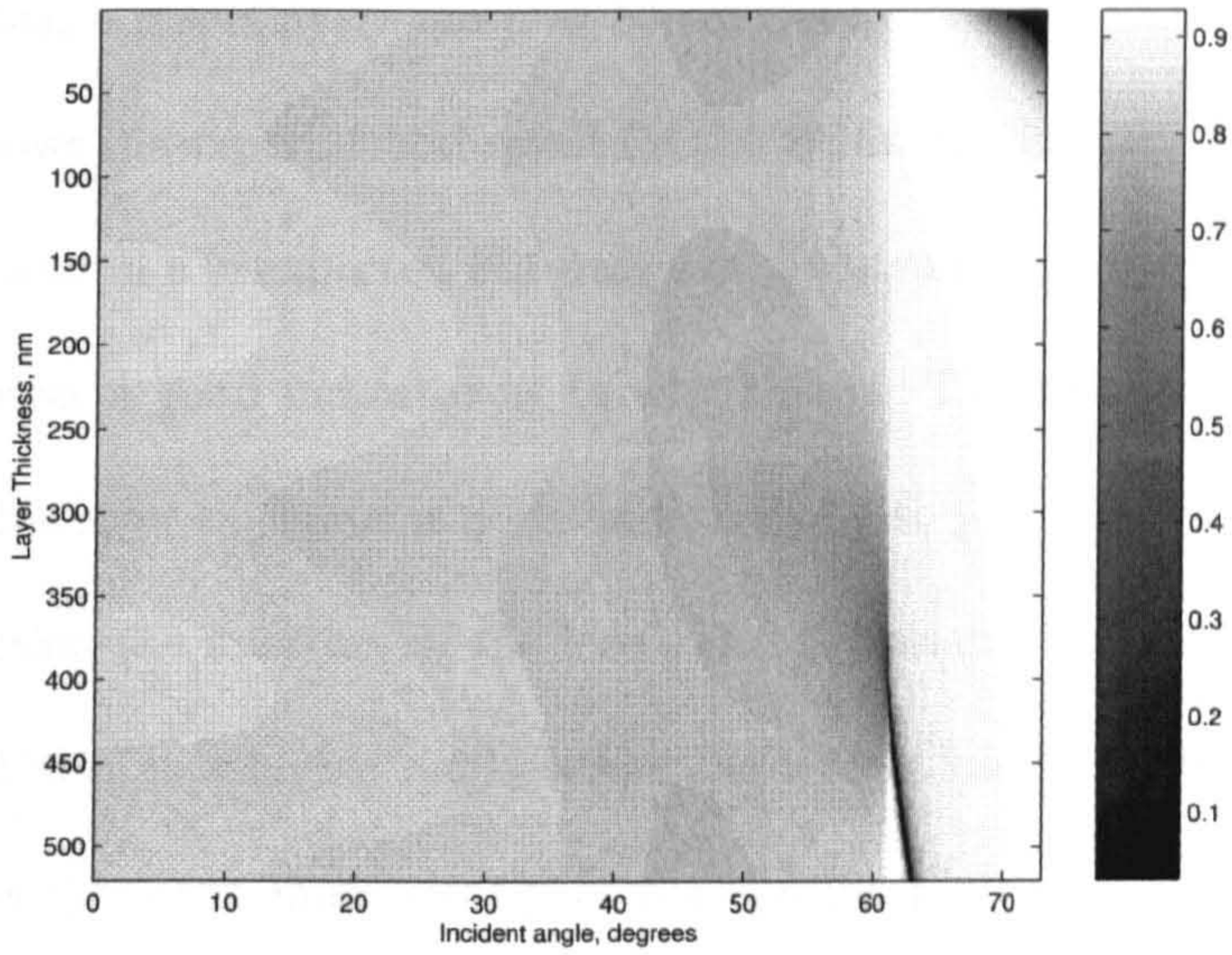

Figure 4.10: *The reflection coefficient Rp plotted as a function of incident angle and layer thickness for a water backed sample*

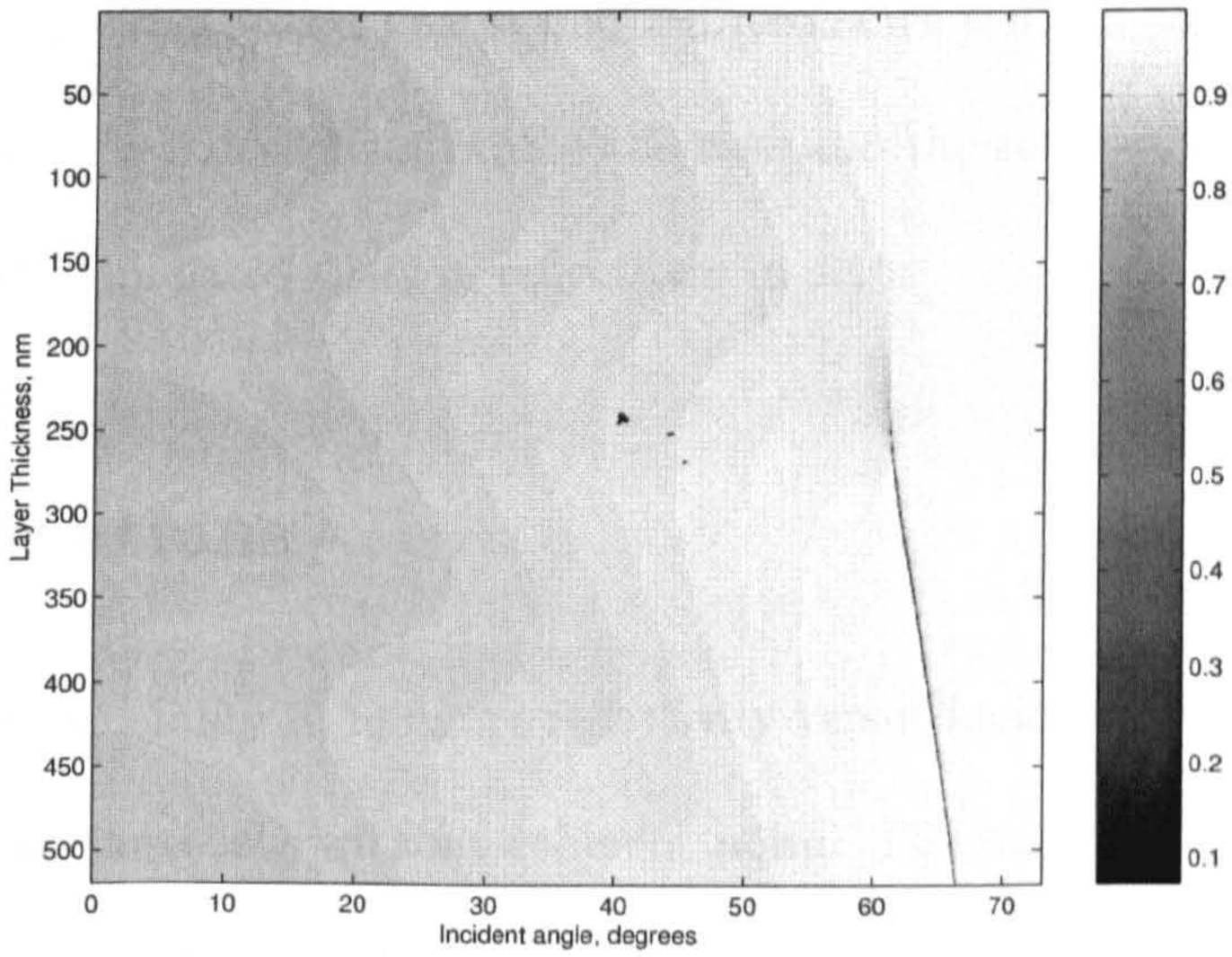

Figure 4.11: *The reflection coefficient Rs plotted as a function of incident angle and layer thickness for a water backed sample*

backing, cases 3 and 5 respectively can now be compared with the simulation.

Figure 4.12 shows the experimental result for the 400nm thick layer. A resonance in p-polarization and in s is expected but only the p resonance is seen. Looking at the simulations gives a good indicator as to why this is. The resonance in the p-polarization for this layer thickness is quite wide and is also just beyond the critical angle and well within the aperture of the lens. The s-resonance on the other hand is very sharp and also at a higher angle where the lens is less likely to work well. Figure 4.13 shows this even more clearly as the specific plots of $(R_p)^2$ and $(R_s)^2$ against incident angle can be seen.

Turning now to case 5, where the thickness of layer is now increased to 520nm we should expect much the same except the resonance angle of the p-polarized resonance should have increased. The s-polarized resonance is again likely to be too fine to observe. This is indeed found to be the case and the result may be seen in figures 4.14 and the simulated plots of reflectance in 4.15.

4.1 Observations

The system shows the ability to measure reflectivity versus incident angle for p and s-polarizations simultaneously without coherent noise. The images are very sharp making sensing possible if the BFP is calibrated and also could allow low resolution imaging by scanning. In fact because the light budget for the microscope was good it would have been possible to increase the magnification of the BFP imaging arm to

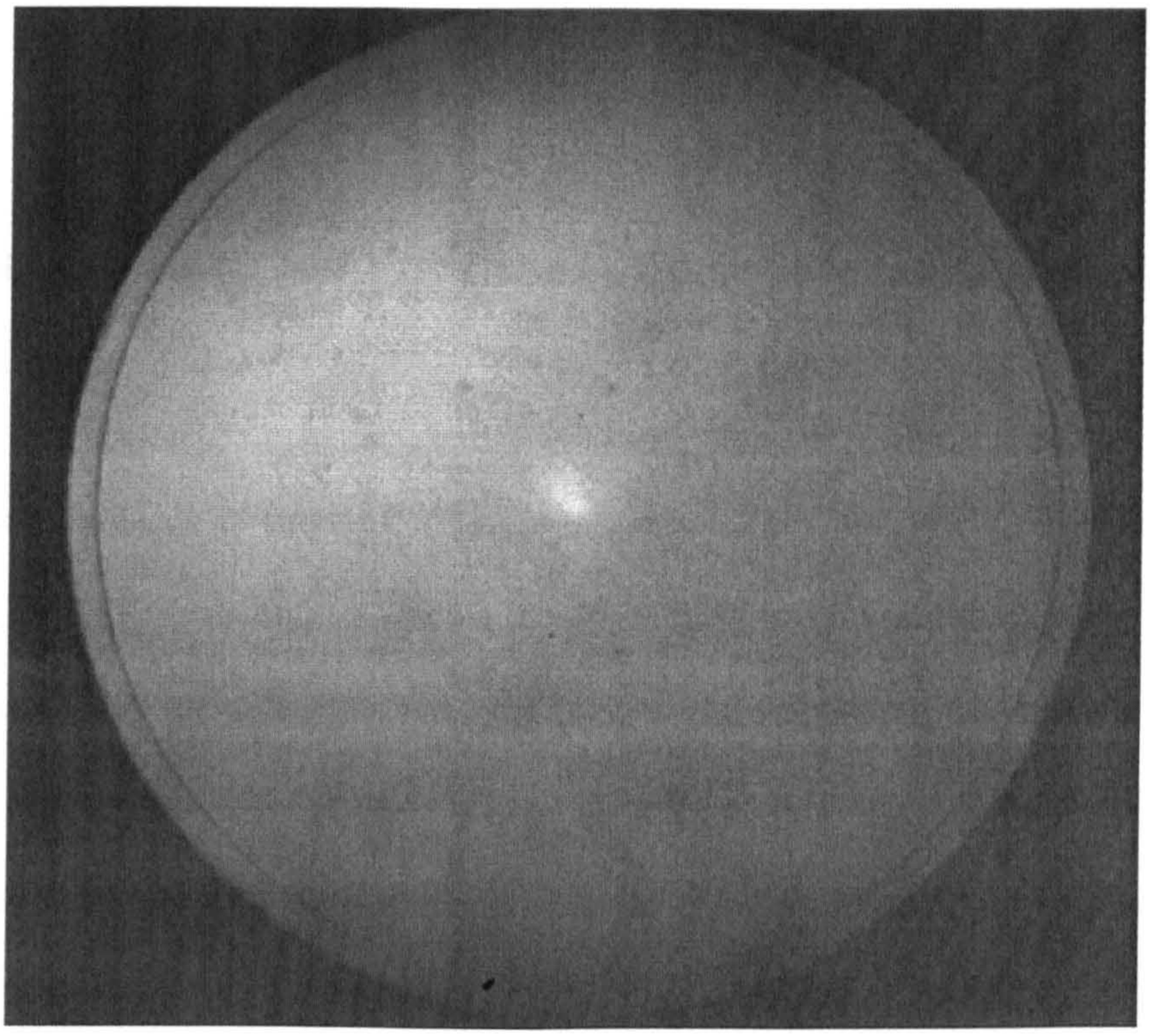

Figure 4.12: *BFP of 43.5nm thick gold with 400nm SiO_2 over layer and water backing*

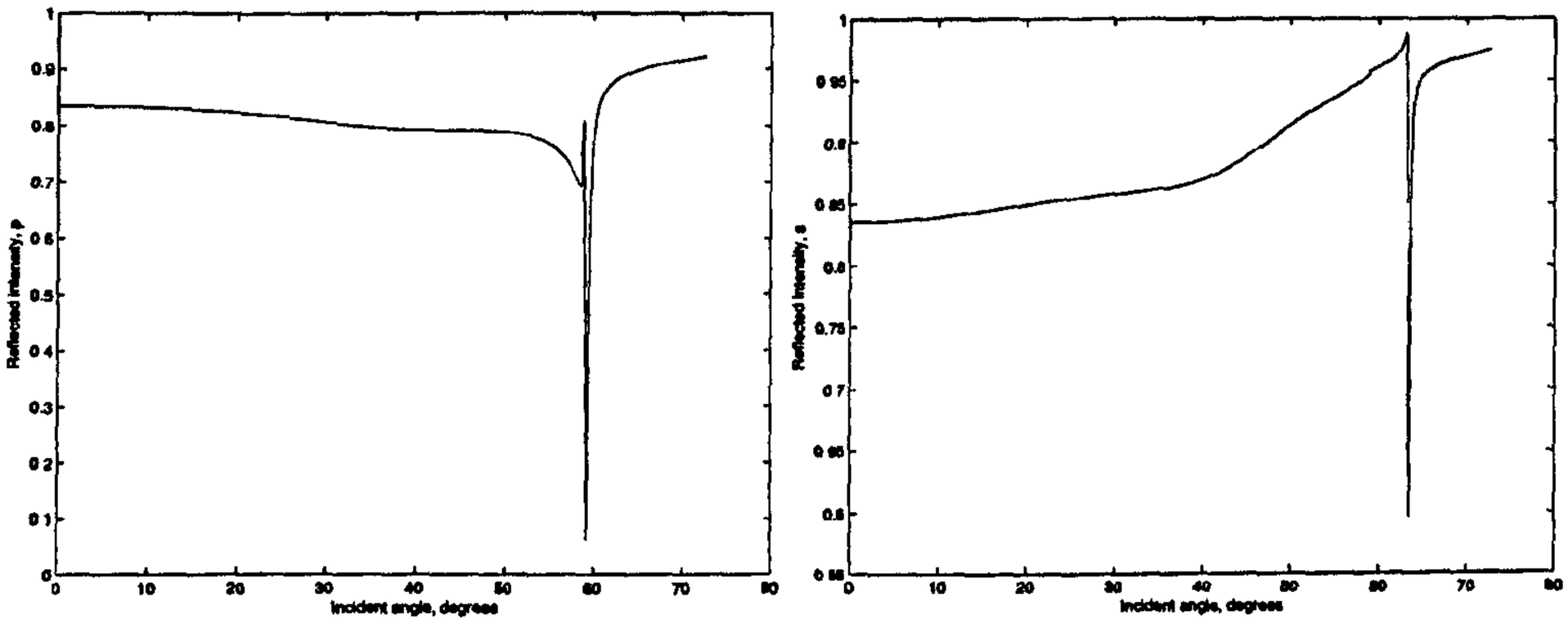

Figure 4.13: *Simulated plots of $(R_p)^2$ and $(R_s)^2$ for 43.5nm thick gold with 400nm SiO_2 over layer and water backing*

image only one side of the BFP. That way greater thickness/index resolution could be obtained in measurement. This would require calibration to known samples but shows a way of increasing the sensitivity without reducing the dynamic range. Further magnification could also be used in order to increase the resolution further but this would result in dynamic range loss as the resonance might may move out of the image area. By mounting the camera on a precise linear stage it might be possible to move the camera to follow the resonance in order to increase the dynamic range of the system.

As the system stands the results still show a large dynamic range, no changes in set up were required when changing samples and multiple resonances in both polarization orientations can be monitored at once. There were however some issues for incident angles close to the aperture of the lens. Beyond the advantages that the instrument provides the results also showed a potentially useful effect. Without a

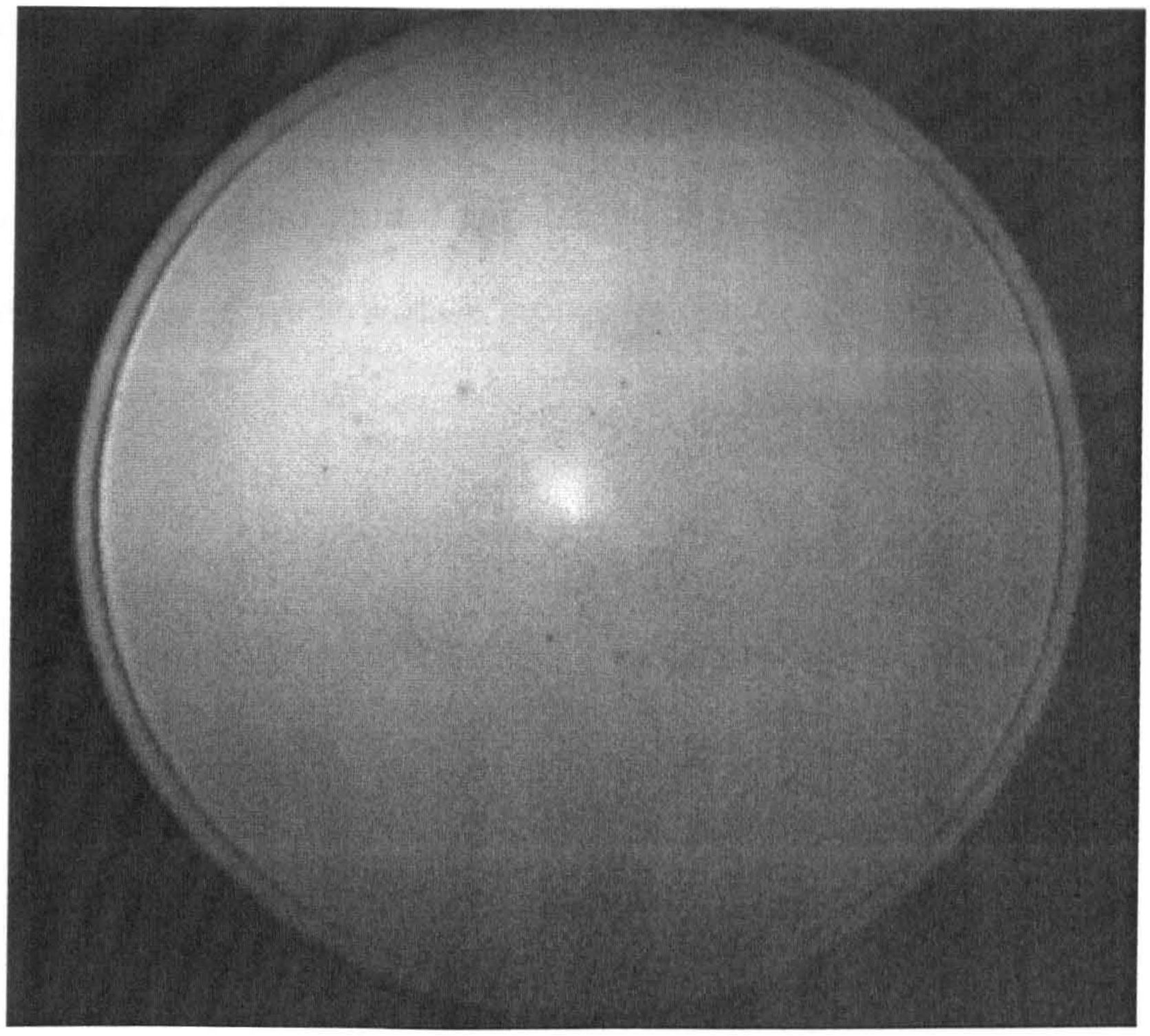

Figure 4.14: *BFP of 43.5nm thick gold with 520nm SiO_2 over layer and water backing*

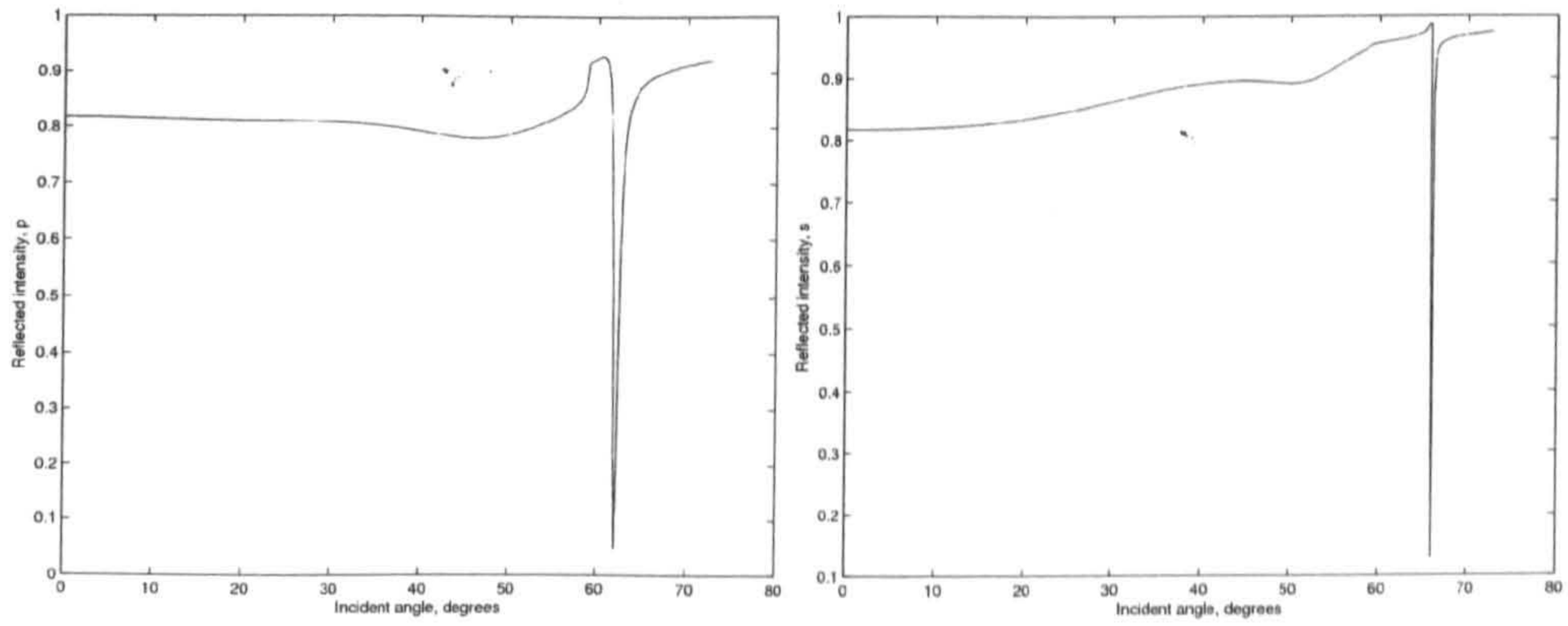

Figure 4.15: *Simulated plots of $(R_p)^2$ and $(R_s)^2$ for 43.5nm thick gold with 520nm SiO_2 over layer and water backing*

layer deposited on the gold it is impossible to excite surface waves using the 1.45NA objective in this system when water or other aqueous samples are used. However, with the addition of the layer guided waves could be produced and despite not being SPs should still be sensitive to surface properties due to the close proximity to the sample region.

Chapter 5

Enhanced Wide field Plasmon Imaging

5.1 Introduction

The sample arm of the system described in chapter 3 is effectively a standard optical microscope with wide field illumination and access to the BFP. This is in its own right a novelty as wide field imaging of plasmon supporting structures had not been seen in the literature using high NA oil immersion objectives [45]. As discussed in chapter 1 the Kretschmann configuration is not ideal for microscopy, requiring objectives with large working distances and inherently low NA. A high NA objective based system offers the advantage of improved imaging quality and resolution, with the added advantage of incoherent illumination removing the effect of coherent noise.

For these reasons images have been recorded in this standard imaging mode and

ways of increasing the contrast have been explored. This will be presented in this chapter.

5.1.1 Conventional imaging results

To begin with, images of two samples were taken in a standard microscopic mode without any form of masking in the BFP or other special techniques. The structure of the two samples may be seen in figure 5.1. The samples will be known as sample A and sample B respectively. In all sample and BFP images the grating will be orientated with the grating vector horizontal to the page.

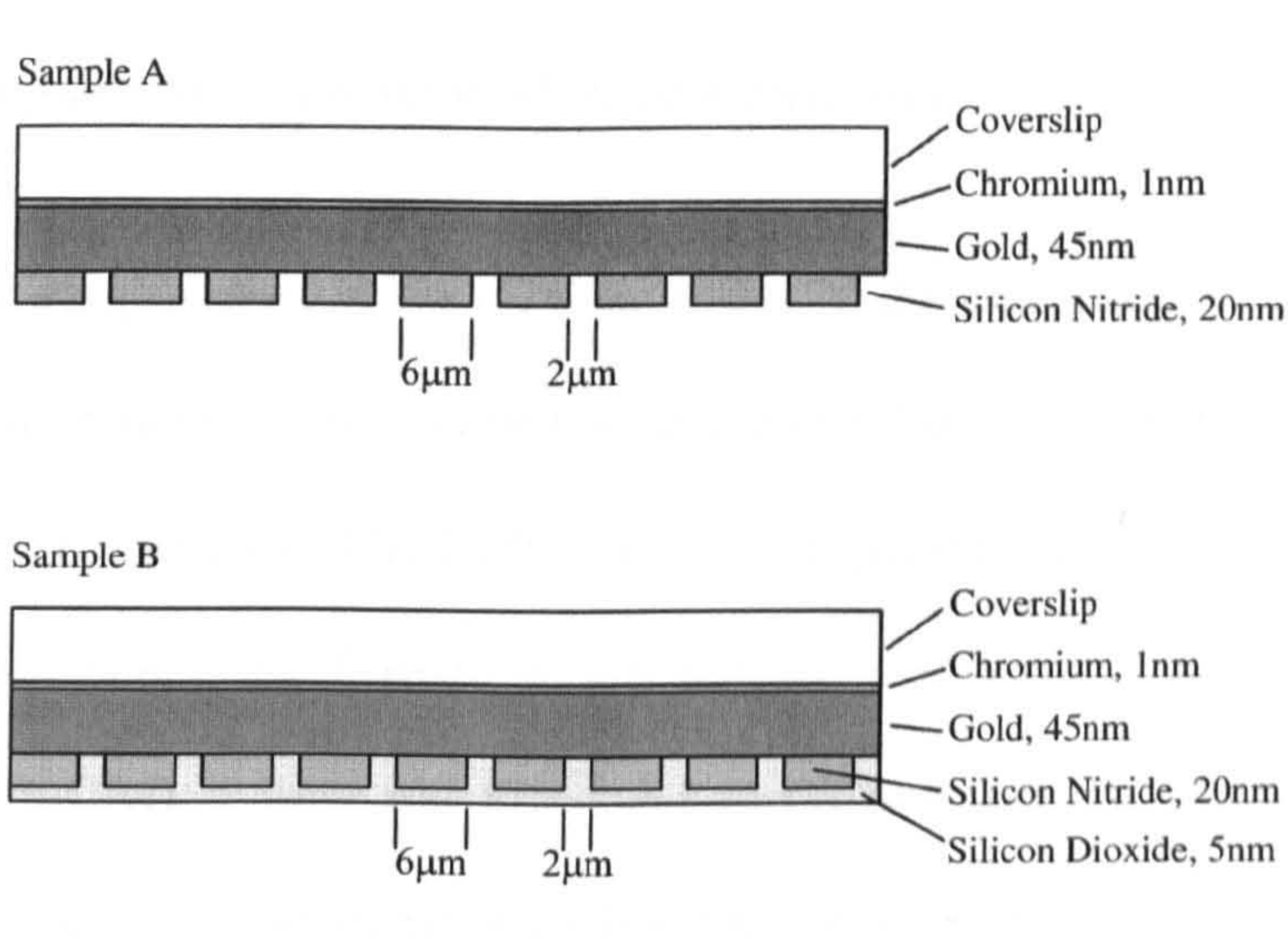

Figure 5.1: *Grating sample structures*

Figure 5.2 shows an image of sample A with the input polarization orientated horizontally. As can be seen there is no discernible contrast in the image. This is

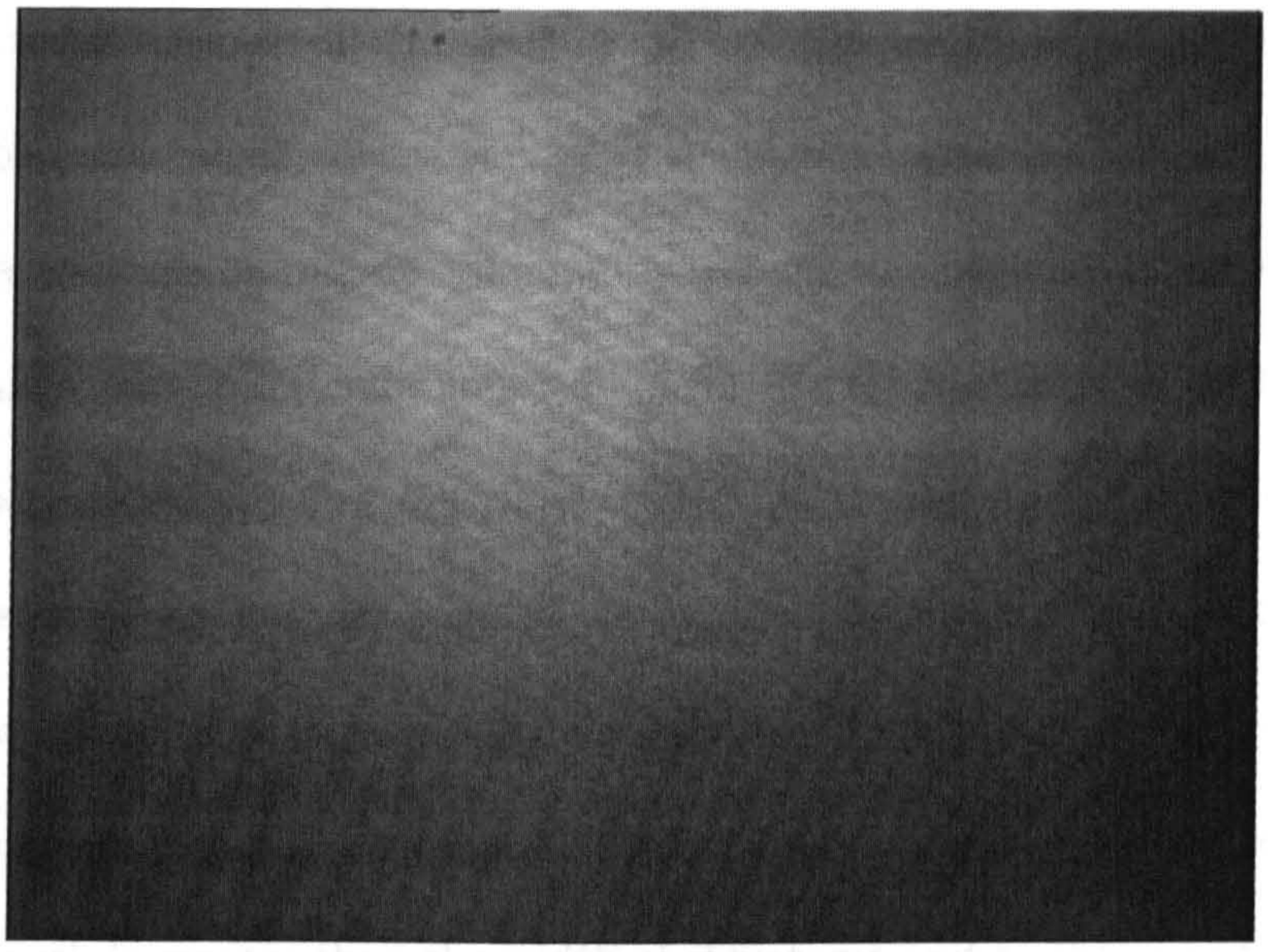

Figure 5.2: *Image of 2-6μmm, 20nm thick SiN_4 grating on 43nm gold film with no imaging polarizer and horizontal input polarization*

not surprising as most of the incident angles in the illumination will not excite SPs. Hence the image has a very large background that drowns out potential contrast and SP induced scattering. The BFP corresponding to this image is seen in figure 5.3 and shows two resonances. Careful measurements of the resonance positions were taken using AutoCAD, a circle was first fitted to the aperture and then concentric circles drawn to check concentricity with the resonance crescents, allowing adjustment of the reference circle. The drawing was then scaled to give an aperture radius of 1.45 which corresponds to the NA of the objective quoted by the manufacturer. Measurements of radial positions of the resonances could be converted into angles using the relation $NA = n\sin(\theta)$ where n=1.518, the refractive index of the oil. The

error found in radii of the resonances was in the order of 1-2°. The inner resonance was found to be at the angle corresponding to the average sample coating, i.e. gold with a 15nm layer of silicon nitride, taking into account the 2-6μm duty cycle of the grating. The angle was confirmed numerically using a Fresnel based matrix method [39]. This observation is just as described by Rothenhäusler et al [21], where the relationship between plasmon propagation length and structure size was explored. Just as in that case, the plasmons are being generated such that they propagate across the boundaries between coated and uncoated gold. In addition, the plasmon propagation length is greater than the width of structures and so the conditions for excitation are averaged. This will discussed in greater detail in section 5.2. The propagation length was calculated to be approximately 11μm for plain gold and 3.5μm for the coated gold according to ref [5]. The outer resonance seen in the BFP corresponds to a wave vector equal to the sum of the plasmon and grating wave vectors. The grating adds momentum to the incident light at a given angle allowing it to excite SPs. This phenomenon was also observed by Rothenhäusler et al.

It was stated earlier that the excited SPs would propagate parallel to the grating vector, however, this is only the case for the light on the x-axis of the BFP. The light off the axis which is no longer purely p-polarized excites SPs that propagate at an angle to the grating vector and see a longer grating period. This means that the angle of the incident k-vector that excites plasmons with the aid of the grating vector is reduced. Because of this the grating resonance seen reduces in diameter with azimuthal angle away from the x-axis.

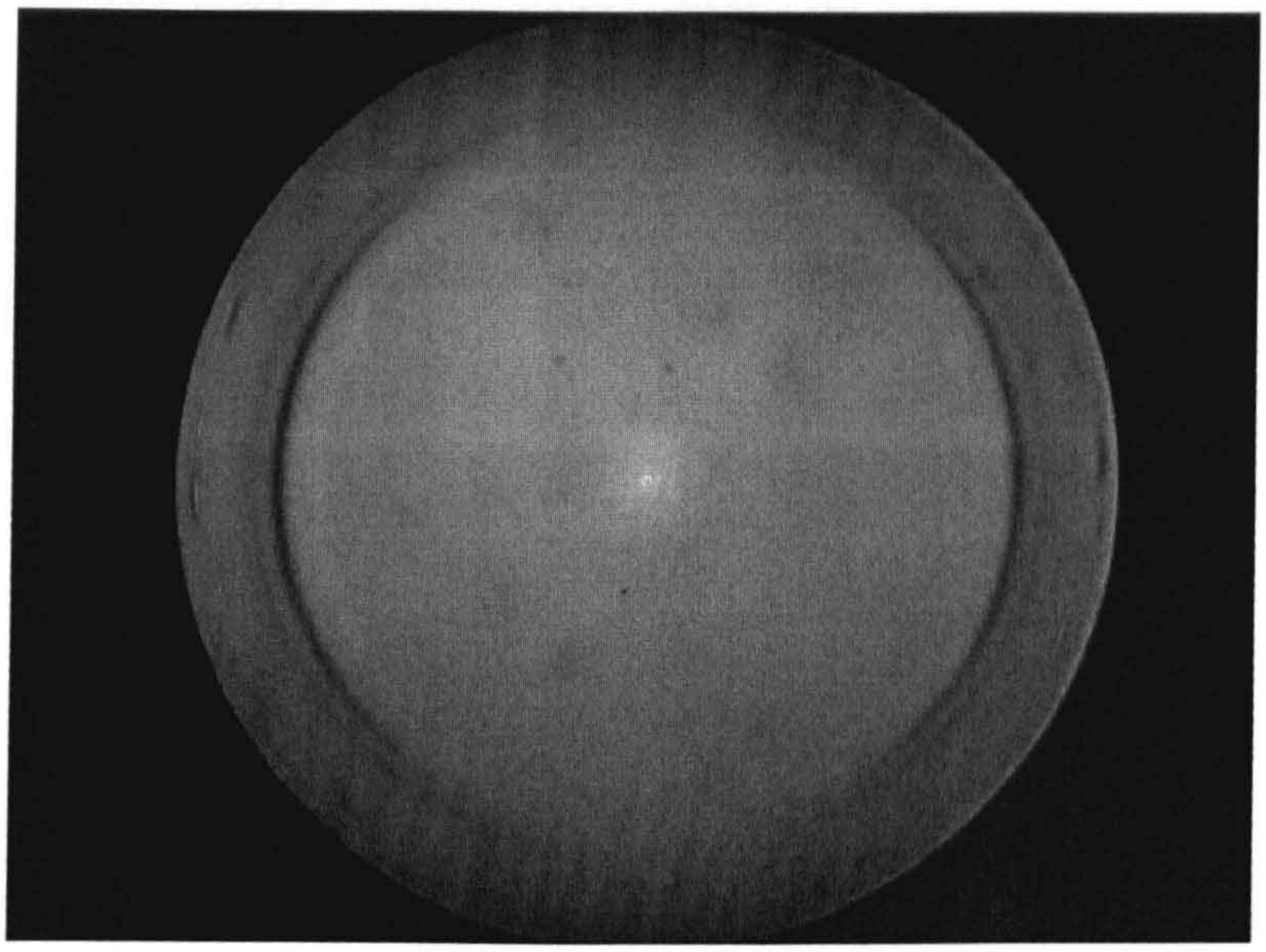

Figure 5.3: *BFP with no imaging polarizer and horizontal input polarization*

An identical imaging experiment was performed for the case of vertical input polarization (image omitted). As for the case of horizontal polarization there was no visible contrast in the image. The back focal plane corresponding to this image may be seen in figure 5.4. Rothenhäusler did not publish results for this orientation of grating and indeed none has been seen in the literature. The distribution is rather more complex now that the SPs are propagating perpendicularly to the grating vector. i.e. down the striped structure. Consider first the resonances seen on the y-axis labeled A and B. On the axis the incident plane waves are p-polarized and the excited SPs will propagate between the material boundaries without crossing them.

This situation is in some ways much like the imaging of a structure much larger

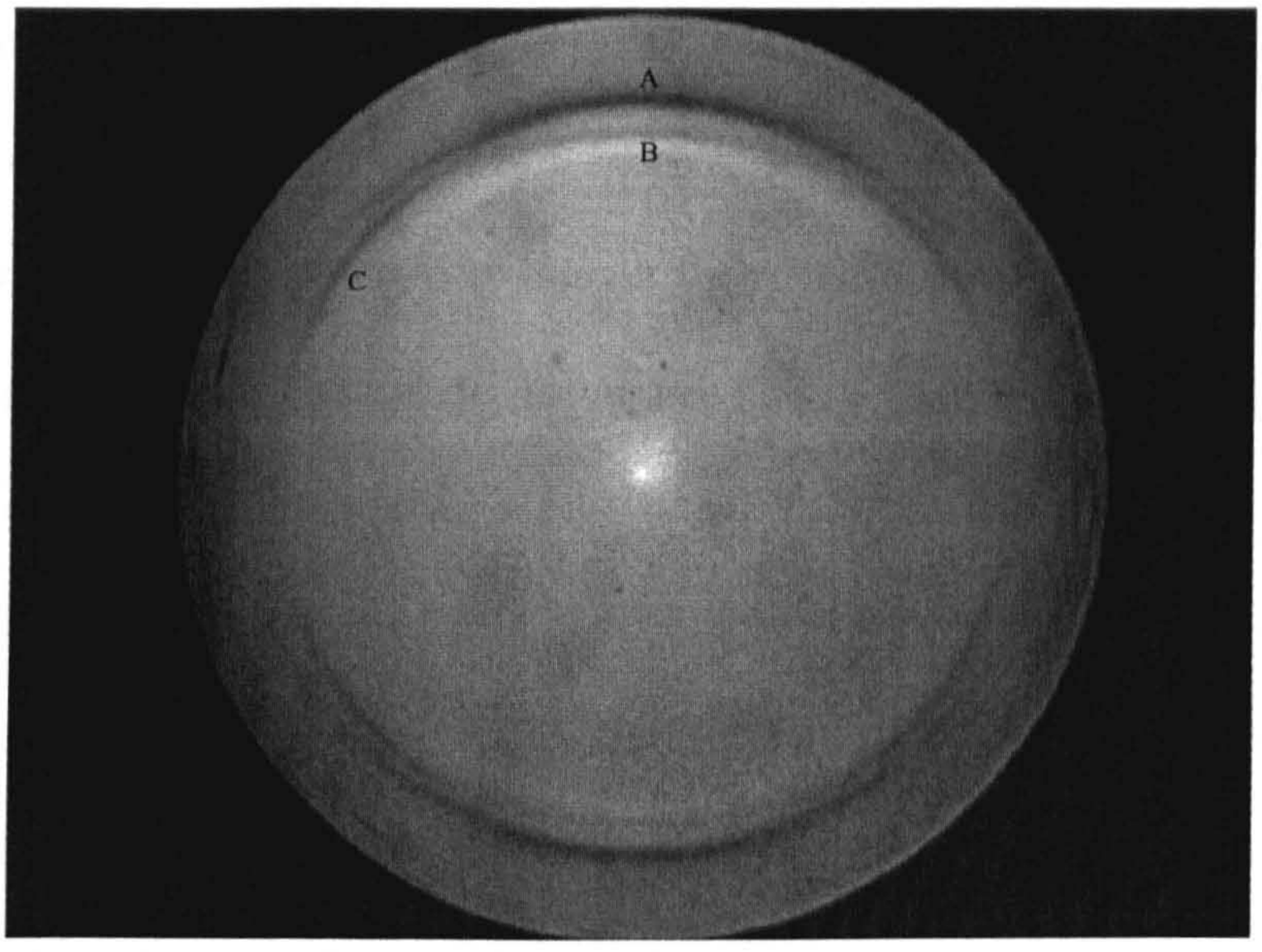

Figure 5.4: *BFP with no imaging polarizer and vertical input polarization*

than the SP propagation length. In that case too, the excited plasmons tend not to cross any boundaries. Rothenhäusler showed that when this is the case that the two materials may be treated individually and that a Fresnel treatment was valid. In this BFP image there are two resonances on the y-axis but they were not found to correspond with the dips of uncoated gold and coated gold respectively. The precise reasons for this are not clear, there is sufficient "room" in each region to support plasmons of the expected k-vector but the regions are narrow so a simple plane wave treatment may still not be valid. If a plane wave illuminates a homogeneous sample at the resonant angle, a "line wave" propagating on the surface of the metal will result. In the case of a narrow feature such as this grating only short sections of the wave can be excited. The surrounding medium applies a boundary condition to

the excitation, changing the exact resonant conditions and hence the resonant angle. This idea could be verified by imaging samples of varying period, unfortunately such samples were not available at the time of the experiments.

Moving away from the y-axis, resonance C can be seen. At this point in the BFP the excited SPs are again propagating across the sample as they did in the case of horizontally polarized light. The difference here is that the p component of the incident light is becoming smaller toward the x-axis before fading totally. The second grating resonance may also be seen where the p-component is larger but the contrast is too low to see it near the x-axis.

In the intermediate azimuthal angles, resonances A and B seem to fade away and are replaced by C and the grating resonance. This probably represents the point at which the structure can no longer support waveguide type surface waves but can support normal plasmons, albeit ones that propagate over the sample structure. It can be seen that resonance B seems to die away first. It is likely that this resonance corresponds to the uncoated gold. The reasons for this are two-fold. Firstly, the resonance is less pronounced. This is not likely to be due to the depth of the resonance but more likely because at that resonant angle a larger portion of the sample is not resonant and reflects specularly so reducing the depth of the observed dip, remembering of course that the uncoated gold represents only a quarter of the sample area. Secondly, the resonance, although modified is relatively close to that of gold and is seen at smaller angles than for the coated material. It is not surprising that the waveguide mode of the uncoated gold region might die away first as it is a

narrower structure. The excited SPs will begin to meet the edges of the 2μm wide regions at smaller angles to the boundaries.

It is clear that in a truly wide field microscopy mode the system is not suitable for surface plasmon microscopy. To boost the contrast, means of reducing the background light levels that do not correspond to plasmon excitation were developed. The first method was to use polarization optics.

5.1.2 Polarization enhanced contrast

To begin with the effects of adding polarizers to the imaging arm of the microscope were investigated. The terms co and cross will be applied to describe a polarizer aligned with or orthogonal to the input polarization respectively.

Figure 5.5 shows an image of sample A with a polarizer added in the imaging arm. This polarizer was aligned with the input polarization, i.e. co-polarized. The input polarization is aligned horizontally. As can be seen the polarizer has no effect on the image contrast. Figure 5.6 shows the corresponding BFP image. Dark patches are visible in all 4 corners, these correspond to regions of the BFP where the polarization state has been altered. This is because the phase of the reflection co-efficients for s and p differ and alter the polarization of the reflected light[36]. The regions where the incident light is purely p or s-polarized are unaffected, as are the more axial regions where the reflection coefficients are very similar. Other than these dark areas the distribution is unaffected. Figure 5.7 and 5.8 show the image and BFP of sample A with vertical input polarization. The results in this

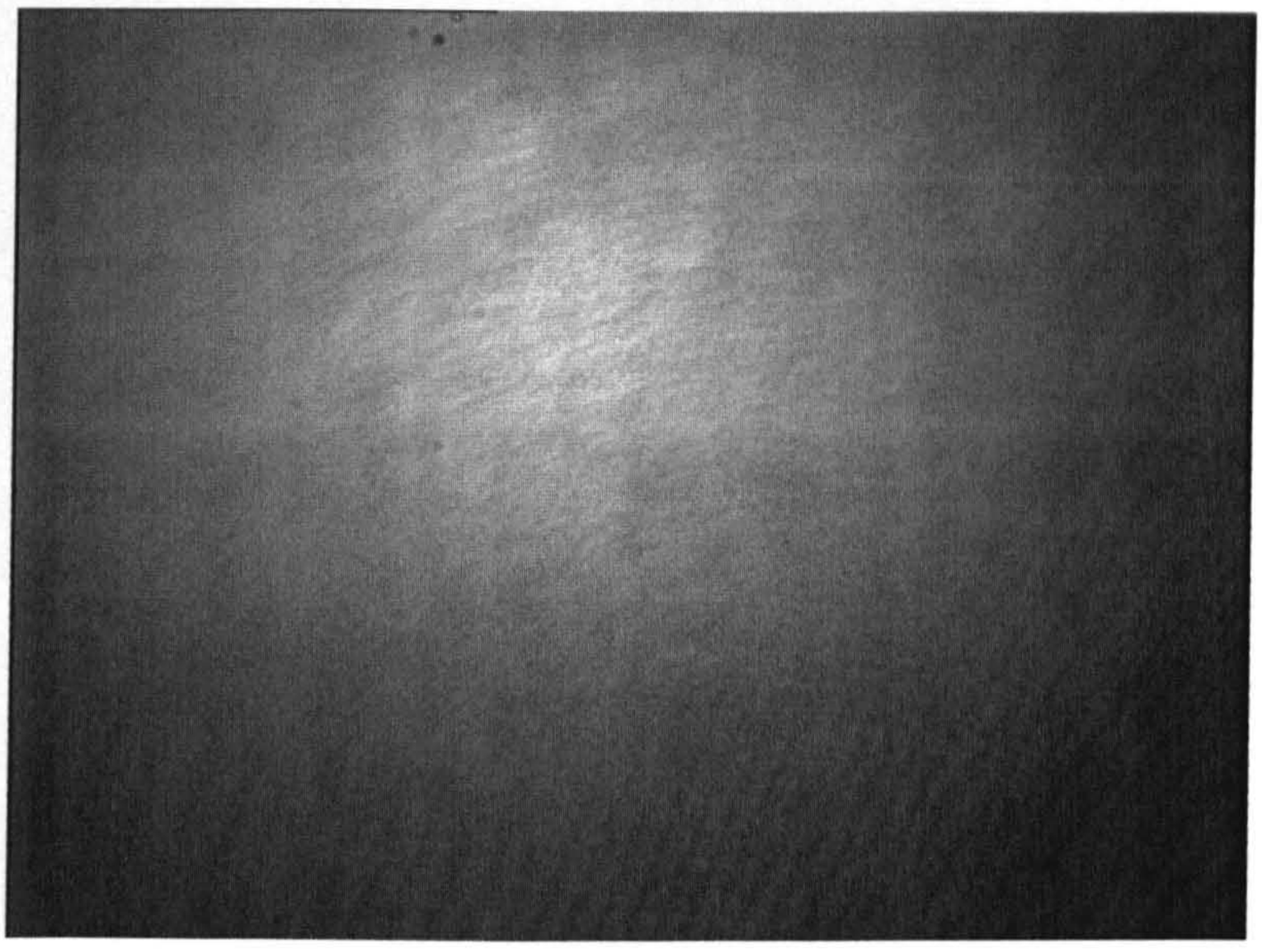

Figure 5.5: *Image of 2-6μm, 20nm thick SiN_4 grating on 43nm gold film with co-aligned analyzer and horizontal input polarization*

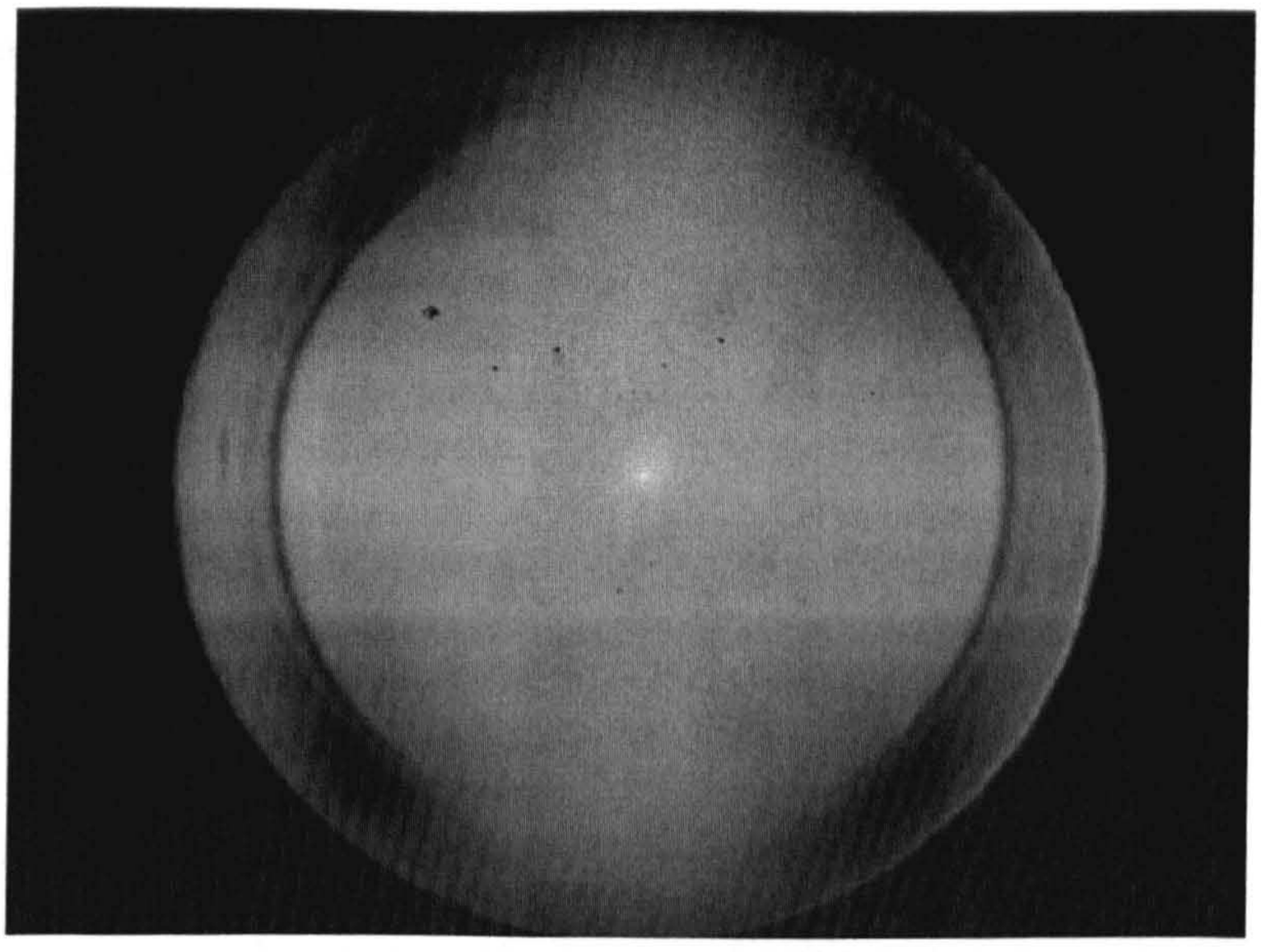

Figure 5.6: *BFP with horizontal polarization and co-polarized analyzer*

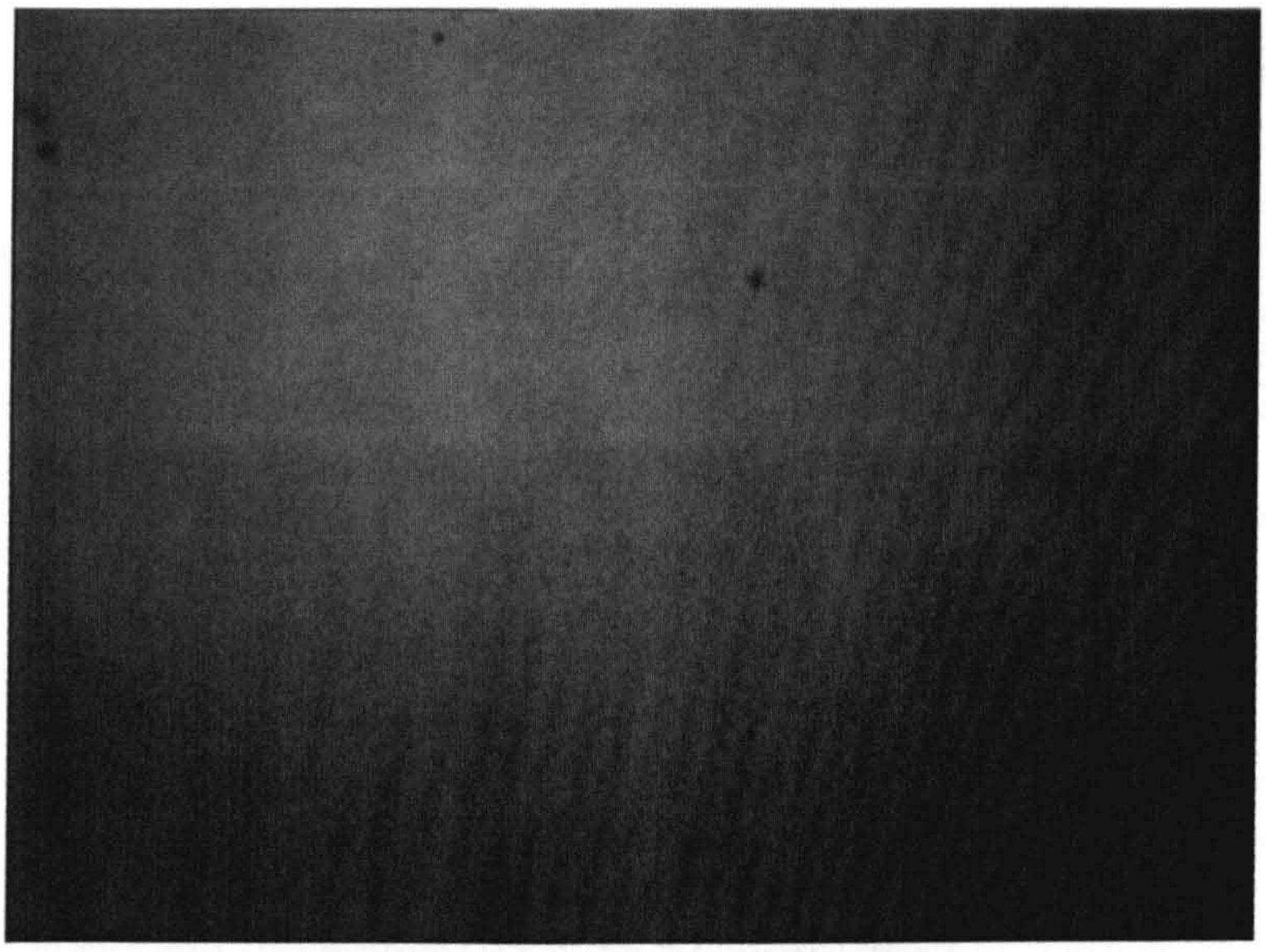

Figure 5.7: *Image of 2-6μm, 20nm thick SiN_4 grating on 43nm gold film with co-aligned analyzer and vertical input polarization*

orientation are much as before, there is no increase in contrast and the only change to the BFP is the addition of dark patches due to polarization change in reflection. If the output polarizer is orientated so as to be orthogonal to the input polarization then rather than block the light that has had its polarization rotated it will pass a portion of it.

The next step was to try a crossed polarizer in the imaging arm. Figure 5.9 shows the image of sample A with horizontal input polarization and with the output polarizer at 90 degrees to the input polarization. In this instance a marked increase in contrast can be seen in the image. Looking at the BFP in figure 5.10 the main reason is evident as the majority of the lower angles have been blocked.

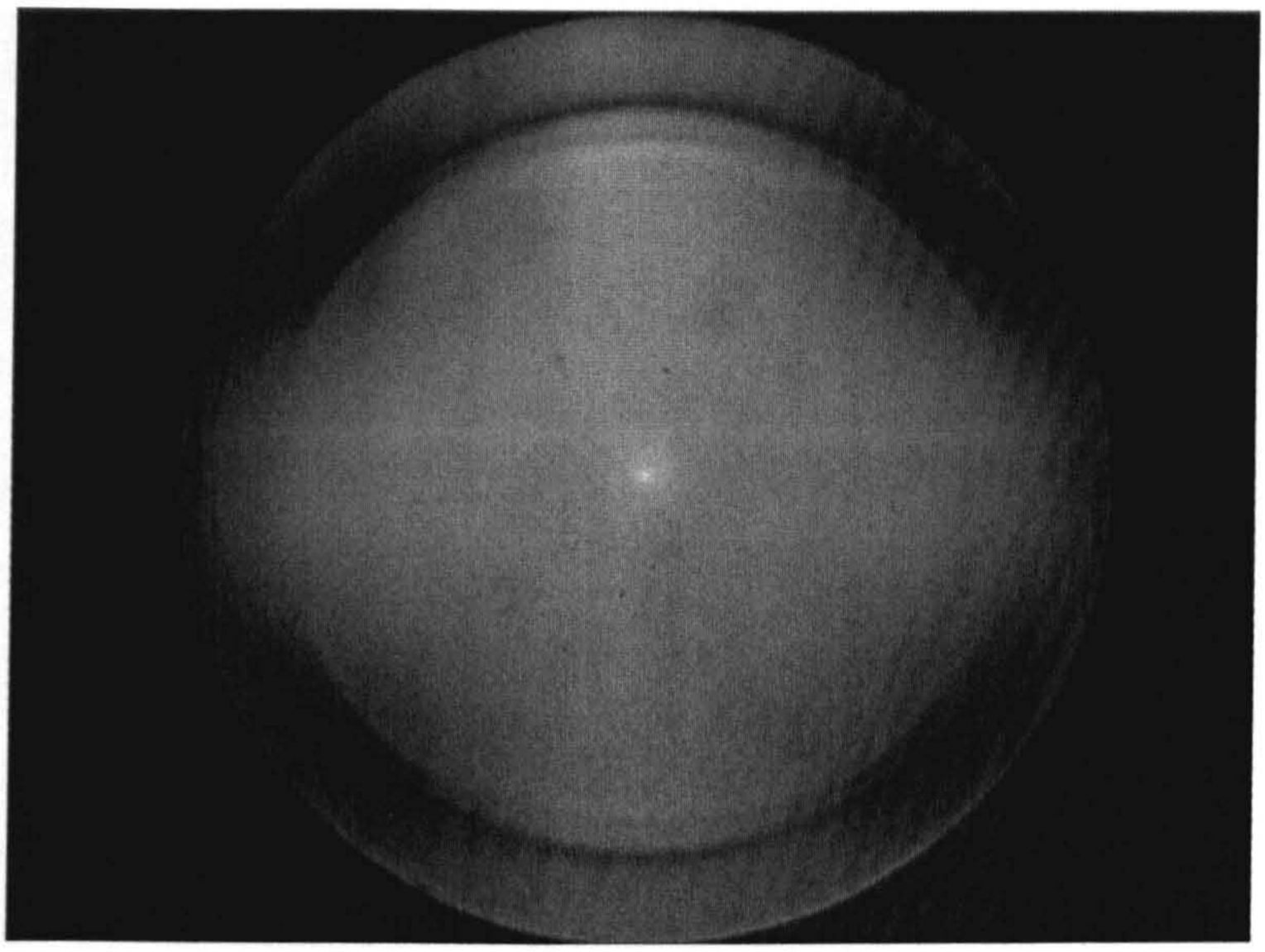

Figure 5.8: *BFP with co-aligned analyzer and vertical input polarization*

This light maintains its polarization and hence is attenuated by the polarizer. The four corners that have their polarization rotated have components that are aligned with the polarizer and so appear light. As well as these features a further resonance appears at the top of the BFP. This corresponds to resonance A seen in figure 5.4 when the input polarization was vertical. The reason that this resonance is not visible in the other BFP images for horizontal input polarization is because as the p-polarized component is very small compared to the s in this region, the effect is normally masked. By adding the polarizer, the light level in this region is reduced because only a portion of the reflected light is co-polarized and so the contrast of the resonance increases. Resonance B can also be seen but it is much less clear.

Looking now at the case of vertical polarization, figure 5.11 and figure 5.12 show

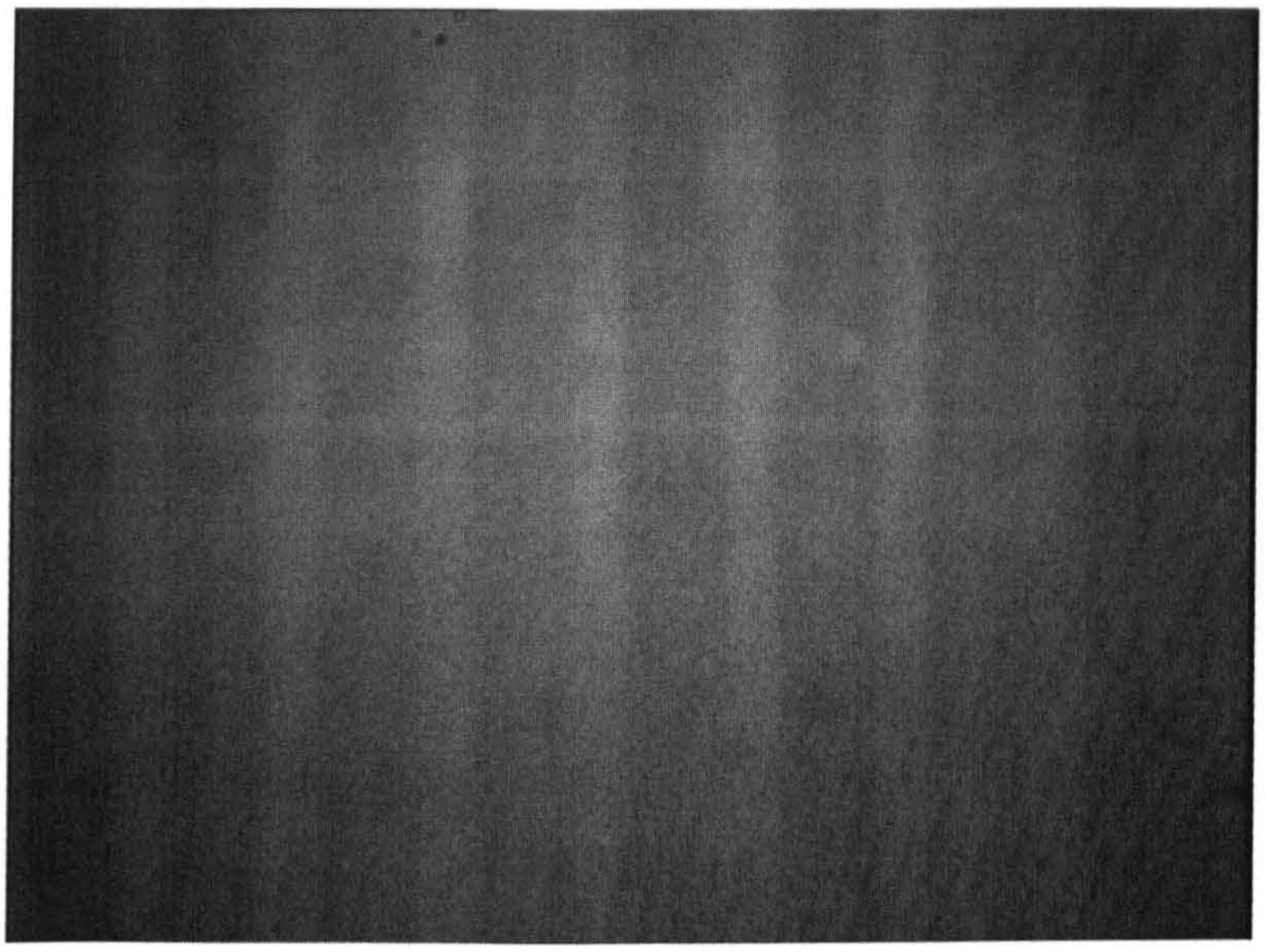

Figure 5.9: *Image of 2-6μm, 20nm thick SiN_4 grating on 43nm gold film with cross-aligned analyzer and horizontal input polarization*

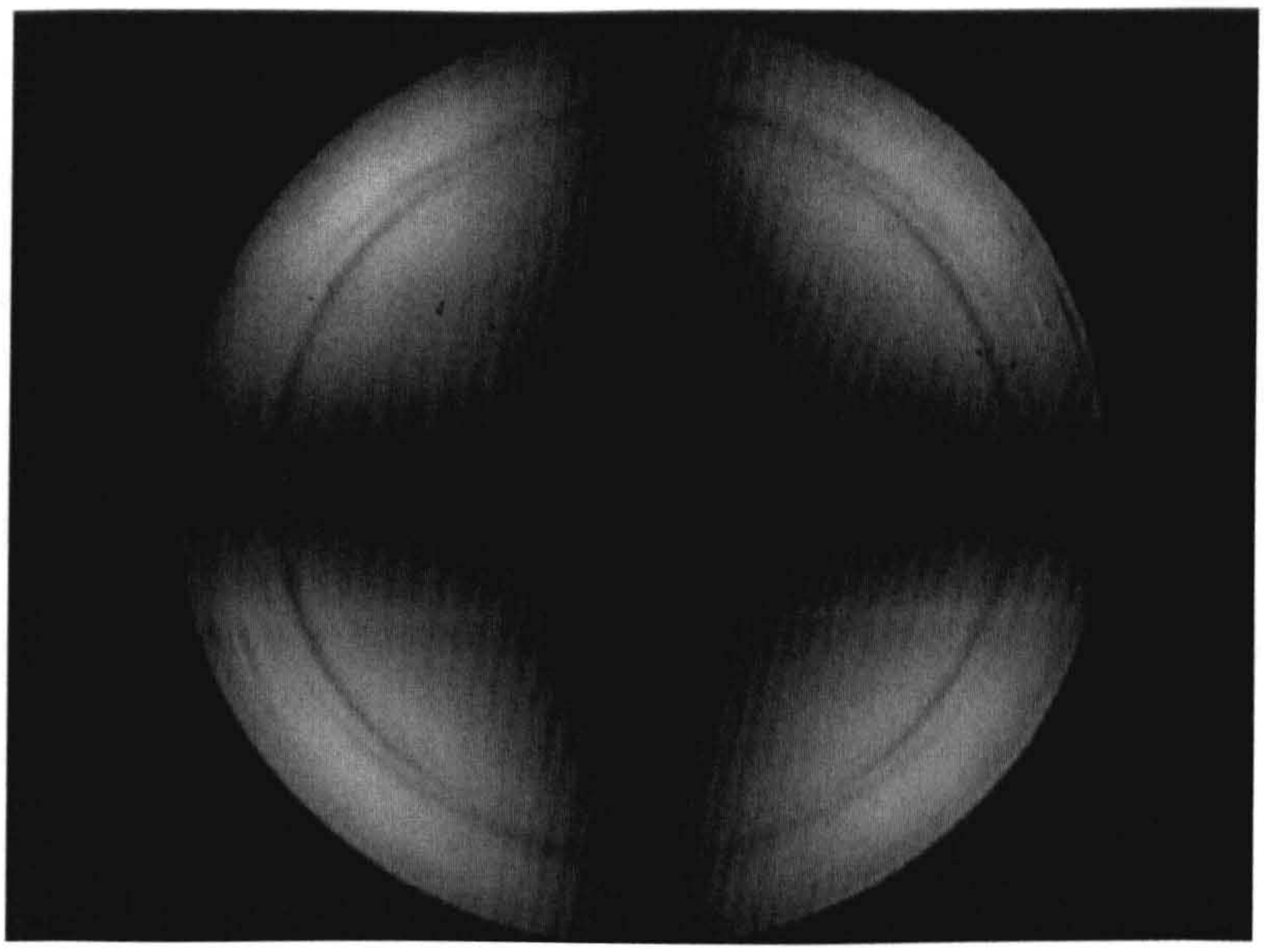

Figure 5.10: *BFP with horizontal polarization and cross-polarized analyzer*

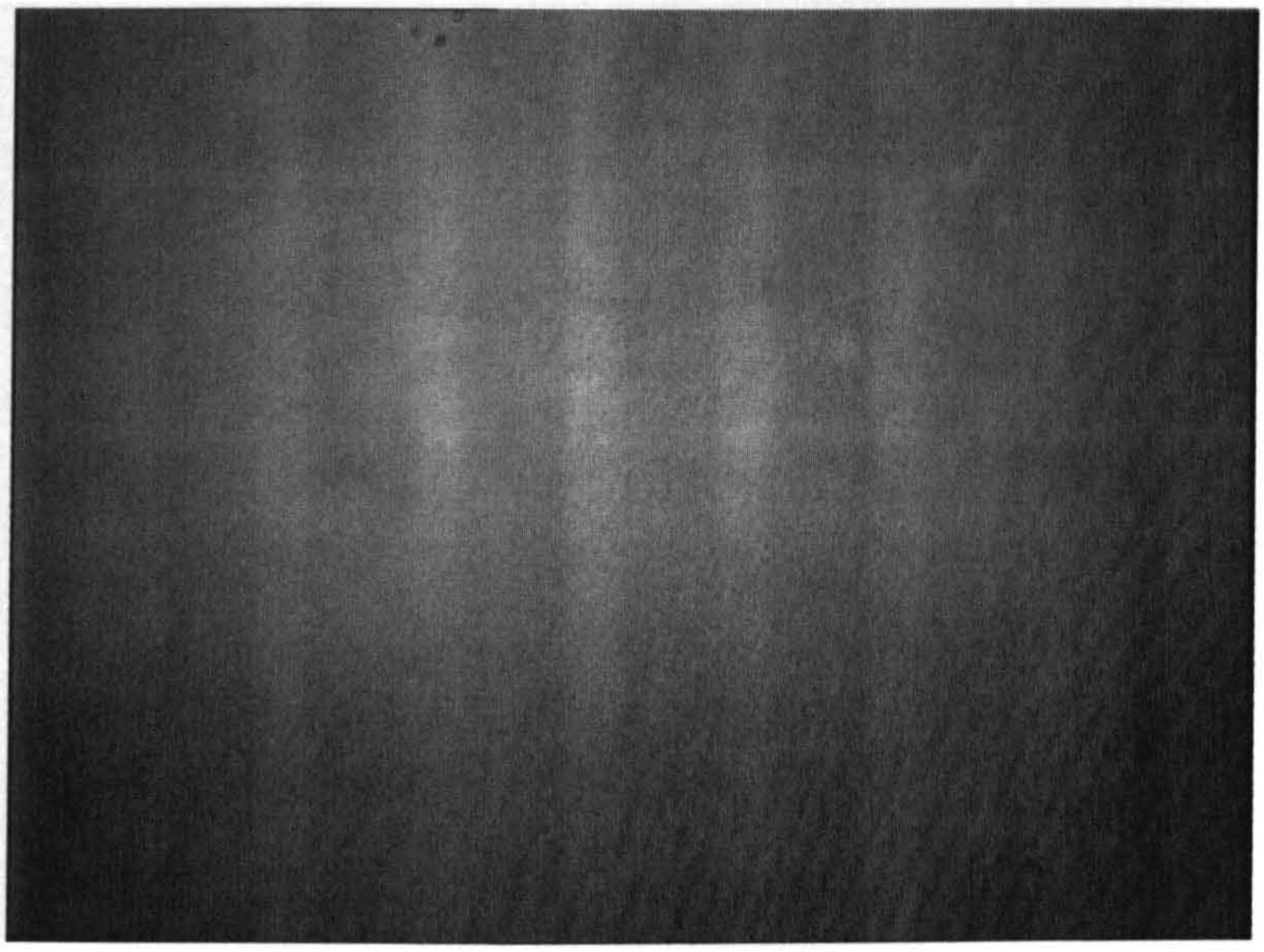

Figure 5.11: *Image of 2-6μm, 20nm thick SiN_4 grating on 43nm gold film with cross-aligned analyzer and vertical input polarization*

the image and BFP of the sample with a cross-polarized polarizer respectively. The resolution is enhanced by the masking effect of the polarizer and the contrast of the resonances in the regions dominated by s-polarized light is increased. It might be noticed that the back focal plane images for both input polarization states when the output polarizer is crossed are identical. This is because the regions that might appear different, on the x and y-axis, are totally dark. In the region between, there is a p-polarized component capable of exciting plasmons over the whole range of azimuthal angles for both polarization directions. Although this might not normally be seen, the reduction in background light makes them visible. The effect of propagation direction on the resolution seen in SP microscopes has been studied widely

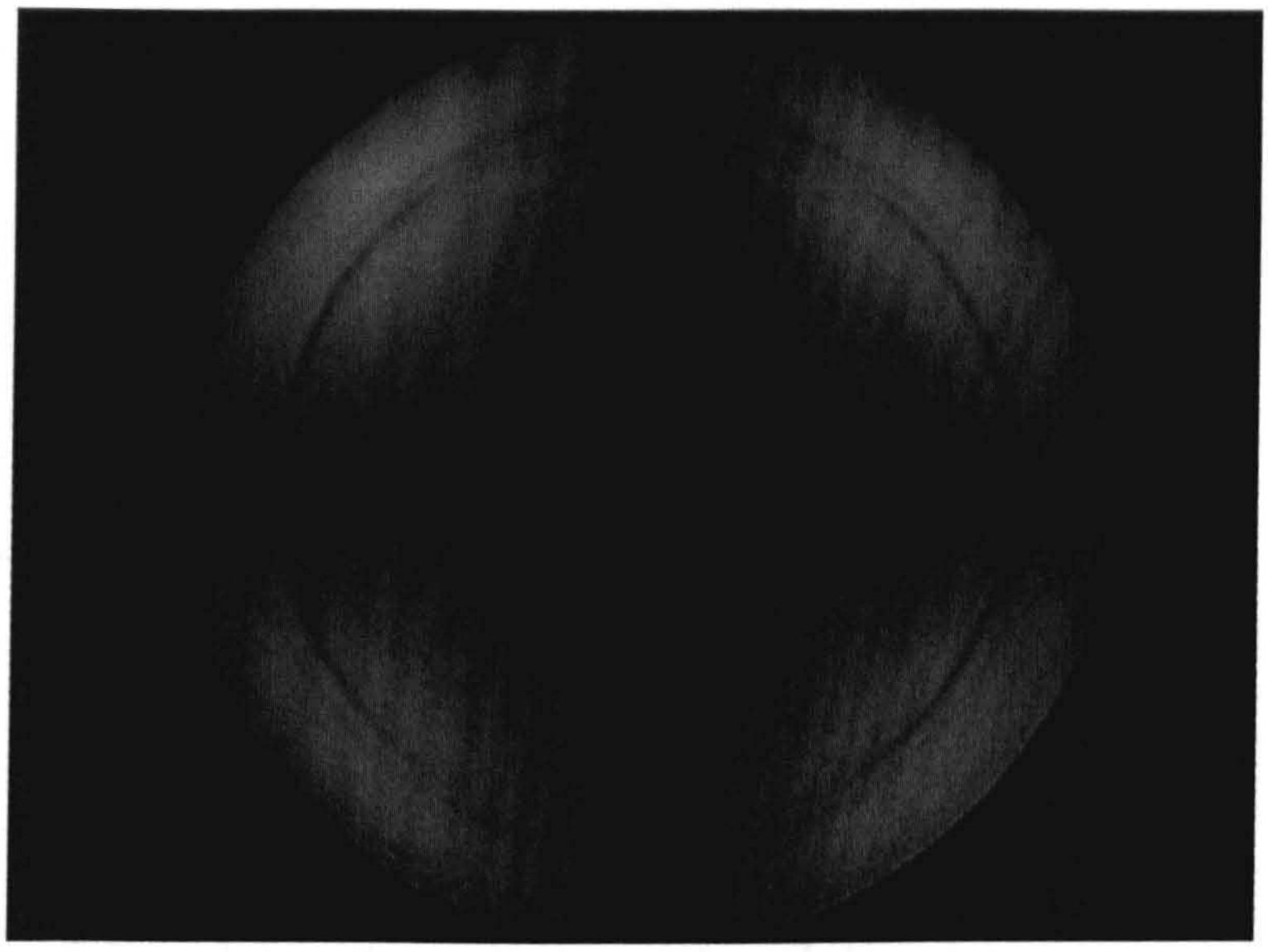

Figure 5.12: *BFP with cross-aligned analyzer and vertical input polarization*

in the literature. If line traces from both images with cross-polarized polarizers are produced the difference in resolution can be compared. Such traces may be seen in figure 5.13. These plots were produced by summing the pixels of the images vertically to remove noise before a low pass filtered version of the plot was subtracted from the line trace to remove the DC. It can be seen that there is no real difference in resolution. The reason for this is that the BFP distributions for both polarization orientations were identical. This is of particular importance when considering the horizontally polarized case as the purely p-polarized light would have propagated parallel to the grating vector causing potential smearing, however, the reflected light at this angle was blocked.

Now some similar images from sample B will be shown. With conventional

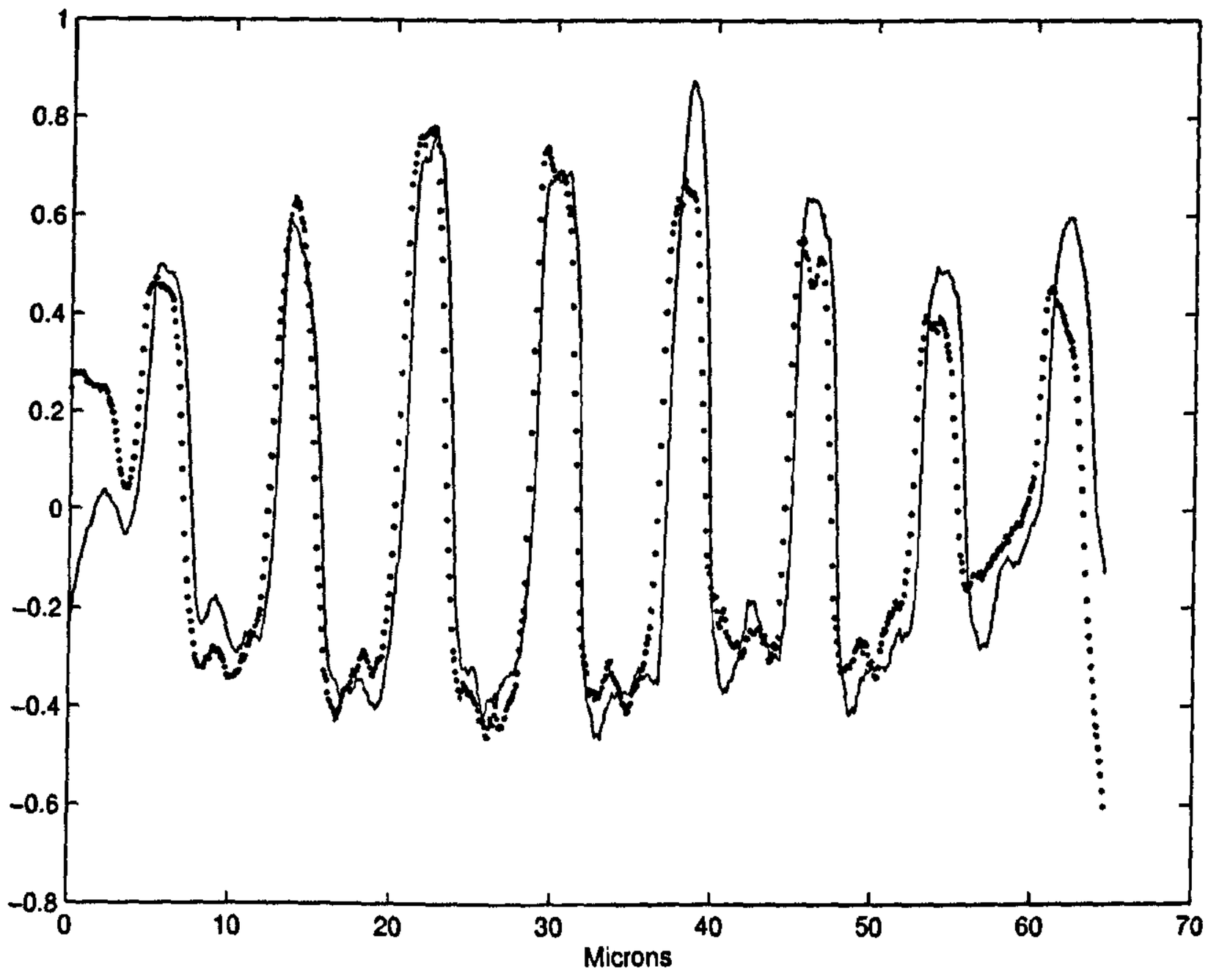

Figure 5.13: *Comparison of line traces for images with vertical(dotted line) and horizontal input polarizations*

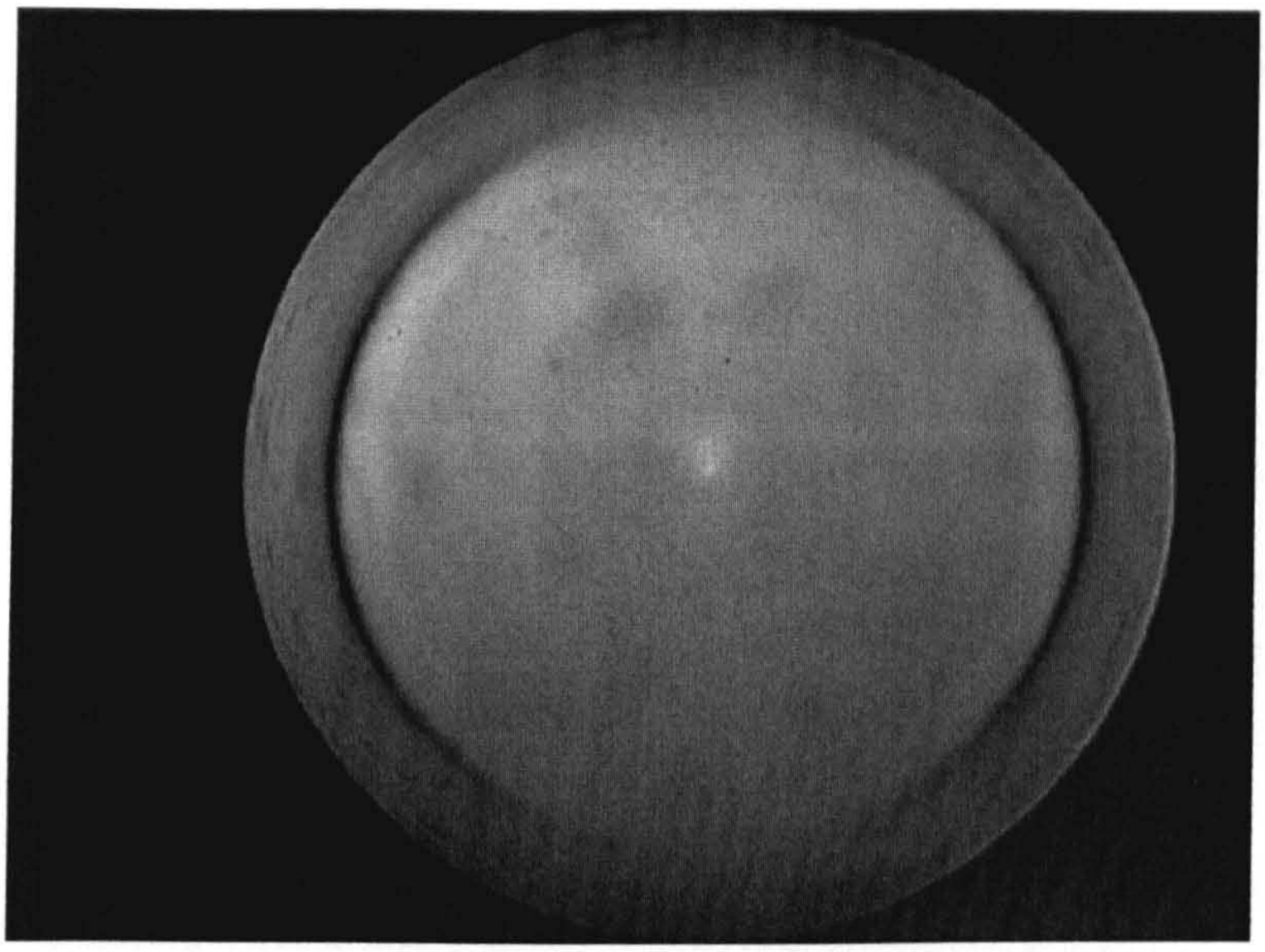

Figure 5.14: *Back focal plane of sample B with horizontal input polarization*

imaging and with no form of masking or filtering no image is seen. Figure 5.14 shows the BFP for this sample when illuminated with the input polarization horizontally. The grating vector is orientated horizontally as it will be for all further images.

Unlike the previous sample there is no visible diffraction pattern of any sort, this is due to the over-layer of silicon dioxide that is reducing the effect of the grating. The resonance is again seen at the average value of the coatings applied.

Looking now at the case of vertical input polarization as seen in figure 5.15 a similar distribution to that of figure 5.4 can be seen, however the effect is much less clear, again probably due to the over layer. If a polarizer is now added in the imaging arm at 90 degrees to the input polarization the BFP distributions shown in figure 5.16 and 5.17 for horizontal and vertical polarizations respectively

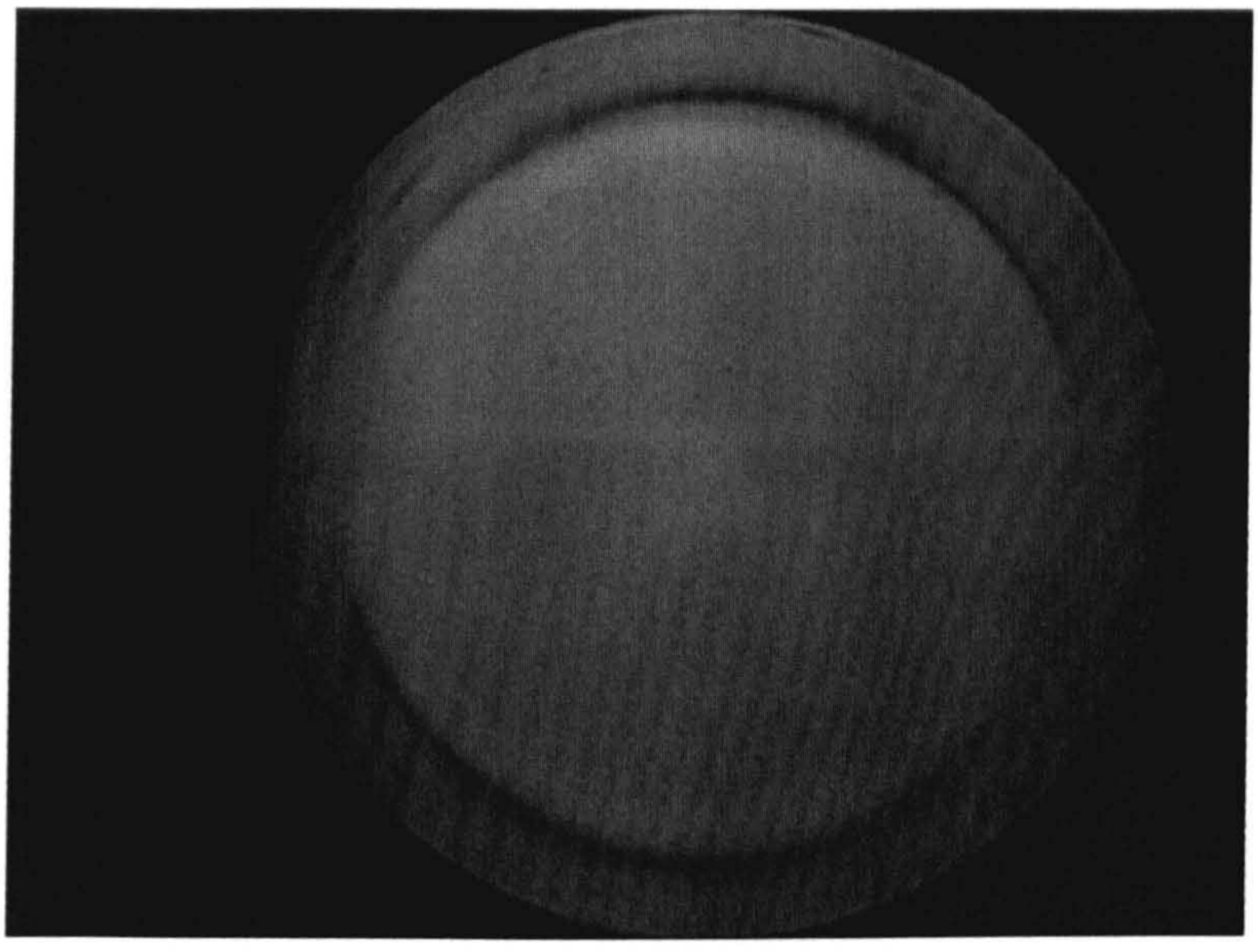

Figure 5.15: *Back focal plane of sample B with vertical input polarization*

are produced. Just as in the case of sample A, both distributions look identical. The images are also virtually identical as can be seen in figures 5.18 for horizontal polarization and 5.19 for vertical. The use of polarization optics is a simple way to boost contrast and should be relatively sample independent. It is certainly a good way to align a system initially when a custom mask is not available. The effect of the crossed polarizer is also interesting. It is normal that in the regions of the BFP where the p-component is smaller than the s that the resonance will not contribute to contrast. By making use of the change in the polarization due to the phase and amplitude differences between R_s and R_p this part of the resonance may be used, as some of the s-polarized light at the resonant angle is filtered.

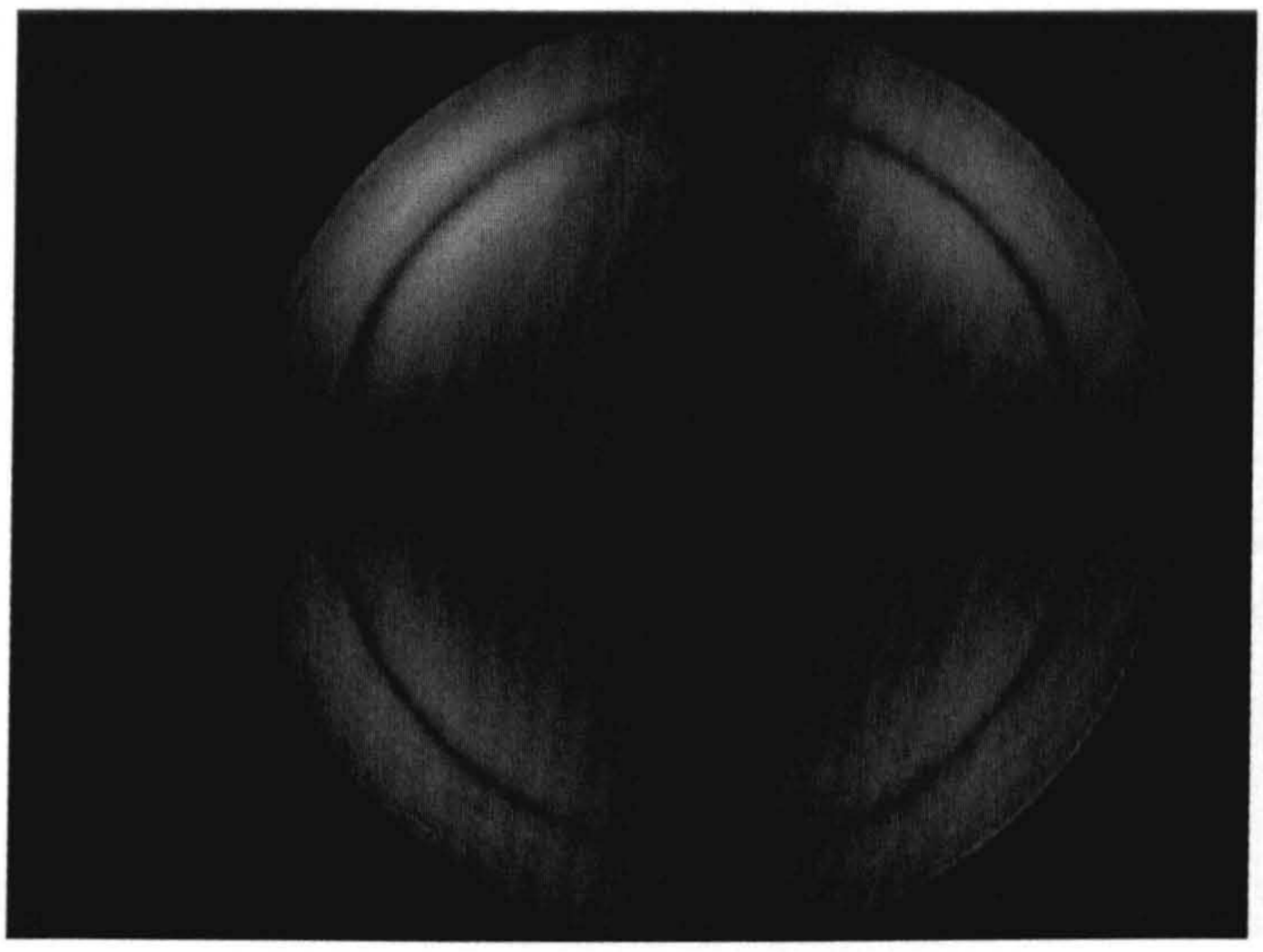

Figure 5.16: *Back focal plane of sample B with a cross-aligned analyzer and horizontal input polarization*

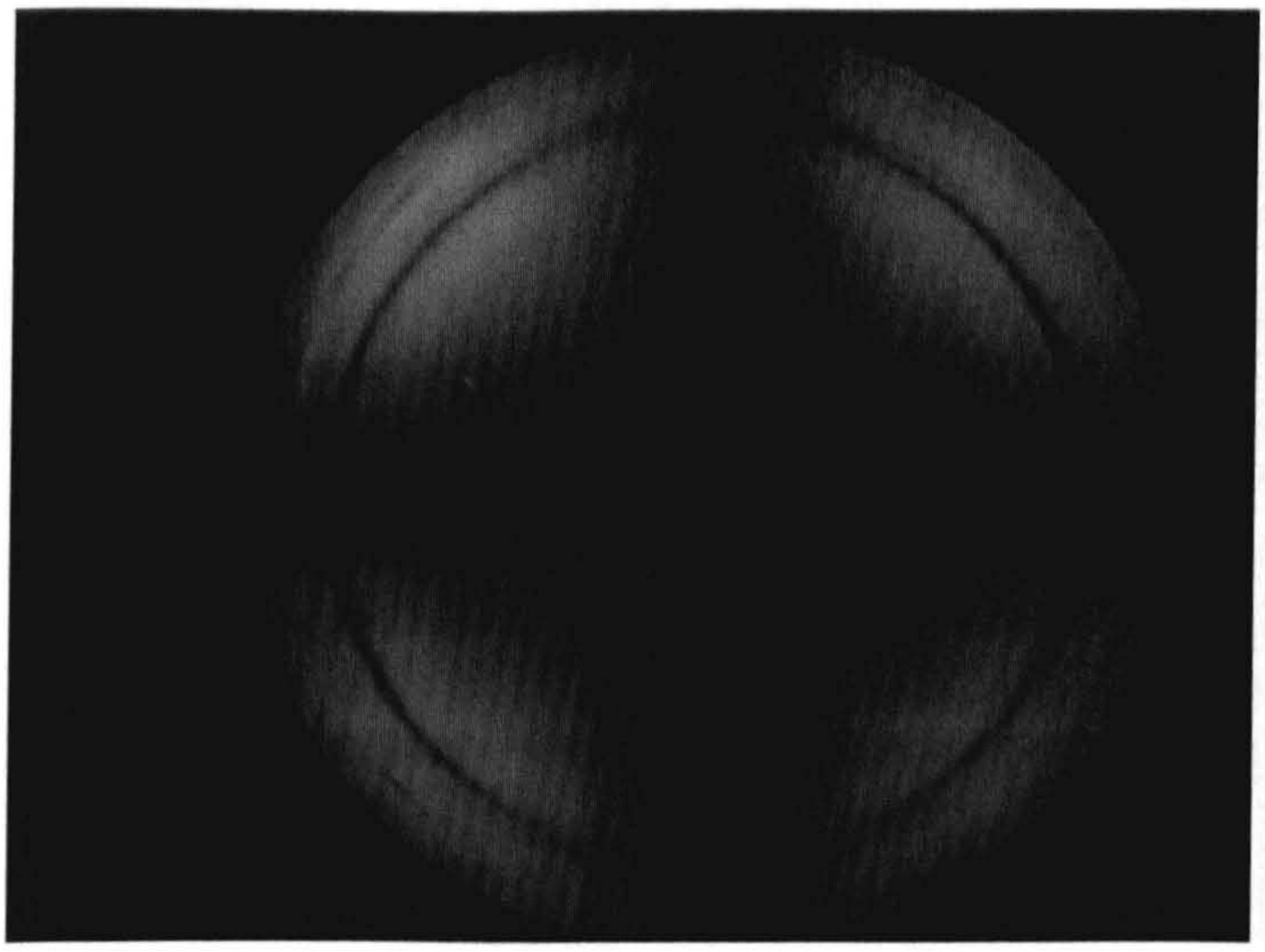

Figure 5.17: *Back focal plane of sample B with a cross-aligned analyzer and vertical input polarization*

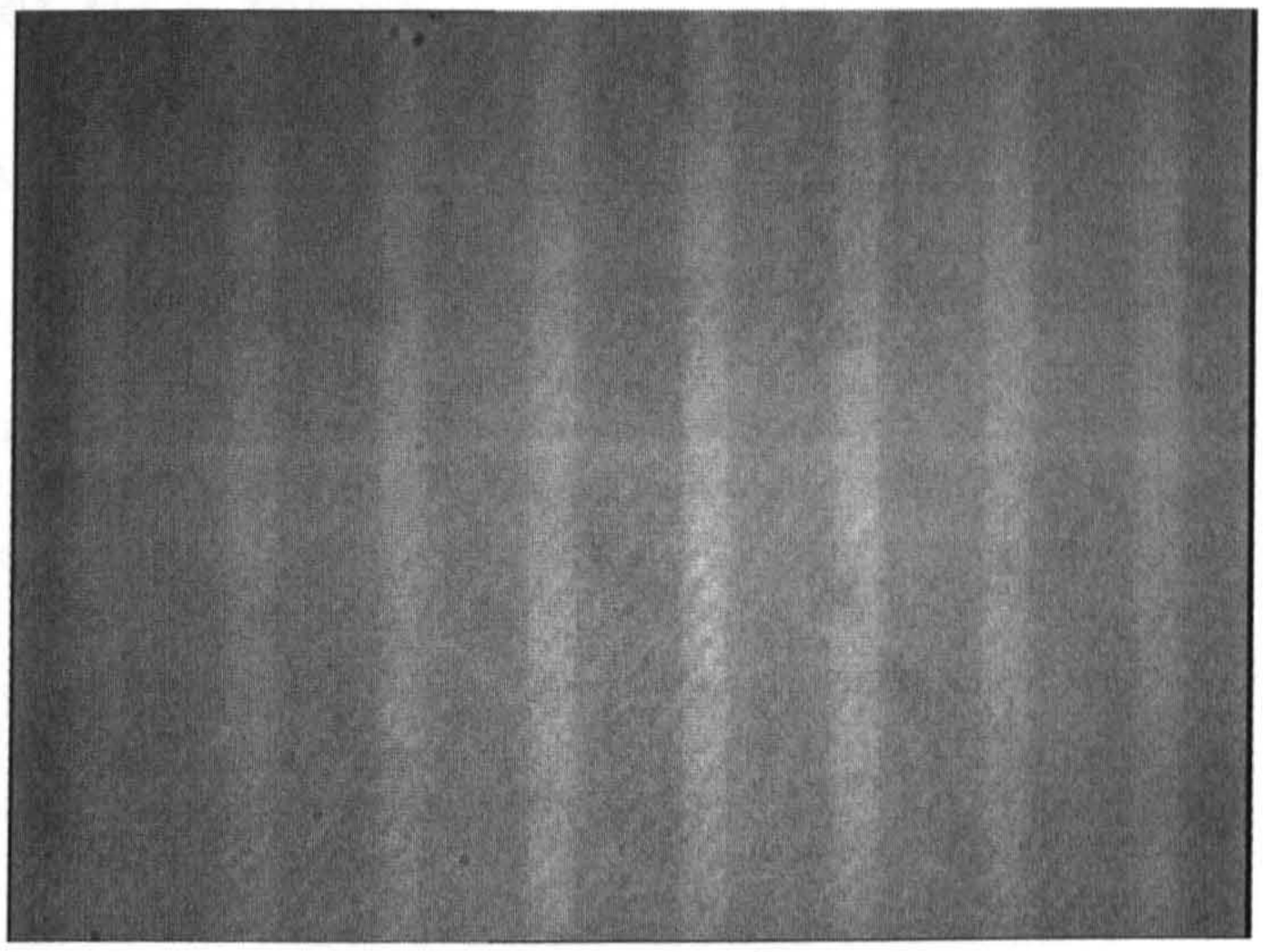

Figure 5.18: *Back focal plane of sample B with a cross-aligned analyzer and horizontal input polarization*

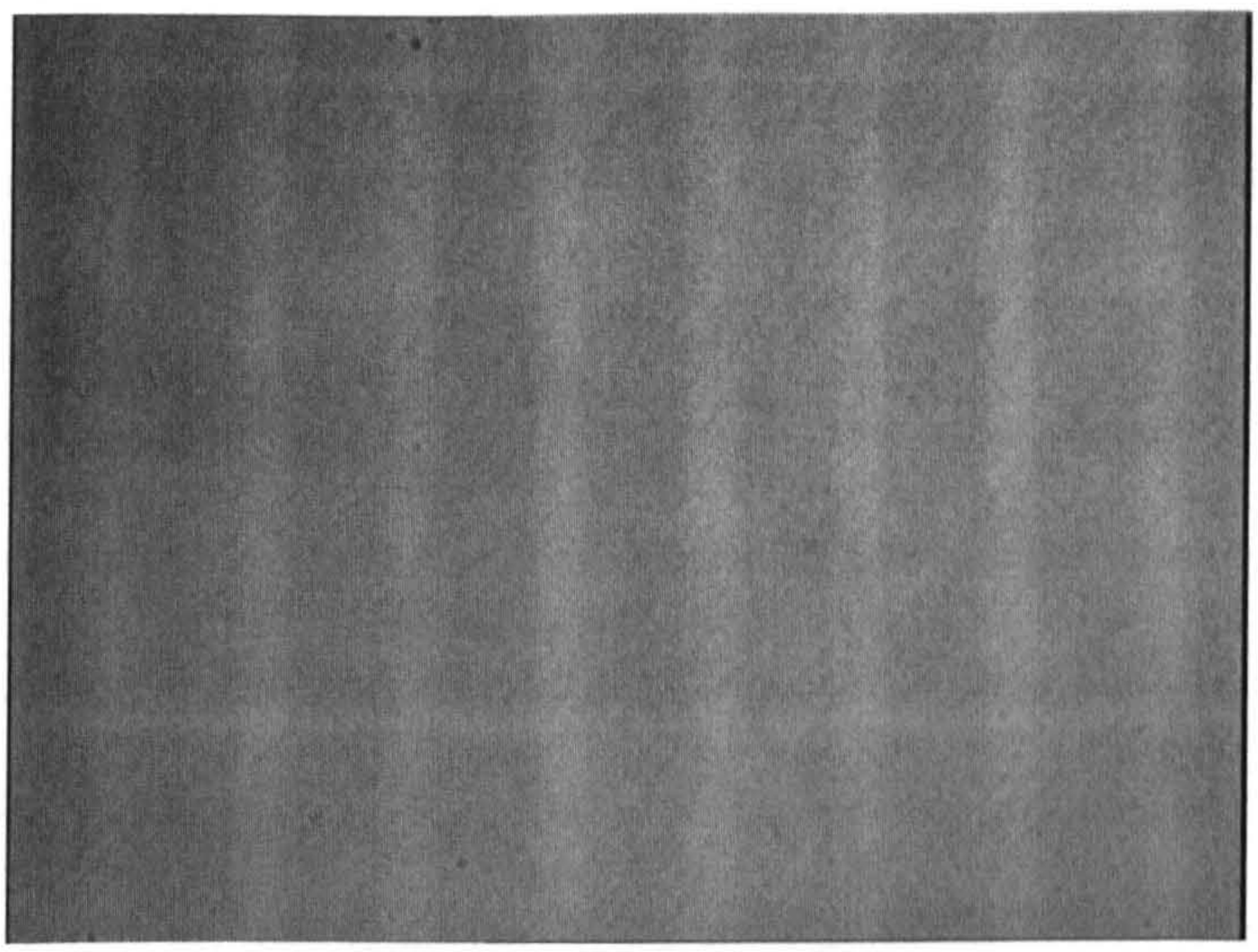

Figure 5.19: *Back focal plane of sample B with a cross-aligned analyzer and vertical input polarization*

5.1.3 Use of BFP masks

In order to further increase the contrast of the basic imaging system, custom masks were placed in a plane conjugate to the BFP. The masks were designed to block out the light illuminating the sample that does not produce SPs. It should be noted that the light exiting the objective is not masked so the image is formed from the entire exit pupil. This is the opposite regime to that seen previously, when filtering was performed after reflection at the sample.

The production of the masks has been covered in chapter 3 and design was relatively straight forward, a graduated glass scale was placed in the plane conjugate to the BFP of the objective. An image of the BFP was then taken and imported into a CAD package. The annular mask could then be designed to block the unwanted incident angles.

Figure 5.20 shows the image produced with horizontal input polarization and figure 5.21 with vertical. The contrast is improved over the the use of a polarizer and a difference can be seen in resolution between the two orientations. To make this more clear, line traces for a single stripe are shown in figure 5.22. The vertical lines denote the theoretical width of the real 2μm stripe. It is clear that the resolution is improved when the sample is illuminated with vertical polarization such that plasmons propagate along the structure rather than across it. From these plots the resolution is thought to be in the region of 1μm for horizontal polarization and 0.5μm for vertical. These figures compare very favourably with those from the literature,

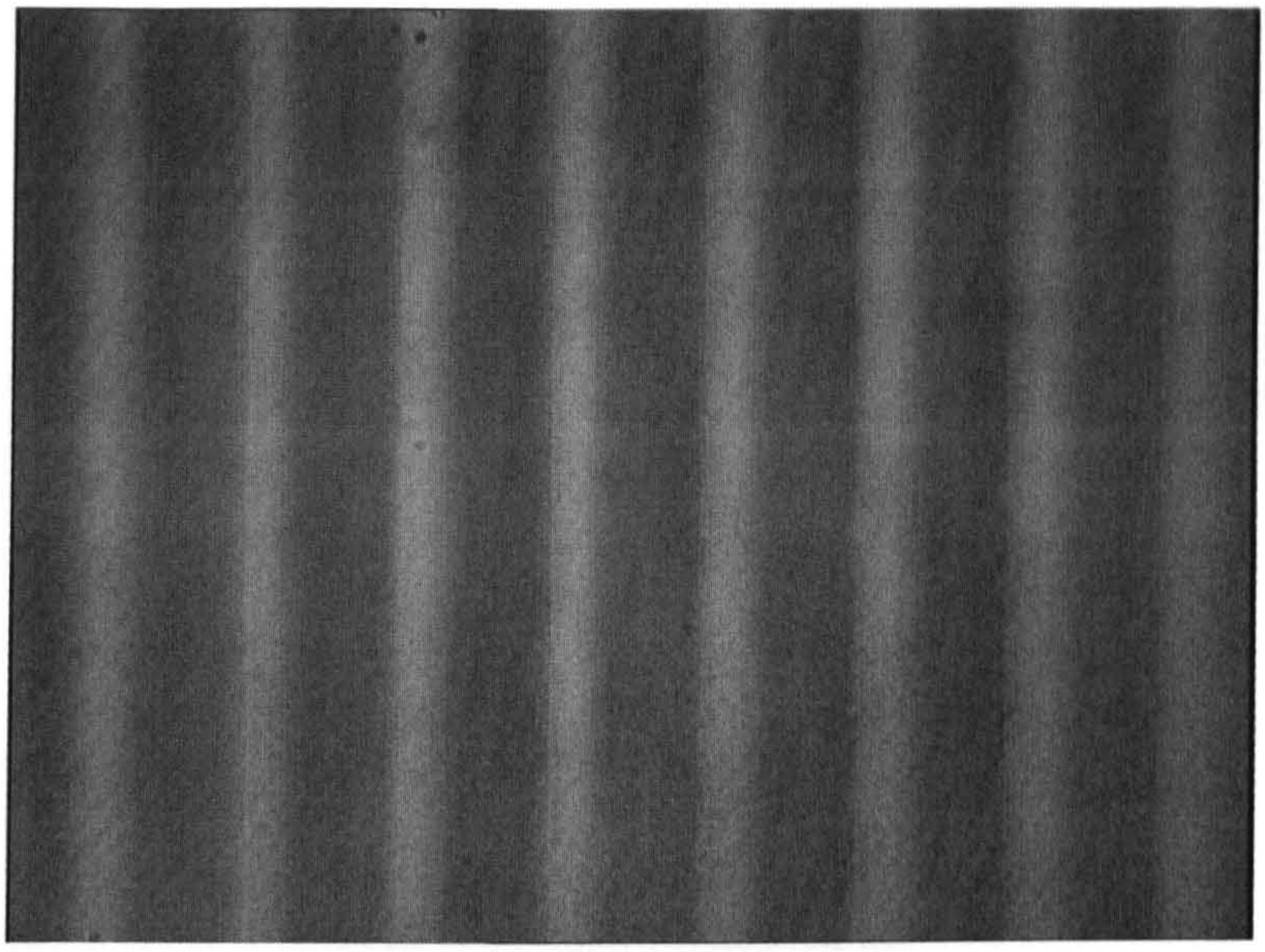

Figure 5.20: *Image of sample A with masked BFP and horizontal input polarization*

even the resolution for SP propagation across the structure is an improvement. The contrast is found to be approximately 30%. The same experiment was repeated for sample B and the results may be seen in figures 5.23 and 5.24 for horizontal and vertical polarization respectively. The resolution is similarly improved over the polarizer method and is better when vertical input polarization is used. The images give identical resolution to that seen for sample A.

5.2 Resonance averaging

Before the mechanism of contrast that allows these structures to be seen is discussed it is necessary to explain further the averaging effect seen in the BFPs for the case

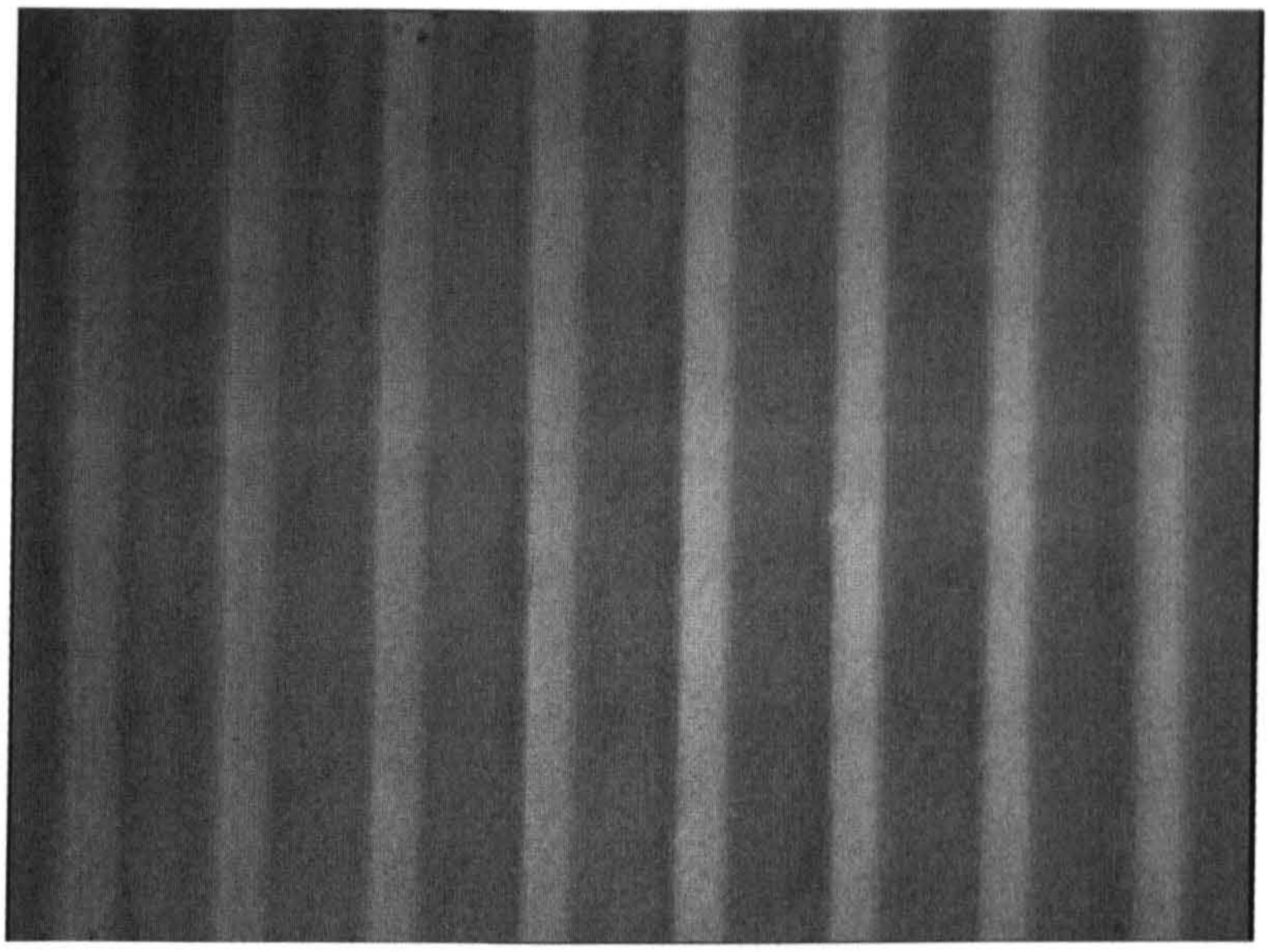

Figure 5.21: *Image of sample A with masked BFP and vertical input polarization*

of SPs propagating parallel to the grating vector. The reason for the explanation is to show that the BFP shows the emitted angular spectrum and does not tell the whole story about the excitation.

For a homogeneous sample and plane wave illumination, the propagation length of the SPs excited is irrelevant as the whole of the metal electron lattice will oscillate resonantly with the incident beam. The lateral propagation of the SP energy is constant over the sample and there is no spatial damping. For this reason such a structure may be considered using a Fresnel theory approach.

A heterogeneous sample with structures larger than the SP propagation length may also be considered using the Fresnel approach when looking at the reflectivity versus incident angle. Rothenhäusler et al considered grating structured at various

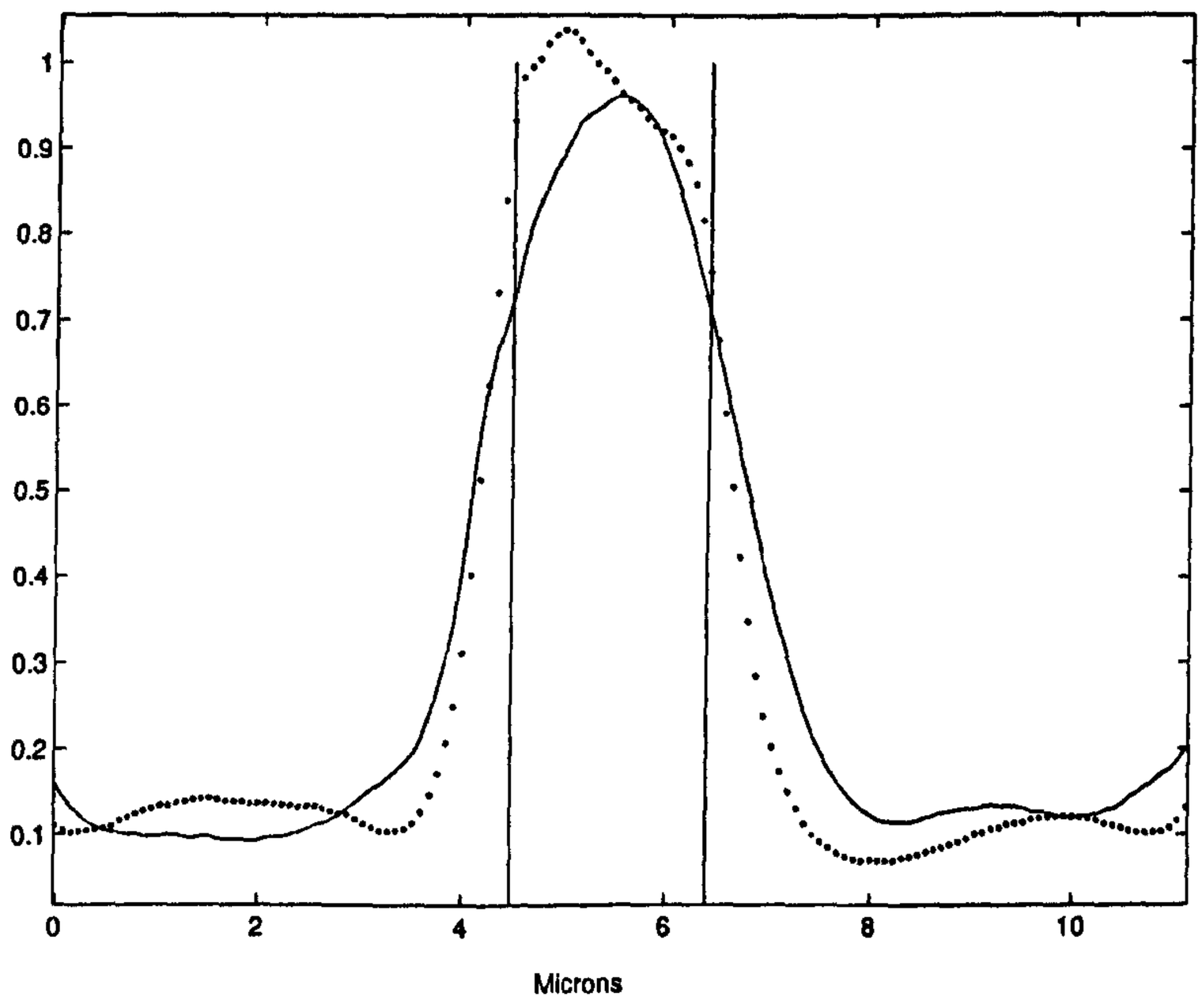

Figure 5.22: *Line trace showing one stripe of SiN4 from figures 5.20(solid) and 5.21(dotted)*

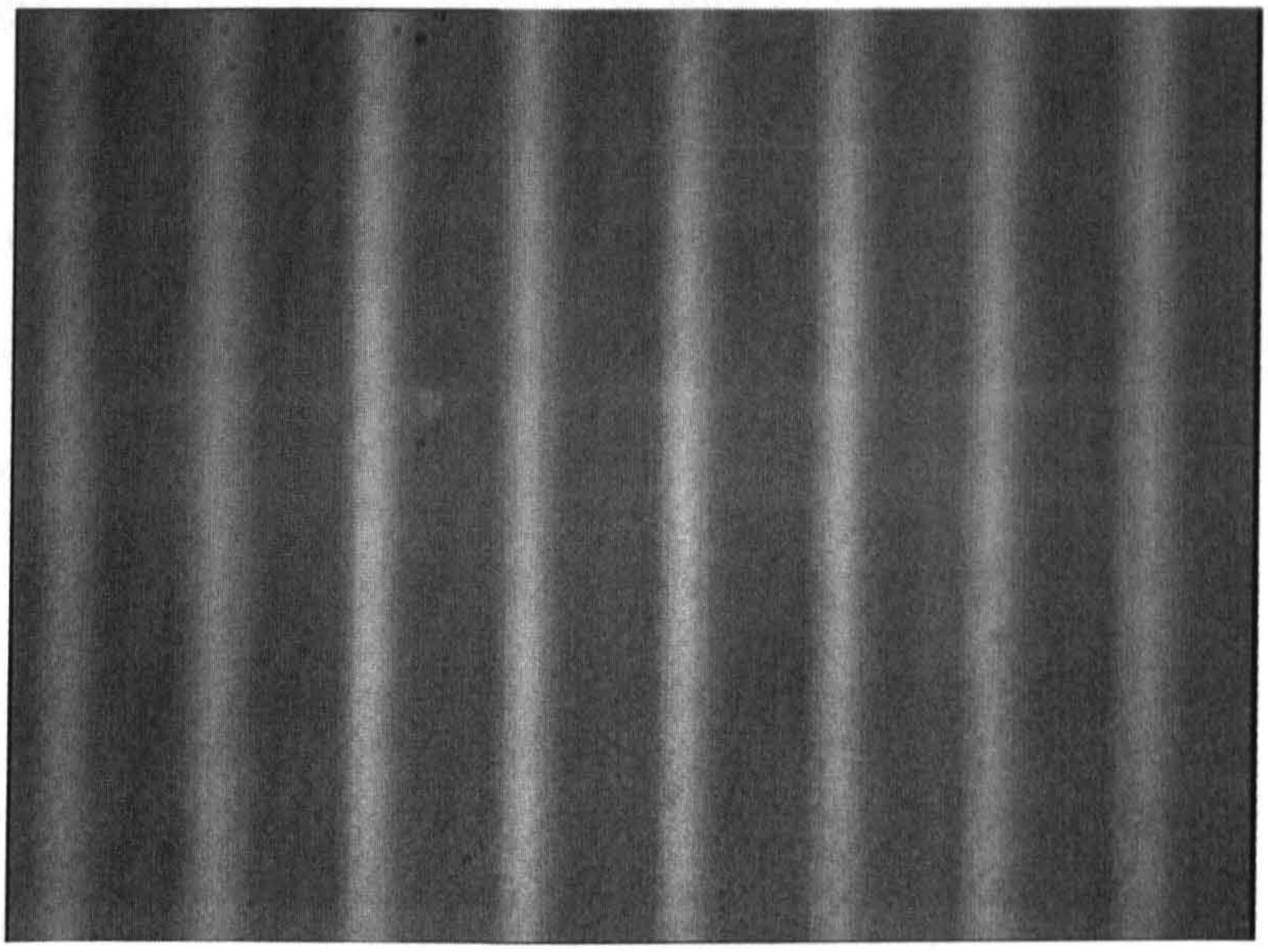

Figure 5.23: *Image of sample B with masked BFP and horizontal input polarization*

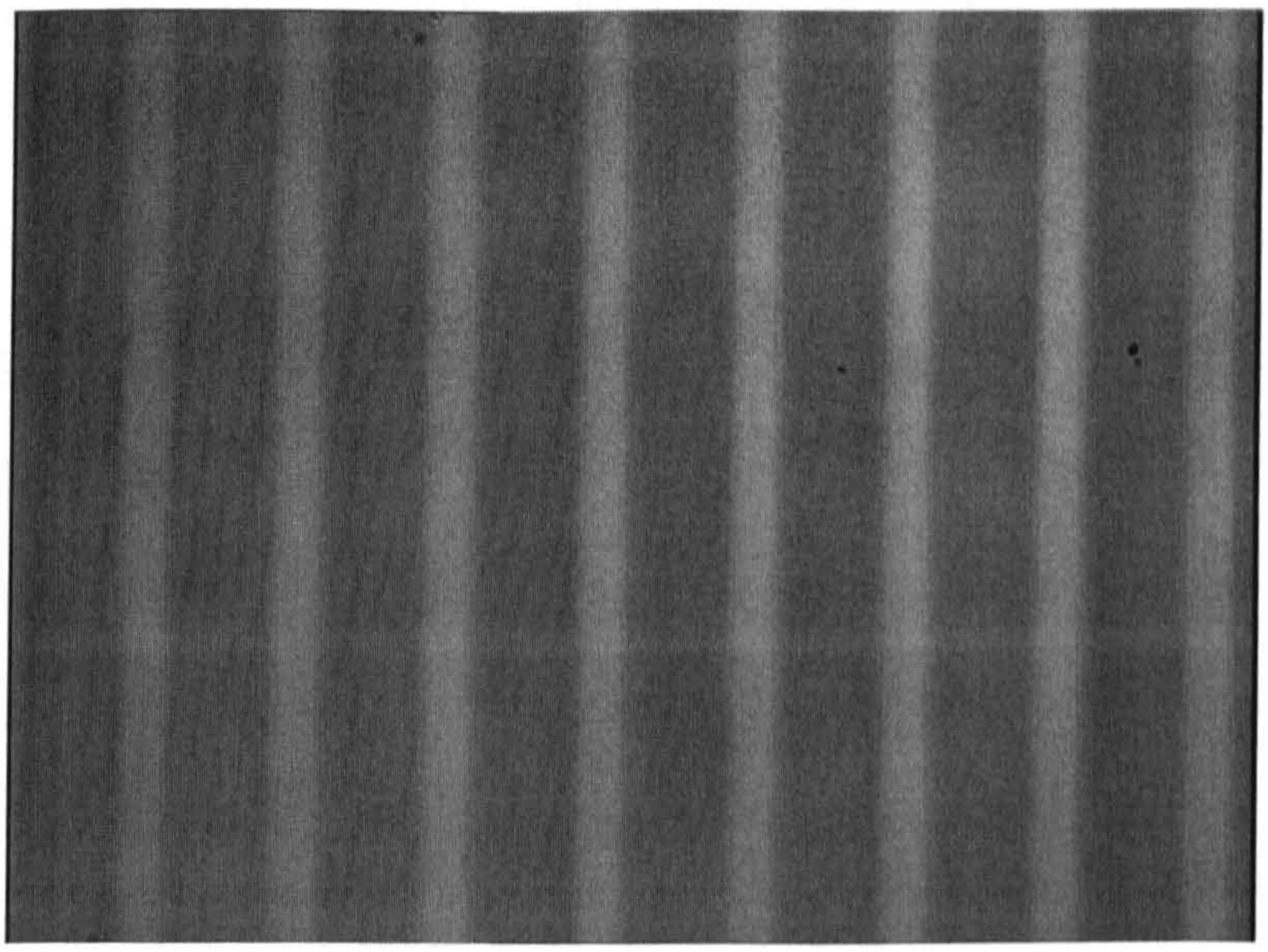

Figure 5.24: *Image of sample B with masked BFP and vertical input polarization*

wavelengths and hence SP propagation lengths [21] . Samples were placed in the Kretschmann configuration and illuminated at a single angle. All reflected, reemitted and diffracted light was collected and measured and plots of reflectivity versus angle were produced. Because the whole of the reflected spectra is detected it is the absorption of the incident light that is recorded. This measurement is subtly different to what is seen in the BFP of the objective. In the exit pupil as was imaged in these experiments the radial position corresponds to light leaving the sample at a specific angle, however, light that emanates at one angle may originate from light incident at another angle as shall be seen. Despite the two experiments not being identical the observed results are very similar but do require slightly different explanations.

Figure 5.25 shows a result from Rothenhäusler's paper, part a) shows the angle versus reflected light plot for a grating sample when the SP propagation length is much smaller than the grating period. Two distinct dips appear that correspond to the homogeneous resonances of the respective structures (coated and uncoated). The depth of these dips is less than for the homogeneous cases as the two responses are effectively added. For example, the light satisfying the resonance of one material will be specularly reflected off the other, reducing the depth of the resonance. Part b) shows the effect of using light of a longer wavelength, the SPs are now of comparative size to the structure and much more likely to cross from resonant to non-resonant regions. The two dips previously seen have merged into a single resonance at an angle corresponding to the average thickness of the sample. Before explaining the

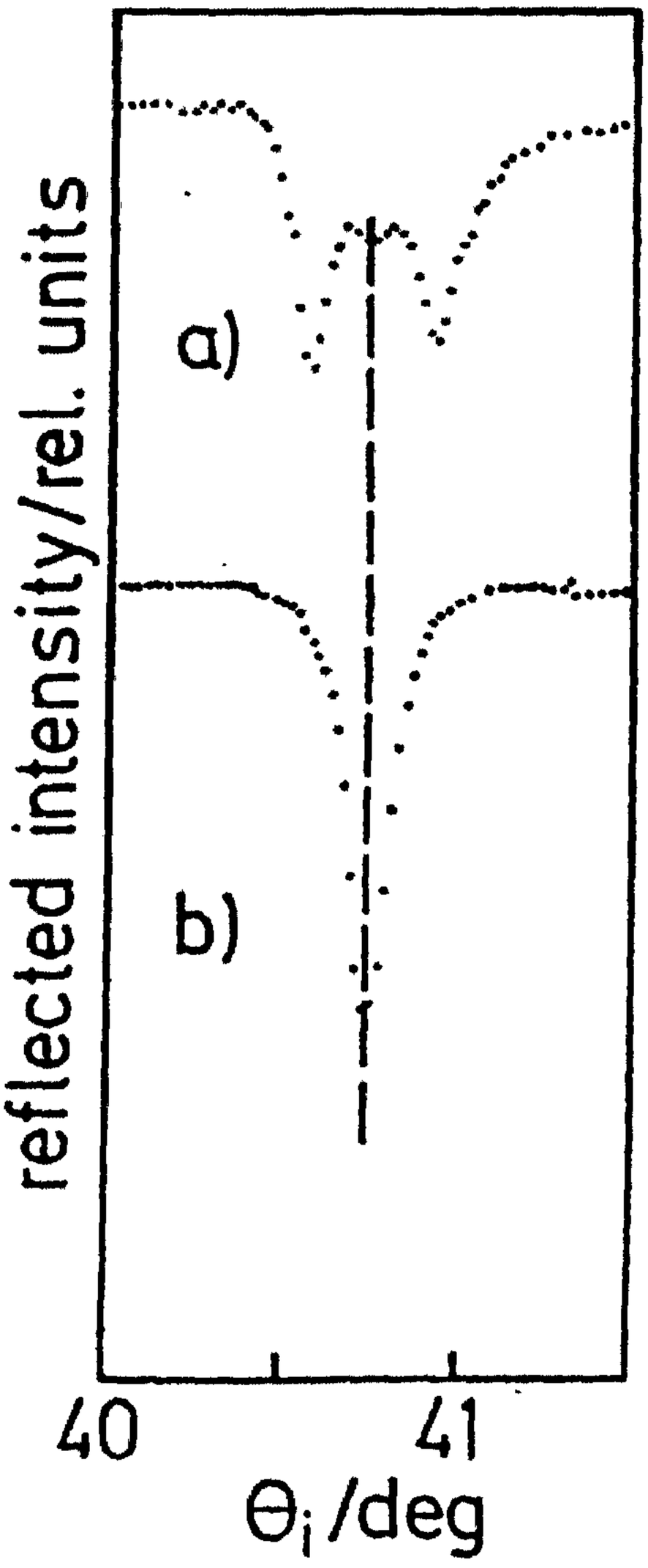

Figure 5.25: *Reflectivity of a grating structure for long (a) and short (b) SP propagation lengths taken from ref. [21]*

second case let us return to the first, figure 5.26 shows the situation for a sample that is large compared the SP propagation length. An incident plane wave strikes the sample at the resonant angle of the coated region, exciting SPs such that they propagate left to right, from coated to uncoated region. In the resonant region little light is reflected but some is reemitted. In the non resonant region most of the light is reflected. At the boundary the SPs excited in the resonant region with wave vector k_0 couple into the resonant mode of the uncoated region, k_1 [23]. This new mode decays as it is not driven by the incident beam. It also reemits energy with wave vector k_1 just as it would have done in the uncoated region with wave vector k_0. The region in which the decaying SP exists can be thought of as an extra area from which energy coupled into plasmons might reemit, the longer the SP propagation length compared to the sample structure the greater this extra area and its effect on the reflectivity is. For the large structure seen in the figure the effect will be small, reducing the depth of the resonance only slightly. Now consider a structure that is of comparable size to the SP propagation length. Figure 5.27 shows such a structure. In this case a grating is considered as it is in ref [21] and this work. Three cases are depicted, the first is illumination at θ_0, the resonant angle for the bare metal. The second at θ_1, the resonant angle for the coated metal. The third is θ_2, an angle lying somewhere between θ_0 and θ_1.

For the first case SPs will be excited in the uncoated regions, reducing the reflected light. In the coated regions, most of the incident light will be reflected. These two effects would normally give rise to a resonance in the reflectivity curve but with

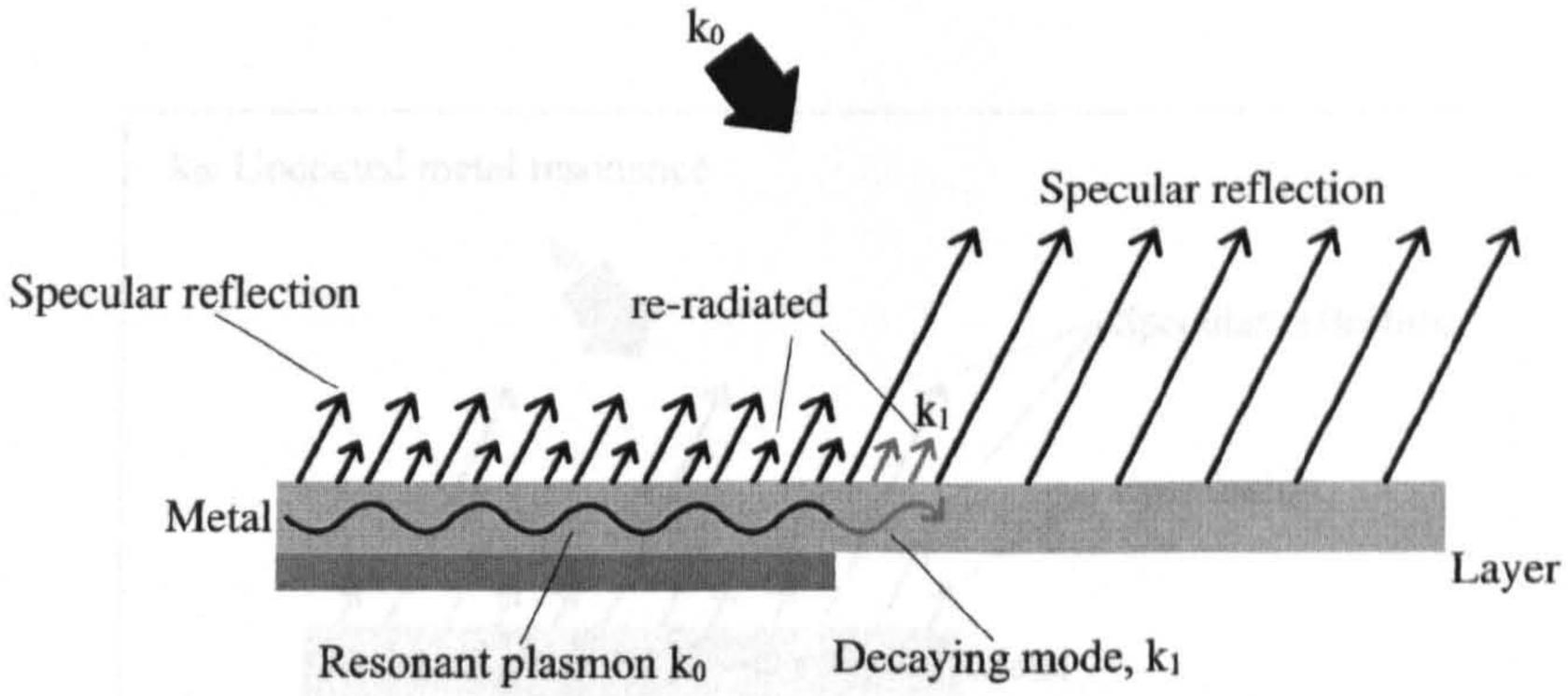

Figure 5.26: *Effects of SP propagation length on a large sample structure*

less depth than that of the homogeneous case due to the specularly reflected light from the off resonance part of the sample. However in this case the decaying SPs must be considered as the propagation lengths cover areas that are comparable to the stripe widths. As before, SPs excited in the uncoated regions with wave vector k_0 couple into SPs with wave vector k_1 in crossing the boundary. Any light reemitted from these SPs will now do so at θ_1, the angle corresponding to the new material. In the case of Rothenhäusler's experiment this light is collected and reduces the depth of the dip seen at k_0. In the case of these experiments it would increase the amplitude of the BFP at the point corresponding to SP excitation at k_1, potentially reducing that dip. Unlike the large structure case, the extra reemission area is half of the total sample area and so the effect will be considerable. The extra light from the reemitting SPs tends to "fill up" the resonance that created them as in

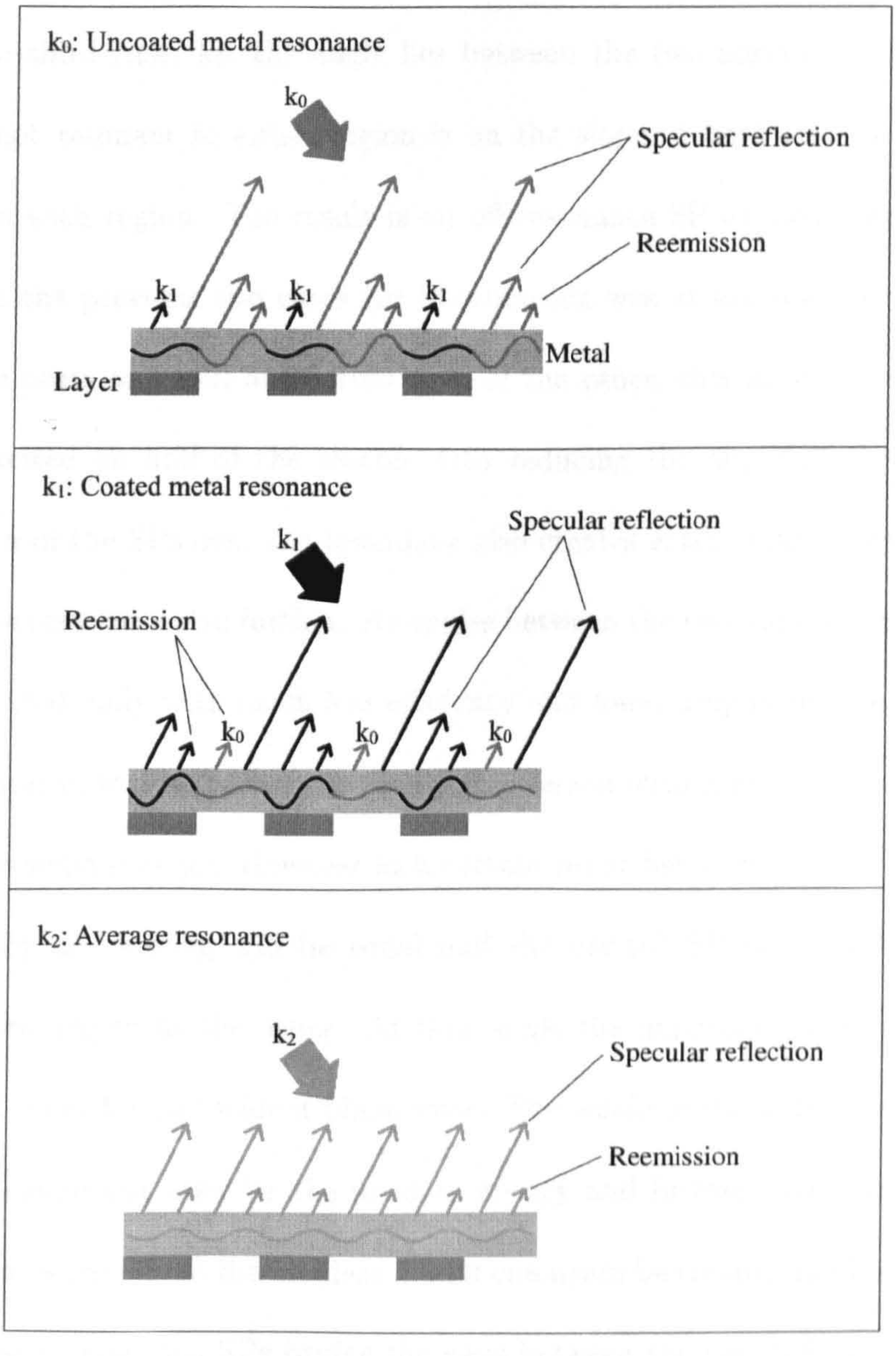

Figure 5.27: *Effects of SP propagation length on a small sample structure*

Rothenhäusler's result or the resonance corresponding to the other part material as per these results.

For the third case, k_2, the angle lies between the two normal resonances and although not resonant in either region is on the slope of both and so is partially resonant in each region. The result is an off-resonance SP excited over the entire sample. In the previous two cases the illumination was at the resonance of one of the sample parts and well away from that of the other, this means that SPs may only be excited on half of the sample area reducing the depth of the dip. The propagation of the SPs over the boundary also creates extra emission reducing the depth of the resonance still further. At angles between the two main resonances, SPs are still excited, only with much less efficiency and lower amplitude. The efficiency of the excitation will be highest in the sample region with a resonant angle closest to the intermediate angle. However at a certain point between the two resonances the efficiency of coupling will be equal and the excited SP mode will be as "at home" in one region as the other. At that angle the maximum coupling into the sample will occur for an incident plane wave. The whole of the sample surface then becomes a catchment area for the incident energy and further more, as the whole sample behaves equally to the incident field it can again be treated as a homogeneous medium, the propagating SPs bridge the gaps between the two differing structures creating a constant field across it.

The example given shows a sample with a duty cycle of 50%. In that case the angle of incidence that creates the homogeneous SP is equal to the resonant angle

of a homogeneous sample with a layer thickness that is half that of the origional grating layer thickness. The grating duty cycle affects the average layer thickness and hence the homogeneous resonance. The resonance will tend to be closer to the angle related to the larger sample surface area, this can be thought of in terms of the fact that the wider stripe will tend to reduce the average thickness if uncoated or increase it if it is coated or it might be imagined that the resonance should match the wider structure more as the homogeneous SP must be "kept going" for longer, the propagating SPs will tend to smooth over the narrower region.

In conclusion, for a sample of comparable dimensions to the SP propagation length the propagation of resonant SPs into neighboring regions tends to increase the overall reflectivity. In this case a new resonance is formed corresponding to the average effect of the structure.

5.3 The imaging mechanism

In chapter 1 several ways of achieving contrast in SP imaging systems were described, the most common is to use a fixed illumination angle and measure the reflected intensity as it varies across the sample. Another method is to again illuminate at a fixed angle but map the phase shift over the sample.

This system differs from those in that the illumination is not at a single angle. Masks were used to reduce the background light levels but illumination included a range of incident angles.

The image is made up from a set of points on the sample that map to conjugate points on the CCD camera, each point and its conjugate, as well as the rays that join them may be thought of as being a single point scanning system. It is known from the literature that such a system can excite SPs in a localized area much smaller than the 2μm width of the uncoated stripes. If a single point pair is considered then it is clear that the BFP contribution for this specific point will have a single resonance just as it does in the scanning systems seen in the literature [28][46]. It is only when all points are considered including the cross coupling via SPs and their contribution to the BFP is integrated that the resonances show an averaging effect. This is a reminder that the imaged BFP distribution maps only the reflected angular spectrum.

Therefore, with a range of incident angles, the only way in which contrast may be seen is by the differing levels of plasmon excitation in each region. Ignoring for now the propagation of SPs as may be done in practice for vertical polarization.

Figure 5.28 shows simulated, normalized, reflected intensities with respect to angle for coated and uncoated sample regions. The resonance of the coated region is substantially widened but has comparable depth to the uncoated gold. The energy coupled into SPs in this material is therefore likely to be less. After integrating these curves the coated regions was found to absorb approximately 10% more light than the uncoated region. This value does not tally with the contrast seen in the images so it would seem likely that the applied mask was actually blocking the inner gold resonance as the edge of the mask was aligned closely with the average reso-

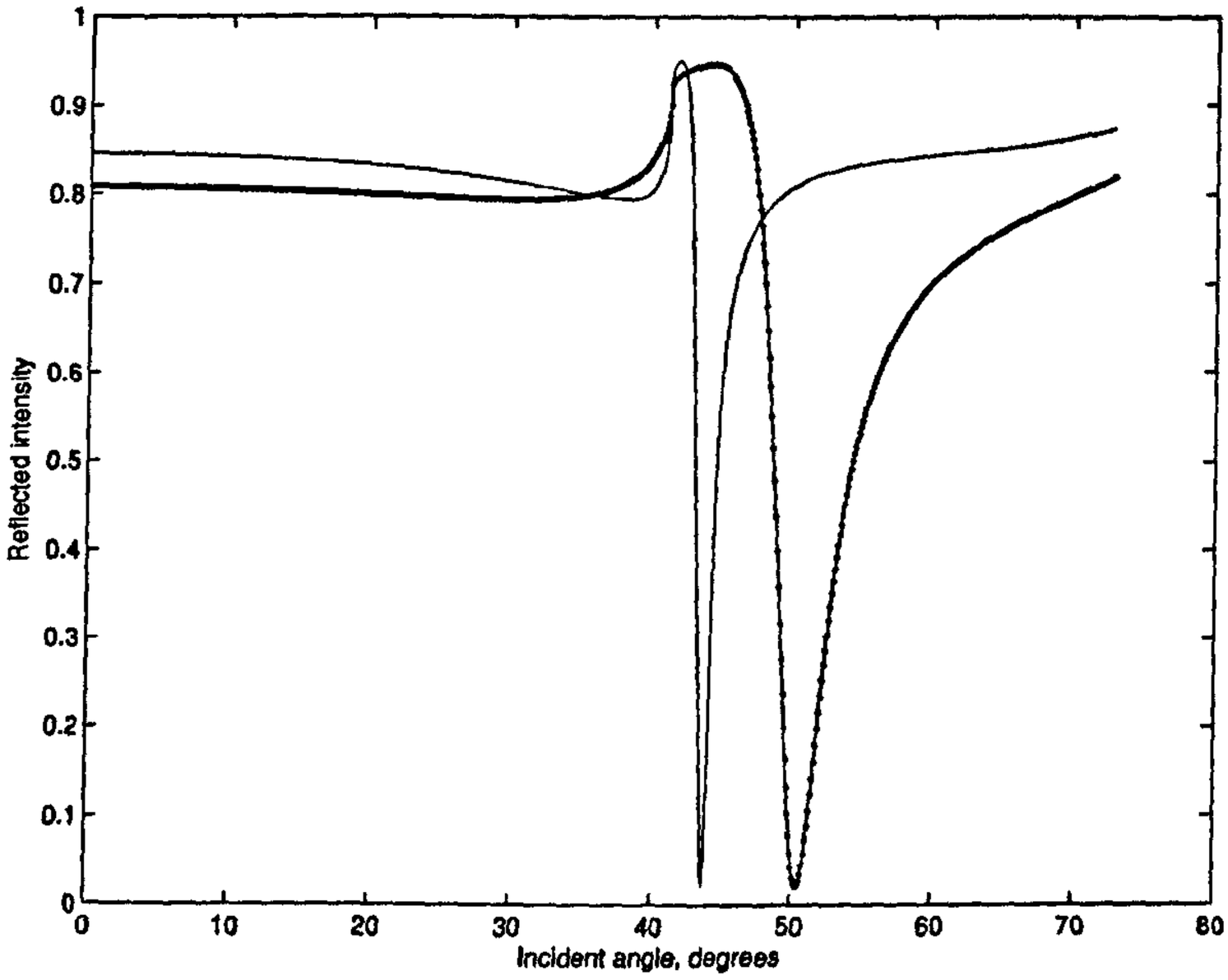

Figure 5.28: *Reflectivity versus angle for 43.5nm thick gold without a coating (solid) and with a 20nm SiO_2 coating (dotted)*

nance. This would also block the pure gold resonance for vertical input polarization. Intergrating the same curves for angles greater than the gold resonance predicts a contrast of upto 40% depending on the position of the exact cut off. An image of the mask was not taken so the exact cut off for the mask cannot be confirmed, nevertheless, this value is quite close to the observed contrast of 30%.

5.4 Summary

The system described shows a simple way of obtaining images with good contrast and good spatial resolution at a minimal cost and complication. Polarization optics

were shown to be a simple way to increase the contrast and revealed some interesting points about changes in polarization of the imaged light and a possible way to exploit this in the future. Masks placed in the back focal plane proved to give even greater contrast although produced a reduction in resolution between images taken with plasmons propagating across the structure rather than along it. The mask had been designed by looking at what could be seen in the BFP and it was serendipity that this produced greater contrast by blocking the resonance in one material. It is clear that this system may not be suitable for very thin films when the two resonances are very close and absorb equal amounts of energy but for fast acquisition of thicker films especially with high dynamic range this system could be wholly suitable. Especially if the mask could be automated via an LCD array or mechanical means. Either way it offers another mode of operation to the final embodiment of the system presented in the next chapter.

Chapter 6

Interferometric Wide field Plasmon Imaging

6.1 Introduction

In this chapter the results from the final embodiment of the system will be presented and the effects of defocus will be shown.

It is important to remember the essential aspects of the original scanning system that produce high resolution and high contrast images. The first point is the use of a high NA objective perpendicular to the sample. The second is the confocal response given by the virtual pinhole of the flat reference beam. Thirdly the system uses the perturbation in the phase of light that excites SPs to unwrap its curved phase front allowing contrast to be gained from the specific angle at which the resonance occurs. This comes from the interference of the relatively flat axial illumination

and the unwrapped portion of the incident light with the reference beam. This contrast mechanism was found to be potentially very sensitive when the objective was defocused and the resolution was found not to be degraded due to SP focusing. The mechanism and the arguments for the high resolution and contrast hold true for the wide field version of the system based on speckle illumination. The confocal response still comes from a pinhole effect but this time the virtual pinhole is produced by speckle correlation. The wide field system may therefore be thought of as many overlapping scanning systems even at defocus.

6.2 Mask design

As the images are taken with a CCD camera with limited dynamic range it is still advantageous to filter out much of the light that is not part of the contrast mechanism. To this end a mask was designed that would allow the passage of only the SP excitation angles and a portion of the more axial rays. The central aperture is a requirement as without it there is no reference with which the light corresponding to excitation may beat.

The mask was manufactured with a lathe as described in section 3.6. The mask may be seen in figure 6.1. The central hole could be blocked if required with a small piece of opaque adhesive tape.

A final note is that the mask only affects the illumination. All reflected light may contribute to the image formation as was the case in the standard imaging mode.

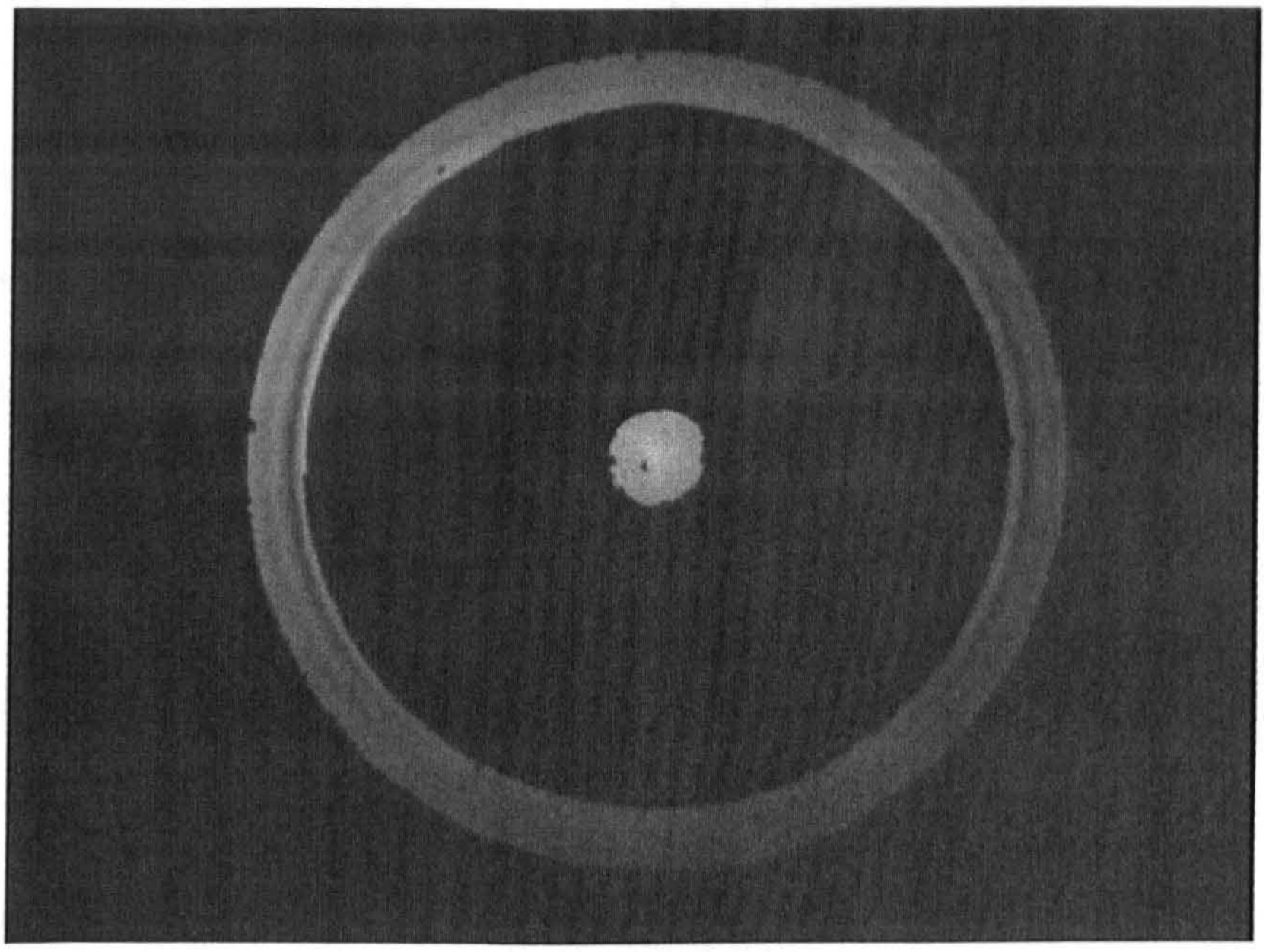

Figure 6.1: *Mask used for interferometric imaging*

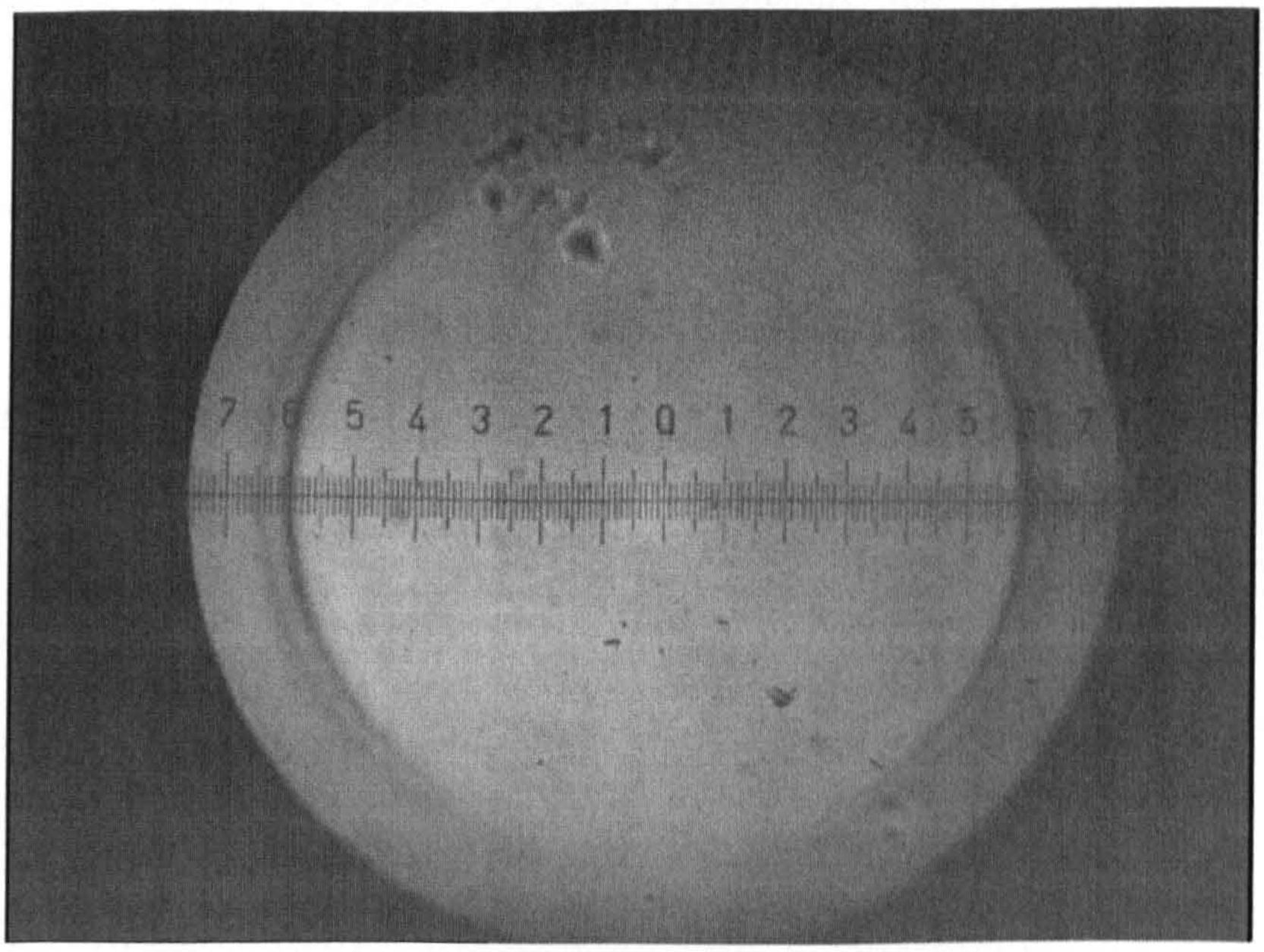

Figure 6.2: *Method of BFP measurement*

6.3 Imaging without central aperture

To prove that the central aperture is indeed required for high resolution a set of images with input polarization orientated horizontally were taken with varying defocus. At each defocus position four images were captured and the reference mirror phase stepped between them. To these images a phase stepping algorithm [47] was applied to extract amplitude and phase information. The amplitude corresponds to the interference term, V. A matrix of amplitude images may be seen in figure 6.3 for sample A as imaged conventionally in chapter 5 and described in figure 5.1. The value marked on each image is the scan position in microns, however, it should be noted that this is with reference to the start of the scan not to the focus. There is no easy way to find the focus with the system fully assembled so it was thought preferable to begin with slight positive defocus. The scan was done such that the sample was brought towards the objective into increasingly negative defocus.

The images show reasonable contrast but poor resolution, this is made more clear in figure 6.4 where averaged (row wise) line scans of a $20\mu m$ wide portion of the sample on the region without defect (a diagonal scratch) are shown. The reason the defect was imaged is that it allowed the sample to be orientated perpendicularly to the objective, the angle of the sample was altered and moved through focus manually until all of the defect came in and out of focus simultaneously.

The experiment was then repeated with the polarization orientated vertically. The image matrix and line scan matrix may be seen in figure 6.5 and figure 6.6

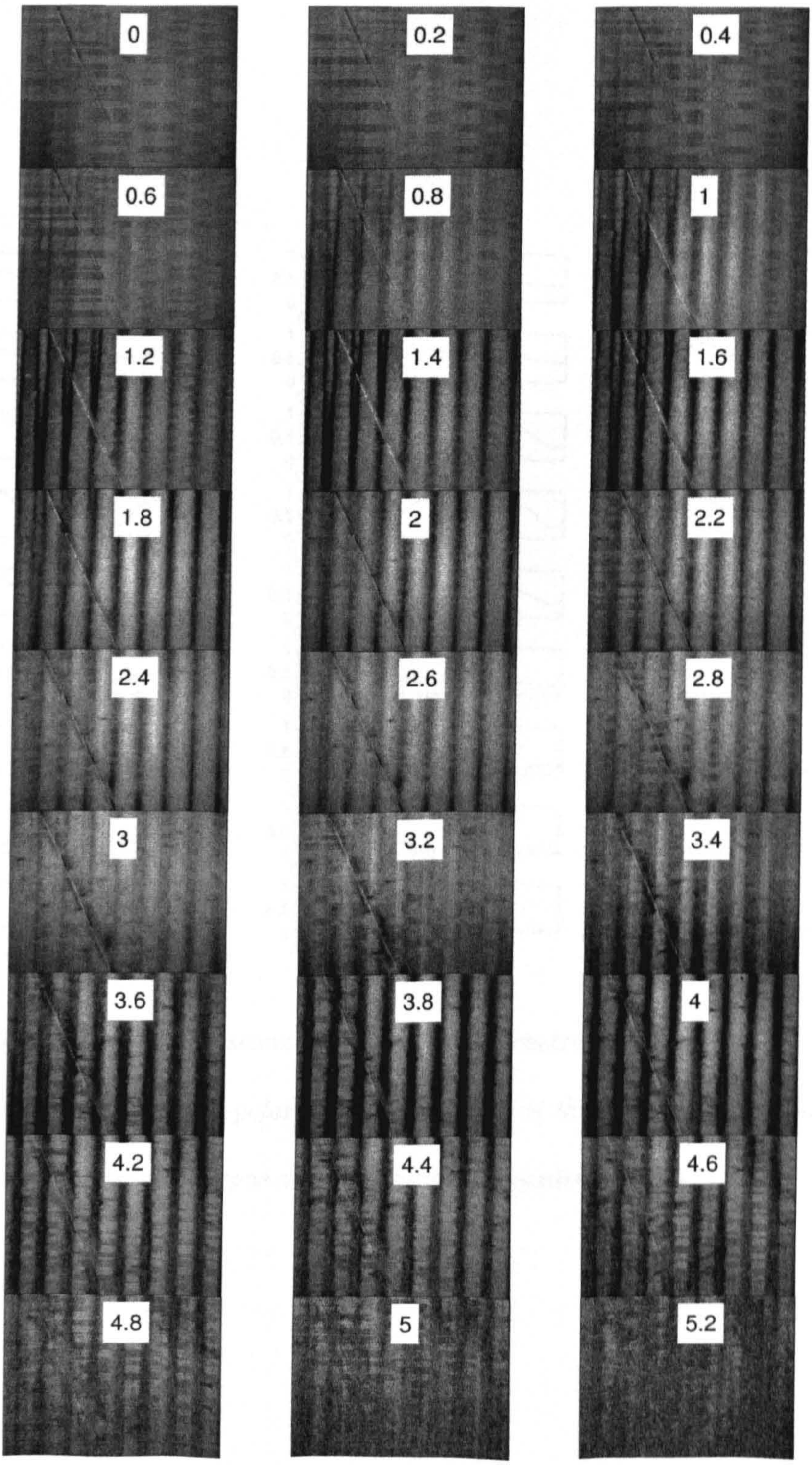

Figure 6.3: *Matrix of images produced interferometrically without reference aperture*

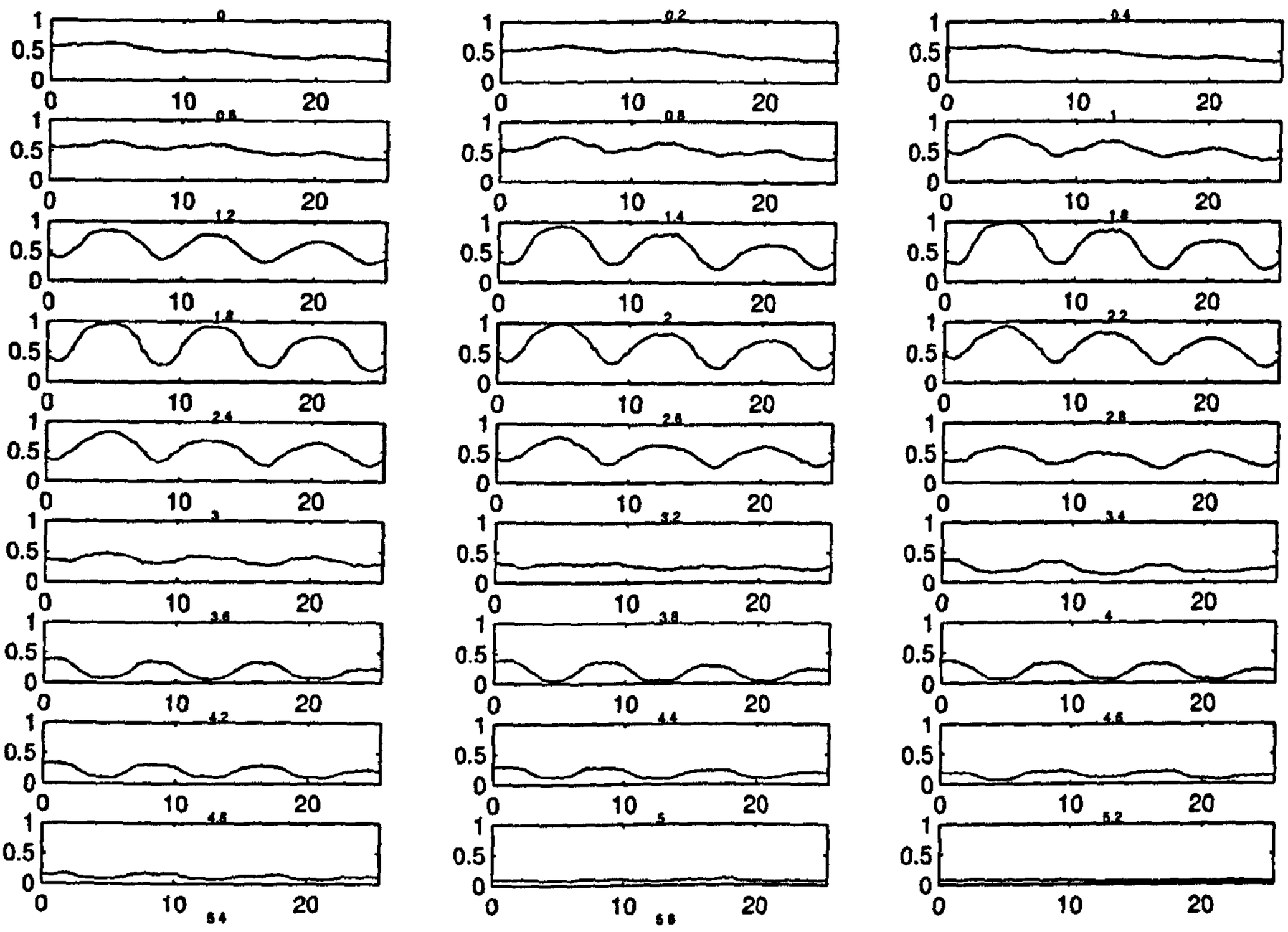

Figure 6.4: *Matrix of line scans produced interferometrically without reference aperture with horizontal input polarization, the y-axis is the normalized amplitude and the x axis distance in microns with increasingly negative defocus*

respectively. The images and line scans are almost identical to those with horizontal polarization.

To clarify the contrast and its reversal, V(z) plots were produced from the image sets it must be noted that the x-axis is reversed when compared to those of chapter 2. The scans were done such that sample began at positive defocus and was moved towards the objective into negative defocus and this ishow they are plotted. Although all the points that make up the phase-stepped images will display the V(z) response, small rectangular areas in each sample region were integrated to remove some of the noise. The V(z) plot for horizontal polarization along with a plot of the difference between the values of V for each region is shown in figure 6.7. A similar plot for vertical polarization may be seen in figure 6.8.

The V(z) plots are almost identical for each polarization orientation. The peak of the V(z) curve should correspond to the focus and there is still some contrast here. This might seem surprising however the phase profile of the unmasked portion of the BFP will differ for each part of the imaged structure. As this it is the only part of the wave front that will contribute to the output, it is likely to be more sensitive to this variation than it would have been for a system with a reference aperture. The lack of resolution is probably due to the suppression of the confocal response of the microscope. The central aperture would normally provide a flat section of wave front for the reemitted SPs to beat with. When this is the case the SPs that are emitted on the axis have greater effect than those off it, without the reference this will not be the case.

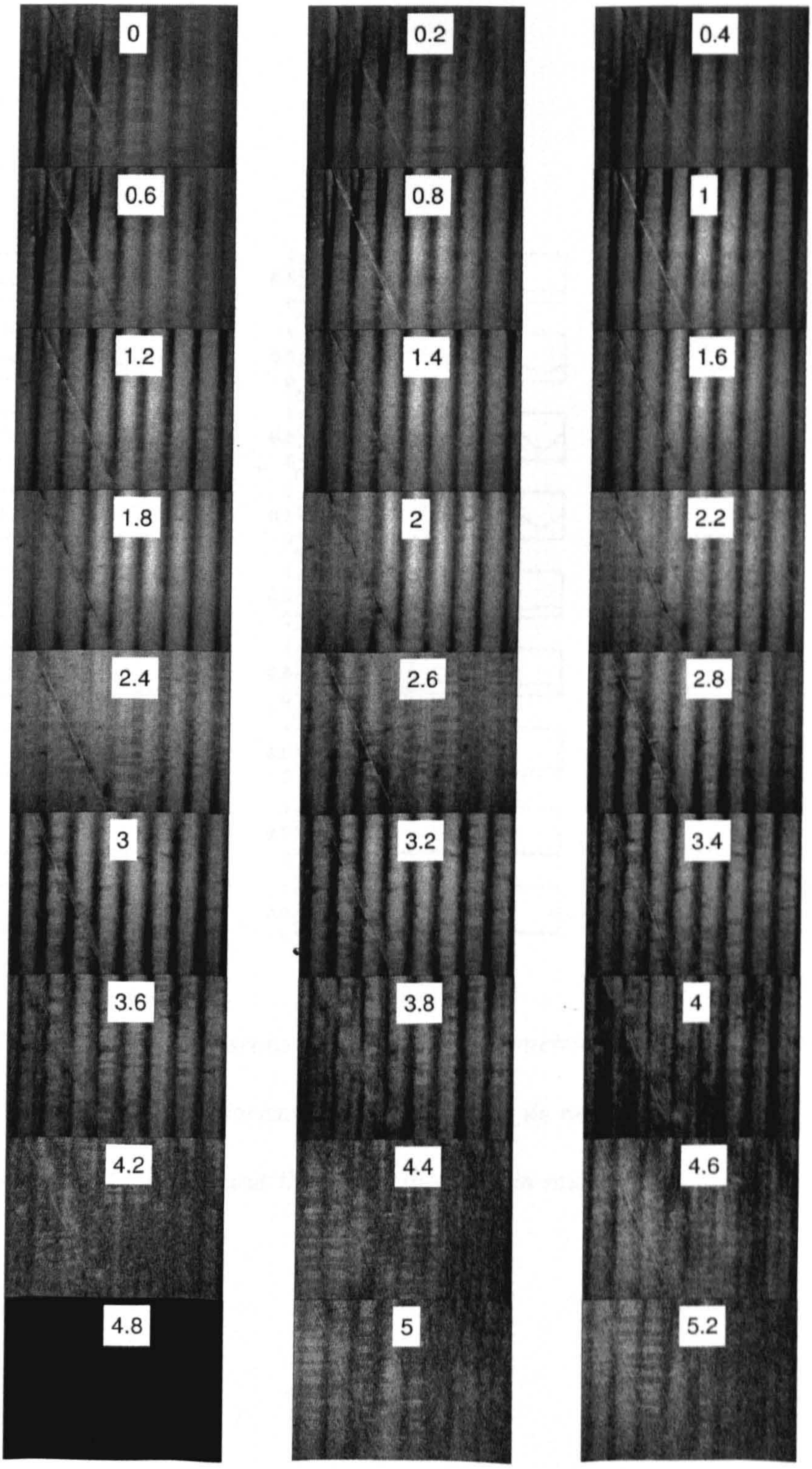

Figure 6.5: *Matrix of images produced interferometrically without reference aperture*

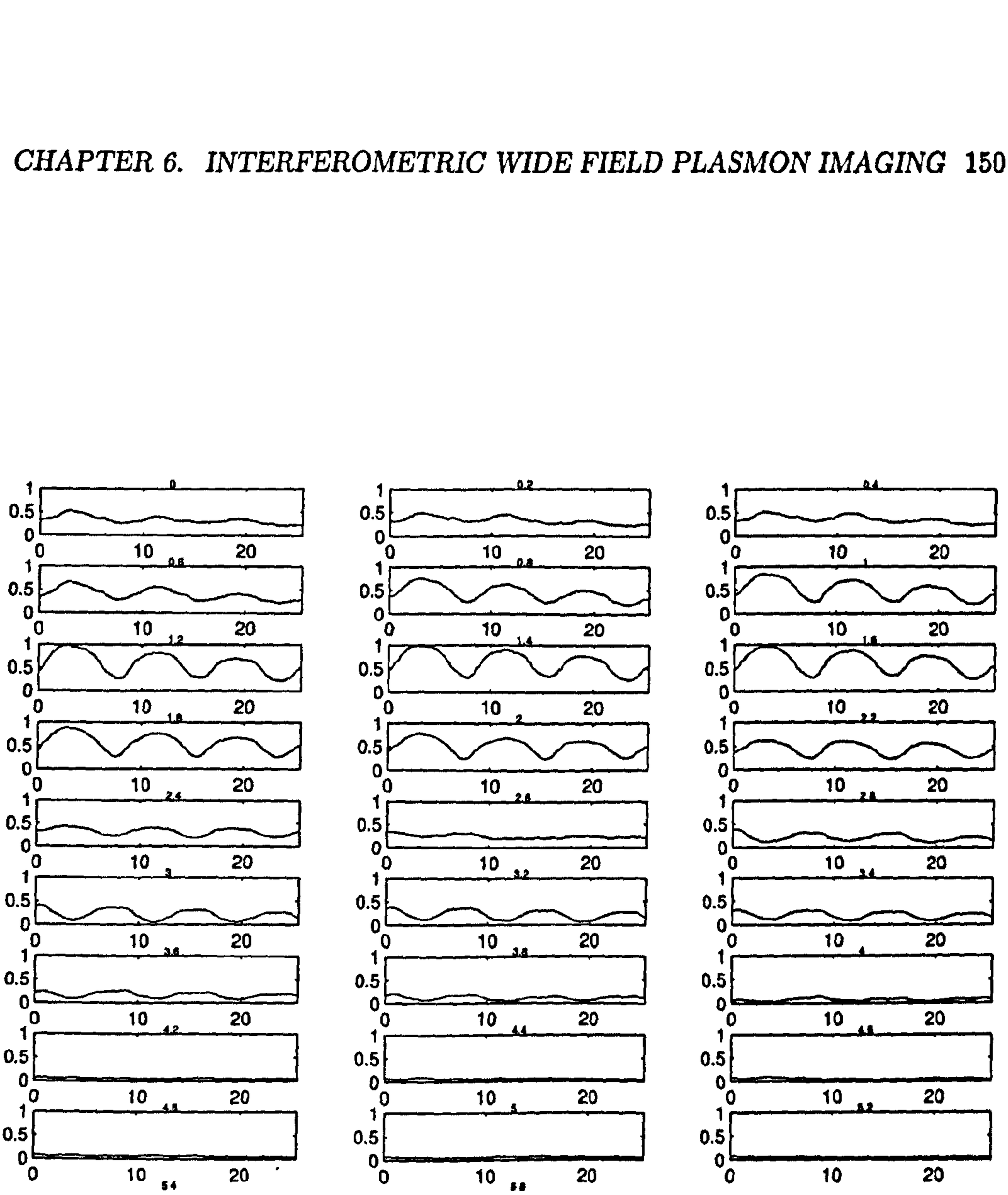

Figure 6.6: *Matrix of line scans produced interferometrically without reference aperture with vertical input polarization with increasingly negative defocus, the y-axis is the normalized amplitude and the x axis distance in microns*

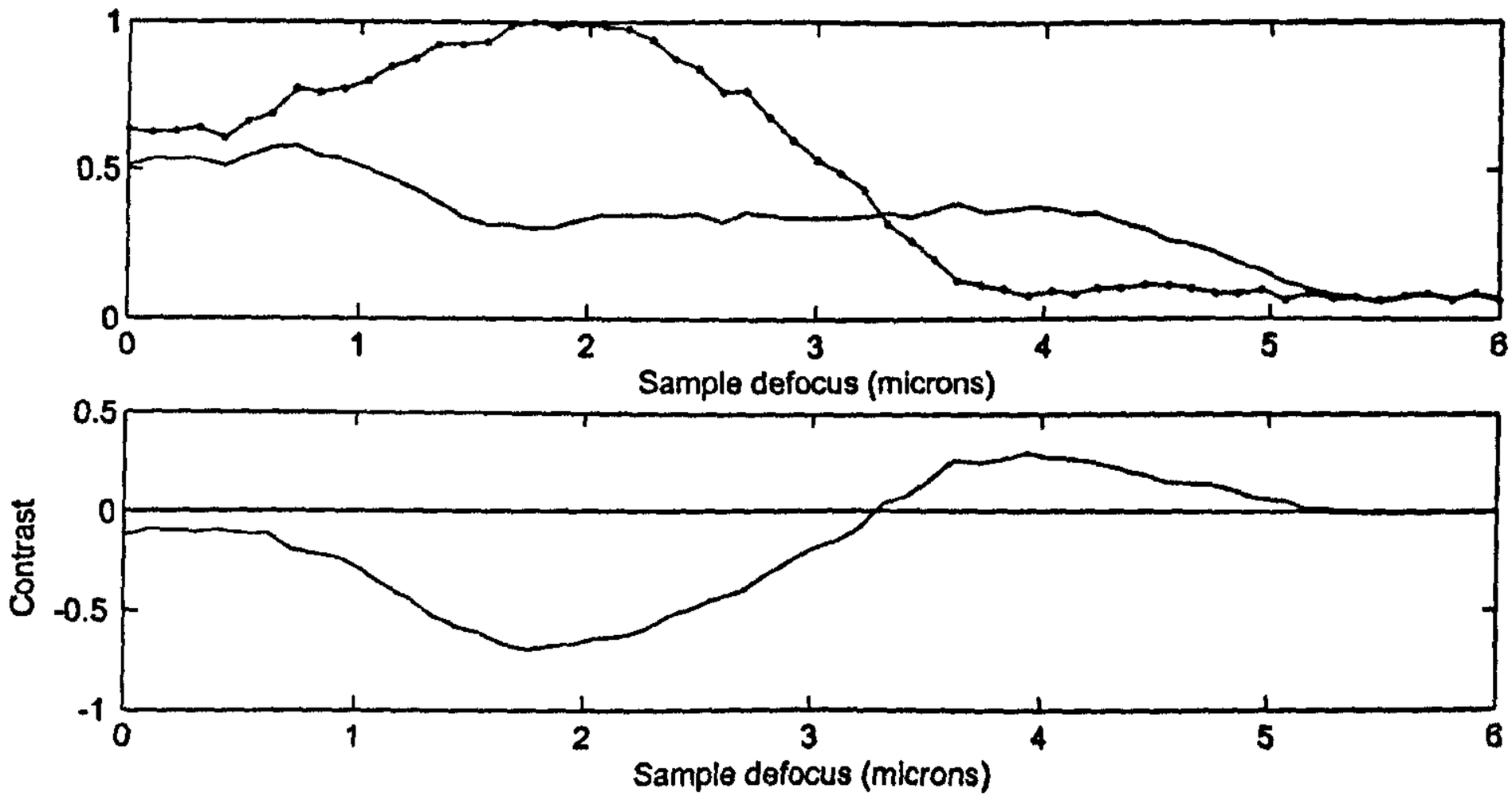

Figure 6.7: *Plots of V(z) without reference aperture for each sample region and a subtraction for horizontal input polarization for increasingly negative defocus, z is relative to the start of the scan not the actual focus*

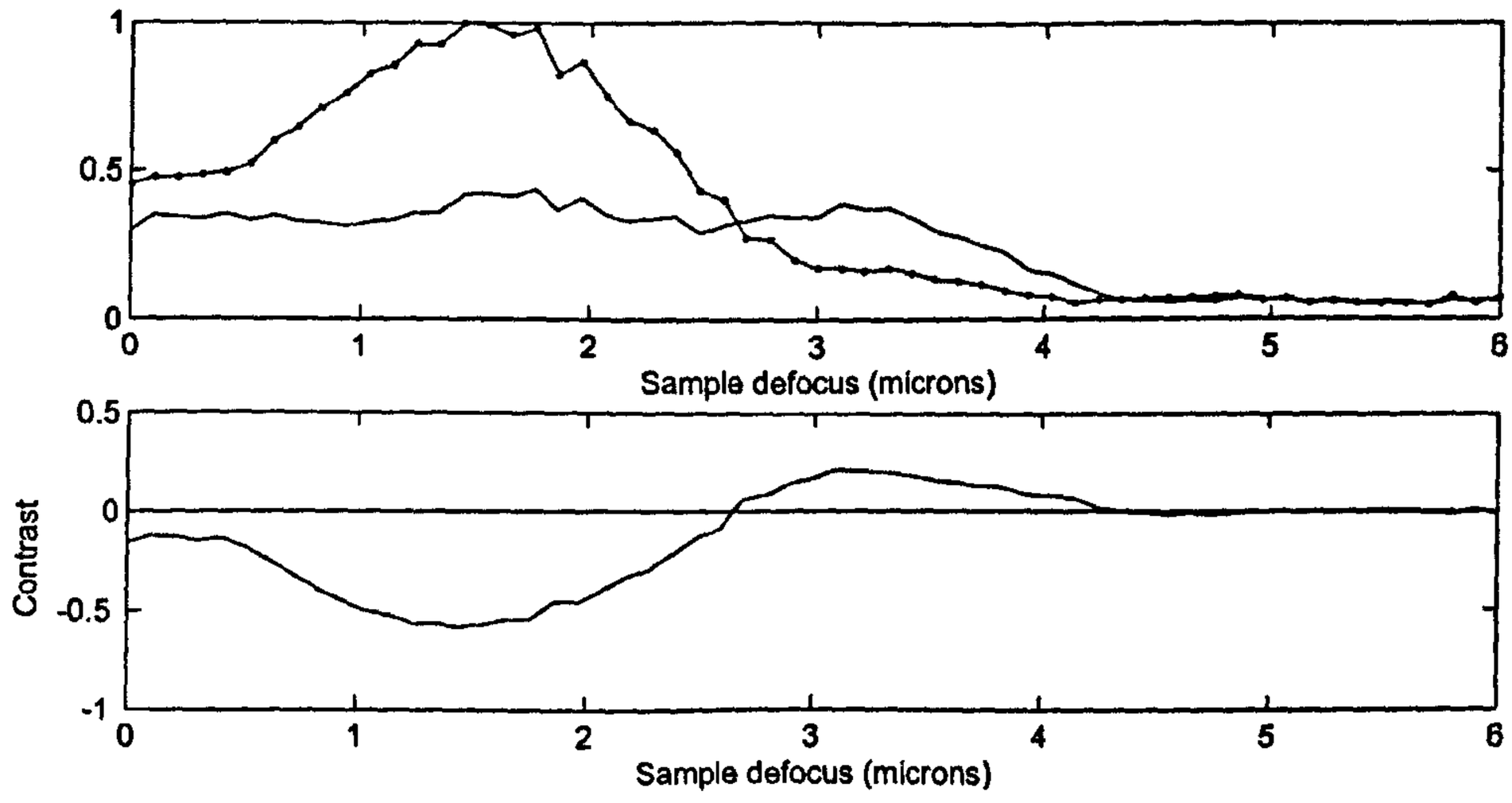

Figure 6.8: *Plots of V(z)without reference aperture for each sample region and a subtraction for vertical input polarization for increasingly negative defocus, z is relative to the start of the scan not the actual focus*

6.4 Imaging with reference aperture

When the aperture is unblocked the images produced are dramatically different, the set of images with horizontal input polarization can be seen in figure 6.9 and the line traces in figure 6.10. Images for vertical input polarization and associated line traces may be seen in figures 6.11 and 6.12 respectively. In terms of the ultimate resolution and contrast the image sets for each polarization orientation are almost identical except for the way the contrast changes with defocus. Each image set goes through several reversals of contrast with points of very low contrast at the transition, when the contrast is low, edge effects can be seen which may correspond to emission into bulk radiation at the boundaries or the addition of a new component in V due to SPs that have traversed the boundary and coupled into new modes. Especially in the case of vertical polarization the edge effects also seem to oscillate which lends credence to this idea.

As before V(z) plots were produced along with the difference between the two which is proportional to the contrast. These may be seen in figure 6.13 and 6.14 for horizontal and vertical polarizations. In both sample regions and for both polarizations a characteristic ripple is seen in the V(z) plots. This in turn produces the contrast and observed contrast reversals. There is a difference between the plots for horizontal and vertical input polarizations for the coated layer, why there is only a major difference in the response for the coated layer is not clear however the differing response with SP propagation direction is not unexpected as the propagation

Figure 6.9: *Matrix of images produced interferometrically with horizontal input po-*

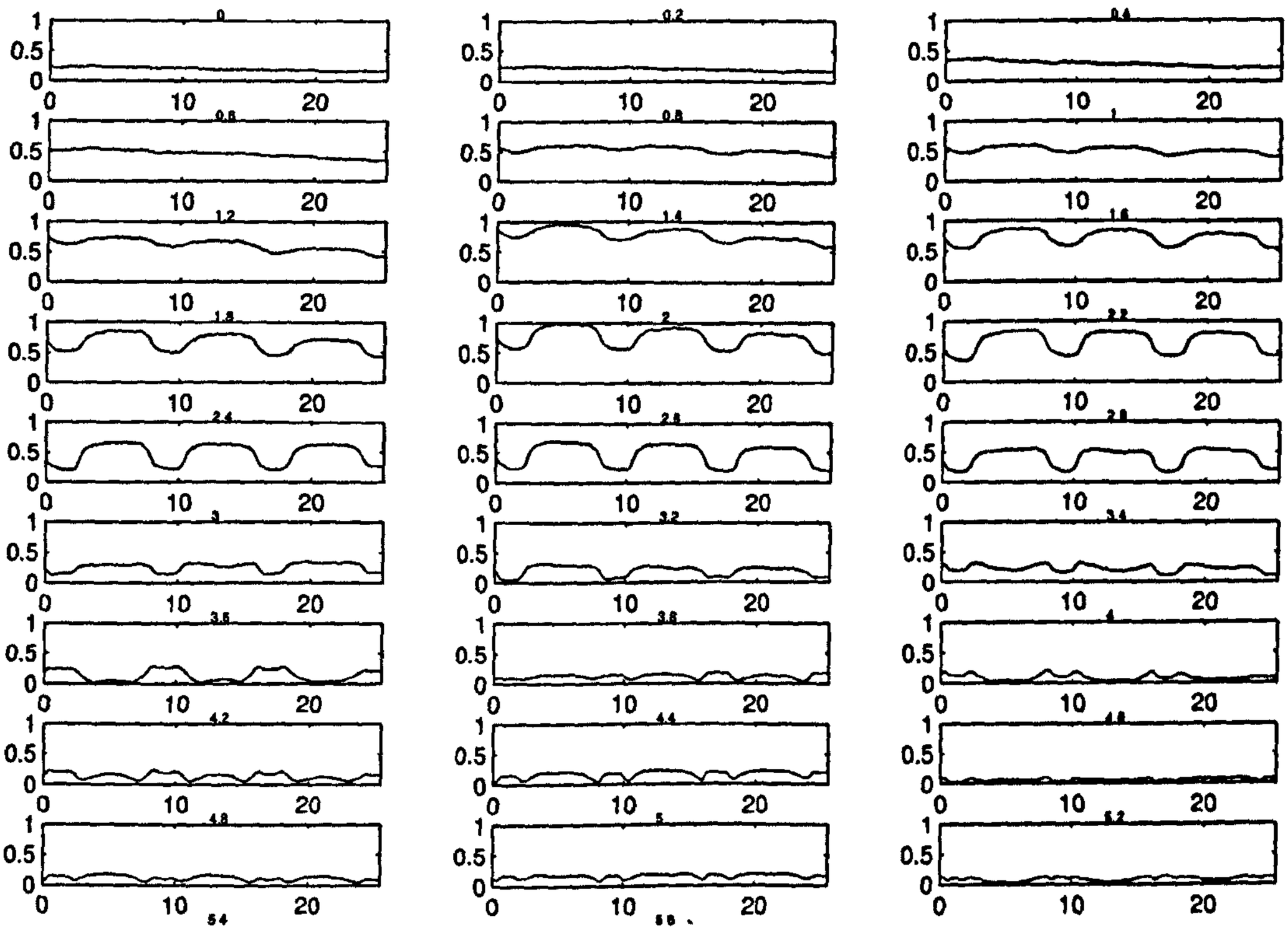

Figure 6.10: *Matrix of line scans produced interferometrically with horizontal input polarization with increasingly negative defocus, the y-axis is the normalized amplitude and the x axis distance in microns*

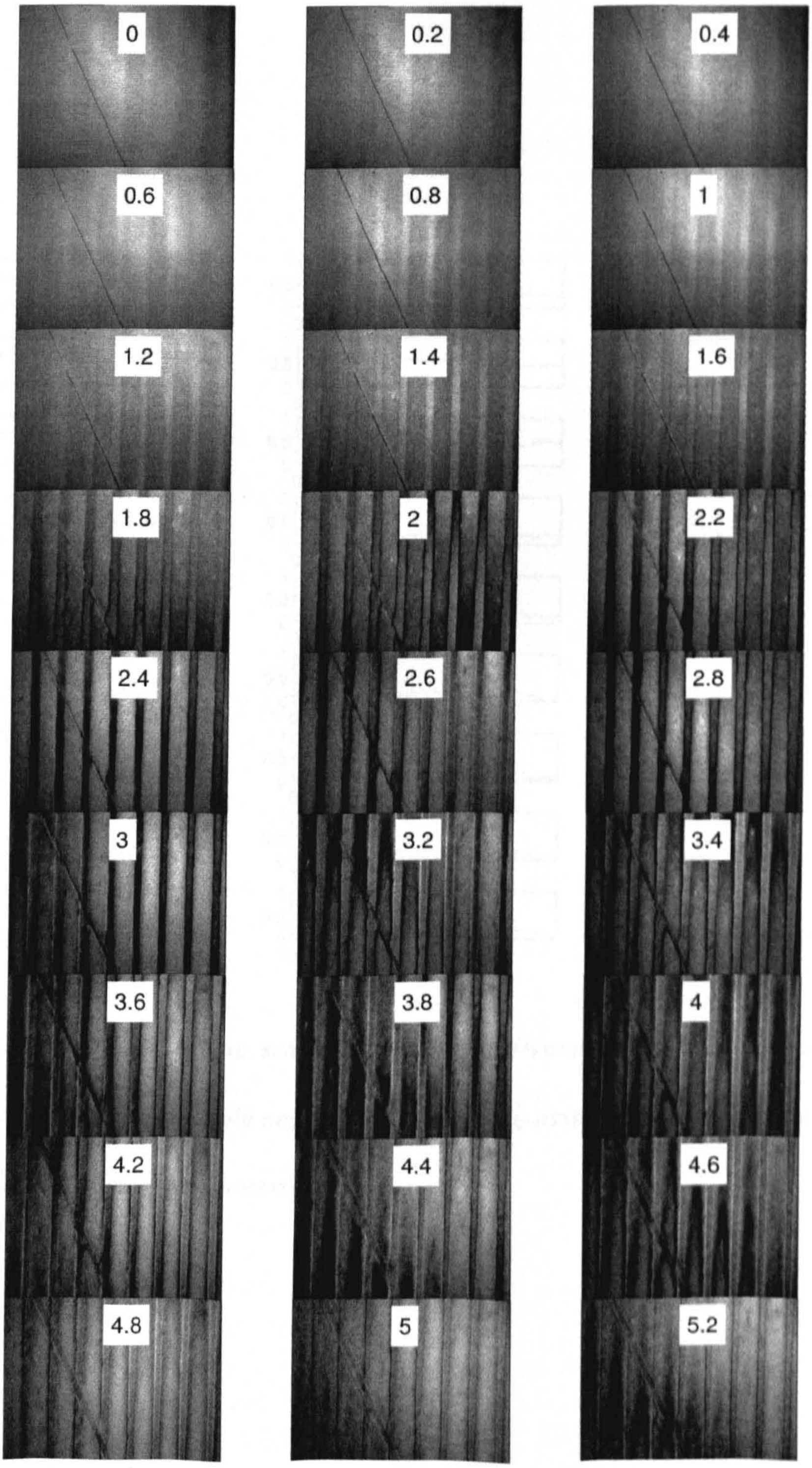

Figure 6.11: *Matrix of images produced interferometrically with vertical input polar-*

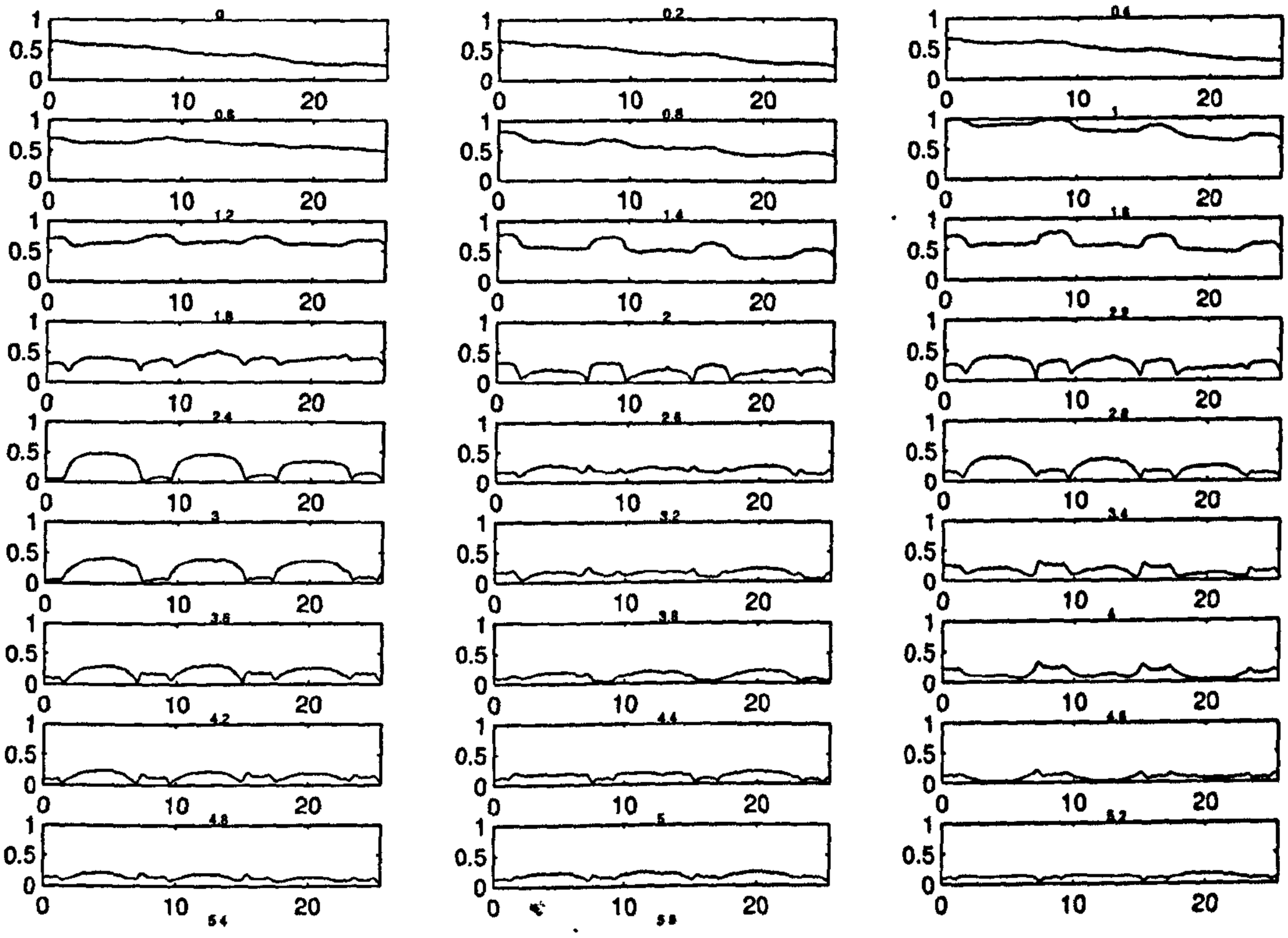

Figure 6.12: *Matrix of line scans produced interferometrically with vertical input polarization with increasingly negative defocus, the y-axis is the normalized amplitude and the x axis distance in microns*

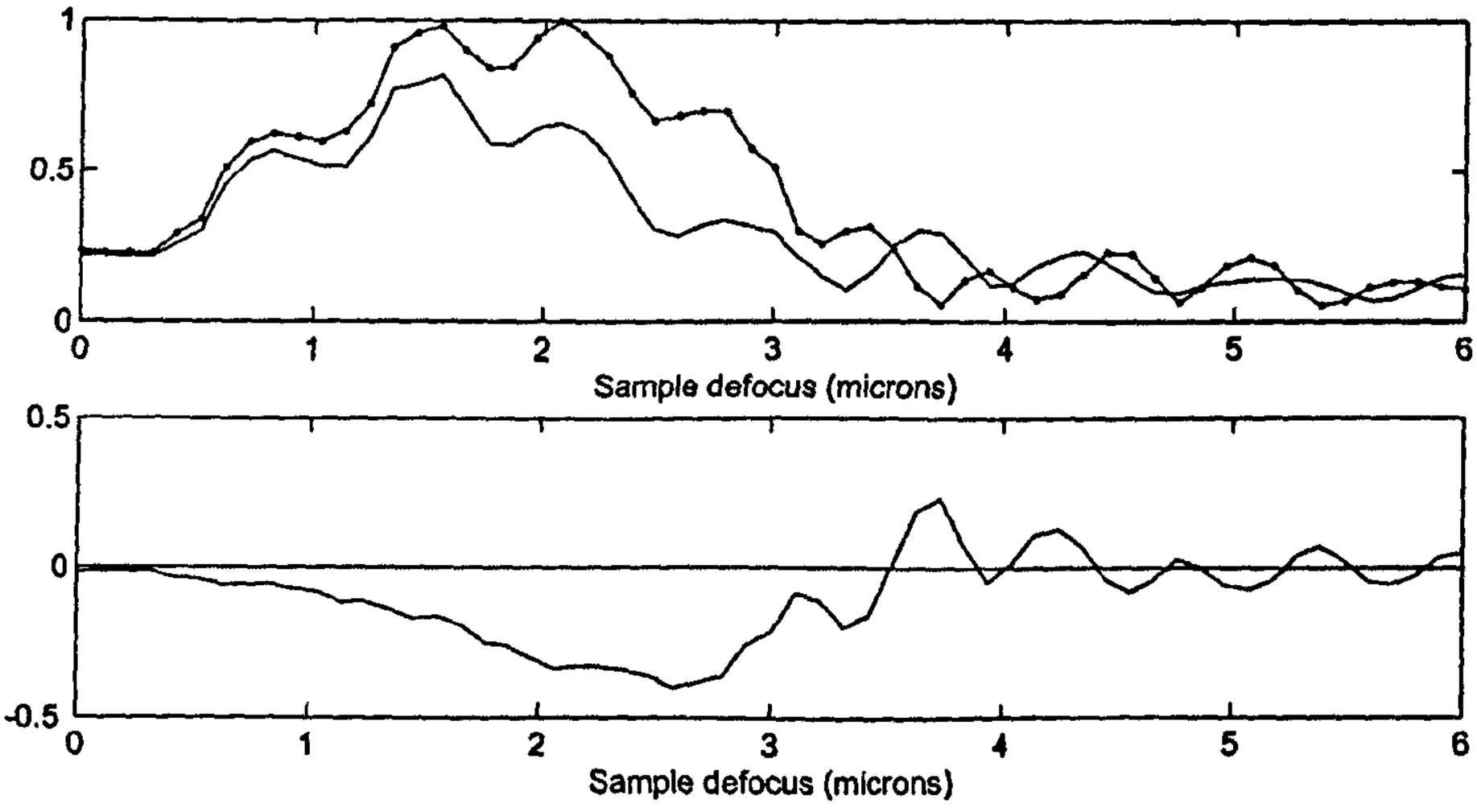

Figure 6.13: *Plots of V(z) with reference aperture for each sample region and a subtraction for horizontal input polarization for increasingly negative defocus, z is relative to the start of the scan not the actual focus*

paths for the SPs will differ between two orientations and this may effect the relative amplitudes of the components that make up V. That does not mean that one orientation is worse than the other, but rather it varies with defocus differently. Of course there may be samples where the response is worse in one orientation than the other but this does not seem to be the case for a grating and the situation is much more complex than for amplitude based SPR microscopes where SP propagation induced smearing is a problem.

Full size images of two defocus positions are shown in figure 6.15 for horizontal input polarization. The first image at a scan position of 2.6μm (1.2μm defocus) has the highest contrast according to figure 6.13. The second image at a defocus

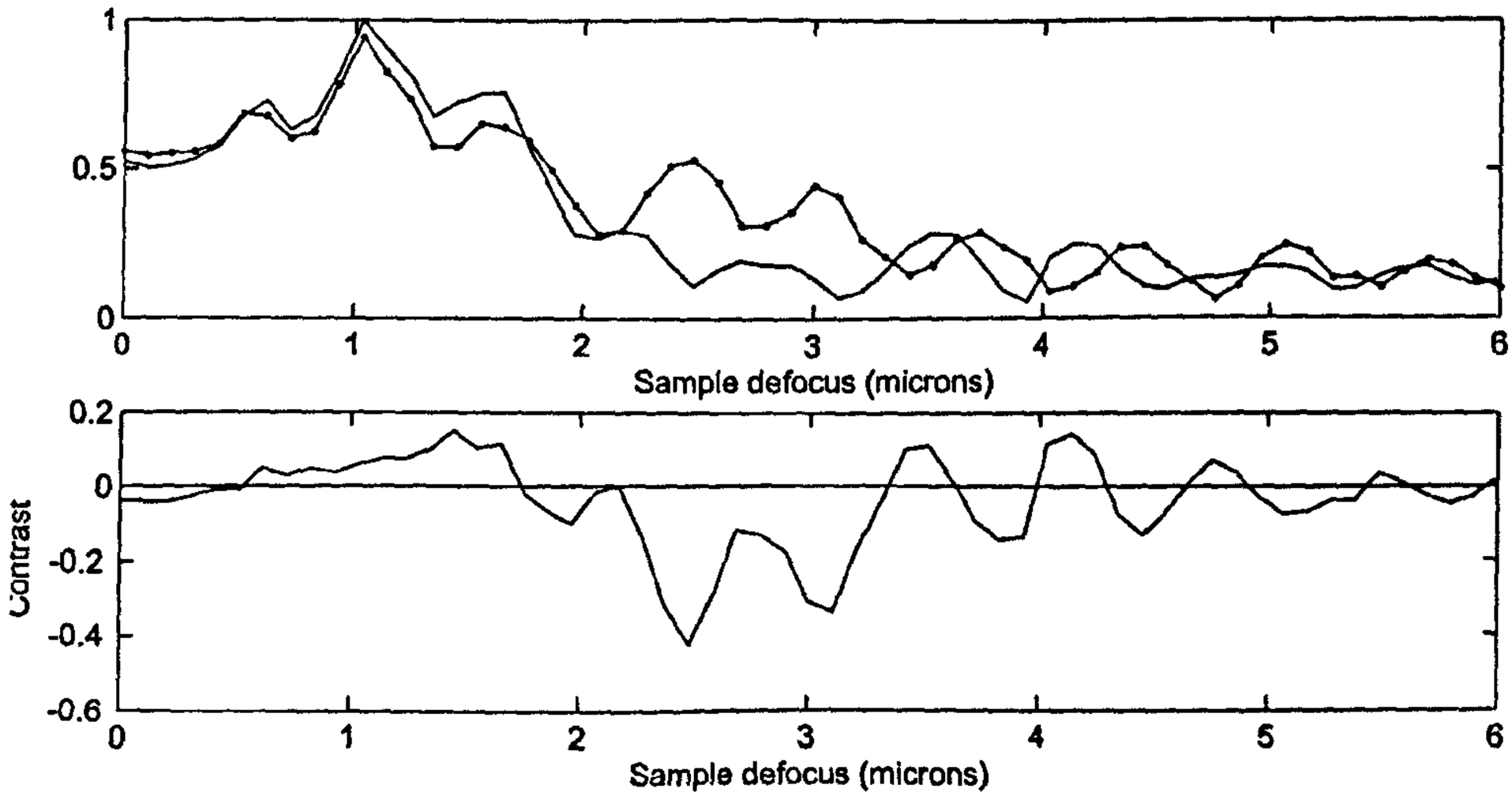

Figure 6.14: *Plots of V(z) with reference aperture for each sample region and a subtraction for vertical input polarization for increasingly negative defocus, z is relative to the start of the scan not the actual focus*

of around 1.6μm seems to have less contrast but higher resolution. Similarly, two images are shown enlarged for vertical input polarization in figure 6.16. The first shows the image at a scan position of 2.4μm (1.4μm defocus). This image has the highest contrast according to figure 6.14. The second image at 3μm scan position (2μm defocus) again seems to have slightly less contrast but higher resolution.

The matrices of images and line scans as well as these specific images show the complex interaction between defocus, contrast and resolution. There seem to be times when some contrast can be traded for resolution. The width of the transitions from 10% and 90% of the total variation is around 0.5μm for each orientation. This is better than seen previously for all but the scanning version of the system and considering the low aquisition time of around 3 seconds represents excellent performance.

6.5 Phase imaging

As well as the amplitude it is also possible to extract the phase of the interference signal via the phase-stepping algorithm. Figure 6.17 shows a single interferogram when the reference mirror is tilted severely to produce fine fringes. As the fringes cross the structure, it can be seen that they become disjointed, suggesting a shift in phase on these regions.

Figure 6.18 shows 4 examples of phase images extracted at 3μm focal position in the defocus scans shown earlier for vertical polarization with aperture, there is

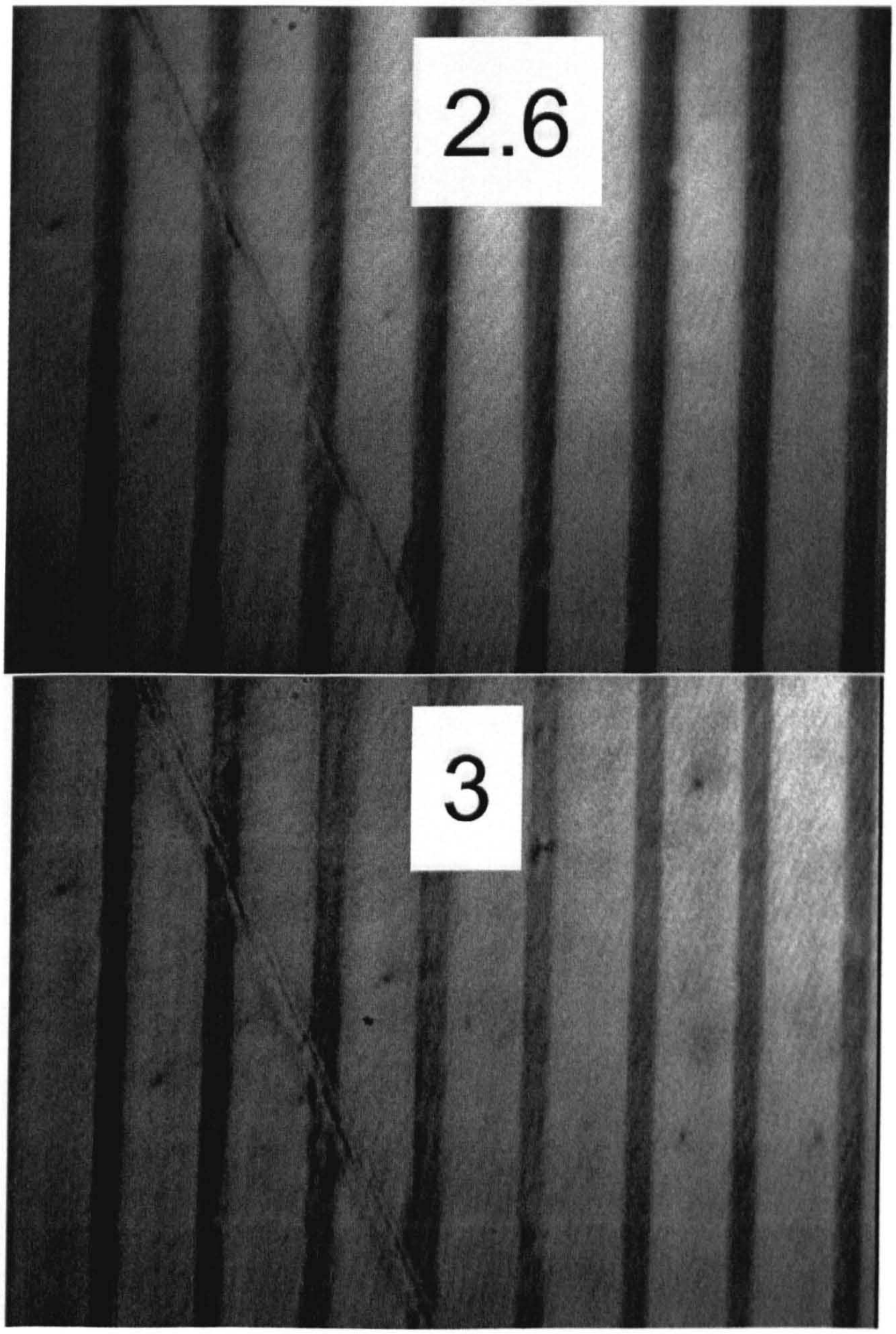

Figure 6.15: *Phase stepped images with horizontal input polarization (scan positions in microns inset)*

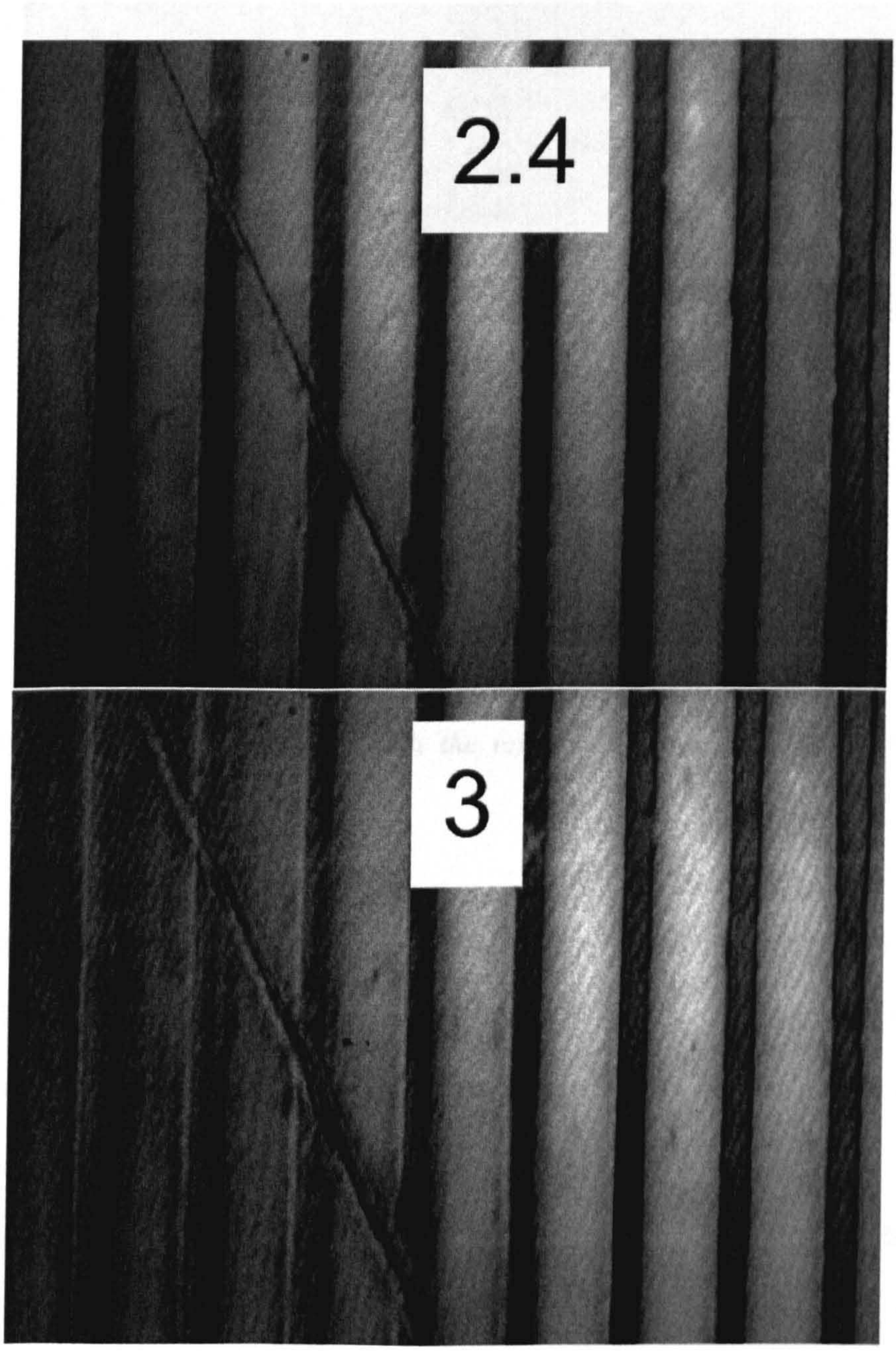

Figure 6.16: *Phase stepped images with vertical input polarization (scan positions in microns inset)*

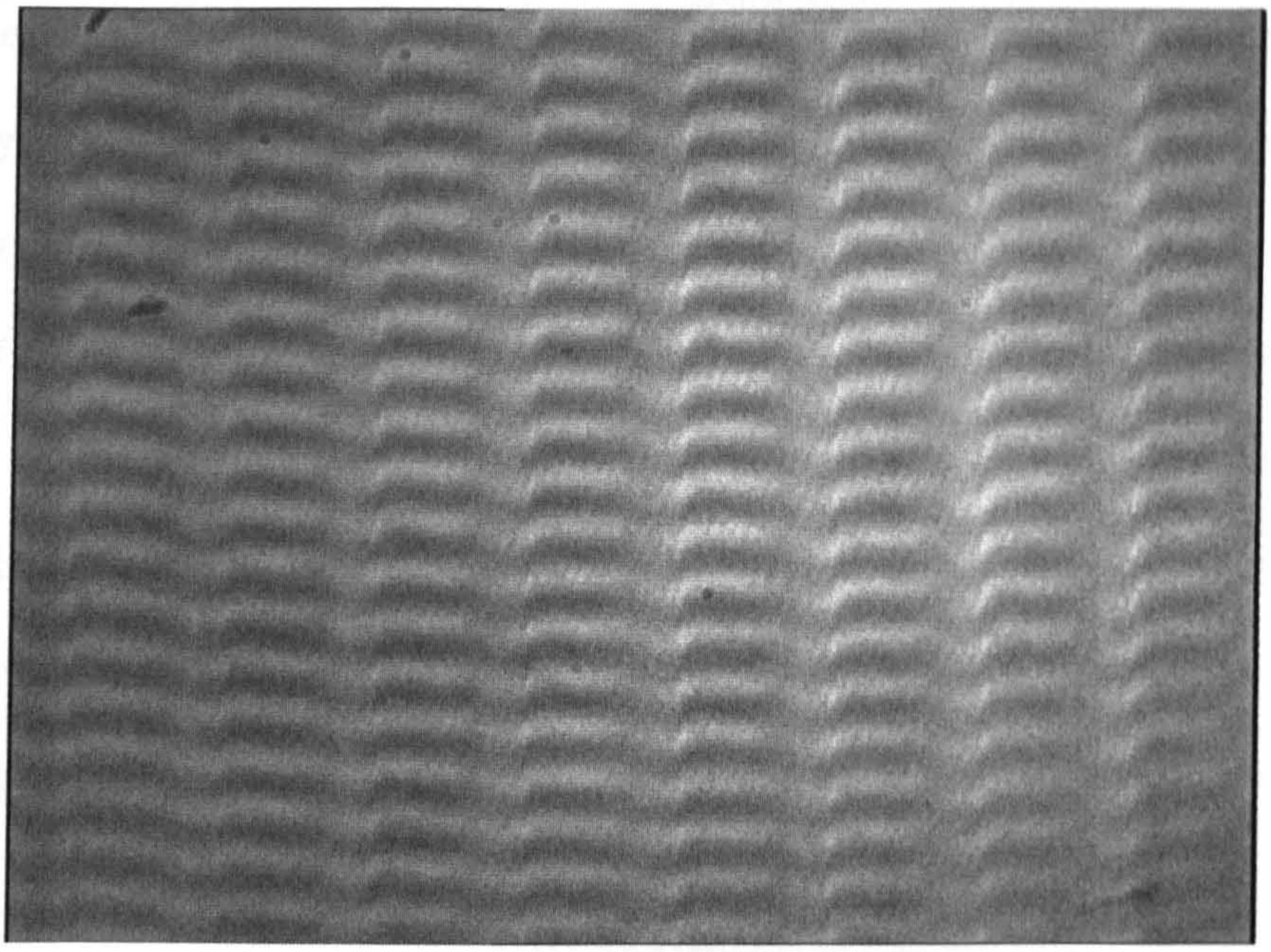

Figure 6.17: *Single interferogram with the reference mirror tilted to produce fine fringes*

a 0.1μm step between each image. The structure can be seen reasonably clearly although the curvature of the wavefront is evident by the circular fringes in the background. Phase variation due to the structure can only be seen at defocus but the general phase curvature makes the phase images less clear.

In an attempt to reveal the structure more clearly a technique by which the differential phase image could be produced was employed. This technique was described by Somekh et al [37] and was used along with an integration to demonstrate the extended focus response of the wide field speckle microscope. In this case only the differential in phase was required, that should show the edges of the structures

most clearly as the phase gradient is greatest there. The method involves simply multiplying the complex form of the image (including amplitude and phase information) by the complex conjugate of a sheared version of itself. The shear was of the order of three pixels in the x direction. The images produced using this technique may be seen in figure 6.19. The images show the edges as light or dark depending on the direction of the transition in phase. The fringes seen before are less visible as they vary slowly. The phase images of standard or differential type do not seem to represent a practical mode of imaging as they offer little more information than the original amplitude images however they do serve as a confirmation to the imaging mechanism being based on the phase of the reflected light.

6.6 Summary

The first thing to be noticed when considering the results presented in this chapter is that the optimum defocus position could not be determined until after the scans were completed and the results analyzed. There seems to be a trade off between resolution and contrast however it is hard to say with this sample if the resolution is actual or virtual. If the results at extreme defocus are considered, the narrower uncoated gold regions actually appear narrower than they should so care is required when quantifying the results. In this case the edge response measurements were taken on an image without edge effects and with good contrast. The image had a sharp appearance and smaller surface irregularities could also be seen, for example

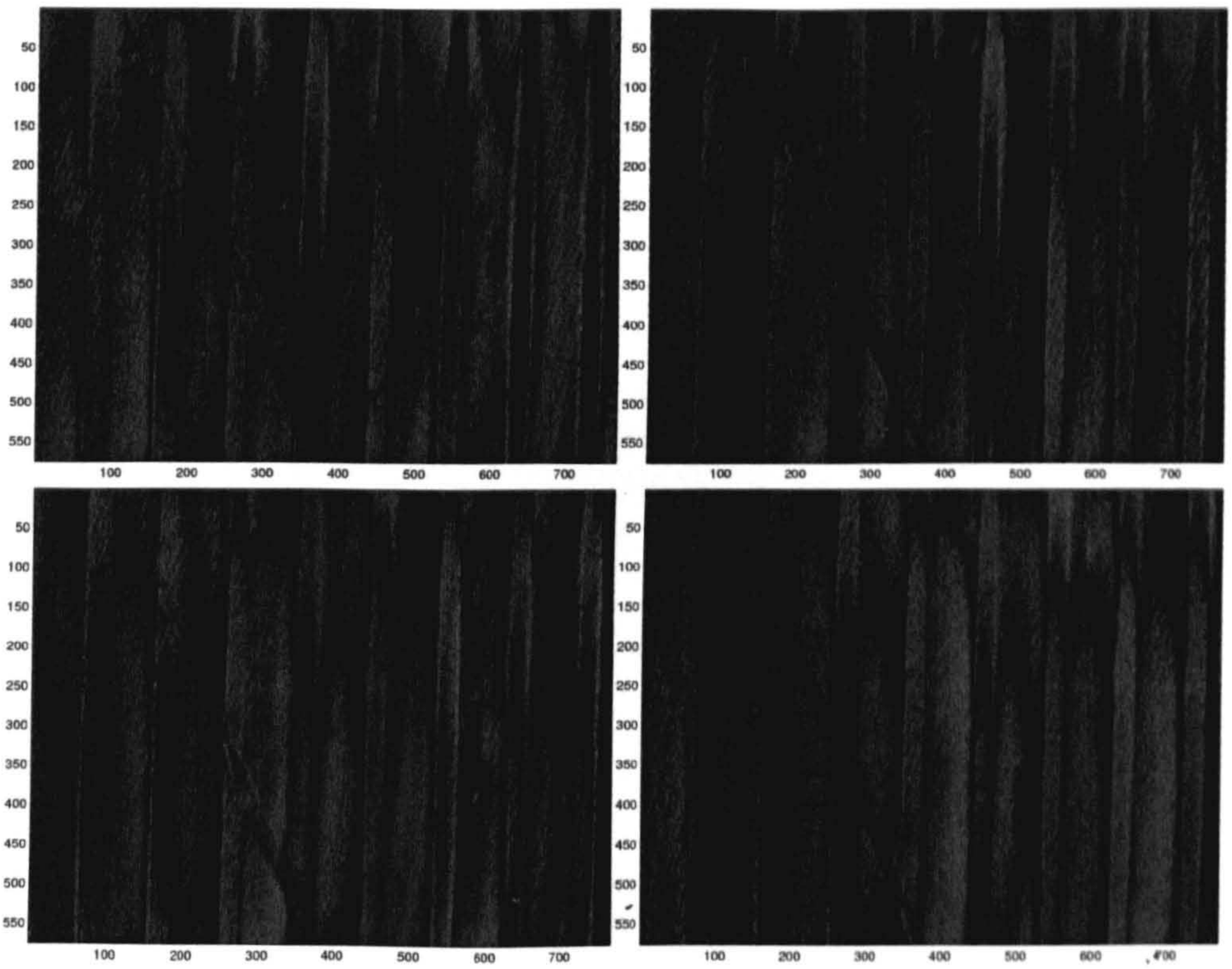

Figure 6.18: *Images of phase extracted at 4 different focal positions 0.1μm apart for vertical polarization*

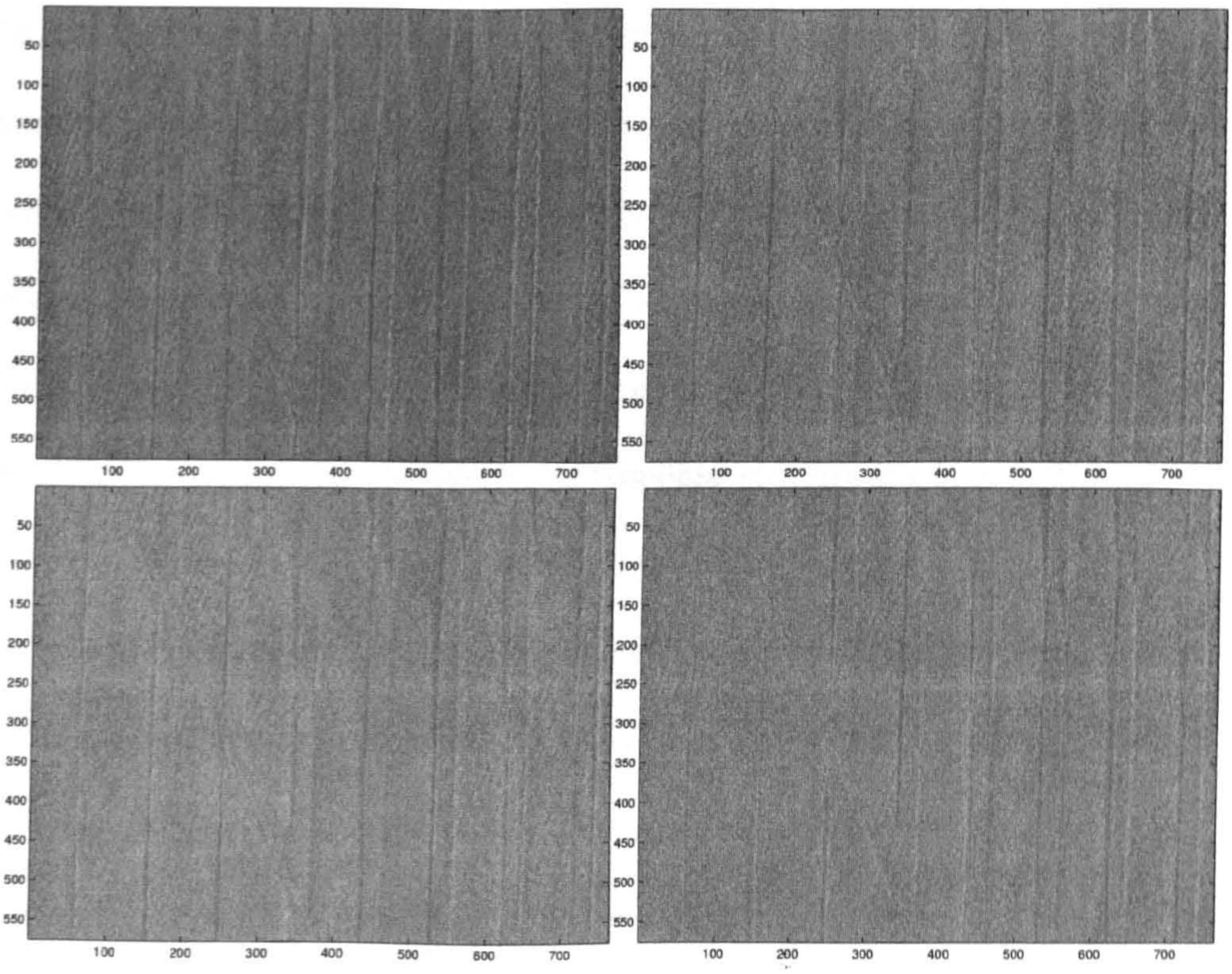

Figure 6.19: *Images of differential phase extracted at 4 different focal positions 0.1μm apart for vertical polarization*

in the case of horizontal polarization the result seen in figure 6.15 with 3μm defocus was used. This appears to be the image that best represents the sample and that looks "right". This subjectivity may seem to be a bad thing but remembering the system is designed as a microscope rather than a sensor the characteristic seems less of a disadvantage. In many conventional microscope systems it is often the job of the operator to interpret the images, especially in systems where depth discrimination is employed. This system although a surface microscope does behave as a confocal microscope in depth, only beam paths are effectively folded onto the sample surface.

On the subject of the edge response the result obtained cannot be considered as the ultimate possible for the system as response to a grating is complicated by the structure. A more exact measurement might be made using a dielectric step, alas this sample was not available at the time of the experimentation. Nevertheless the results are encouraging and represent a case that would normally result in very poor performance from the surface plasmon microscopes seen in the literature.

Finally although the response of the microscope is affected by the propagation direction the performance does not seem to be. For a totally consistent response, circular polarization might be employed to produce pseudo-radial polarization with minimum complication.

In the following chapter the results presented in this and preceding chapters will be summarized and conclusions drawn. Also potential further work will be suggested.

Chapter 7

Conclusions

In the following, the main themes of each chapter will be summarized and conclusions drawn. Further work will also be suggested.

In chapter 1, a general introduction to the phenomenon and use of surface plasmon propagation was presented followed by historical review of the evolution of surface plasmon microscopy techniques. This began with the Kretschmann configuration based amplitude techniques that were shown to be heavily affected by propagation length and direction. A number of techniques to improve the resolution of these systems were then shown. Systems that make use of the highly sensitive phase shift in the reflection co-efficient for p-polarized light were then described and shown in imaging modes. SP excitation with an oil immersion objective lens and the concept of SP focusing on a surface or "localization" was reviewed. Two scanning systems making use of the response seen in the BFP of the exciting objective were also described and the results obtained compared to those of conventional surface

plasmon microscopy. Finally a system using an oil immersion objective and the phase shift of the reflection co-efficient was described. The system forms the basis of this work and was shown to exhibit high contrast and resolution at defocus.

In chapter 2, some of the basic theory required for the understanding of the system developed are presented. The analysis of a lens as a Fourier transformer and the representation of an optical field in terms of an angular spectrum is briefly described. This is related to the distributions seen in the BFP of the imaging objective, these distributions are of key importance to understanding the excitation of SPs on structured samples and for the design of masks. Then the basic concept of the determination of the Fresnel reflection coefficients is described as this is key to the understanding of the concept of phase shift in reflection coefficients and in the analysis of the system developed. An in depth review of the scanning system that forms the basis of that developed in this work was presented. This covered the optical system, the theory behind the contrast and the reasons for operating in defocus. Suggestions are also made as to why this system retains high resolution with defocus for various sample types. Finally a review of a wide field system analogous to the scanning system previously presented is described. This system forms the basis of the evolution of the scanning surface plasmon microscopy to wide field operation.

In Chapter 3, the design considerations and final implementation of the system are presented. The importance of illumination and the effects on field of view are discussed. A short description of the mechanical and automation aspects of the

microscope as well as the alignment procedure is also covered. Finally the production of optical masks used in the BFP of the sample objective is described.

In Chapter 4 images of the BFP distribution are shown for a variety of planar layered samples. The results are shown to correspond to simulated results and also to be of higher quality than those shown in the literature. As such the system operating in this mode could form part of a sensitive sensing system with high dynamic range or a low resolution scanning system. The layered structures also showed the generation of non SP guided wave resonances in the s-polarized direction as well as the p. These resonances were still present with the addition of water backing suggesting the potential use of such layers when imaging aqueous samples.

In Chapter 5 the reference arm of the full system was omitted to allow conventional imaging to be performed. Masks were used to cut down the amount of background light in order to increase the contrast. Initially polarizing optics were added to the imaging arm and these did indeed provide notable contrast enhancement and symmetrical response in terms of polarization orientation. Then results for custom designed mechanical masks were shown with much improved contrast and resolution in the same order of magnitude of better than most surface plasmon microscopy systems. This time a dependence on propagation direction was observed although it was minimal. This system could provide a cost effective means of imaging structures however the contrast obtained may be somewhat sample specific.

In Chapter 6 the results from the completed microscope. A mask was used as it was in the standard imaging configuration to reduce the background light levels

however in this instance an aperture in its centre was required to form a reference. Images of a grating structure were produced in the interferometric mode without the central aperture and the results were poor. Very low resolution resulted although some contrast was seen.

Then imaging results for the same sample were presented but with the central aperture, this time the results were much improved with excellent contrast and sub micron edge response. Images were taken for horizontal and vertical input polarizations and these were almost identical in terms of the resolution and contrast although the response with defocus was distinctly different. For each orientation the best results were obtained at a specific defocus, this would suggest that a truly live feed of the phase stepped images would be beneficial as it would allow the operator to adjust the defocus while monitoring the image.

The system displays almost identical performance to the scanning version with several key improvements. First and foremost the speed is much improved, in the scanning system the image would be built up point by point. In this system the results can be taken in a number of seconds. This is advantageous on several counts. Firstly it speeds the general acquisition of the images, secondly it allows the correct defocus to be found giving the best results for the specific sample, thirdly it allows the possibility of viewing surface reactions in real time and finally the instrument is less sensitive to vibration and other external influences. Another general improvement is the simplicity of the system, it consists essentially of a conventional Linnik interferometer, most of the optics required are as for a conventional microscope, it

was also shown that a low NA objective could be used successfully in the reference arm. Very little ancillary equipment is required only a PC, piezo stage/driver and CCD cameras are absolutely required. Further to this the microscope offers other imaging modes such as conventional microscopy both for SP and non SP samples and also sensing via the imaging of the BFP.

7.1 Further Work

There are several areas in which the current work could be extended directly. To begin with it would be beneficial to produce more samples from which a greater diversity of results could be obtained. This would allow the experimental investigation of the resolution on a edge and the effects of structures on excitation in both polarization states. It might also allow the absolute limits of sensitivity and resolution in refractive index and thickness to be determined. Similarly reference samples could allow the microscope operating as a sensor to be investigated more thoroughly.

As well as further experimental work it would be useful to expand the numerical model of the V(z) shown in chapter 2 to deal with non homogeneous samples. As the wide field microscope can be thought of as many scanning microscopes in parallel it would produce valid and enlightening results that may also help in the design in masks and the determination of the correct defocus. As well as these practical advantages it could explain the exact mechanism of contrast for a variety of sample

types and show the relative weighting of each.

The next and most important modification to the current system is an increase in acquisition speed. Compared to the scanning system the speed was excellent, image capture took around 2—3 seconds. If the speed could be increased to around 10–15 frames per second then the system could be used as a conventional microscope and the defocus adjusted manually by the operator(via micrometer or keypad) for the best image.

There are several ways of achieving this goal. Sawyer et al[48] showed a means of producing 4 phase-stepped images on a single CCD camera via the application of polarization optics. This means that the image production is limited by the camera capture time and computer processing speed. Fast capture can be performed with progressive scan CCD cameras and the system has sufficient light for short exposure times. The fast diffuser disk means that streaking should also not be seen. Adding a second counter-rotating diffuser disk would also increase the speed of speckle evolution. The problem with this technique is that the CCD camera is not used efficiently. The second disadvantage is the difficulty in alignment and complexity of the optical system. Other methods might also be used to produce images more quickly, if the reference mirror piezo stage was driven sinusoidally then a photo diode might be used to trigger the PS-CCD to capture at the relevant points. The whole of the CCD could then be used and the optical set up would be trivial. Work is also being undertaken in the group on the development of modulated light cameras using photo diodes and in built processing optics, these might also be used for ultra

fast acquisition when they come to fruition.

In terms of the commercial application of the microscope developed in this thesis the components are relatively economic, the most expensive component by far is the oil immersion objective. To this end work is being carried out on the use of solid immersion lenses. These low-cost hemispherical lenses can be used to increase the effective NA of long working length low NA objectives and have recently been shown to be applicable to SP excitation [49].

7.2 Summary

The goal of the work carried out was to produce a high resolution wide field surface plasmon microscope. This goal has been achieved and in addition two extra modes of operation have been shown that have not been seen before. The sensing mode based on the BFP distributions of the sample objective provides BFP images much clearer than those before and could yield highly sensitive sensing with high dynamic range. The "conventional" imaging mode was also shown to produce images comparable with those in the literature and improved over prism based microscopes. The final system was shown to be capable of producing high resolution high contrast images comparable to those of the scanning system on which it was based but at much higher speed and with less complexity. The instrument is hence a highly useful and practical device with direct applications to many areas of science.

Bibliography

[1] S. Liu, *Optical microscopy for high resolution and high sensitivity imaging of biological samples.* PhD thesis, The University of Nottingham, 2002.

[2] E. M. Yeatman, "Resolution and sensitivity in surface plasmon microscopy and sensing," *Biosensors and Bioelectronics*, vol. 11, no. 6, pp. 635–649, 1996.

[3] M. Petty, *Langmuir-Blodgett films.* Cambridge University Press, 1996.

[4] E. Kretschmann, "Decay of non radiative surface plasmons into light on rough silver films. comparison of experimental and theoretical results," *Optical Communications*, vol. 6, pp. 185–187, 1972.

[5] H. Raether, *Surface Plasmons on smooth and rough surfaces and on gratings.* Springer-Verlag, 1988.

[6] T. Inagaki and K. Kagami, "Photoacoustic observation of nonradiative decay of surface plasmons in silver," *Physical Review B*, vol. 24, no. 6, pp. 3644–3646, 1981.

[7] B. Rothenhäusler, J. Rabe, P. Korpiun, and W. Knoll, "On the decay of plasmon surface polaritons at smooth and rough ag-air interfaces: A reflectance and photo-acoustic study," *Surface Science*, vol. 137, pp. 373–383, 1984.

[8] C. Nylander, B. Liedberg, and T.Lind, "Gas detection by means of surface-plasmon resonance," *Sensors and Actuators*, vol. 3, pp. 79–88, 1982.

[9] K. Matsubara, S. Kawata, and S. Minami, "Optical chemical sensor based on surface-plasmon measurement," *Applied Optics*, vol. 27, pp. 1160–1163, 1988.

[10] I. Pockrand, "Surface plasma oscillations at silver surfaces with thin transparent and absorbing coatings," *Surface Science*, vol. 72, pp. 577–588, 1978.

[11] M. T. Flanagan and R.H.Pantell, "Surface plasmon resonance and immunosensors," *Electronics Letters*, vol. 20, no. 23, pp. 968–970, 1984.

[12] H. E. de Bruijn, R. P. H. Kooyman, and J. Greve, "Choice of metal and wavelength for surface-plasmon resonance sensors: some considerations," *Applied Optics*, vol. 31, no. 4, pp. 440–442, 1992.

[13] E. Yeatman and E. A. Ash, "Surface plasmon microscopy," *Electronics Letters*, vol. 23, no. 20, pp. 1091–1092, 1987.

[14] B. Rothenhäusler and W. Knoll, "Surface-plasmon microscopy," *Nature*, vol. 332, pp. 615–617, 1988.

[15] W. L. Barnes and J. R. Sambles, "Re-radiation from surface plasmon polaritons," *Solid State Communications*, vol. 55, no. 11, pp. 921–923, 1985.

[16] Z. Schlesinger and A. J. Sievers, "Infrared surface wave interferometry," *Applied Physics Letters*, vol. 36, no. 6, pp. 409–412, 1980.

[17] G. I. Stegeman, A. A. Maradudin, and T. S. Rahman, "Refraction of the surface polariton by an interface," *Physical Review B*, vol. 23, no. 6, pp. 2576–2585, 1981.

[18] A. A. Maradudin, R. F. Wallis, and G. I. Stegerman, "Surface polariton reflection and transmission at a barrier," *Solid State Communications*, vol. 46, no. 6, pp. 481–485, 1983.

[19] T. A. Leskova, "Theory of a fabry-perot type interferometer for surface polaritons," *Solid State Communications*, vol. 50, no. 9, pp. 869–873, 1984.

[20] B. Rothenhäusler and W. Knoll, "Total internal diffraction of plasmon surface polaritons," *Applied physics letters*, vol. 51, no. 11, pp. 783–785, 1987.

[21] B. Rothenhäusler, "On the influence of the propagation length of plasmon surface polaritons in the visible energy range for the optical characterization of heterogeneous thin films," *Surface Science*, vol. 191, pp. 585–594, 1987.

[22] B. Rothenhäusler and W. Knoll, "Surface plasmon interferometry in the visible," *Applied Physics Letters*, vol. 52, pp. 1554–1556, 1988.

[23] B. Rothenhäusler and W. Knoll, "Interferometric determination of the complex wave vector of plasmon surface polaritons," *Journal of the Optical Society of America B*, vol. 5, no. 7, pp. 1401–1405, 1988.

[24] C. E. H. Berger, R. P. H. Kooyman, and J. Greve, "Surface plasmon propagation near an index step," *Optics Communications*, vol. 167, pp. 183–189, 1999.

[25] M. E. Caldwell and E. M. Yeatman, "Performance characteristics of surface plasmon liquid crystal light valve," *Electronics Letters*, vol. 27, no. 16, pp. 1471–1472, 1991.

[26] H. E. de Bruijn, R. P. H. Kooyman, and J. Greve, "Surface plasmon resonance microscopy: improvement of the resolution by rotation of the object," *Applied Optics*, vol. 32, no. 13, pp. 2426–2430, 1993.

[27] C. E. H. Berger, R. P. H. Kooyman, and J. Greve, "Resolution in surface plasmon microscopy," *Review of scientific instruments*, vol. 65, no. 9, pp. 2829–2836, 1994.

[28] H. Kano, S. Mizuguchi, and S. Kawata, "Excitation of surface-plasmon polaritons by a focused laser beam," *Journal of the Optical Society of America B*, vol. 15, pp. 1381–1386, 1998.

[29] M. Stalder and M.Schadt, "Linearly polarized light with axial symmetry generated by liquid-crystal polarization converters," *Optics Letters*, vol. 21, pp. 1948–1950, 1996.

[30] H. Kano and W. Knoll, "Locally excited surface-plasmon-polaritons for thickness measurement of lbk films," *Optics Communications*, vol. 153, pp. 235–239, 1998.

[31] H. Kano and W. Knoll, "A scanning microscope employing localized surface-plasmon-polaritons as a sensing probe," *Optics Communications*, vol. 182, pp. 11–15, 2000.

[32] T. Tanaka and S. Yamamoto, "Laser-scanning surface plasmon polariton resonance microscopy with multiple photodetectors," *Applied Optics*, vol. 42, no. 19, pp. 4002–4007, 2003.

[33] S. G. Nelson, K. S. Johnston, and S. S. Lee, "High sensitivity surface plasmon resonance sensor based on phase detection," *Sensors and Actuators B*, vol. 35-36, pp. 187–191, 1996.

[34] A. V. Kabashin and P. I. Nikitin, "Surface plasmon resonance interferometer for bio- and chemical-sensors," *Optics Communications*, vol. 150, pp. 5–8, 1998.

[35] A. N. Grigorenko, P. I. Nikitin, and A. V. Kabashin, "Phase jumps and interferometric surface plasmon resonance imaging," *Applied Physics Letters*, vol. 75, no. 25, pp. 3917–3919, 1999.

[36] A. V. Kabashin, V. E. Kochergin, and P. I. Nikitin, "Surface plasmon resonance bio- and chemical sensors with phase-polarization contrast," *Sensors and Actuators B*, vol. 54, pp. 54–56, 1999.

[37] M. G. Somekh, C. W. See, and J. Goh, "Wide field amplitude and phase confocal microscope with speckle illumination," *Optics Communications*, vol. 174, pp. 75–80, 2000.

[38] A.Atalar and H.Koymen, "V(z) of the surface acoustic-wave focusing system," *IEEE Transactions on ultrasonics ferroelectrics and frequency control*, vol. 34, pp. 387–388, 1987.

[39] R. Azzam and N. Bashara, *Ellipsometry and polarized light.* North-Holland personal library, 1977.

[40] M. G. Somekh, S. G. Liu, T. S. Velinov, and C. W. See, "Optical v(z) for high-resolution 2π surface plasmon microscopy," *Optics letters*, vol. 25, no. 11, pp. 823–825, 2000.

[41] E. Hecht, *Optics, third edition.* Addison-Wesley, 1998.

[42] M. Petran, M. Hadraysky, M. Egger, and R. Galambos, "Tandem-scanning reflected-light microscope," *Journals of the Optical Society of America*, vol. 58, p. 661, 1968.

[43] T. Wilson, R. Justaitis, M. Neil, and M. Kozubek, "Confocal microscopy by aperture correlation," *Optics Letters*, vol. 21, p. 1879, 1996.

[44] M. Neil, R. Juskaitis, and T. Wilson, "Method of obtaining optical sectioning by using structured light in a conventional microscope," *Optics Letters*, vol. 22, p. 1905, 1997.

[45] G. Stabler, M. G. Somekh, and C. W. See, "High-resolution wide-field surface plasmon microscopy," *Journal of Microscopy*, vol. 214, no. 3, pp. 328–333, 2003.

[46] H. Kano and W. Knoll, "A scanning microscope employing localized surface-plasmon-polaritons as a sensing probe," *Optics Communications*, vol. 182, pp. 11–15, 2000.

[47] K. Creath, "Comparison of phase-unwrapping algorithms by using gradient of first failure," *Applied Optics*, vol. 35, pp. 5108–5114, 1996.

[48] N. Sawyer, S. Morgan, M. Somekh, C. See, and X. Cao, "Wide field amplitude and phase confocal microscope with parallel phase stepping," *Review of scientific instruments*, vol. 3793, pp. 3793–3801, 2001.

[49] J. Zhang, C. W. See, M. G. Somekh, M. C. Pitter, and S. G. Liu, "Wide field surface plasmon microscopy with solid immersion excitation," *Applied physics letters, awaiting publication*, 2004.